

 TU Delft Shell

July 26-28, 2000

# TNF5

Delft, The Netherlands

**5<sup>th</sup>** *International Workshop*

*on Measurement and*

*Computation of Turbulent*

*Non-Premixed Flames*

# *Proceedings*

J.M. Burgerscentrum



Warmte en Stroming  
Thermal and Fluids Sciences

**Proceedings of the 5<sup>th</sup> International Workshop On  
Measurement and Computation of Turbulent Non-  
Premixed Flames.  
26<sup>th</sup> – 28<sup>th</sup> July 2000. Delft, The Netherlands**

**Editors**

Aristide Mbioc<sup>\*</sup>, Dirk Roekaerts<sup>#</sup>, and Robert Barlow<sup>\*\*</sup>

<sup>\*</sup> Thermal and Fluids Sciences, Department of Applied Physics, Faculty of Applied Sciences, Delft University of Technology, Lorentzweg, 1, 2628 CJ Delft, The Netherlands

<sup>#</sup> Shell Global Solutions International BV, Amsterdam, The Netherlands

<sup>\*\*</sup>Combustion Research Facility, Sandia National Laboratories, Livermore, CA 94551, USA

**TNF Organizing Committee**

R. Barlow, R. Bilger, J.-Y. Chen, E. Hassel, J. Janicka, A. Masri, N. Peters, H. Pitsch, S. Pope, D. Roekaerts.

**Local Host Committee**

Tieying Ding, Maggy Doolhoff, Mike Golombok, Werner Huebner, Denis Krasinsky, Aristide Mbioc, Bertrand Naud, Dirk Roekaerts, Joan Teerling.

## Contents (PDF Version)\*

Summary and Conclusions  
Recommended Restrictions on the Use of TNF Proceedings  
Preface  
Agenda  
List of Participants

SECTION 1: Piloted CH<sub>4</sub>/Air Jet Flames and Related Issues  
Coordinated by Robert S. Barlow

- Update on Piloted CH<sub>4</sub>/Air Jet Flames – R. Barlow
- Partially Premixed Laminar Flame Comparisons
- Chemistry Issues in C/H/N/O Systems for C<sub>1</sub>/C<sub>2</sub> Fuels – P. Lindstedt
- Update on Radiation Issues
- Parametric Studies on Mixing Models – J.-Y. Chen
- Numerical Errors in PDF Methods – S. Pope
- Note on Turbulence Models and Inlet Profiles – D. Roekaerts

SECTION 2: Computation of Bluff-Body Stabilised Jets and Flames  
Coordinated by Assaad R. Masri

SECTION 3: Confined TECFLAM Swirl Burner: Experimental Investigations and Numerical Simulations  
Coordinated by Andreas Dreizler

SECTION 4: Poster Abstracts

- List of Authors and Titles
- Poster Abstracts

\* This pdf version of the TNF5 Proceedings includes additional material that was not in the printed proceedings.

## SUMMARY AND CONCLUSIONS

### **Fifth International Workshop on Measurement and Computation of Turbulent Nonpremixed Flames**

**26-28 July 2000  
Delft, The Netherlands**

**Robert Barlow and Dirk Roekaerts**

#### **INTRODUCTION:**

The series of workshops on Measurement and Computation of Turbulent Nonpremixed Flames (TNF Workshops) is intended to facilitate collaboration and information exchange among experimental and computational researchers in the field of turbulent nonpremixed combustion. The emphasis is on fundamental issues of turbulence-chemistry, as revealed by comparisons of measured and modeled results for selected flames.

TNF5 was hosted by the Thermal and Fluid Sciences Section, Delft University of Technical and was attended by 68 researchers from 11 countries. Thirty posters were contributed and abstracts are included in the proceedings. Calculated and measured results were compared for three target flames:

- Piloted CH<sub>4</sub>/air jet flame series, with emphasis on extinction/re-ignition and NO formation
- Bluff-body stabilized flows and flames
- The TECFLAM burner for confined swirling natural gas flames

In addition, there were presentation and discussions on specific modeling issues, including:

- Accuracy of chemical mechanisms in calculations of laminar, opposed-flow, partially-premixed CH<sub>4</sub>/air flames
- Adequacy of the optically thin radiation model
- Sensitivity of piloted flame results to the choice of mixing model
- Sensitivity of results to changes (uncertainties) in inflow conditions
- Statistical accuracy of pdf calculation

As in previous TNF workshops there was an open and productive atmosphere with numerous discussions in small groups, during breaks and poster sessions, as well as larger discussions, during the technical session. It is this situation, together with the exchange of information during the year among collaborating groups at various locations, which forms the basis for progress on the selected target flames. TNF participants are encouraged to continue and expand these collaborations and discussions, as we pursue a better understanding of turbulent combustion.

This summary briefly outlines accomplishments on the three target flames and other focus topics. It also summarizes discussions at TNF5 regarding research priorities and planning for the next workshop (TNF6). The TNF5 Proceedings are available in pdf format on the web at [www.ca.sandia.gov/tdf/Workshop](http://www.ca.sandia.gov/tdf/Workshop). The pdf file includes all materials from the proceedings notebook that was distributed to workshop participants in Delft (preface, agenda, list of attendees, selected comparisons of measured and modeled results for the three target flames, information on

other focus topics, and poster abstracts). Several vugraph presentations have also been included. The pdf file has 236 pages taking roughly 22 Mb, and it includes bookmarks and thumbnails for navigation.

### **ACCOMPLISHMENTS:**

Accomplishments on various topics are outlined in the order of the TNF5 agenda.

#### **Piloted Flames:**

- **General Progress** – Significant progress has been made in recent years in the modeling of the piloted CH<sub>4</sub>/air jet flames. It can be concluded that it is now possible to obtain very good agreement between model and experiment. In particular, the pdf calculations contributed by Tang, Xu, and Pope (Cornell) and by Lindstedt, Louloudi, and Vaos (Imperial College) each do well in accounting for local extinction, as well as getting reasonably good agreement on Favre averaged profiles, conditional means, and fluctuations. These calculations, which are described in more detail in papers contributed to the 28<sup>th</sup> Combustion Symposium, are representative of the state of the art in modeling turbulent jet flames with local extinction. We have also achieved a better understanding of several aspects of the models and the sensitivity of results to the choice of chemical mechanism, radiation model, mixing model and mixing constants, constants in turbulence models, and boundary conditions.
- **Chemical Mechanisms** – Comparisons of measured and modeled results in steady, opposed-flow, partially premixed laminar flames served to clarify the similarities and differences among various detailed chemical mechanisms for methane combustion. It may be concluded that the detailed mechanisms used in the various calculations of the target flames (the Lindstedt mechanism and versions of GRI Mech ) yield similar results for the major species profiles in laminar flames and that predictions agree with experiments. There are large differences among mechanisms, with regard to the prediction of NO. The proceedings include laminar flame results using mechanisms from Lindstedt, Li & Williams, Warnatz, and GRI-Mech (2.11, 3.0, and reduced versions of these). More work is needed to fully compare the available data with calculations using all the major mechanisms. However, the comparisons contained in the TNF5 proceedings show that GRI 3.0 significantly over predicts NO levels in lean and near-stoichiometric regions of the laminar flames, while GRI 2.11 under predicts NO levels in fuel-rich conditions. Calculations from Lindstedt and from Li & Williams appear to do a better job than GRI-Mech in predicting the measured shape of the NO profile.
- **Radiation** – Accurate modeling of radiation is important in the context of NO formation. Measured radiant fractions are now available for many of the jet flames in the TNF data library, and these are reported by Frank et al. (28<sup>th</sup> Combustion Symposium). There is some evidence to suggest that the optically thin model recommended for TNF calculations over predicts the radiant fraction in all of the TNF jet flames except for the H<sub>2</sub> flames. The strength of absorption of the 4.3-micron band of CO<sub>2</sub> is the main issue. Further work is needed in this area to quantify the absorption effect and, if necessary, to develop an improved radiation model that is not computationally expensive.
- **Mixing Models and Constants** – The measured degree of local extinction in the piloted flame series is expected to be difficult to reproduce in calculations. Therefore, it is important to emphasize that calculations from the groups at Cornell and Imperial College each show good

results on extinction. The Cornell group used the EMST mixing model, while the Imperial College group used the modified Curl's model. Both groups made adjustment to the mixing model constant in order to achieve agreement with measurements. This suggests that both mixing models are capable of capturing the main features of the local extinction process. However, it also demonstrates the sensitivity of extinction results to the choice of the mixing model and constants. Parametric calculations of flame F by J-Y Chen also show that different mixing models yield significantly different results, when constants are not tuned. The Cornell group has also demonstrated that the degree of extinction is very sensitive to inflow conditions. Specifically, they observed that  $\pm 10\text{K}$  changes in the pilot temperature produced significant differences in burning index for flame F.

- **Unfinished Business** – Comparisons of results for piloted flame D, which were presented first in TNF3 (Boulder, 1998), showed that the steady flamelet model and the CMC model yielded significantly higher levels of CO and H<sub>2</sub> in fuel-rich conditions, as compared to pdf models and the measurements. The reasons for these differences are still not fully understood. Laminar flame comparisons have shown agreement between measured and calculated results for partially premixed flames at relevant strain rates. Thus, the problem appears to be with something other than the chemistry.

#### **Bluff Body Flames:**

- **Flow Field** – In contrast to the situation for piloted flames, predictions of the flow field for the bluff-body flames are not yet in satisfactory agreement with measurements. Computations of the velocity and turbulence fields are adequate in the upstream regions of the jet covering the recirculation zone and the necking zone. However, further downstream and starting at about two bluff-body diameters, calculations show increasing deviation from the measurements. This is true regardless of the numerical approach used and of the modifications made to the model constants. For the results at this workshop the contributions using modified eddy viscosity models did get better results than those using second moment closure approaches without modifications.
- **Chemistry** – The chemistry models used were simple and were based on one of the following assumptions: flamelet, fast chemistry, full or constrained equilibrium. Computations were presented for temperature and the mass fractions of OH and NO in the recirculation zones. It was clearly concluded that detailed chemical kinetics are needed to adequately compute the mass fraction of minor species such as OH and NO even in regions where local extinction is not prevalent such as in the recirculation zone.
- **New Wall Temperature Data** – Measurements of the temperature of the ceramic face of the bluff-body yielded 650 C for flame HM1 and 750 C for flame HM2. These new boundary conditions should be implemented in future calculations.
- **New CO Data** – Data on CO collected using LIF was presented in a poster by Dally et al. showing a vast improvement on the existing Raman CO measurements. These data, which were acquired during the original experiment but only processed recently, will be added to the current bank on bluff-body stabilized flames.

In the closing discussion it was agreed that focus should now shift to compute the compositional structure in the recirculation zone of bluff-body stabilized flames. Measurements show that, the mean radial location of the reaction zone shifts from the inner edge (close to the fuel jet) of the

large vortex to the outer edge (close to the air side) depending on the fuel jet velocity and the fuel mixture. This is an important issue and a good test case for the computations. A list of candidate flames, having the mean reaction zone occurring at different locations in the recirculation region, will be made available as target flames for TNF6.

### **TECFLAM Burner:**

For the TECFLAM burner the main accomplishment was the presentation of a complete, consistent data set. First modeling results are encouraging, but the problem of getting good agreement with experiment is even more open than in the case of the bluff body flames due to the complexity of the flow. The question is which strategy now has to be followed. Is it possible to identify the minimal ingredients both in turbulence modeling and in turbulence-chemistry interaction model to get at least the flow field to agree well. Incorporation of radiation in the model here needs more than an emission only assumption, which adds to the complexity.

### **RESEARCH PRIORITIES:**

- **Piloted Flames** – There is no longer a strong incentive to keep the piloted jet flames as primary target flames for future TNF workshops because they have been extensively studied over the past years, and some good results are being published. Nevertheless, some arguments in favour of keeping them were given. Since the correct prediction of the velocity field is easily possible, the discussion can focus on detailed issues related to chemistry and turbulence-chemistry interaction. Piloted flames will remain useful as a test for NO and radiation modeling. Further comparison of micromixing models to better document the true reasons for success are to be made (e.g. compare EMST model and modified Curl model). It was also suggested that updated measurements in piloted flames of pure methane (or  $\text{CH}_4/\text{N}_2$ ) and new data in ethylene flames would be of interest.
- **More Complicated Flames** – The main challenge for the TNF workshop participants is to extend the success obtained for partially premixed methane/air piloted jet flames to more complicated flames. Good datasets should be selected and made available on the web. Flame types that are in the picture are bluff-body flames, swirl flames, and opposed jet flames. With each of these geometries the accurate documentation of inflow and boundary conditions will be very important. Due to the difficulty in modeling just the flow field in these cases, it may be appropriate to consider bluff-body and swirl flames with little or no local extinction. Modelers should always first try to produce correct flow fields and mean mixture fraction profiles for the new flames. This needs understanding of the turbulence and a certain minimal level of chemistry model. The second step, is to get the profiles of main combustion species (including hydrogen and CO) right. The third and final step focuses on the prediction of minor species as NO. The successful completion of the third step will need a completion of the discussion on radiation modeling started at TNF5
- **LES** – Large eddy simulation should also be done, because of its intrinsic value and because of the light it may shed on some of the modeling issues in PDF, CMC or flamelet models. Setting up LES may require a preliminary study on inlet boundary conditions.
- **Chemical Mechanisms** – The GRI mechanisms and various reduced versions are widely available. However, other mechanisms have shown better agreement with measurements of

NO in partially premixed CH<sub>4</sub>/air flames. Therefore, it would be beneficial if detailed and reduced versions of mechanisms from Lindstedt, Li & Williams, and perhaps Miller could be made available on the web in broadly compatible format with corresponding thermodynamic data.

- **Laminar Flame Comparisons** – More work is needed to complete and fully document the cross comparison of various measurements and calculations of NO and other scalars in laminar flames. It was suggested that additional data at lower strain rates and lower fuel-side equivalence ratios would be useful. Detailed laminar flame data from ethylene flames was also requested.
- **Scalar Dissipation** – Available models of scalar dissipation in jet flames are not in agreement with each other. It appears that further work is needed in the area of experimental validation of scalar dissipation models.
- **Other Fuels** – In general, changing the fuel leads to mean reaction zones at different locations relative to shear layers and recirculation zones (because of other stoichiometry) and therefore changes in regime of turbulence-chemistry interaction. Therefore, it can be interesting to plan experiments with other fuels, in either piloted or a bluff-body geometry providing new challenges. In the case of piloted flames, it can be interesting to turn to the more difficult case of pure methane. Also ethylene was suggested as an interesting fuel because it is a key component in many combustion processes. Two candidate fuels for bluff body flames are CH<sub>4</sub> (for which some results are already available) and H<sub>2</sub>/CO. The turbulent diffusion flame lab in Sandia is available for experiments, but there is a need for someone to do the measurements: e.g. visiting students from groups worldwide

### **ORGANIZATION OF TNF6:**

The Sixth TNF Workshop will be held in Japan in 2002 just before the 29<sup>th</sup> Combustion Symposium. Details regarding target problems, location, and dates will be announced.

Arguments were put forward to enlarge the scope of the TNF workshop to include also spray flames and even premixed flames. The preliminary conclusion on this was that such excursions are possible provided a sufficient number of both experimentalists and modelers are actively involved. It is the strength of the group of contributors to TNF workshops that there is a strong interaction between modellers and experimentalists and this should be maintained.

### **ACKNOWLEDGMENTS**

Sponsorship by Shell and the J. M. Burgerscentrum are gratefully acknowledged. Sandia contributions to the TNF Workshops are supported by the DOE Office of Basic Energy Sciences.

### **RECOMMENDED RESTRICTIONS ON USE OF THE TNF PROCEEDINGS:**

Results in this and other TNF Workshop proceedings are contributed in the spirit of open collaboration. Some results represent completed work that has been or will be published in the archival literature. Others results represent work in progress, which may or may not be published as it appears here. Readers should keep this in mind when reviewing these materials. It may be inappropriate to quote or reference specific results from these proceedings without first checking with the individual authors for permission and for their latest information on results and references. It should also be noted that several papers relevant to the target flames were presented at the 28<sup>th</sup> Combustion Symposium in the Colloquium on Non-Premixed Turbulent Combustion, and these papers contain more detailed descriptions and comparisons than are included here.

# Fifth International Workshop on Measurement and Computation of Turbulent Nonpremixed flames

Dish Hotel, Delft, The Netherlands, July 26—28, 2000

## Preface

The series of workshops on Measurement and Computation of Turbulent Nonpremixed Flames (TNF-workshops) is intended to facilitate collaboration and information exchange among experimental and computational researchers in the field of turbulent nonpremixed combustion. The emphasis is on fundamental issues of turbulence-chemistry interactions as revealed by comparisons of measured and computed results for selected flames. The first four workshops were held in Naples(1996), Heppenheim(1997), Boulder(1998), and Darmstadt(1999). More information on the previous workshops and links to related web sites can be found at the main website which is at <http://www.ca.sandia.gov/tdf/Workshop.html>. The website for the present workshop is at <http://www.ws.tn.tudelft.nl/tnf5>

For TNF5 the following three target problems have been put on the agenda:

1. Piloted CH<sub>4</sub>/air flames with emphasis on resolution of differences in fuel-rich results and on detailed consideration of NO formation.
2. Bluff-body CH<sub>4</sub>/H<sub>2</sub> flame with emphasis on prediction of NO in the recirculation zone.
3. The TECFLAM burner for confined swirling natural gas flames

For each of the target problems in these proceedings the respective coordinators report on the progress made in the last year, on the contributions received and the issues to be addressed in discussions at the workshop.

Parametric studies that isolate the sensitivity of results to changes in a single submodel or parameter were encouraged. Areas of special interest include: Influence of mixing models of rich-side chemistry; Influence of scalar dissipation models; More accurate modeling of radiation; Comparison of different chemical mechanisms; Treatment of wall interactions; Sensitivity of results to boundary conditions.

In addition, there is ongoing experimental and modeling work on other current and prospective target flames, as well as ongoing work on submodel development. A lot of that work is presented at the workshop in the form of posters, the abstracts of which are included in these proceedings.

Aristide Mbiocq, Dirk Roekaerts and Robert Barlow

## Acknowledgements:

The TNF5 workshop is hosted by Delft University of Technology, Thermal and Fluids Sciences Section. Special thanks to Maggy Doolhof and Joan Teerling.

The workshop is sponsored by:

- J.M. Burgers Centre (<http://ic-server.stm.tudelft.nl/~burgers/>)
- Shell International BV (<http://www.shell.nl/nl-nl/>) (<http://www.shell.com/royal-en/>)

**Organising Committee:** R. Barlow, R. Bilger, J.-Y. Chen, E. Hassel, J. Janicka, A. Masri, N. Peters, H. Pitsch, S. Pope, D. Roekaerts.

**Local Host Committee:** Tieying Ding, Maggy Doolhoff, Mike Golombok, Werner Huebner, Denis Krasinsky, Aristide Mbiocq, Bertrand Naud, Dirk Roekaerts, Joan Teerling.

## Fifth International Workshop on Measurement and Computation of Turbulent Nonpremixed Flames

Delft, Holland  
July 26 – 28, 2000

### Final Program

#### Wednesday Afternoon Session

16.00 – 17.00	Registration ( <i>Business Corner I</i> ) and installation of posters ( <i>Meeting Room I</i> )
17.00 – 18.00	Poster hour with refreshments ( <i>Meeting Room I</i> )
18.00 – 18.30	Introductory remarks (G. Ooms, D. Roekaerts, R. Barlow) ( <i>Meeting Room II</i> )
18.30 – 20.00	Buffet dinner ( <i>Restaurant 2<sup>nd</sup> floor</i> )
20.00 – 21.30	Poster session with informal discussions ( <i>Meeting Room I</i> )

#### Thursday Session

from 07.00 – 08.30	Buffet breakfast ( <i>Restaurant 2<sup>nd</sup> floor</i> )
08.00 – 08.30	Postertime after breakfast ( <i>Meeting Room I</i> )
08.30 – 10.15	<b>Session 1</b> ( <i>Meeting Room II</i> ) <ul style="list-style-type: none"><li>• Piloted flame review and update</li><li>• Chemical kinetics and laminar flame comparisons</li><li>• Panel: Barlow, Bilger, Chen, Lindstedt, Pope, Roekaerts, Williams</li></ul>
10.15 – 10.45	Coffee Break
10.45 – 12.30	<b>Session 2</b> ( <i>Meeting Room II</i> ) <ul style="list-style-type: none"><li>• Radiation</li><li>• Mixing models, statistical errors in pdf calculations, extinction/re-ignition</li><li>• Scalar dissipation measurements and models</li><li>• Panel: Barlow, Bilger, Chen, Gore, Lindstedt, Pope, Roekaerts, Weber</li></ul>
12.30 – 17.00	Lunch followed by Delft Historical City Tour and Lab-tour
17.00 – 18.00	Poster hour ( <i>Meeting Room I</i> )
18.00 – 19.30	Buffet dinner ( <i>Restaurant 2<sup>nd</sup> floor</i> )
19.30 – 21.00	<b>Session 3</b> ( <i>Meeting Room II</i> ) <ul style="list-style-type: none"><li>• Turbulence models, effects of inlet profiles</li><li>• General discussion on simple- and piloted jet flame and fundamentals</li><li>• Summary issues and conclusions from Sessions 1 and 2</li><li>• Panel: Barlow, Bilger, Chen, Janicka, Jones, Lindstedt, Pope, Roekaerts</li></ul>
21.00	Close

## Friday Session

from 07.00 – 08.30	Buffet breakfast ( <i>Restaurant 2<sup>nd</sup> floor</i> )
08.00 – 08.30	Postertime after breakfast ( <i>Meeting Room I</i> )
08.30 – 10.15	<b>Session 4: Masri</b> ( <i>Meeting Room II</i> ) <ul style="list-style-type: none"><li>• Bluff body flames</li><li>• Wall interactions</li></ul>
10.15 – 10.45	Coffee Break
10.45 – 12.30	<b>Session 5: Dreisler, Janicka</b> ( <i>Meeting Room II</i> ) <ul style="list-style-type: none"><li>• Tecflam</li><li>• Other target flames, progress on measurements and models</li></ul>
12.30 – 13.30	Lunch ( <i>Restaurant 2<sup>nd</sup> floor</i> )
13.30 – 15.00	<b>Session 6: Roekaerts</b> ( <i>Meeting Room II</i> ) <ul style="list-style-type: none"><li>• Summary of accomplishments and conclusions</li><li>• Research priorities, open questions, who will do what</li><li>• TNF6 planning</li></ul>
15.00 -	Close and refreshments
15.30 -	Meeting of the organising committee and selected contributors (if needed). Write outline or rough draft summarizing main points of discussions.

Optional: - Additional Labtour -

%%

### ***Location of rooms in the Dishotel:***

Restaurant for your meals:	2 <sup>nd</sup> floor
Business Corner I:	1 <sup>st</sup> floor
Meeting Room I:	1 <sup>st</sup> floor
Meeting Room II:	2 <sup>nd</sup> floor
Business Corner II:	2 <sup>nd</sup> floor (between Restaurant and Meeting Room II)

During the workshop, you can find the TNF-administration-office in Business Corner II.  
The bar of the hotel will be open daily until 23.00 hours.

## TNF5 WORKSHOP PARTICIPANTS

1	Name	Company/university	Town	Country
2	Bajaj, Dipl.Ing. Pankaj <a href="mailto:Bajaj@ltnt.iet.mavt.ethz.ch">Bajaj@ltnt.iet.mavt.ethz.ch</a>	Swiss Federal Inst. of Technology (ETHZ)	Zürich	Switzerland
3	Barlow, Robert <a href="mailto:Barlow@ca.sandia.gov">Barlow@ca.sandia.gov</a>	Sandia National Laboratories	Livermore, CA	USA
4	Bilger, Robert <a href="mailto:Bilger@mech.eng.usyd.edu.au">Bilger@mech.eng.usyd.edu.au</a>	University of Sydney	Sydney	Australia
5	Cabra, Ricardo <a href="mailto:Ricardo@newton.berkeley.edu">Ricardo@newton.berkeley.edu</a>	University of California	Berkeley CA	USA
7	Dally, Dr. Bassam <a href="mailto:Bassam.dally@adelaide.edu.au">Bassam.dally@adelaide.edu.au</a>	University of Adelaide	Adelaide	Australia
8	Demiraydin, Dr. Lâle <a href="mailto:Demiraydin@ltnt.iet.mavt.ethz.ch">Demiraydin@ltnt.iet.mavt.ethz.ch</a>	ETH-Zurich	Zürich	Switzerland
9	Dibble, Prof. Robert <a href="mailto:Rdibble@firebug.me.berkeley.edu">Rdibble@firebug.me.berkeley.edu</a>	University of California	Berkeley CA	USA
10	Donbar, Jeff <a href="mailto:Donbarjm@possum.appl.wpafb.af.mil">Donbarjm@possum.appl.wpafb.af.mil</a>	Air Force Research lab. WPAFB, OH	Wright-Patterson AFB, OH	USA
11	Dreizler, Dr. Andreas <a href="mailto:Dreizler@hrz2.hrz.tu-darmstadt.de">Dreizler@hrz2.hrz.tu-darmstadt.de</a>	TU Darmstadt Inst. of Energy and Powerplant Technology	Darmstadt	Germany
12	Düsing Dipl.-Ing. Michael <a href="mailto:Duesi@hrzpub.tu-darmstadt.de">Duesi@hrzpub.tu-darmstadt.de</a>	TU Darmstadt, Institute of Energy and Powerplant Techn.	Darmstadt	Germany
13	Gass, Dr. Jürg <a href="mailto:Gass@ltnt.iet.mavt.ethz.ch">Gass@ltnt.iet.mavt.ethz.ch</a>	Inst. of Energy Technology ETHZ	Zürich	Switzerland
14	Gerlinger, dr. Peter <a href="mailto:Peter.Gerlinger@dlr.de">Peter.Gerlinger@dlr.de</a>	DLR Stuttgart	Stuttgart	Germany
15	Geyer, Dirk <a href="mailto:Geyer@hrz2.hrz.tu-darmstadt.de">Geyer@hrz2.hrz.tu-darmstadt.de</a>	TU Darmstadt Inst. of Energy and Powerplant Technology	Darmstadt	Germany
16	Girard, James <a href="mailto:Girardj@newton.me.berkeley.edu">Girardj@newton.me.berkeley.edu</a>	University of California	Berkeley CA	USA
17	Gore, Prof. Jay P.	Purdue University	West Lafayette Indiana	USA

	<a href="mailto:Gore@ecn.purdue.edu">Gore@ecn.purdue.edu</a>			
18	Hassel, Egon <a href="mailto:Egon.hassel@mbst.uni-rostock.de">Egon.hassel@mbst.uni-rostock.de</a>	Universitaet Rostock	Rostock	Germany
19	Heikkinen, Johanna <a href="mailto:Johanna.heikkinen@tut.fi">Johanna.heikkinen@tut.fi</a>	Tampere University of Technology	Tampere	Finland
21	Hewson, John <a href="mailto:Jchewso@sandia.gov">Jchewso@sandia.gov</a>	Sandia National Laboratory	Livermore CA	USA
22	Hoffmann, Axel <a href="mailto:Axel.Hoffmann@urz.uni-heidelberg.de">Axel.Hoffmann@urz.uni-heidelberg.de</a>	Ruprecht-Karls-Universitaet Heidelberg	Heidelberg	Germany
23	Homma, Ryoji <a href="mailto:Homma@tokyo-gas.co.jp">Homma@tokyo-gas.co.jp</a>	Tokyo Gas Co., Ltd	Tokyo	Japan
24	Huh, Prof. Kang Yul <a href="mailto:Huh@postech.ac.kr">Huh@postech.ac.kr</a>	Pohang University of Science and Technology	Pohang	Korea
25	Ikeda, Yuji <a href="mailto:Ikeda@mech.kobe-u.ac.jp">Ikeda@mech.kobe-u.ac.jp</a>	Kobe University, Department of mechanical engineering	Kobe	Japan
26	Janicka, Prof.dr.-Ing. Johannes <a href="mailto:Janicka@hrzl.hrztu-darmstadt.de">Janicka@hrzl.hrztu-darmstadt.de</a>	TU Darmstadt, Institute of Energy and Powerplant Techn.	Darmstadt	Germany
27	Jones, Prof. W.P. <a href="mailto:w.jones@ic.ac.uk">w.jones@ic.ac.uk</a>	Imperial College London	London	UK
28	Keck, Dipl.Phys. Olaf <a href="mailto:Olaf.keck@dlr.de">Olaf.keck@dlr.de</a>	DLR Stuttgart	Stuttgart	Germany
29	Kempf, Dipl.-Ing. Andreas <a href="mailto:Skrmppg@gmx.net">Skrmppg@gmx.net</a>	TU Darmstadt, Institute of Energy and Powerplant Techn.	Darmstadt	Germany
30	Kojima, Jun <a href="mailto:Kojima@ms-5.mech.kobe-u.ac.jp">Kojima@ms-5.mech.kobe-u.ac.jp</a>	Kobe University	Kobe	Japan
31	Kim, Yongmo <a href="mailto:Ymkim@email.hanyang.ac.kr">Ymkim@email.hanyang.ac.kr</a>	Hanyang University		Korea
32	Kim, Seong-Ku With Yongmo Kim	Hanyang University		Korea
33	Kunz, Oliver <a href="mailto:Oliver.kunz@dlr.de">Oliver.kunz@dlr.de</a>	German Aerospace Center DLR Institute of Combusion Technology	Stuttgart	Germany

34	Kunzelmann Thomas <a href="mailto:Tkunzelm@ix.urz.uni-heidelberg.de">Tkunzelm@ix.urz.uni-heidelberg.de</a>	Universitaet Heidelberg	Heidelberg	Germany
35	Lindstedt, Prof. Peter <a href="mailto:p.lindstedt@ic.ac.uk">p.lindstedt@ic.ac.uk</a>	Imperial College	London	UK
36	Liu, Kai <a href="mailto:K147@cornell.edu">K147@cornell.edu</a>	Cornell University	Ithaca NY	USA
37	Long, Prof. Marshall <a href="mailto:Marshall.long@yale.edu">Marshall.long@yale.edu</a>	Yale University	New Haven CT	USA
38	Maas, Prof. Ulrich (Replaced by Boris Steiner) <a href="mailto:Maas@itv.uni-stuttgart.de">Maas@itv.uni-stuttgart.de</a>	Stuttgart University	Stuttgart	Germany
39	Mahmud, dr. Tariq <a href="mailto:T.Mahmud@leeds.ac.uk">T.Mahmud@leeds.ac.uk</a>	University of Leeds	Leeds	UK
40	Malalasekera, dr. W. <a href="mailto:w.malalasekera@lboro.ac.uk">w.malalasekera@lboro.ac.uk</a>	Loughborough University	Loughborough	UK
41	Martinelli Paolo <a href="mailto:Paolo.martinelli@pirelli.com">Paolo.martinelli@pirelli.com</a>	Pirelli Cavi e Sistemi S.p.A.	Milano	Italy
42	Masri, Prof. Assaad <a href="mailto:Masri@mech.eng.usyd.edu.au">Masri@mech.eng.usyd.edu.au</a>	The University of Sydney	Sydney	Australia
43	Massimo, Nutini <a href="mailto:Massimo.nutini@pirelli.com">Massimo.nutini@pirelli.com</a>	Pirelli Milano	Milano	Italy
45	Meier, Dr. Wolfgang <a href="mailto:Wolfgang.meier@dir.de">Wolfgang.meier@dir.de</a>	DLR Institute of Combustion Tech.		Germany
46	Merci, Ir. Bart <a href="mailto:Bart.Merci@rug.ac.be">Bart.Merci@rug.ac.be</a>	Ghent University	Ghent	Belgium
47	Mueller, Dr.-ing. Christian <a href="mailto:Christian.mueller@abo.fi">Christian.mueller@abo.fi</a>	Åbo Akademi University, Process Chemistry Group	Turku	Finland
48	Muradoglu, Metin <a href="mailto:Metinm@mae.cornell.edu">Metinm@mae.cornell.edu</a>	Cornell University	Ithaca NY	USA
49	Pitts, dr. William M. <a href="mailto:Wpitts@nist.gov">Wpitts@nist.gov</a>	National Institute of Standards and Technology	Gaithersburg, MD	USA
50	Pope, Prof. Stephen B. <a href="mailto:Pope@mae.cornell.edu">Pope@mae.cornell.edu</a>	Cornell University	Ithaca NY	USA
51	Renfro, Michael <a href="mailto:Renfro@ecn.purdue.edu">Renfro@ecn.purdue.edu</a>	Purdue University	West Lafayette Indiana	USA

52	Repp, Stephan <a href="mailto:Srepp@hrzpub.tu-darmstadt.de">Srepp@hrzpub.tu-darmstadt.de</a>	Darmstadt University of Technology, Institute of Energy & Power Plant Technology	Darmstadt	Germany
53	Riesmeier, Elmar <a href="mailto:Riesmeier@itm.rwth-aachen.de">Riesmeier@itm.rwth-aachen.de</a>	Institut fuer Technische Mechanik, RWTH Aachen	Aachen	Germany
54	Roekaerts, Prof. dr. D. <a href="mailto:Dirkr@ws.tn.tudelft.nl">Dirkr@ws.tn.tudelft.nl</a>	Delft University of Technology	Delft	NL
55	Sadiki, Dr. Amsini <a href="mailto:Sadiki@hrz2.hrz.tu-darmstadt.de">Sadiki@hrz2.hrz.tu-darmstadt.de</a>	TU-Darmstadt, TU Darmstadt, Institute of Energy and Powerplant Techn.	Darmstadt	Germany
57	Schmidt, Dietmar <a href="mailto:Schmidt@itv.uni-stuttgart.de">Schmidt@itv.uni-stuttgart.de</a>	Stuttgart University	Stuttgart	Germany
58	Schneider, Christoph <a href="mailto:Cschneid@hrz2.hrz.tu-darmstadt.de">Cschneid@hrz2.hrz.tu-darmstadt.de</a>	TU Darmstadt Inst. of Energy and Powerplant Technology	Darmstadt	Germany
59	Solero, Giulio <a href="mailto:Giulio.solero@polimi.it">Giulio.solero@polimi.it</a>	Politecnico di Milano	Milano	Italy
60	Sou, Dr. Akira <a href="mailto:Sou@mech.kobe-u.ac.jp">Sou@mech.kobe-u.ac.jp</a>	Kobe University Department of mechanical Engineering	Kobe	Japan
61	Tang, Qing <a href="mailto:Qtang@mae.cornell.edu">Qtang@mae.cornell.edu</a>	Cornell University	Ithaca NY	USA
62	Walter, Dipl.-Ing. <a href="mailto:Uta.walter@mbst.uni-rostock.de">Uta.walter@mbst.uni-rostock.de</a>	Universität Rostock	Rostock	Germany
63	Wel, Marco C. van der <a href="mailto:m.c.vanderwel@wbmt.tudelft.nl">m.c.vanderwel@wbmt.tudelft.nl</a>	TU Delft Mechanical Engineering and marine Technology, Section thermal Power Engineering	Delft	
64	Williams, Prof. F.A. <a href="mailto:Faw@mae.ucsd.edu">Faw@mae.ucsd.edu</a>	University of CA San Diego	La Jolla CA	USA
65	Weber, dr. Roman <a href="mailto:Roman.weber@ifrf.net">Roman.weber@ifrf.net</a>	IFRF Research Station	IJmuiden	NL
66	Ooms, Prof. dr.ir. Gijs <a href="mailto:g.ooms@siep.shell.com">g.ooms@siep.shell.com</a>	J.M. Burgerscentrum	Delft	NL

67	Ding, Ir. T. <a href="mailto:Tieying@ws.tn.tudelft.nl">Tieying@ws.tn.tudelft.nl</a>	TU Delft – TN WS		NL
68	Golombok, Dr. Michael <a href="mailto:Mike.m.golombok@opc.shell.com">Mike.m.golombok@opc.shell.com</a>	TU Delft – TN WS		NL
69	Hübner, Dipl.Ing. Werner <a href="mailto:Werner@ws.tn.tudelft.nl">Werner@ws.tn.tudelft.nl</a>	TU Delft – TN WS		NL
70	Krasinsky, Dr. Denis <a href="mailto:Dkr@ws.tn.tudelft.nl">Dkr@ws.tn.tudelft.nl</a>	TU Delft – TN WS		NL
71	Mbiock, Dr. Aristide <a href="mailto:Aristide@ws.tn.tudelft.nl">Aristide@ws.tn.tudelft.nl</a>	TU Delft – TN WS		NL
72	Naud, Ir. Bertrand <a href="mailto:Bertrand@ws.tn.tudelft.nl">Bertrand@ws.tn.tudelft.nl</a>	TU Delft – TN WS		NL
73	Teerling, Joan <a href="mailto:Joan@ws.tn.tudelft.nl">Joan@ws.tn.tudelft.nl</a>	TU Delft - TN WS		NL
74	Tummers, Dr. Mark <a href="mailto:Mark@ws.tn.tudelft.nl">Mark@ws.tn.tudelft.nl</a>	TU Delft – TN WS		NL

# SECTION 1

## Piloted Flames and Related Issues

**Fifth International Workshop on Measurement and Computation  
of Turbulent Nonpremixed Flames**  
Delft, The Netherlands  
26-28 July 2000

**Update on Piloted CH<sub>4</sub>/Air Jet Flames**

Robert S. Barlow, Sandia National Laboratories

**Introduction:**

The piloted CH<sub>4</sub>/air jet flames have served as target cases for TNF3, TNF4, and TNF5. A total of more than twenty calculations have been submitted for flame D, and a smaller but still significant number of calculations have been completed on other flames in the series. Two of the more significant and thorough studies, those by Tang et al. and Lindstedt et al., will be presented at the 28<sup>th</sup> Combustion Symposium and reflect the state of the art in pdf calculations. A third significant study, by Pitch and Steiner (Phys. Fluids, submitted), used the D flame as a target for LES calculations, which employed an unsteady flamelet model. These papers include detailed comparisons with experimental data, and each study can be described as very successful, although none gets everything right.

At past workshops we have presented detailed comparisons of measured and calculated results for these flame. However, because of the large number of calculations and the need to avoid duplication of Symposium presentations, this TNF5 Workshop does not include the same sort of detailed comparisons of piloted flame calculations. An overview of newly contributed calculations is included here, along with some highlights and limited comparisons. However, the main story on some calculations must be reserved for the Symposium. Instead, the program for the first three sessions of this workshop focuses on specific issues and problem areas that were identified in the TNF4 Summary as high priorities for research related to the piloted flame problem. These include:

- Validation of chemical mechanisms for partially-premixed methane-air combustion
- Resolution of questions regarding the accuracy of measured radiant fractions and the validity of the optically-thin radiation model for the workshop target flames
- Further work to understand the influence of mixing models on rich-side predictions
- Further work to more fully specify boundary conditions and determine the sensitivity of results to changes in the inflow conditions
- Testing of the influence of the number of particles in pdf calculations and issues involving the statistical accuracy of pdf calculations

Some new results are available on these topics and will be presented by various contributors. This section provides an update on contributed calculations of the piloted flames, as well as some fuel for discussion on radiation. Contributions from several groups regarding comparisons of measured and calculated scalar profiles in laminar partially-premixed flames are provided in sections that follow.

## Overview of Newly Contributed Calculations of the Sandia Piloted Jet Flames

Six groups contributed new results on one or more of the piloted flames, with “new” meaning that the results were not included in previous workshop comparisons.

- Chen (Berkeley)  
Joint scalar pdf calculations of flames D and F, using the modified Curl’s mixing model and a 13-step reduced chemistry derived from GRI 3.0
- Demiraydm and Gass (ETH Zurich) Presented on a TNF5 poster  
Pdf calculation of flame E, using 4-step chemistry
- Merci, Roekaerts, Peeters, and Dick (Ghent/Delft) Presented on a TNF5 poster  
Assumed pdf calculations of flame D, using constrained equilibrium
- Pitsch and Steiner (Stanford) Submitted to Phys. Fluids  
LES calculation of flame D, using a Lagrangian flamelet model and a reduced version of GRI 2.11
- Robert and Fuchs (Lund) Presented on a TNF5 poster  
Calculation of flame D using 2-step chemistry
- Tang, Xu, and Pope (Cornell) 28<sup>th</sup> Combustion Symposium paper  
Velocity-scalar pdf calculations of flames D, E, and F, using the EMST mixing model and a reduced mechanism derived from GRI 2.11

One-page summaries of these calculations are included here. Summaries of previously contributed calculations that are used in the present comparison plots may be found in the TNF4 Proceedings, which are available on the web.

## **PDF Calculations of Piloted Flames D and F**

J.-Y. Chen  
Department of Mechanical Engineering  
University of California, Berkeley

**Flow Model:** Reynolds stress model parabolic code

**Turbulence-Chemistry Interaction Model:** Joint Scalar PDF

**Chemistry Model:** Reduced Chemistry 13-step with NO<sub>x</sub> developed from GRI30

**Grid Size:** 70 cells across half of the jet: 400 Particles/cell

**Radiation Model:** included with H<sub>2</sub>O, CO, CO<sub>2</sub>, CH<sub>4</sub> recommended by workshop web information (prior to June updated on CO<sub>2</sub>)

**Mixing Model:** Modified Curl's Mixing Model with standard constant

**Special near field treatment:** For flame F used flamelet model without NO ( $a=100/s$ )  
from  $x/D=0$  to  $x/d=7.5$

# Numerical Simulation of a Piloted Methane/Air flame (Flame E) using PDF Transport Equations Model

L. Demiraydin , J. Gass

Institute of Energy Technology, ETH Zurich  
Laboratory of Thermodynamics in Emerging Technologies  
LOW C1, ETH-ZENTRUM, CH-8092 Zurich Switzerland  
e-mail : [demiraydin@lnt.iet.mavt.ethz.ch](mailto:demiraydin@lnt.iet.mavt.ethz.ch)

**Turbulence Model:** Flow field calculations are done with k- $\epsilon$  turbulence model by using a sophisticated Finite volume commercial code. Turbulent viscosity is calculated via

$$\nu_t = C_\mu / \sigma_f \cdot \tilde{k}^2 / \tilde{\epsilon}$$

**Coupling model:** With the assumption of steady state hydrodynamics, the coupling of flow field solution is done with an Eulerian composition Finite Difference PDF/Monte Carlo method via constant density. [1] An ensemble of  $\{Z_{\text{mix}}, n_{\text{CH}_4}, n_{\text{CO}}, n_{\text{tot}}, n_{\text{H}}\}$  is chosen for the description of system.

**Solution Domain:** Assuming axis-symmetry: grid consists of 120x90 nodes which has a grid-refinement in the nozzle-exit.

**Boundary Conditions:** Boundary conditions are supplied from the documentation and linearly interpolated to the grid points.

**Chemistry model and kinetic mechanism:** Reduced 4-step mechanism with 8 species ( $\text{CH}_4, \text{O}_2, \text{CO}_2, \text{H}_2\text{O}, \text{CO}, \text{H}_2, \text{H}, \text{N}_2$ ) from Rogg and Peters/Kee. [2,3]

**Turbulent Transport modeling :** Gradient Diffusion Assumption

**Mixing model:** LMSE Model with 100 particles /cell

**Location of start of computation:** Computation starts at  $x/d=0$ .

**Convergence Criteria:** After a converged steady solution is reached for flow field calculations, PDF calculations are achieved with  $10^{-4}$  s. for each step.

**Computer Facility:** The computations required about 120 h total computational time on a Silicon Graphics Octane™ 2 300 MHz IP30 processors.

**Comments:** Along the centerline, after  $x/d=50$ , some problems arised concerning the axial profiles of mixture fraction and species.  $\text{CH}_4$  concentrations showed a sudden increase and this caused high temperatures, high product concentrations and low  $\text{O}_2$  concentrations compared to experiments .

## **References:**

- [1] A. Laxander, Numerische Simulation von turbulenten Diffusionsflammen mit einem PDF-Transportgleichungsmodell, Ph. D. Thesis Universität Stuttgart, 1996
- [2] B. Rogg, Sensitivity Analysis of Laminar Premixed  $\text{CH}_4$  – Air Flames using full and reduced Kinetic Mechanisms and Asymptotic Approximations for Methane – Air Flames, Volume 384 of Lecture Notes in Physics, page 159-192, Springer Verlag, 1991
- [3] N. Peters and R.J. Kee, The Computation of stretched laminar methane- air diffusion flames using a reduced four-step mechanism, Combustion and Flame, 68:17-29,1987

# Large-Eddy Simulation of a Turbulent Piloted Methane/Air Diffusion Flame (Sandia Flame D)

H. Pitsch and H. Steiner

Center for Turbulence Research

Department of Mechanical Engineering

Stanford University

## Modeling Procedure

Spatially filtered equations for continuity, momentum, and the mixture fraction are solved in the low Mach number limit. All sub-grid quantities are determined using the dynamic model.

## Numerical Method

The equations are solved using a second order Adams-Bashford-Molton projection method on a staggered grid. Second derivatives are evaluated using central differences. A robust globally second order scheme is used for the convection terms.

## Chemistry Model

The Lagrangian Type Flamelet model has been used in the simulations. Unsteady flamelets are introduced at the inflow boundary. These flamelets then move downstream, essentially by convective transport. Filtered quantities are then obtained by the solution of the unsteady flamelet equations with the GRI 2.11 mechanism and a presumed  $\beta$ -function sub-grid pdf of the mixture fraction.

## Solution Domain

The solution is obtained for 78 diameters in the downstream direction. A spherical coordinate system is used with the axis normal direction varying from approximately 7 diameter in the nozzle plane to 36 diameter at the maximum nozzle distance. The computational mesh consists of 192, 110, and 48 cells in the radial (downstream), tangential, and azimuthal directions, respectively.

## Boundary and Inlet Conditions

Inlet conditions for velocity and mixture fraction have been prescribed according to the experimental data. A convective boundary condition is used at the outflow and a traction-free boundary condition at the lateral boundary.

## Computational Time

Statistically converged results are obtained after approximately two flow through times. The computational time on an SGI 2000 for this period is approximately 800 CPU h.

## References

1. Pitsch, H., Steiner, H., Large-Eddy Simulation of a Turbulent Piloted Methane/Air Diffusion Flame (Sandia Flame D), accepted for publication in *Physics of Fluids*, 2000.
2. Pitsch, H., Steiner, H., Scalar Mixing and Dissipation Rate in Large-Eddy Simulations of Non-Premixed Turbulent Combustion, accepted for presentation at the Twenty-Eighth Symposium (International) on Combustion, 2000.
3. <http://www.stanford.edu/hpitsch/>

# Numerical Simulation of the Piloted Flame Type D

*Szasz Robert, Laszlo Fuchs*  
*Lund Institute of Technology, Dept. of Heat and Power Engineering*  
*Ole Römersväg 1, 22100, Lund, Sweden*  
*szrobi@mail.vok.lth.se*

Overview about models, boundary and initial conditions, and comments on the simulation.

## **Turbulence model:**

Reynolds Stress Model [1].

## **Chemistry Model and Kinetic Mechanism:**

2 step reaction mechanism.

## **Mixing Model:**

Generalized gradient diffusion model of Lien et al. [2].

## **Coupling Model:**

SIMPLE method for pressure-velocity coupling.

## **Solution Domain:**

Axis-symmetric domain, axial length 900 mm, radial length 1500 mm.

## **Boundary Conditions:**

The boundary conditions are assigned according to documentation on the web. [3].

## **Location of start of computation:**

Computation starts at  $x=0$  mm.

## **Convergence Criteria or Length of Calculation:**

The residuals should decrease with 3 orders of magnitudes, except for the energy equation, in which they should decrease 6 orders.

## **Machine used and Approx. CPU Time:**

IRIX 10000, 16 processors, 175 Mhz. Only one processor was used, the approximate CPU time is 46 hours.

## **Comments:**

The above mentioned CPU time includes the cold-flow run, the solution of the problem with standard  $k-\epsilon$  model, the results being used as initial guess for the RSM calculations.

## References:

1. B.E.Launder, G.J.Reece, and W.Rodi. Progress in Development of a Reynolds-Stress Turbulent Closure. J. Fluid Mech., 68(3):537-566, April 1975.
2. F.S.Lien and M.A.Leschziner. Assessment of Turbulent Transport Models Including Non-Linear RNG Eddy-Viscosity Formulation and Second-Moment Closure. Computers and Fluids, 23(8):983-1004, 1994.
3. [www.ca.sandia.gov/tdf/workshop.html](http://www.ca.sandia.gov/tdf/workshop.html)

## **PDF/ISAT Calculations of Piloted-jet Non-premixed Turbulent Flames**

Qing Tang, Jun Xu and Stephen B. Pope  
Cornell University

- Models:
  - Joint velocity-composition-frequency PDF model;
    - velocity: simplified Langevin model;
    - mixing: EMST model (Subramaniam and Pope, 1998) without differential diffusion effects;
    - frequency: stochastic model (Xu and Pope, 1999);
  - ISAT (Pope, 1997): error tolerance  $5e-5$ ;
  - Chemistry mechanism: augmented reduced mechanism with NO developed from GRI2.11;
  - Radiation: Optical thin limit model with absorption coefficients of H<sub>2</sub>O, CO<sub>2</sub>, CH<sub>4</sub> and CO calculated by RADCAL (Grosshandler, 1993);
  - No artificial ignition is needed.
- Numerics:
  - Grids: 61x61;
  - Domain: 120x25 R<sub>jet</sub>;
  - Particles: 100/cell;
  - Starting location of computation:  $x/D=0.0$ ;
  - Machine: IBM SP2 (5 processors);
  - CPU time: ~100 hours;
  - B.C.'s: same as TNF web for both flames

## Comparisons of Measured and Modeled Results

In the following comparisons, only those calculations that include NO are considered. Readers are reminded that extensive comparisons of measured and modeled results for flames D, E, and F are included in the TNF4 Proceedings (66 pages of plots, in addition to summary comments and model descriptions). Most of the observations that were documented in the TNF4 Proceedings are also valid for the new contributions. Therefore, the limited comparisons here will serve to review some of the main observations and point to a few issues that may motivate further discussion and research. A selection of new and previously submitted results is used.

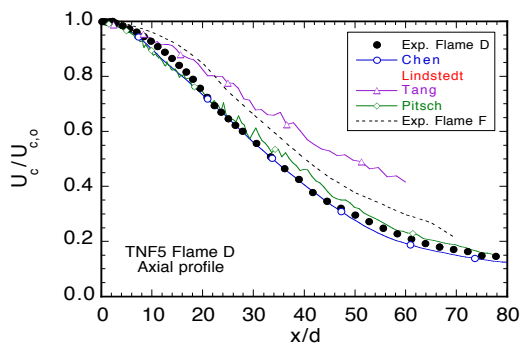
Comparison plots include:

- Axial profiles of  $U/U_0$ ,  $u''$ ,  $f$ , and  $f''$  in flames D and F
- Measured axial profiles of  $f$  and  $T$  in flames C, D, E, and F
- Conditional means of  $T$ ,  $CO$ ,  $H_2$ , and  $NO$  at  $x/d=30$  in flame D
- Scatter plots of  $T$ ,  $CO$ ,  $H_2$ , and  $NO$  at  $x/d=15$  and  $x/d=30$  in flames F

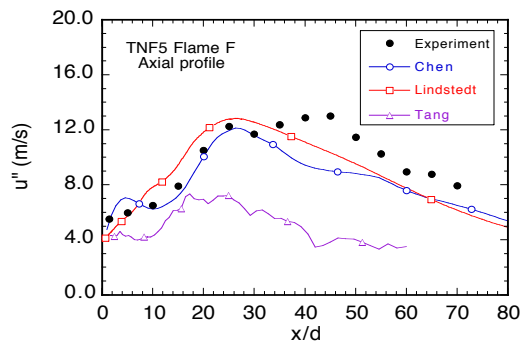
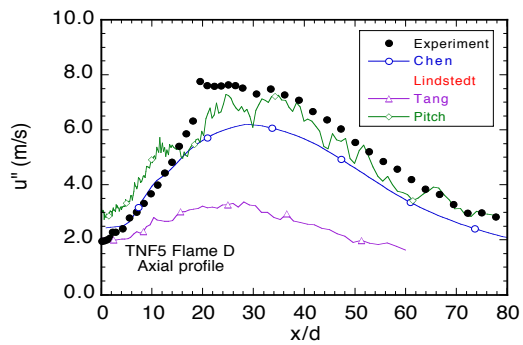
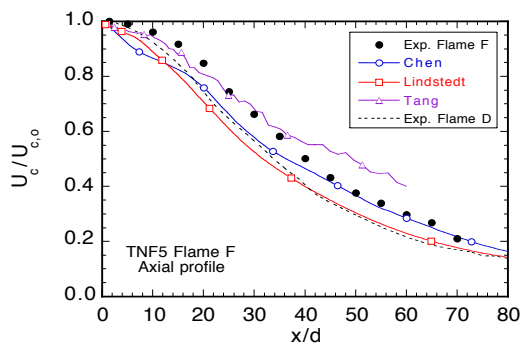
Experimental data in these plots are from Sandia (scalar measurements) and from the Darmstadt University of Technology (velocity measurements).

## Axial Profiles

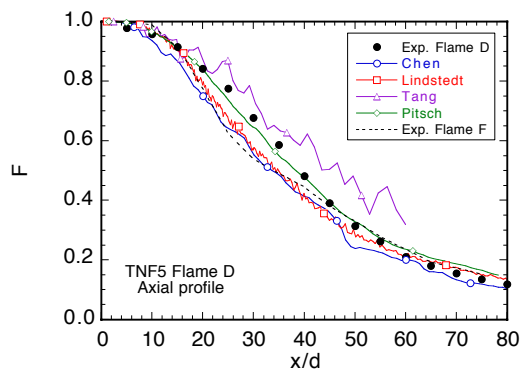
### Flame D



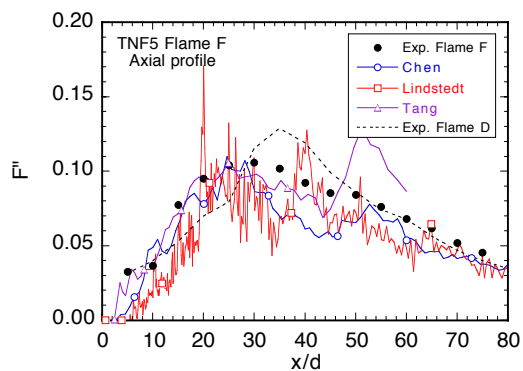
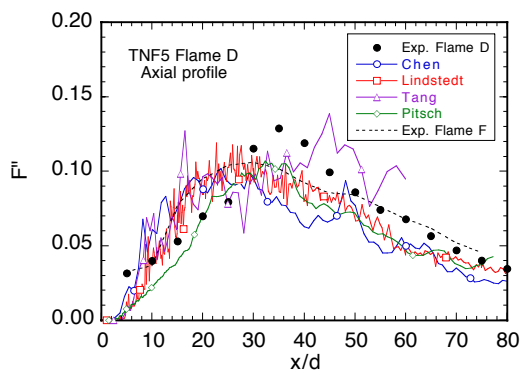
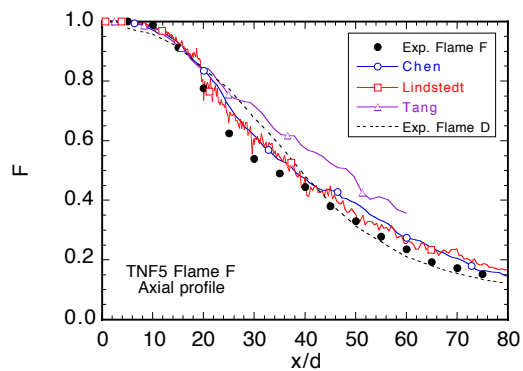
### Flame F



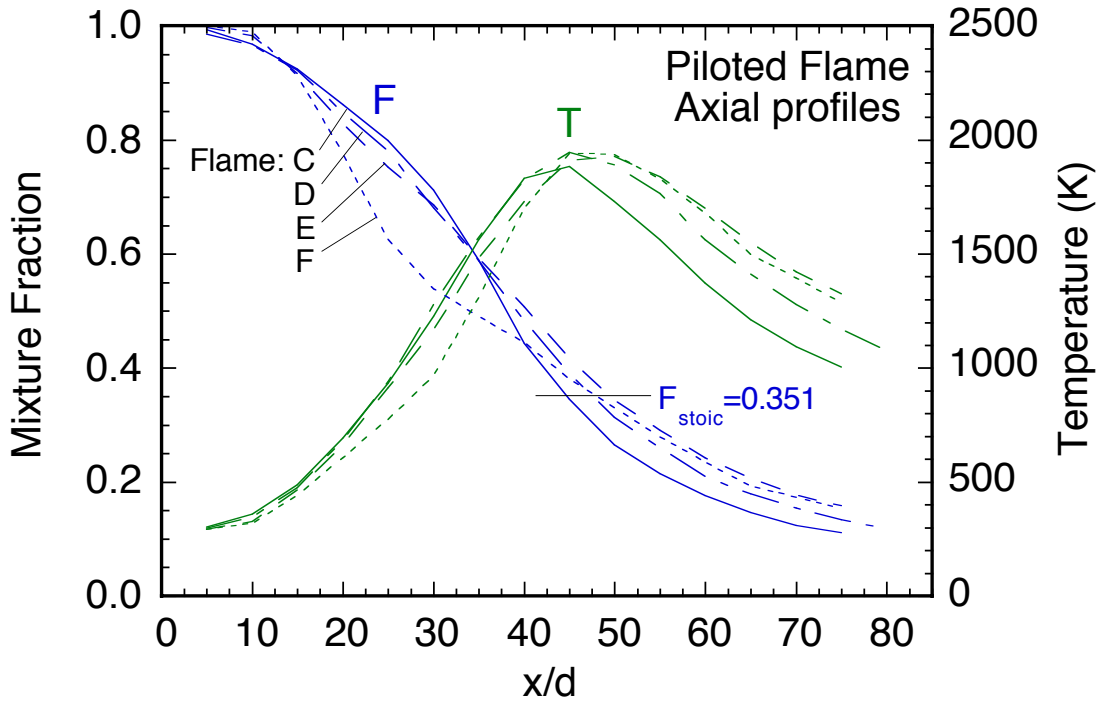
### Flame D



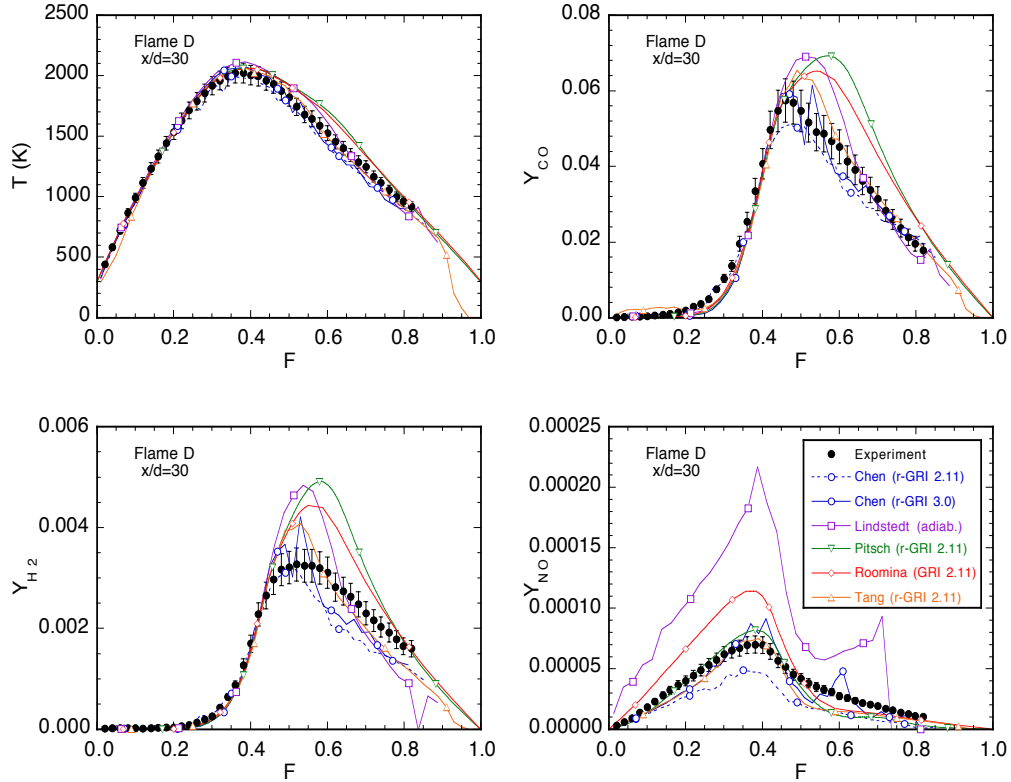
### Flame F



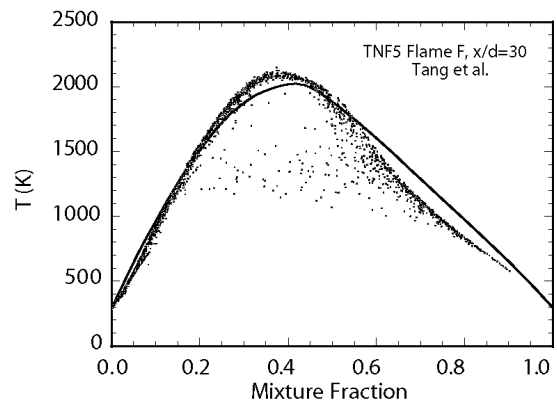
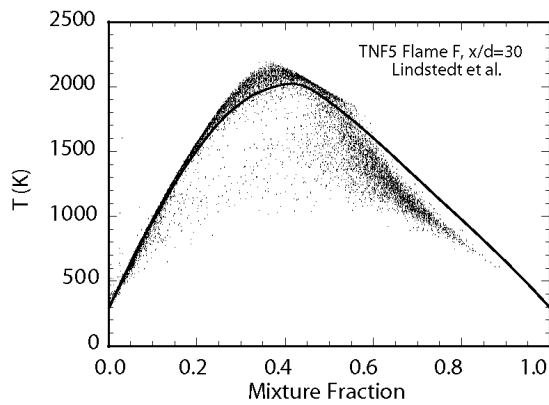
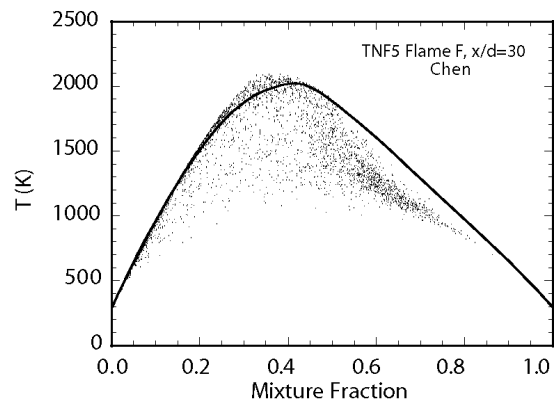
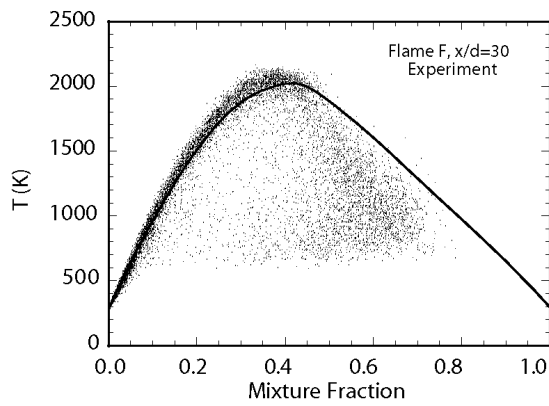
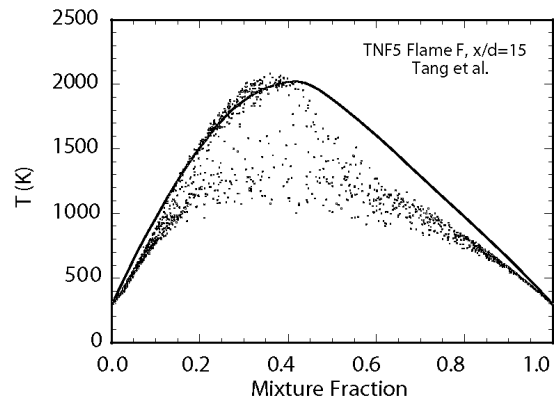
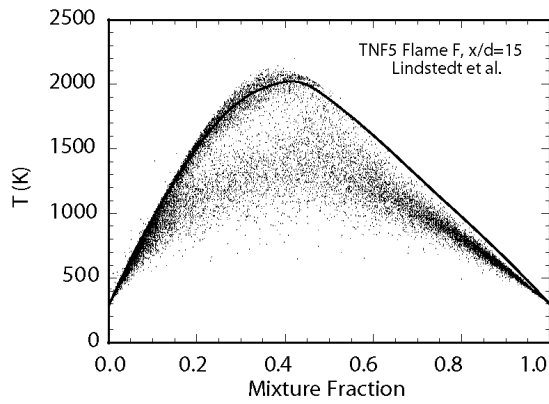
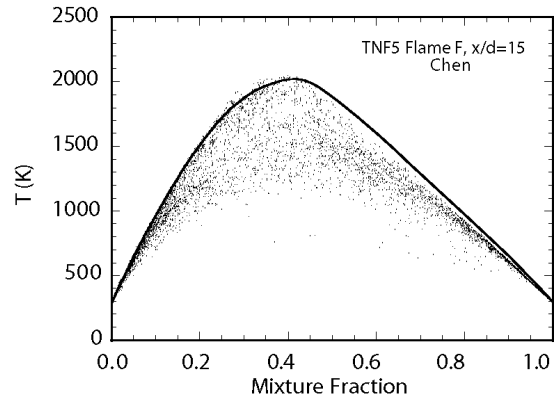
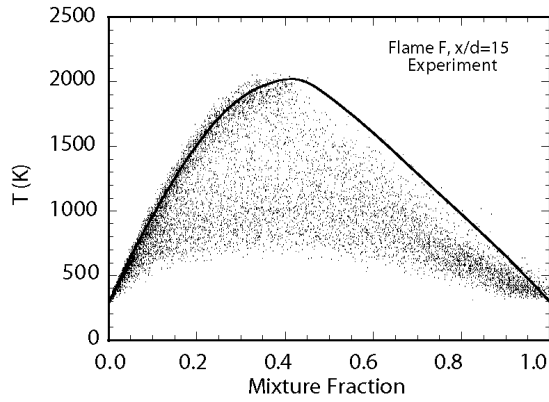
### Measured Axial Profiles



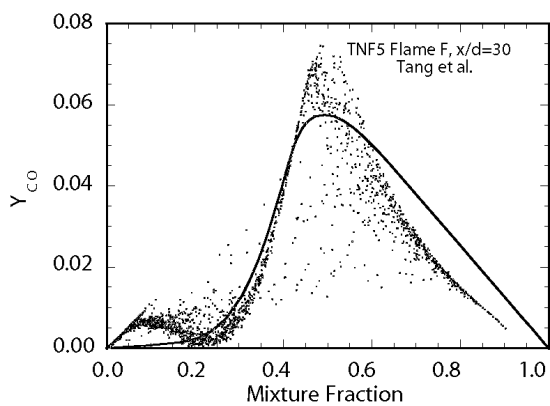
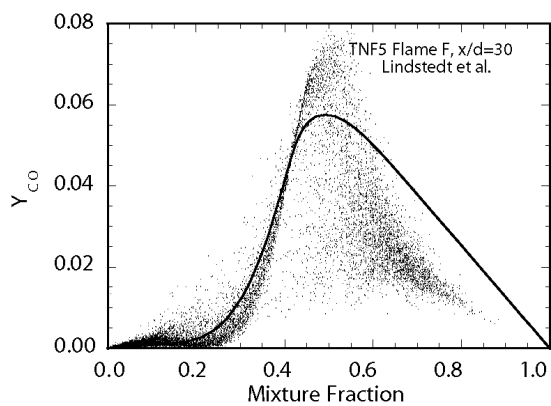
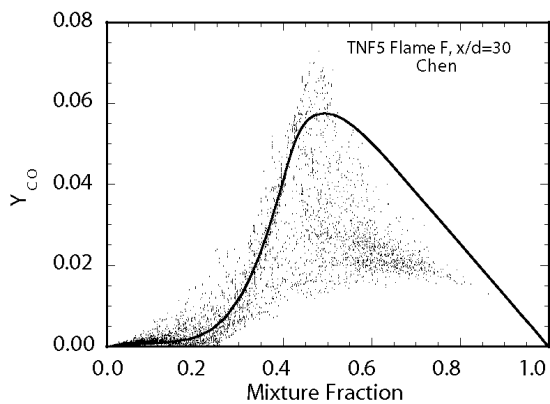
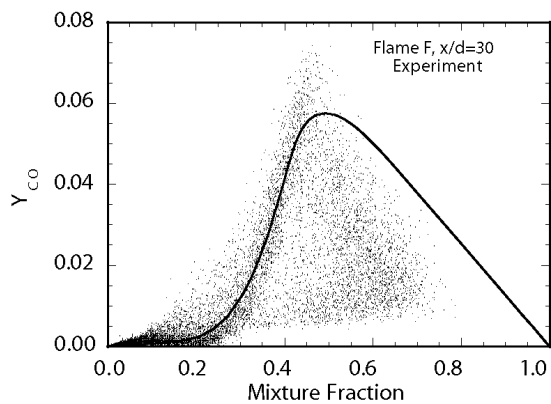
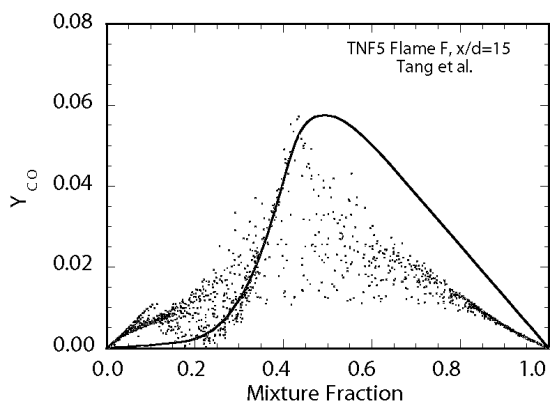
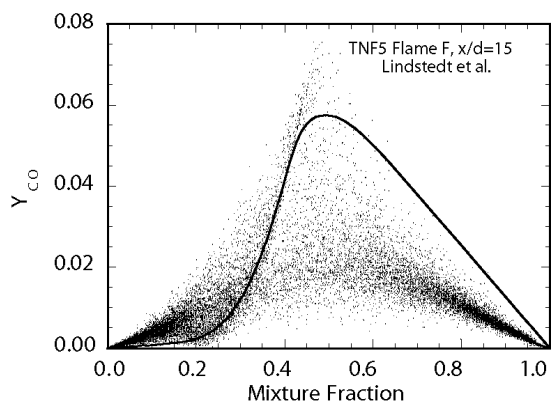
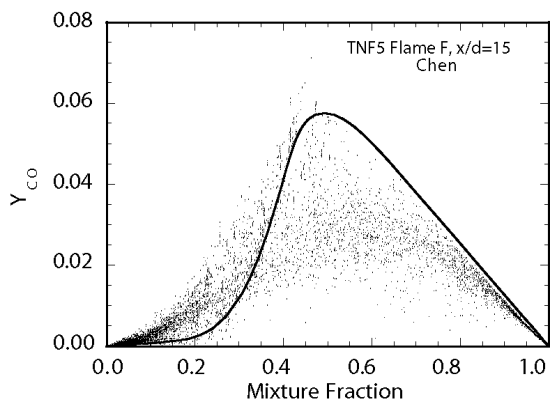
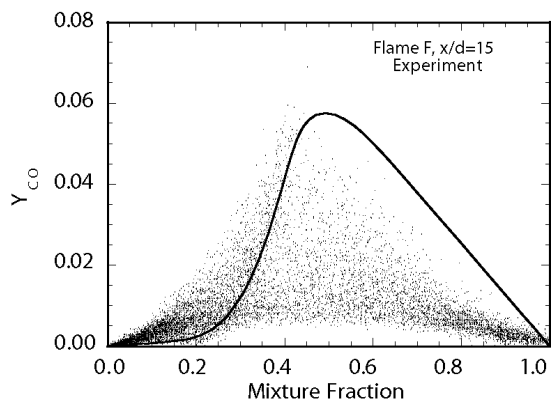
### Conditional Means at $x/d=30$ in Flame D



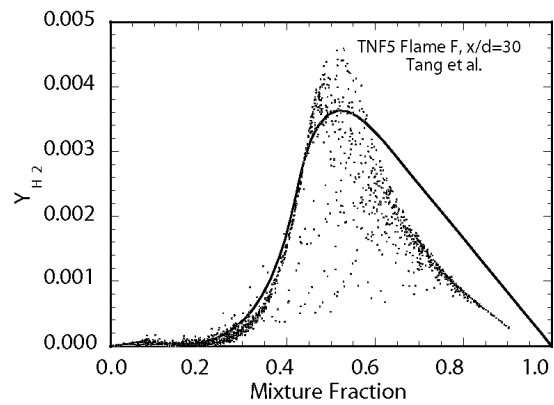
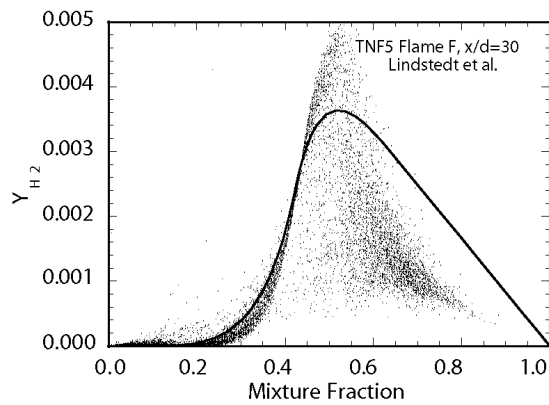
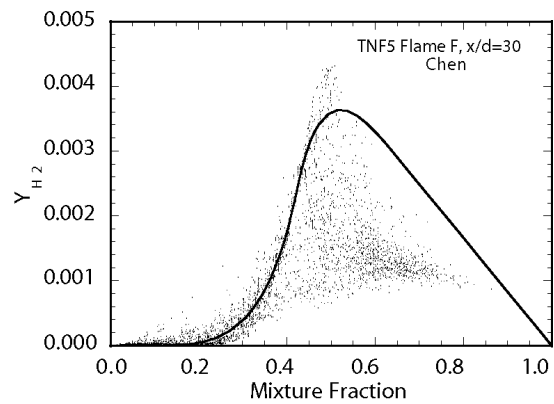
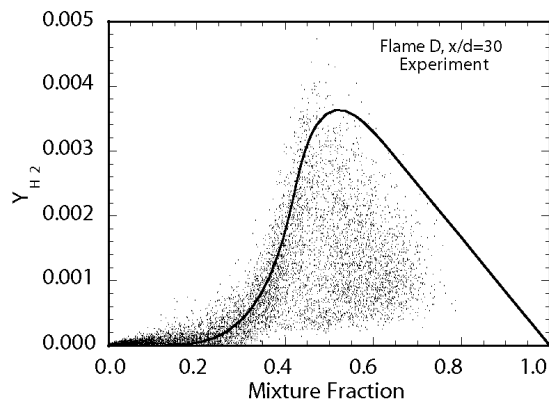
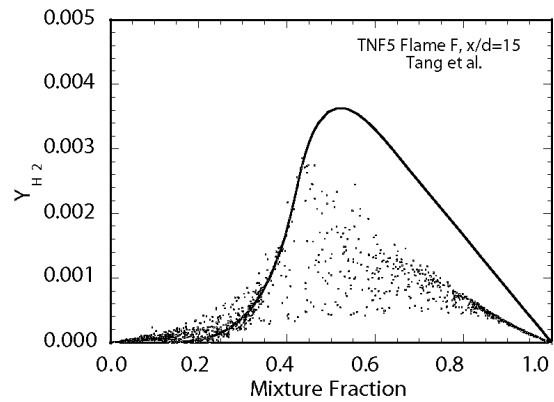
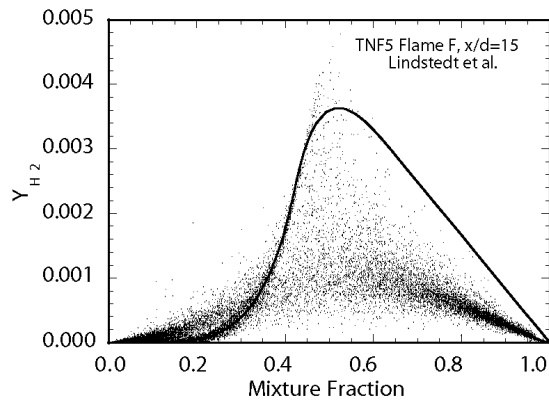
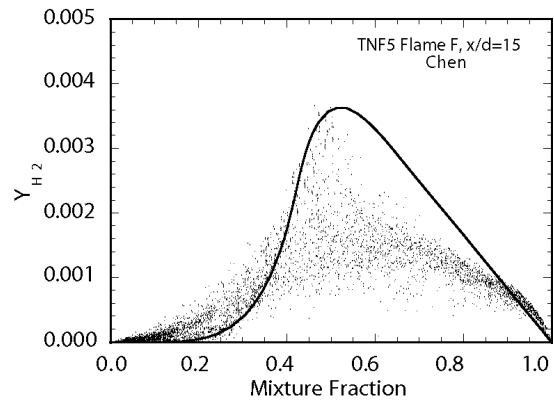
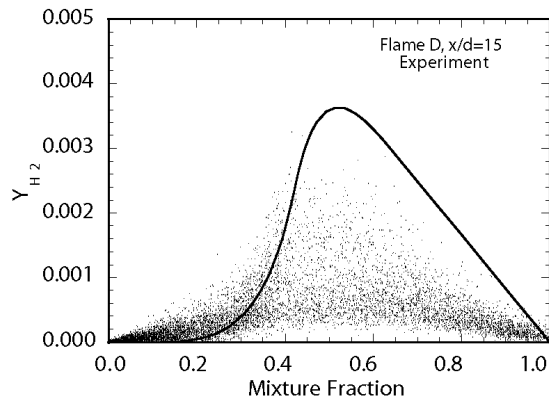
# Flame F Scatter Plots of Temperature at $x/d=15$ and $x/d=30$



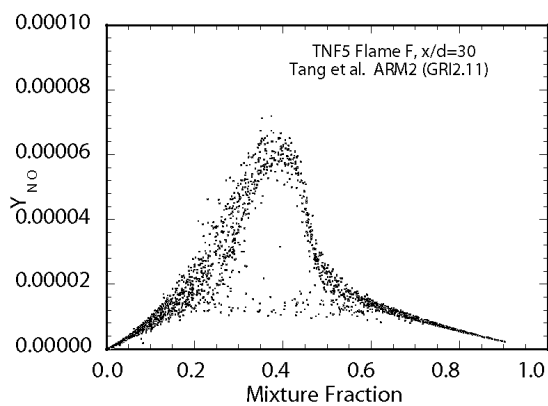
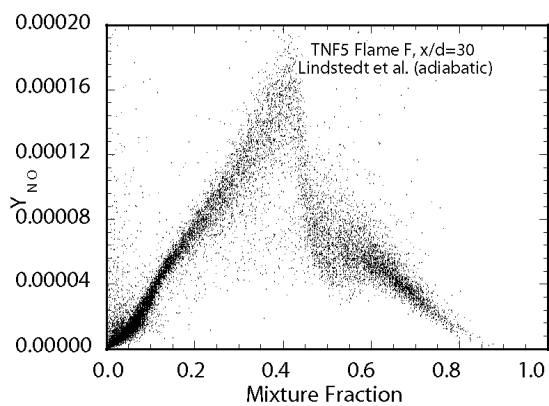
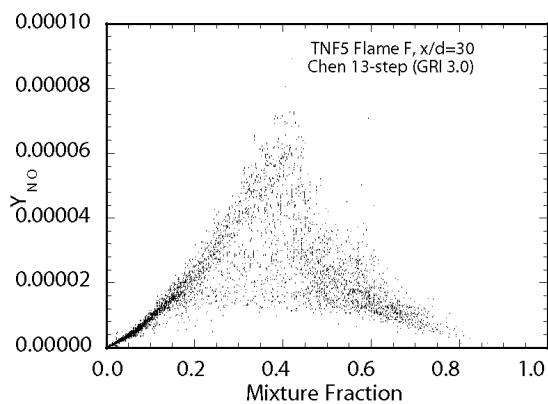
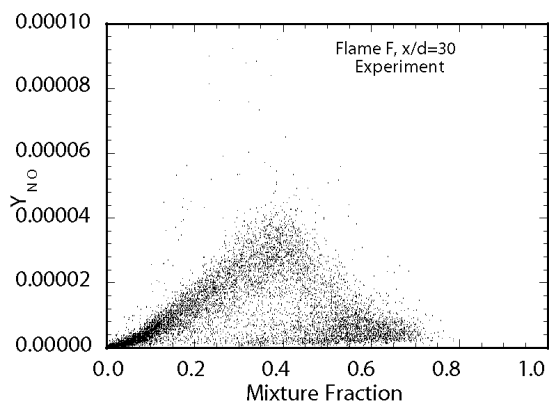
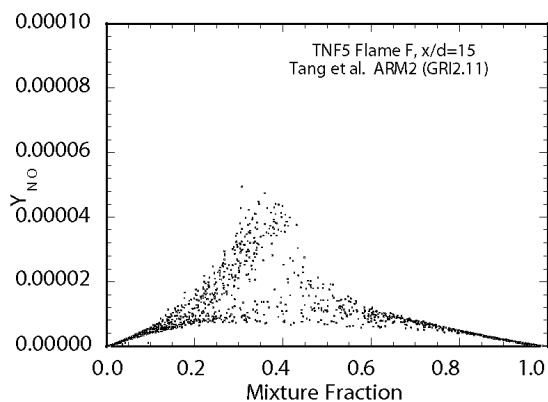
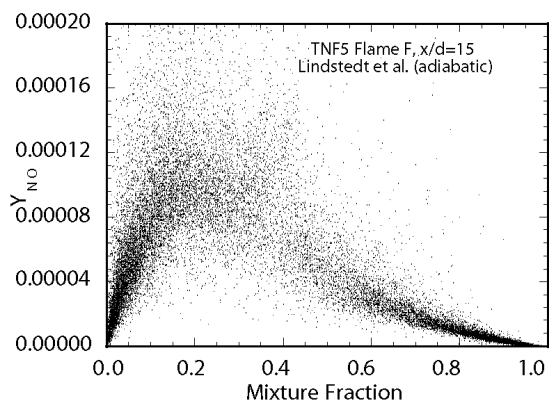
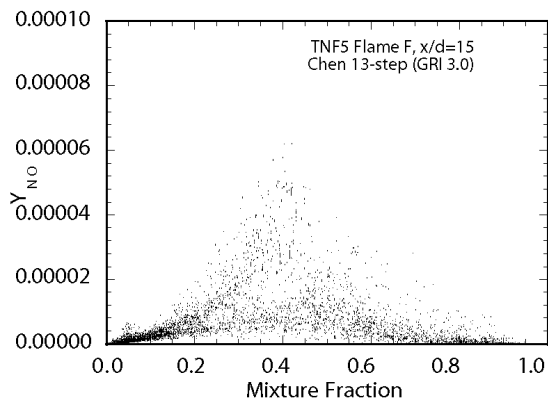
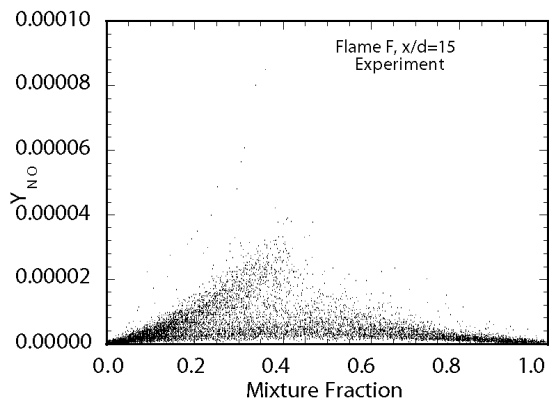
# Flame F Scatter Plots of CO Mass Fraction at $x/d=15$ and $x/d=30$



# Flame F Scatter Plots of H<sub>2</sub> Mass Fraction at x/d=15 and x/d=30



# Flame F Scatter Plots of NO Mass Fraction at $x/d=15$ and $x/d=30$



## Observations Regarding the Piloted Flame Comparisons

1. Current combustion models are capable of yielding reasonably good agreement with measurement on the overall velocity and mixture fraction fields in these flame. However there are some areas of disagreement. In particular,  $u''$  in the calculation by Tang et al. appears low. Radial profiles of velocity and mixture fraction, shown in the Symposium paper by Lindstedt et al., also support this observation, as do some of the calculations from previous workshops.
2. All the models considered here yield similar results for  $f''$  and agree with the measurements.
3. The better results from pdf methods show good agreement with the experiment with regard to extinction at  $x/d=15$ . Agreement is generally not as good at  $x/d=30$ , where the measurements show a slower recovery of flame F than is seen in the models. The models do not show the same strong effect that the high degree of local extinction in flame F has on the axial profile of mixture fraction. However, flame F is not far from blowout, making it something of a special case. The probability of extinction in this flame is particularly sensitive to details of boundary conditions and several submodels.
4. Conditional means of T, CO, and H<sub>2</sub> at  $x/d=30$  in flame D are consistent with trends noted in previous workshops. For example, the CMC and LES/unsteady flamelet results show higher temperature and higher mass fractions of CO and H<sub>2</sub> in fuel-rich conditions, as compared to pdf calculations using the same chemistry. The Lindstedt calculation yields slightly high peak levels of CO. This may be due to differences between chemical mechanisms, as all the other calculations use GRI-based mechanisms.
5. Some of the NO calculations show excellent agreement with the measurements. However, uncertainties in the chemistry and radiation models must be resolved before a conclusion can be drawn that the right answers are obtained for the right reasons.
6. The NO results contain some apparent puzzles that should be discussed.
  - The scatter data from the Lindstedt calculation behave differently than those from the other calculations, particularly at  $x/d=15$  in flame F.
  - All of the calculations included here, except for the adiabatic calculation of Lindstedt et al., use nominally the same radiation model. Previous results from Roomina (CMC) and Chen (pdf) have shown roughly a factor of two decrease in NO, when radiation is included. However, Tang et al. report very little difference between radiative and adiabatic calculations.
  - The Chen/GRI-3.0 calculation and the GRI-2.11-based calculations of Pitsch and Tang are all in good agreement with the measurements, but we expect these two versions of GRI mech to produce significantly different results for NO.

**Fifth International Workshop on Measurement and Computation  
of Turbulent Nonpremixed Flames**  
Delft, The Netherlands  
26-28 July 2000

**Partially-Premixed Laminar Flame Comparisons**

Contributions by:

P. Bajaj, J. Gass, and D. Poulidakos, ETH Zurich  
R. S. Barlow and J. H. Frank, Sandia National Laboratories  
J.-Y. Chen, University of California at Berkeley  
S. C. Li and F. A. Williams, University of California at San Diego  
R. P. Lindstedt, Imperial College  
I. K. Puri, University of Illinois at Chicago  
R. V. Ravikrishna and N. M. Laurendeau, Purdue University

**Introduction**

Comparisons of piloted flame D results at previous workshops have revealed significant differences among predictions of conditional means of species mass fractions for fuel-rich conditions. This is illustrated in Fig. 1, using results from the Boulder workshop (TNF3), in which each calculation used the full GRI 2.11 mechanism. The CMC (Roomina and Bilger) and Monte-Carlo flamelet (Chen) results yield a greater degree of partial oxidation of CH<sub>4</sub> in fuel-rich conditions, such that mass fractions of CO and H<sub>2</sub> are higher than in the PDF calculation and the experiment. Validation of chemical mechanisms for partially-premixed combustion is an important step in gaining a better understanding of the causes of these differences. Of particular interest with regard to major species is whether the detailed mechanisms correctly predict the progress of partial oxidation on the fuel-rich side at low strain rates, which allow these relatively slow reactions to progress. Validation of chemical mechanisms for NO formation in partially-premixed flames is also a high priority because there are significant differences (factor of two) among the available detailed mechanisms, when it comes to NO predictions.

Published measurements in steady, laminar, opposed-flow, partially-premixed CH<sub>4</sub>/air flames are limited, but recent work is adding to the picture. Li and Williams (C&F 118:399-414, 1999) reported temperature and species measurements and calculations for four flames with fuel-side equivalence ratios of  $\phi=1.5, 2.0, 2.5$  and  $3.0$ . Ravikrishna and Laurendeau (accepted to C&F) have measured temperature and NO in several partially-premixed CH<sub>4</sub>/air flames and have compared their results to calculations using GRI 2.11. Recent measurements of steady laminar flames in the Tsuji geometry were obtained by Barlow and Frank in the TDF lab at Sandia and are presented here along with calculations by J-Y Chen. Bajaj et al. (see poster) have run calculations of the Li and Williams flames using GRI and Warnatz mechanisms. Li and Williams have run calculations of the Sandia flames using their mechanism. Lindstedt has also generated comparisons for these flame.

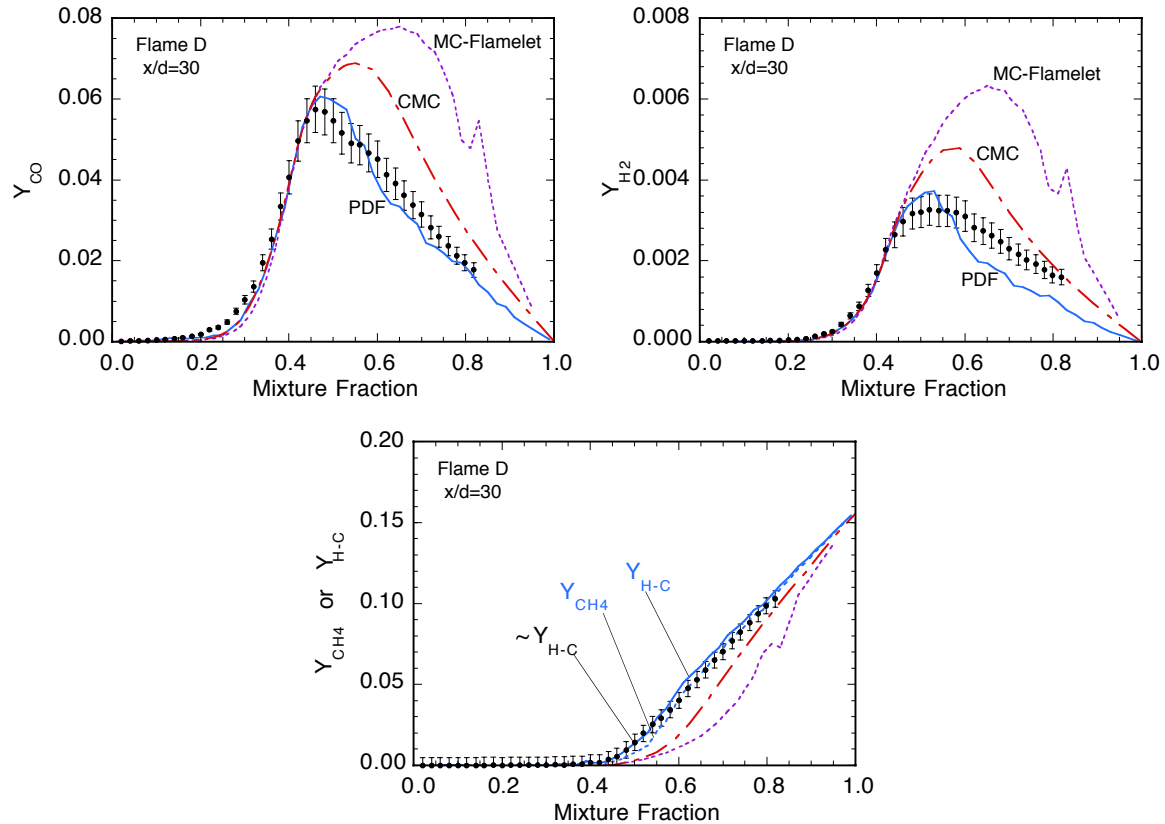


Fig. 1. Measured and calculated conditional mean mass fractions of CO, H<sub>2</sub>, and CH<sub>4</sub> at x/d=30 in piloted flame D. Results are taken from calculations contributed to the TNF3 Workshop (Boulder, 1998) by Roomina and Bilger (CMC) and by Chen (PDF and Monte Carlo flamelet). All calculations used the full GRI 2.11 mechanism.

Our objectives with regard to NO are to use these various comparisons and cross comparisons to:

1. Determine whether the measurements are consistent with each other. (Note that this can only be done in reference to calculations because there are no cases where the same flame has been measured in different laboratories.)
2. Gain a better understanding of the differences among various mechanisms, with regard to NO chemistry.
3. Attempt to reach some conclusions regarding that accuracy with which current mechanisms can be expected to predict NO levels in partially-premixed flames.
4. Identify areas where further work is needed.

This section includes the following contributed comparisons:

- Barlow, Frank, and Chen: Multi-species measurements for flames with  $\phi=2.2$  and 3.17, with adiabatic and radiative calculations based on GRI 2.11 and GRI 3.0.

- Ravikrishna and Laurendeau: Temperature and NO measurements for flames with  $\phi=1.45, 1.6, 1.8,$  and  $2.0,$  with radiative calculations based on GRI 2.11 and GRI 2.11 with a modified rate.
- Li and Williams: Measurements from flames with  $\phi=1.5, 2.0, 2.5,$  and  $3.0,$  with radiative calculations using their mechanism and GRI 3.0. Comparisons of the Barlow and Frank measurements with radiative calculations using the Li and Williams mechanism.
- Bajaj et al.: Adiabatic calculations of the Li and Williams flames, using GRI and Warnatz mechanisms.
- NO results for various flames from Lindstedt, using various mechanisms.

### **Contribution from Barlow, Frank, and Chen**

Measurements were obtained in laminar partially-premixed flames in the Tsuji geometry (porous cylinder in crossflow) using the Rayleigh/Raman/LIF system of the TDF lab at Sandia. Two flames are considered, having fuel-side equivalence ratios of  $\phi=3.17$  and  $\phi=2.2$ . The first case corresponds to the fuel composition used for the piloted jet flames (25% CH<sub>4</sub> and 75% air). Strain rate was not measured, so the calculated strain rate was adjusted to match the measured profile of mixture fraction in each flame.

Results of adiabatic and radiative (optically thin) calculations using GRI 3.0 and GRI 2.11 are compared in Fig. 2 to the measurements in the  $\phi=3.17$ . Agreement on major species is generally excellent, when radiation is included. The two versions of GRI mech yield nearly identical results for all plotted species except NO, and only GRI 3.0 results are shown for those species. Measured mass fractions of H<sub>2</sub> are above the radiative calculation, but the H<sub>2</sub> measurements have an estimated uncertainty of  $\pm 20\%$  at intermediate temperatures, and may suffer from additional interferences in these laminar flames. Therefore, it is not clear that the difference is outside the uncertainty in the measurements. CO results near the peak include a small ( $\sim 7\%$ ) non-resonant contribution from hydrocarbon interference, which has not been subtracted from these data, so agreement on CO is even better than indicated by Fig. 2.

Figure 2 illustrates the fact that the two versions of GRI mech differ significantly in their predictions of NO. In this flame GRI 2.11 yields better agreement with the measurements in fuel-lean and near-stoichiometric conditions. However, GRI 2.11 under predicts NO on the fuel-rich side of the flame. GRI 3.0 agrees with the measurements in the very rich part of the flame but significantly over predicts NO levels in the rest of the flame. In Fig. 3., measured profiles of CO, H<sub>2</sub>, and NO are compared in mixture fraction coordinates with radiative calculations using GRI 2.11 and GRI 3.0, as well as reduced versions of each mechanism. Differences between full and reduced mechanisms are relatively small. Measured and computed results for the flame with  $\phi=2.2$  are shown in Figs. 4 and 5, and results are consistent with those for the  $\phi=3.17$  flame. Figure 6 shows measured and calculated results for the C/H ratio, providing a check on the consistency of the carbon and hydrogen species measurements across different regions of the

flame. Figure 7 shows RADCAL calculations that support the use of the optically –thin model for radiation in these laminar flames.

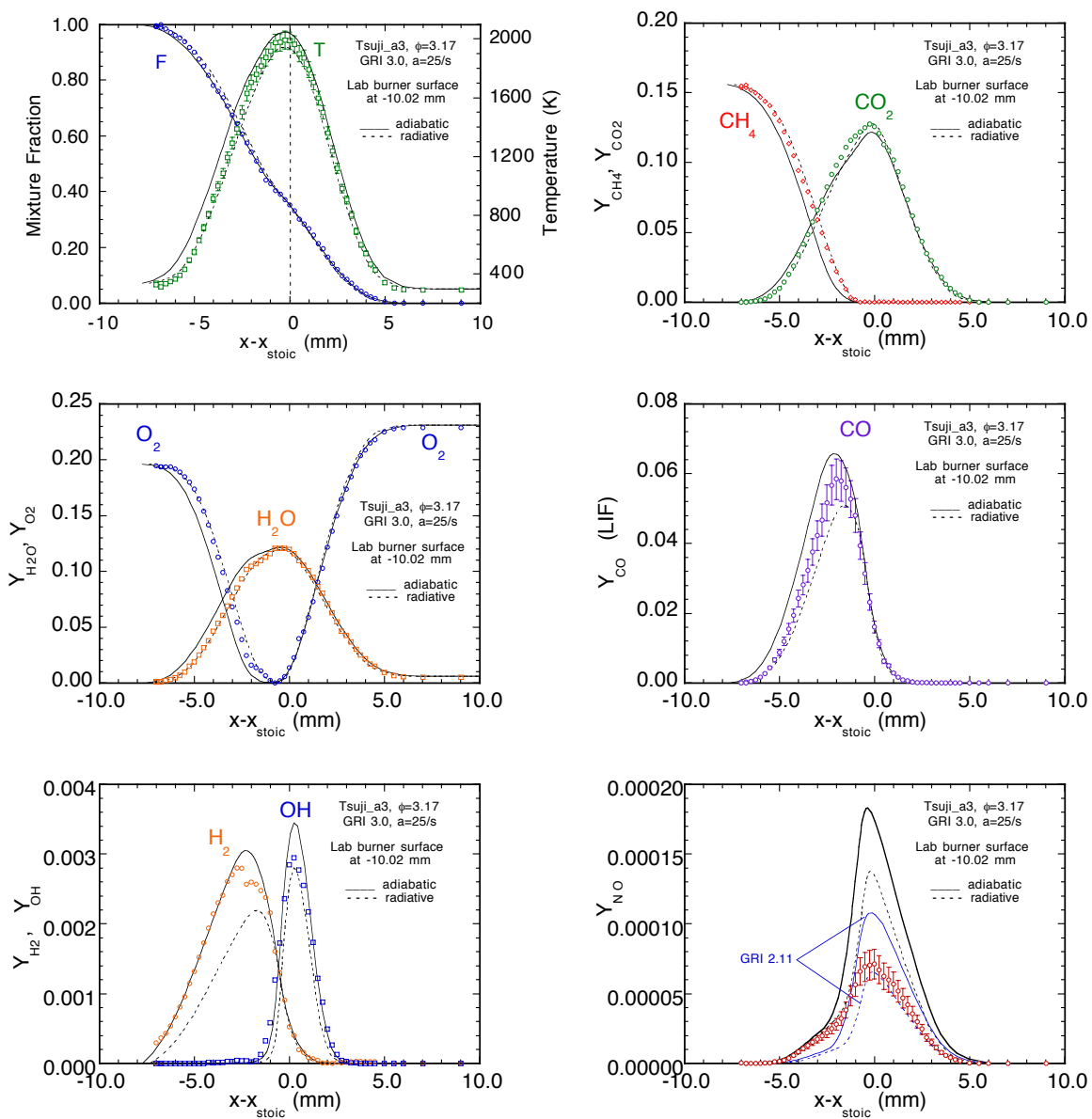


Fig. 2. Measured and calculated profiles of temperature and species mass fractions in the flame with  $\phi=3.17$  (from Barlow, Frank and Chen) show good agreement on major species when radiation is included. An exception is  $H_2$ , which is discussed in the text. GRI 2.11 and GRI 3.0 yield significantly different results for NO, with GRI 2.11 giving better agreement with measured results in fuel-lean and near-stoichiometric parts of the flame.

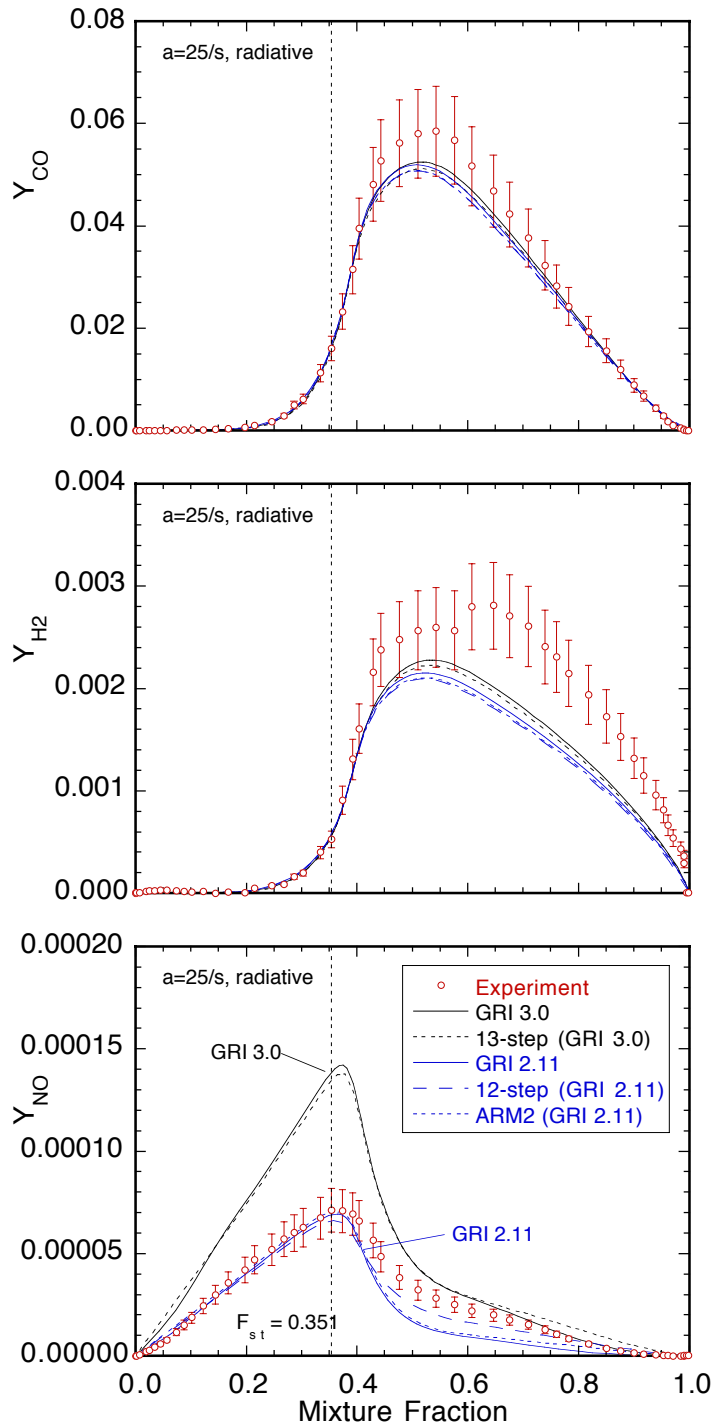


Fig. 3. Radiative calculations using detailed and reduced versions of GRI Mech are plotted versus the measured mixture fraction at each location in the flame profile. Differences among the calculated results for CO and H<sub>2</sub> are small. For NO the differences between reduced mechanisms and their starting mechanism are small compared to the difference between GRI 2.11 and GRI 3.0.

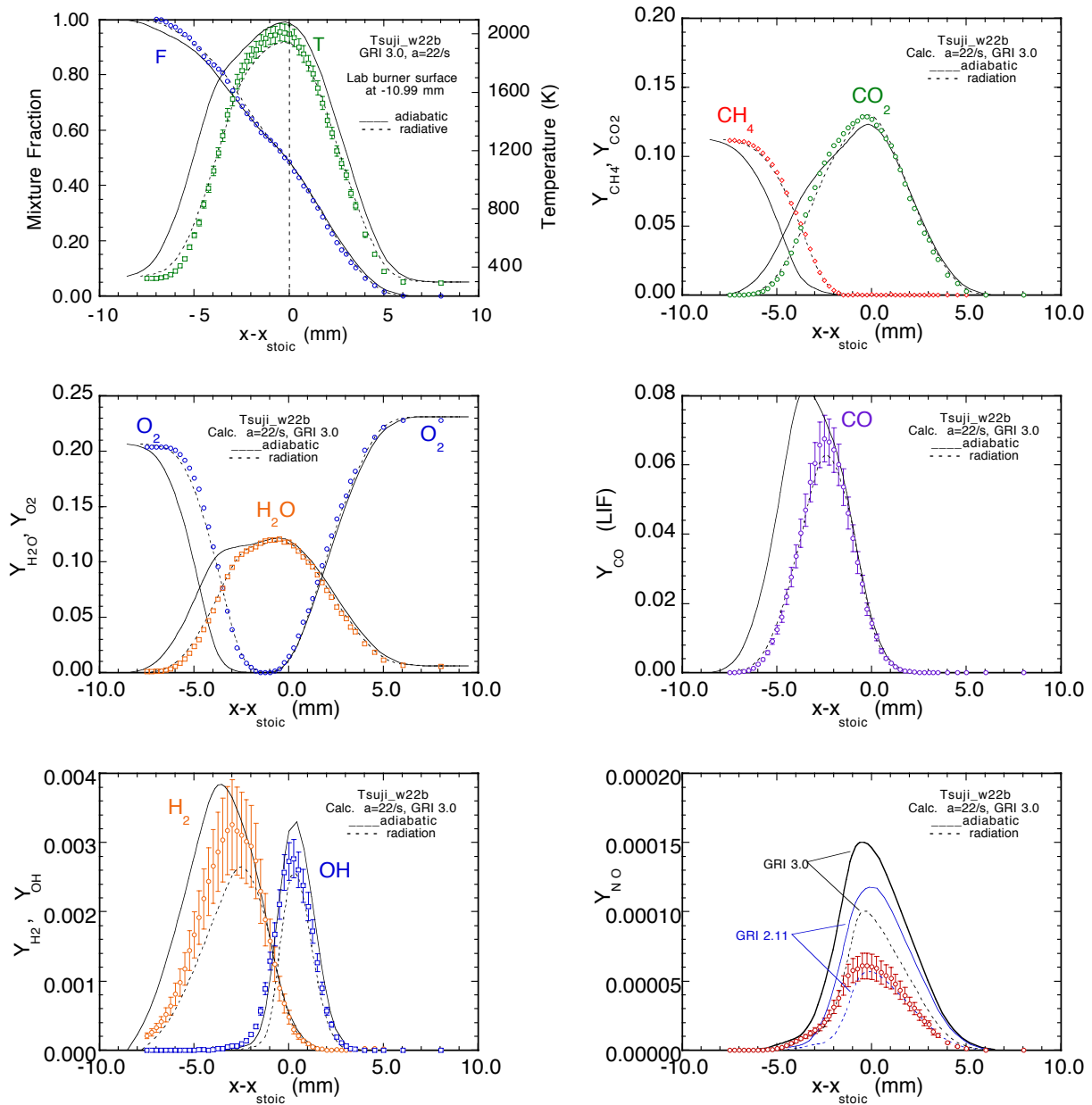


Fig. 4. Results for the  $\phi=2.2$  case are consistent with those from the  $\phi=3.17$  case, showing agreement between the radiative calculation and the measurements. Again, GRI 2.11 agrees with the measured NO peak, while the GRI 3.0 result is well above measurements. It is clear from this figure and the following plots versus mixture fraction that radiation has a strong influence on the calculated flame profile, particularly with regard to the progress of partial oxidation of the fuel in this partially-premixed flame.

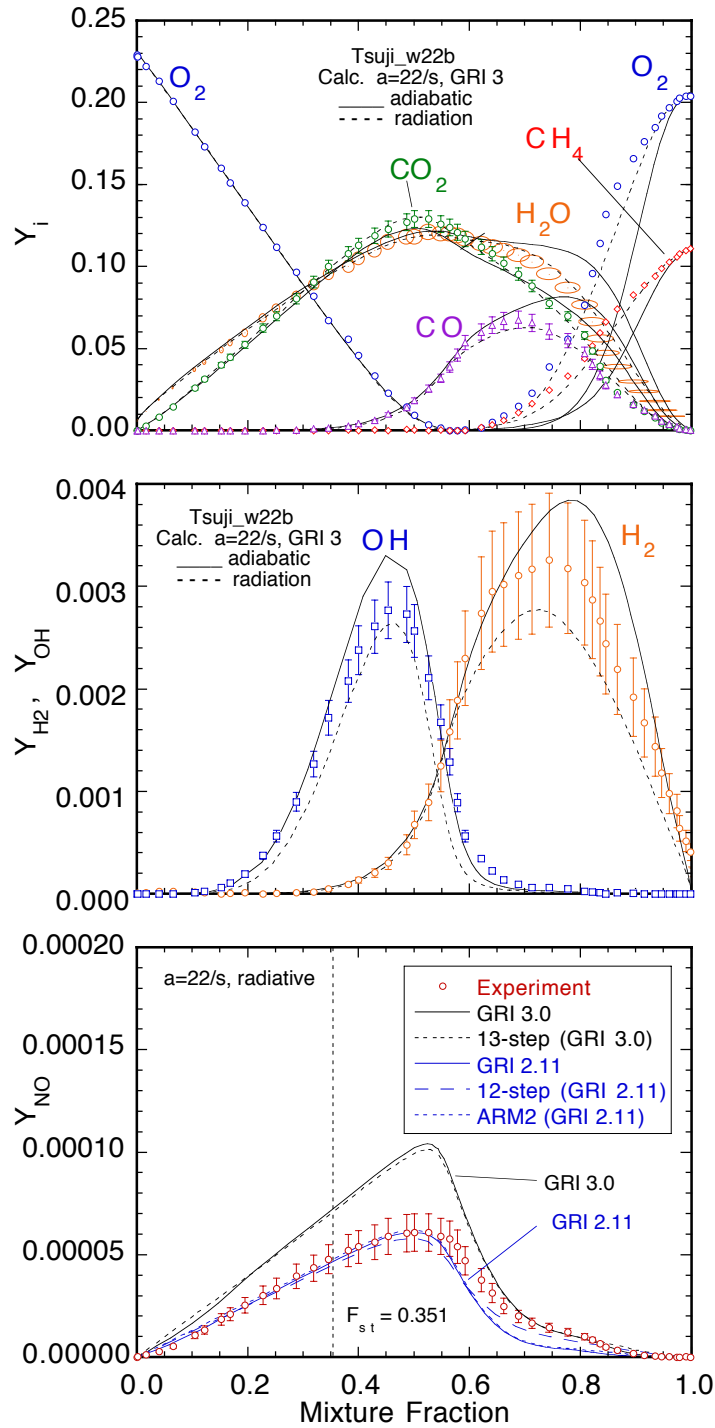


Fig. 5. Comparison of measured and calculated results plotted versus mixture fraction for a steady laminar opposed-flow flame (Tsuji geometry) with  $\phi=2.2$  in the fuel stream. Note the large differences between adiabatic and radiative results in the fuel-rich part of the flame ( $f > 0.6$ ). (Note that the label and dashed line marking the stoichiometric value of mixture fraction are incorrect for this flame.)

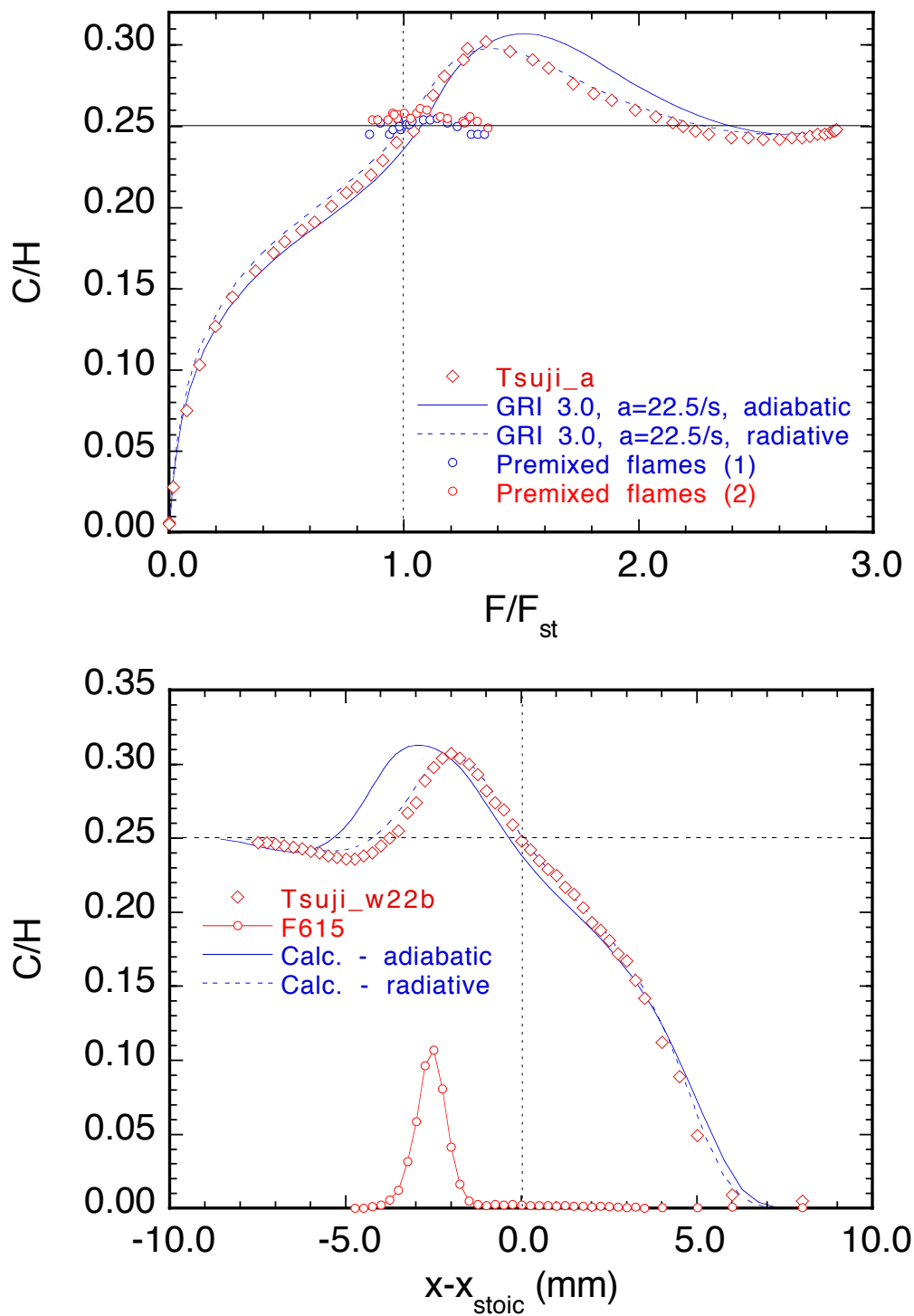


Fig. 6. The  $C/H$  ratio provides a useful check on the consistency of the species measurements across the flame. The measured  $C/H$  profiles in two laminar flames ( $\phi=3.17$  above,  $\phi=2.2$  below) show good agreement with calculations. Note that humidity in the air stream causes  $C/H$  to go to zero at the boundary of the flame. Results from flat flame calibrations (upper graph), taken before and after the Tsuji flame measurements, show the expected value of  $C/H=0.25$ .

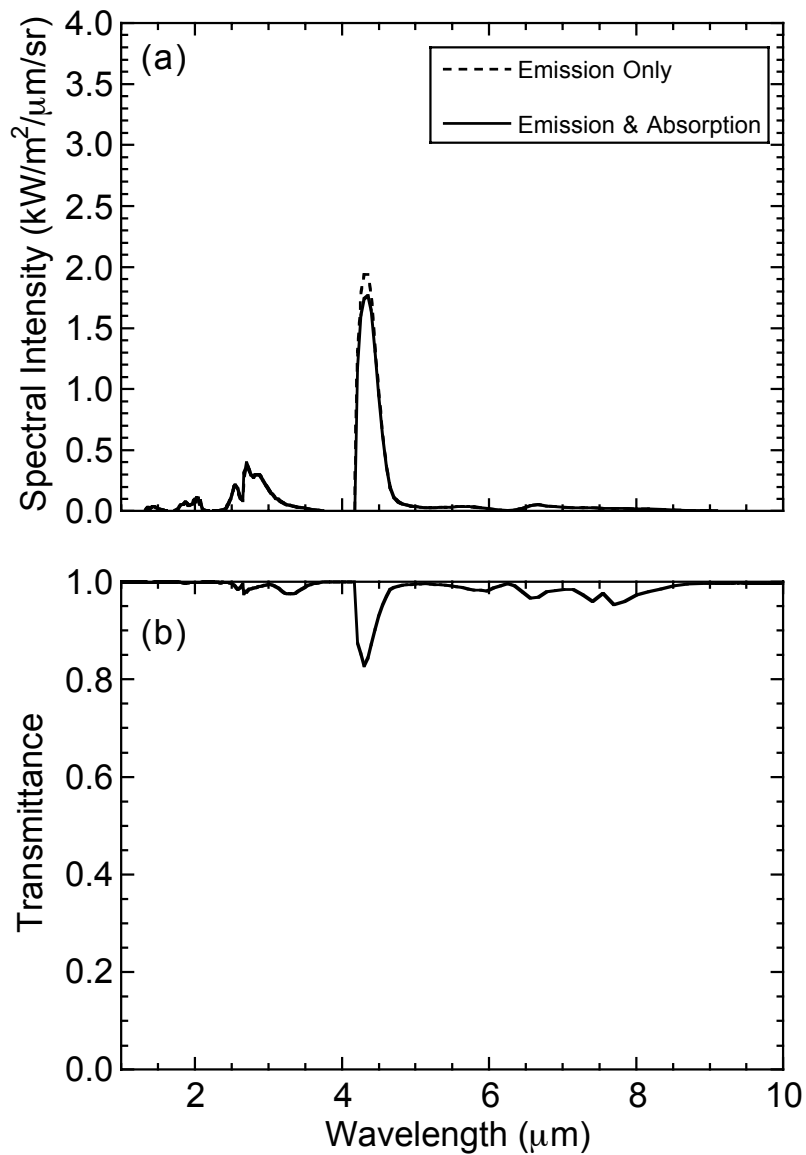
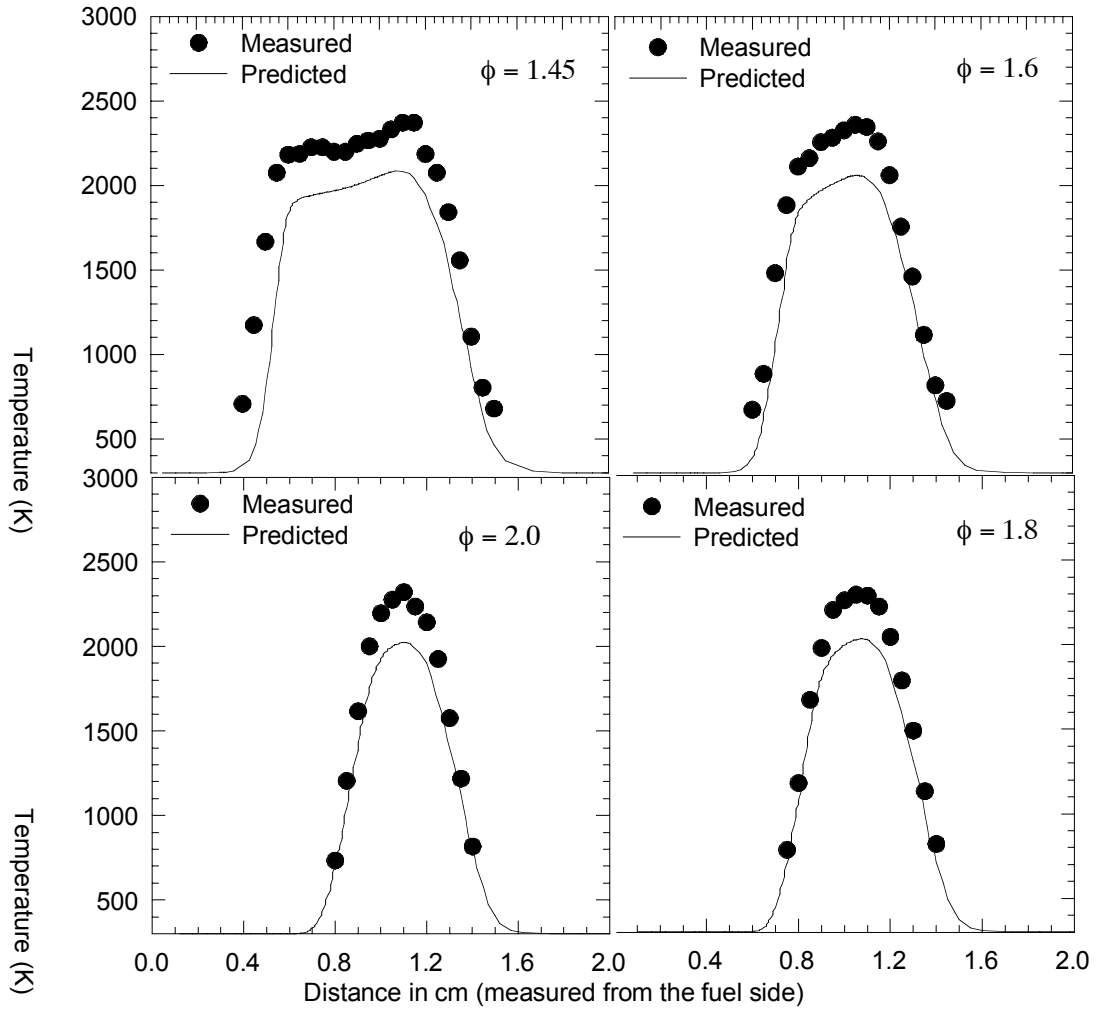
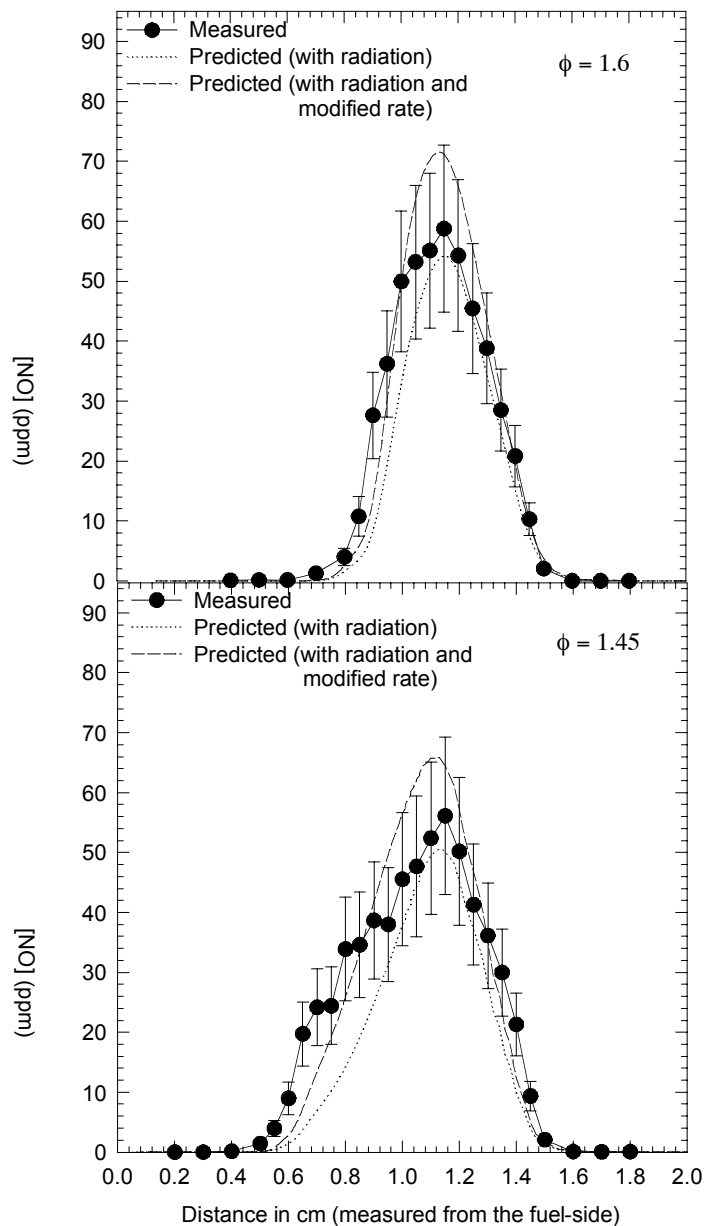


Fig. 7. Spectral intensity and transmission from RADCAL, using the measured profiles of temperature and species ( $\text{CO}_2$ ,  $\text{H}_2\text{O}$ ,  $\text{CH}_4$ , and  $\text{CO}$ ) in the flame with  $\phi=2.2$ . The integrated intensity differs by only  $\sim 5\%$  between the emission-only and emission-absorption calculations. The minimum in spectral transmittance is roughly 0.83 at the peak of the 4.3-micron band of  $\text{CO}_2$ . This supports the use of the optically thin assumption for radiative calculations of these laminar flames.

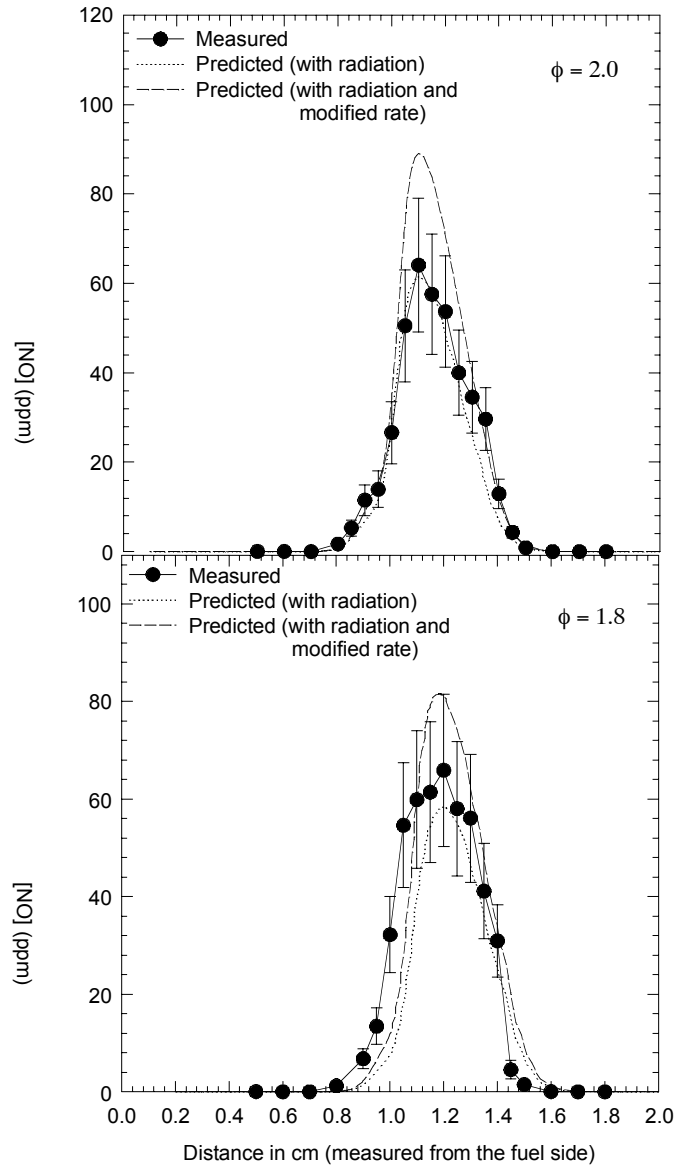
**Contribution from Ravikrishna and Laurendeau:**



Comparison of measured and predicted temperatures in the counterflow partially-premixed flames with fuel-side equivalence ratios of 1.45, 1.6, 1.8, and 2.0 (from Ravikrishna and Laurendeau, "Laser-Induced Fluorescence Measurements of Nitric Oxide in Counterflow Partially-Premixed Flames, *Combust. Flame*, to appear).

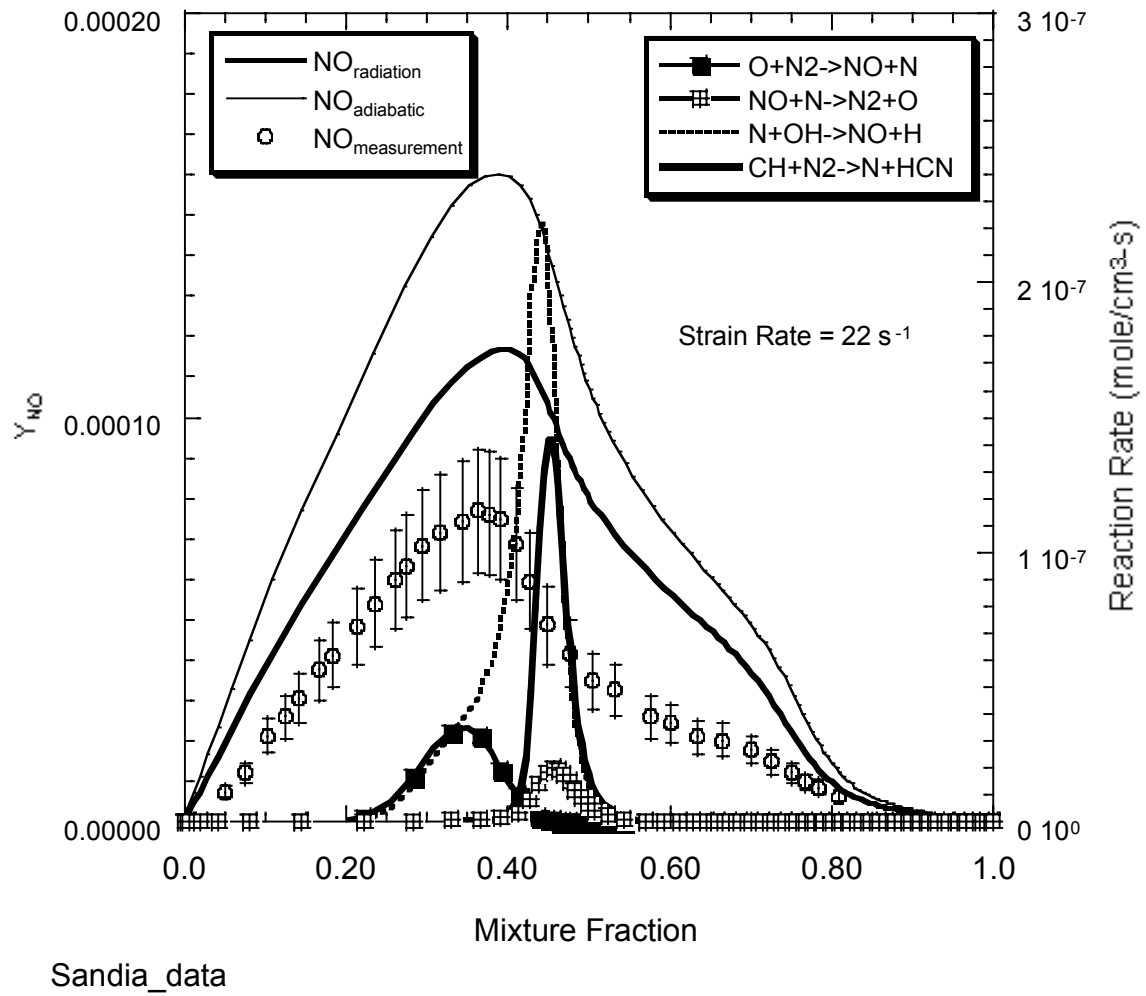


Comparison of LIF [NO] measurements and model predictions with radiation in the counterflow partially-premixed flames with fuel-side equivalence ratios of 1.45 and 1.6. The dotted line represents the predictions of the model with radiation using the GRI mechanism (version 2.11) in its original form. The dashed line represents the model with radiation using a modified rate coefficient for the prompt-NO initiation reaction. . (From Ravikrishna and Laurendeau, *Combust. Flame*, to appear).

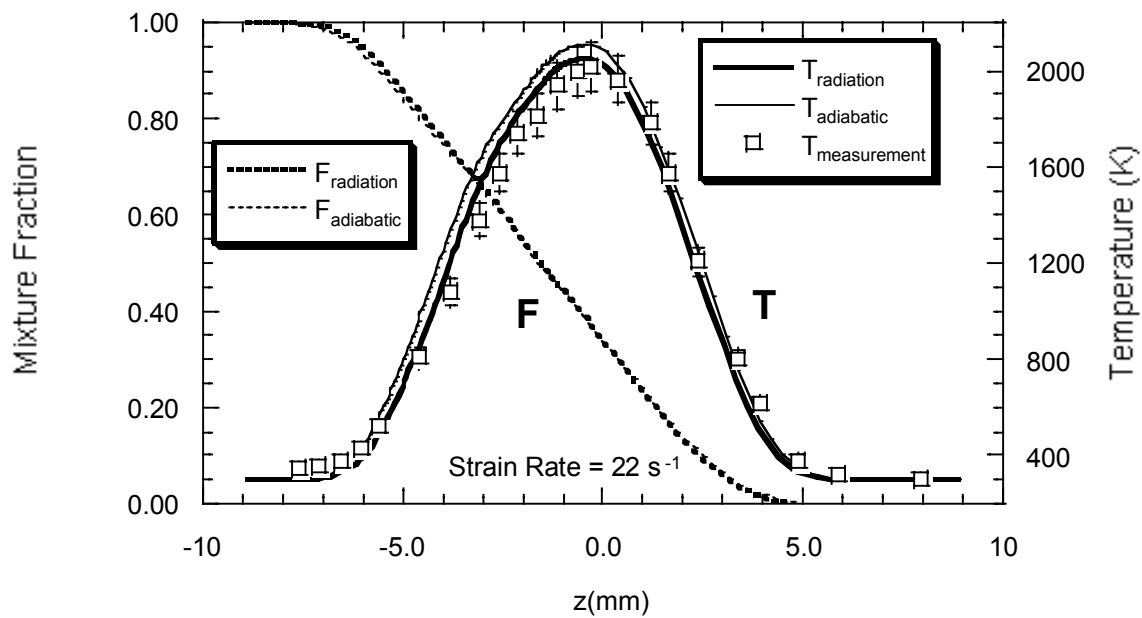
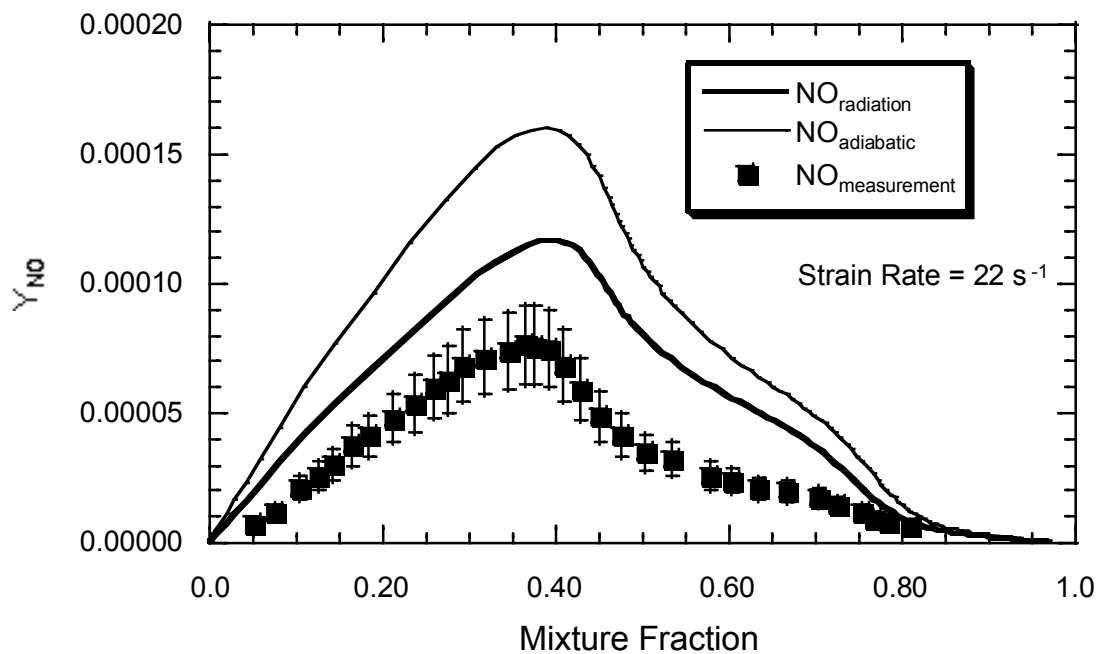


Comparison of LIF [NO] measurements and model predictions with radiation in the counterflow partially-premixed flames with fuel-side equivalence ratios of 1.8 and 2.0. The dotted line represents the predictions of the model with radiation using the GRI mechanism (version 2.11) in its original form. The dashed line represents the model with radiation using a modified rate coefficient for the prompt-NO initiation reaction. (From Ravikrishna and Laurendeau, *Combust. Flame*, to appear).

**Contribution from Li and Williams (UC San Diego):**



Adiabatic and radiative calculations of NO mass fraction in the  $\phi=3.17$  flame of Barlow and Frank, using the Li and Williams mechanism (C&F 118:399-414, 1999).



Adiabatic and radiative calculations of NO mass fraction and temperature in the  $\phi=2.2$  flame of Barlow & Frank, using the Li and Williams mechanism (C&F 118:399-414, 1999).

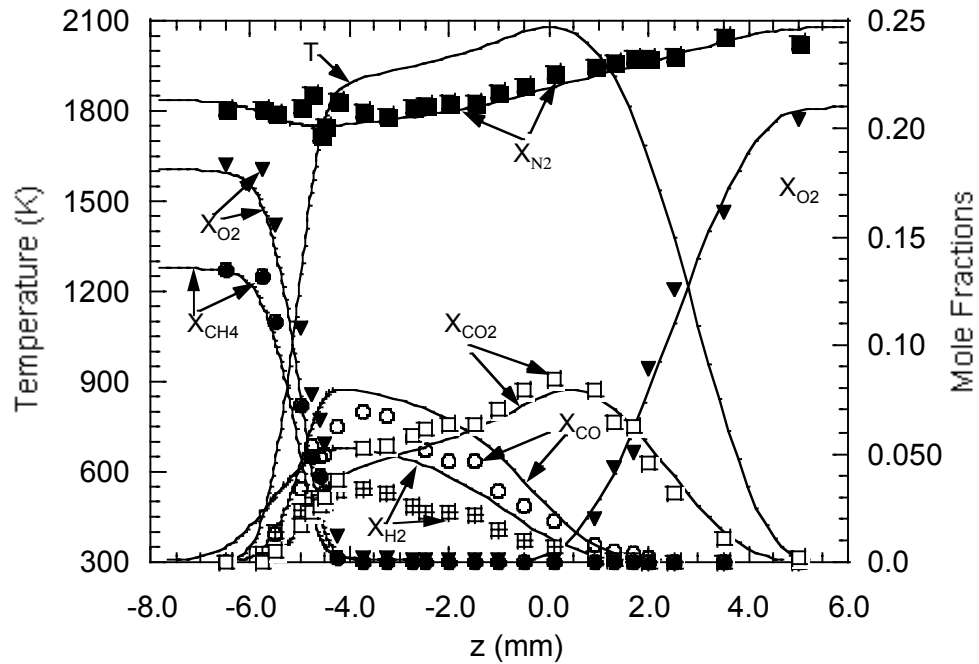


Fig.4(a): Comparison between measured and prediction for concentration profiles of major species for  $\Phi = 1.5$  and strain rate  $a = 50 \text{ s}^{-1}$ .

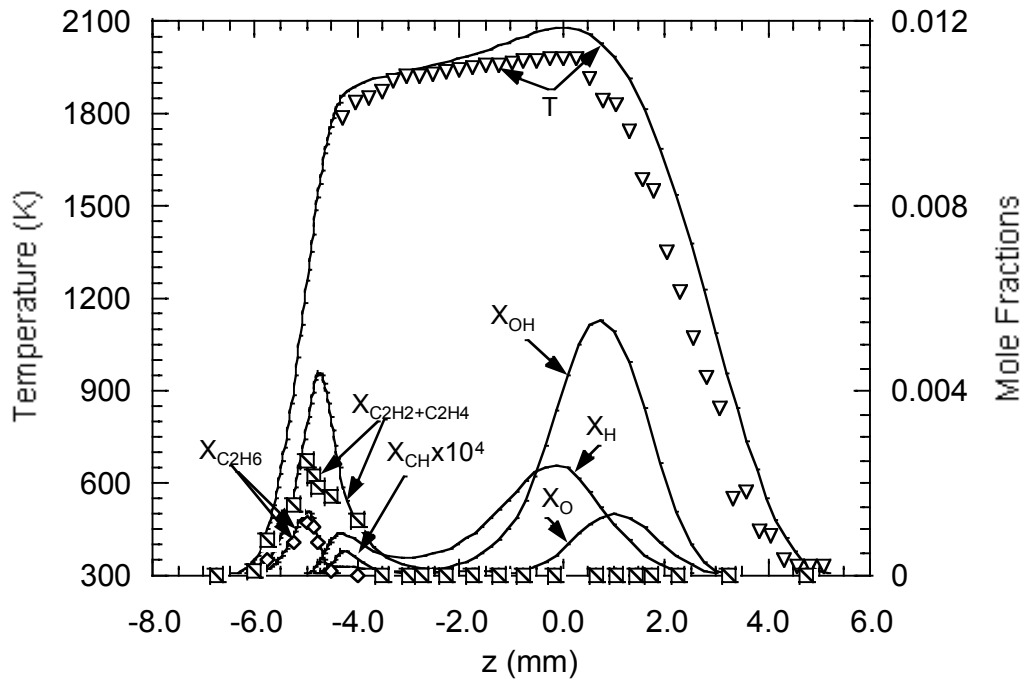


Fig.4(b): Comparison between measurement and prediction for profiles of temperature and concentrations of radicals and  $C_2$  species for  $\Phi = 1.5$  and strain rate  $a = 50 \text{ s}^{-1}$ .

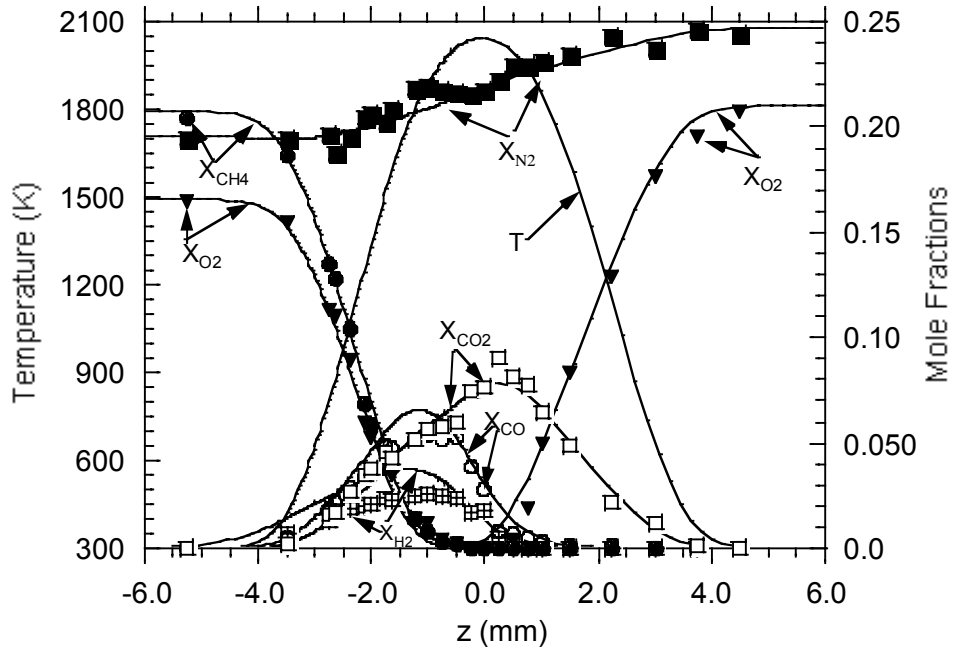


Fig5a: Comparison between measurement and prediction for concentration profiles of major species for  $\Phi = 2.5$  and strain rate  $a = 50\text{s}^{-1}$ .

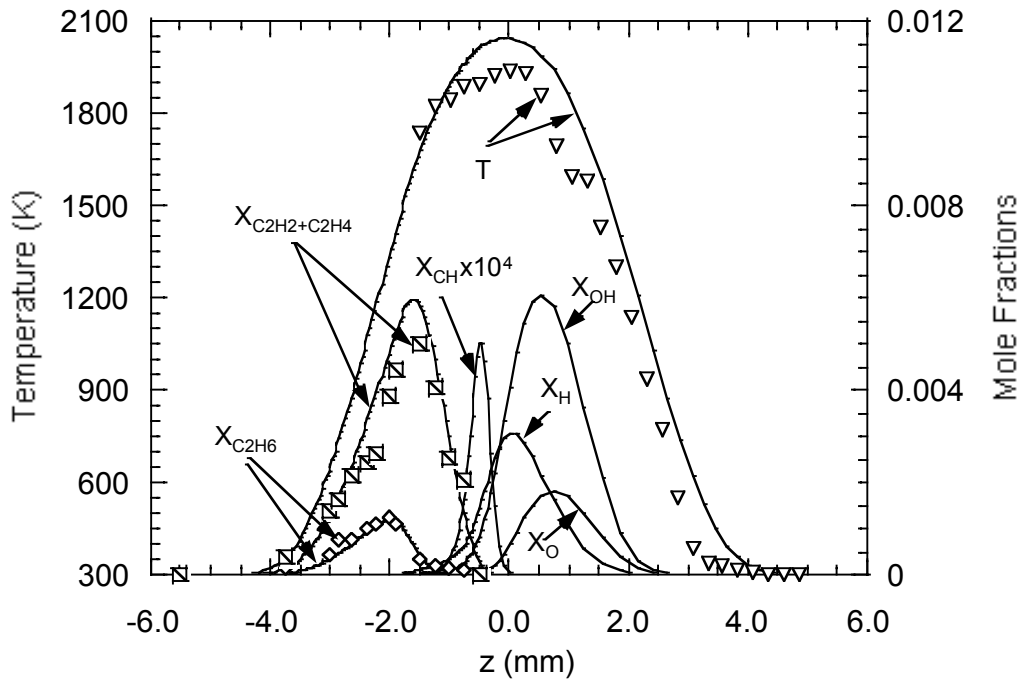


Fig.5(b): Comparison between measurement and prediction for profiles of temperature and concentrations radicals and  $C_2$  species for  $\Phi = 2.5$  and strain rate  $a = 50\text{ s}^{-1}$ .

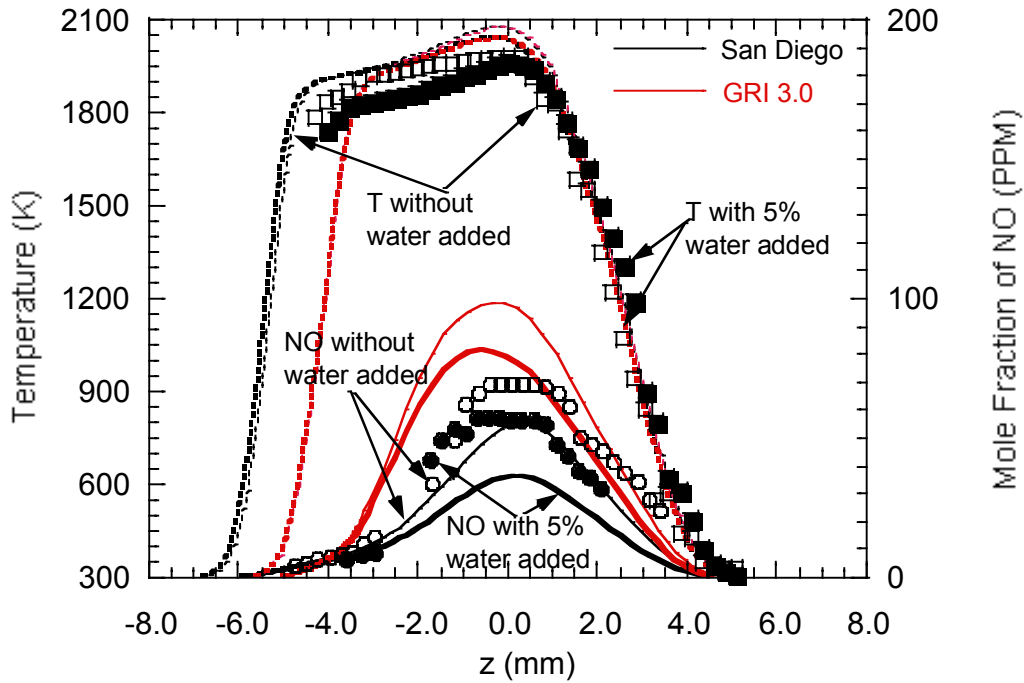


Fig.6: Comparison between measurement and prediction for profiles of NO concentration and temperature with  $\Phi = 1.5$  and strain rate  $a = 50 \text{ s}^{-1}$ .

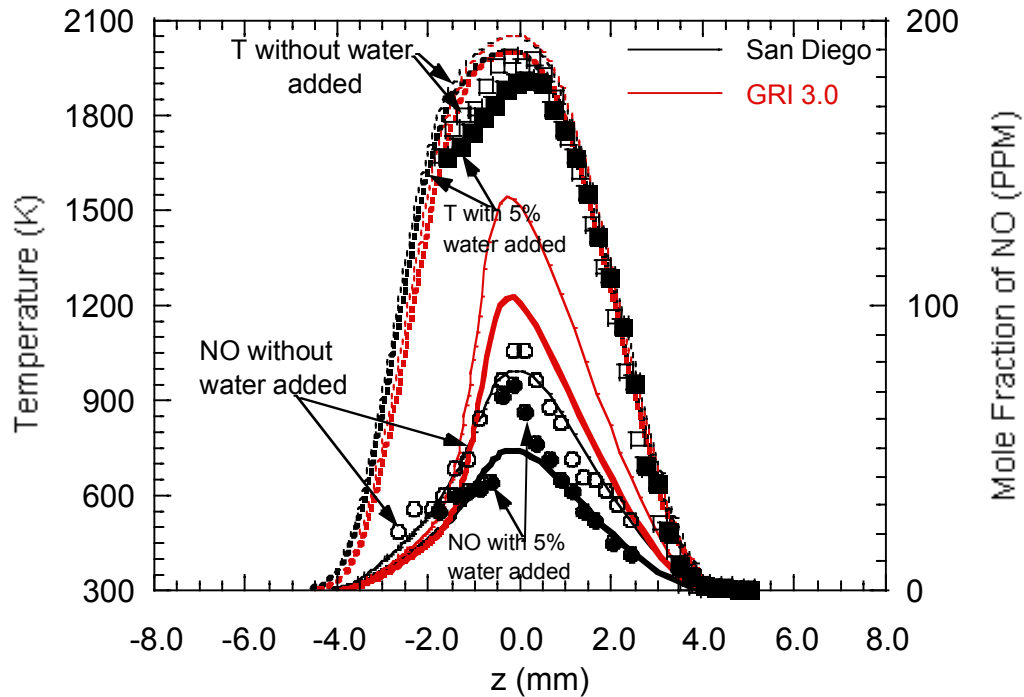


Fig.7: Comparison between measurement and prediction for profiles of NO concentration and temperature with  $\Phi = 2.0$  and strain rate  $a = 50 \text{ s}^{-1}$ .

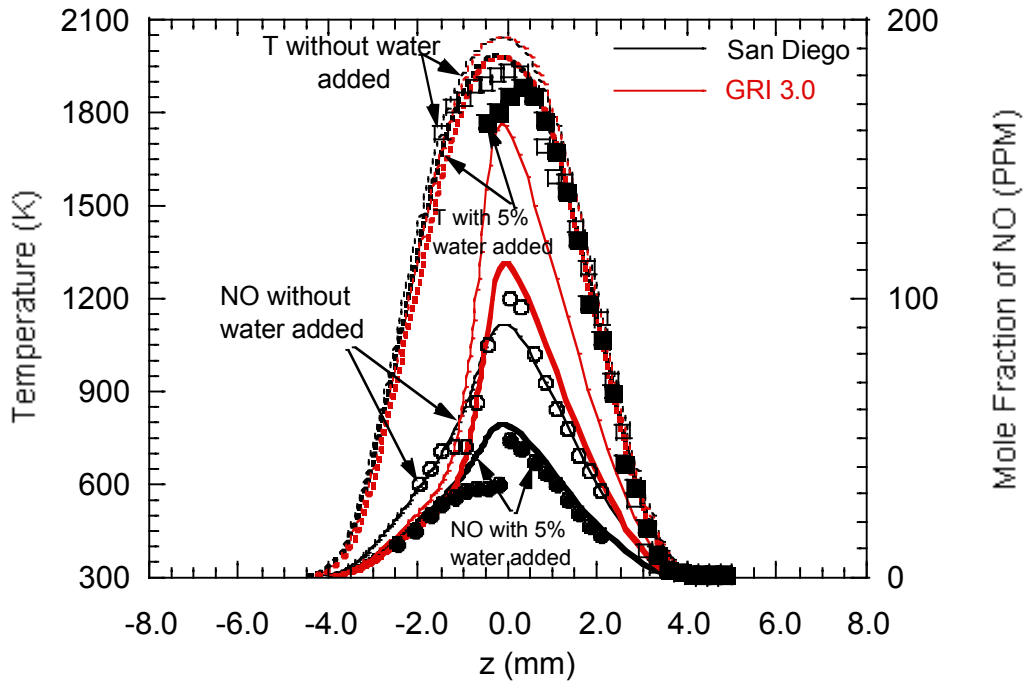


Fig.8: Comparison between measurement and prediction for profiles of NO Concentration and temperature with  $\Phi = 2.5$  and strain rate  $a = 50 \text{ s}^{-1}$ .

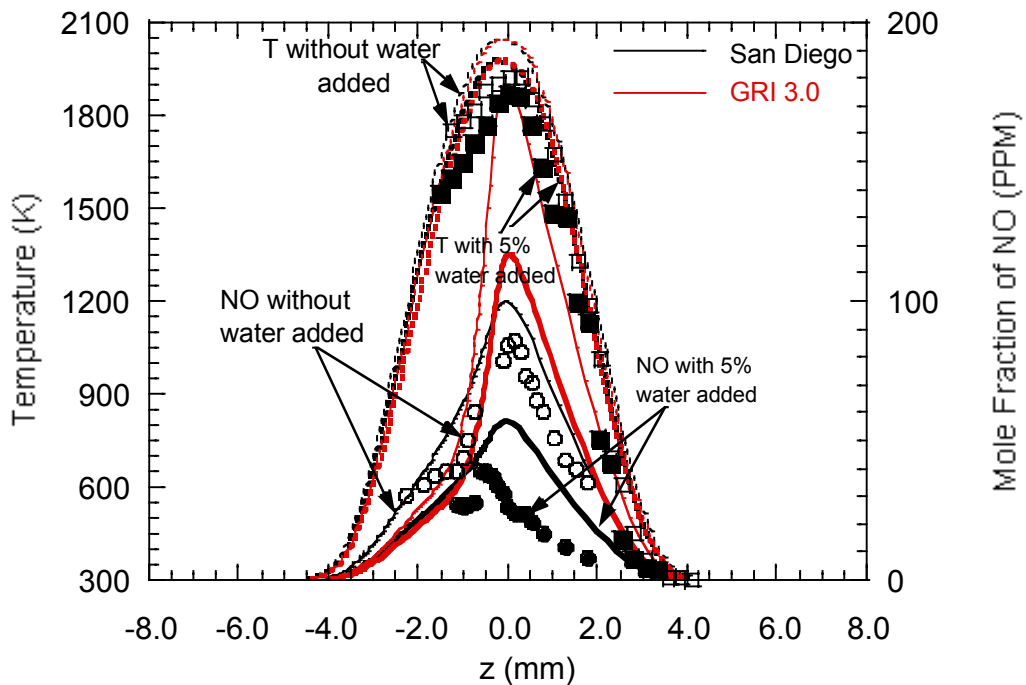
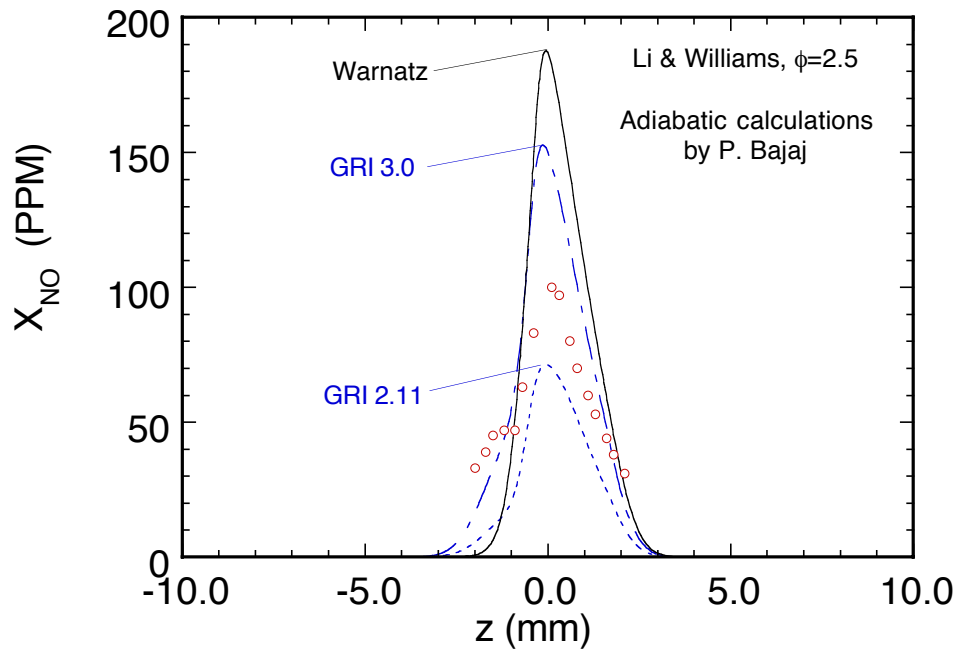
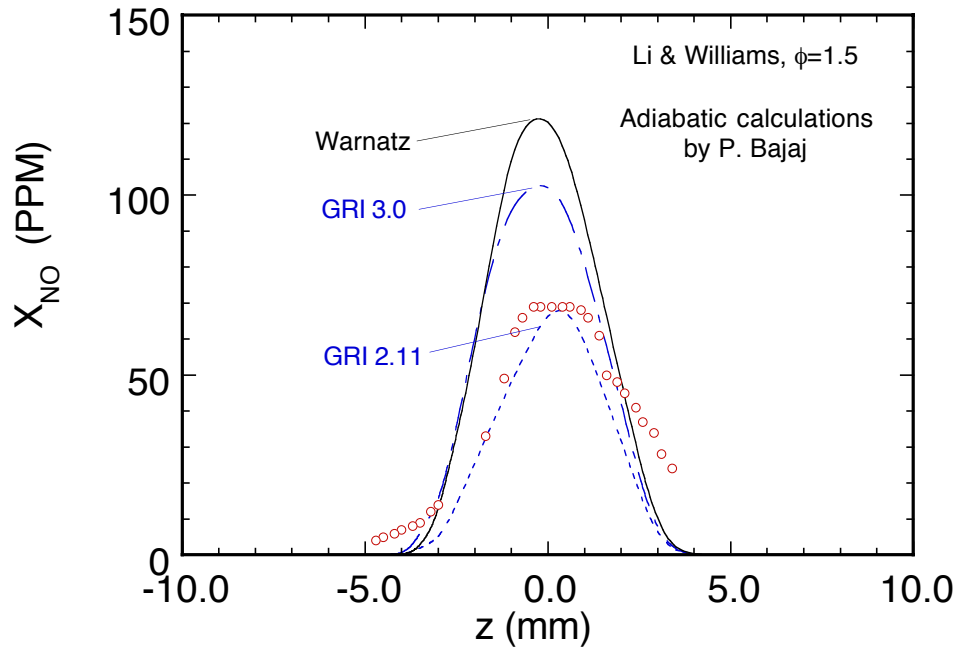


Fig.9: Comparison between measurement and prediction for profiles of NO concentration and temperature with  $\Phi = 3.0$  and strain rate  $a = 50 \text{ s}^{-1}$ .

## Contribution from Bajaj, Gass, Poulidakos, and Puri

(see poster for details)



Comparison of the Li & Williams NO measurements in flames with  $\phi=1.5$  and  $\phi=2.5$  with *adiabatic* calculations, using GRI 2.11, GRI 3.0, and the Warnatz mechanism.

**Contribution from R.P. Lindstedt and M.P. Meyer.**

Please note that the heat loss factor is denoted by  $\beta$  in the captions below. Additional discussion of results and further comparisons of flames will form part of the TNF5 Workshop.

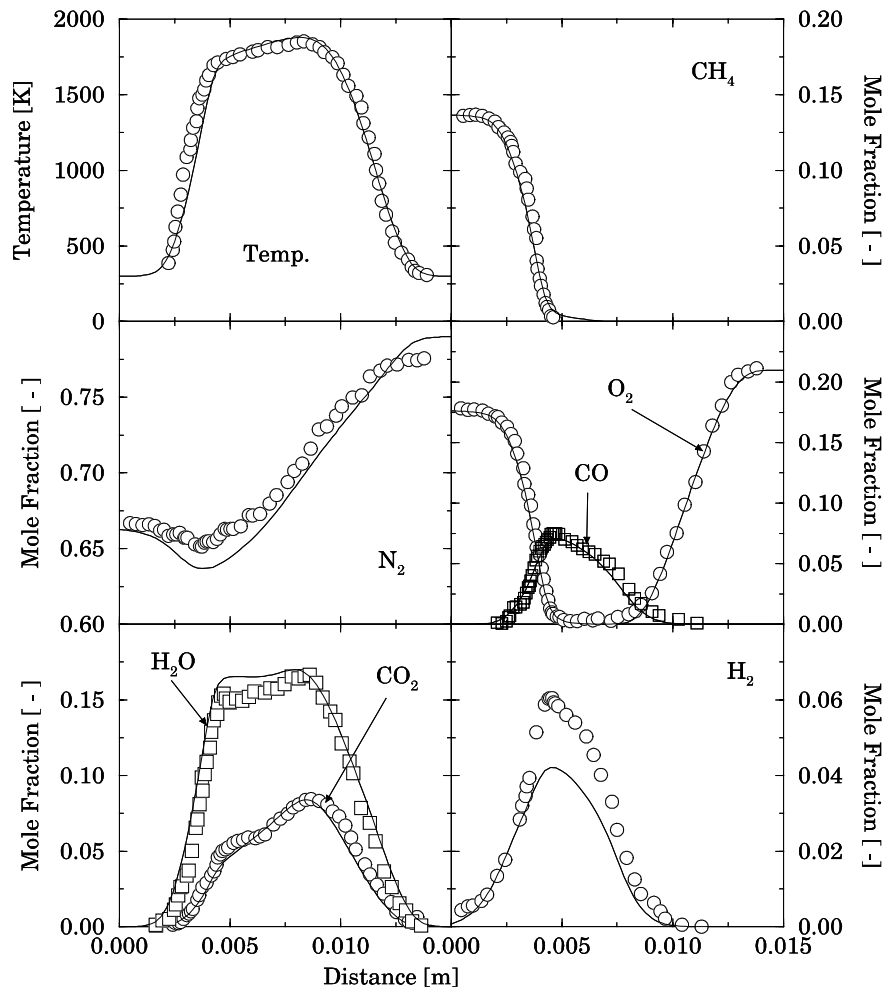


Fig. 1. Flame Structure for the Partially Premixed ( $\phi=1.5$ ;  $a = 30$  /s;  $\beta = 0.10$ ) Flame of Tsuji & Yamaoka (1976). Mechanism of Lindstedt & Skevis (1997).

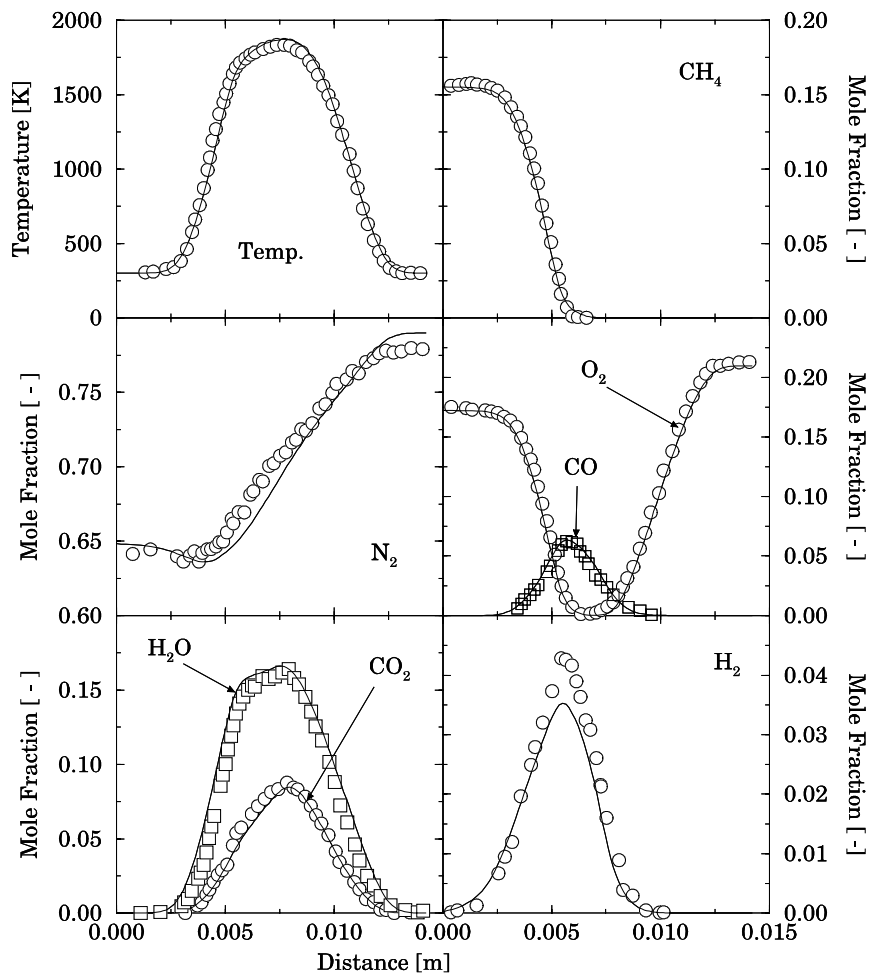


Fig. 2. Flame Structure for the Partially Premixed ( $\phi=1.8$ ;  $a = 30$  /s;  $\beta = 0.10$ ) Flame of Tsuji & Yamaoka (1976). Mechanism of Lindstedt & Skevis (1997).

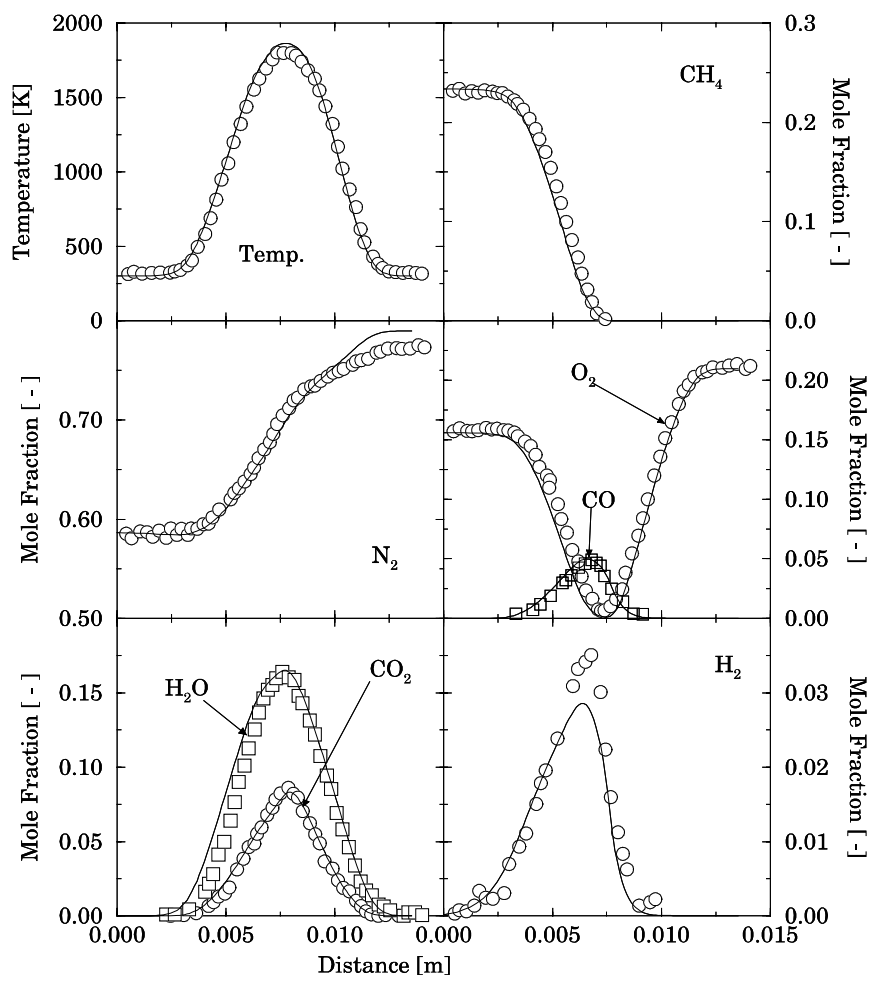


Fig. 3. Flame Structure for the Partially Premixed ( $\phi=3.0$ ;  $a = 30$  /s;  $\beta = 0.10$ ) Flame of Tsuji & Yamaoka (1976). Mechanism of Lindstedt & Skevis (1997).

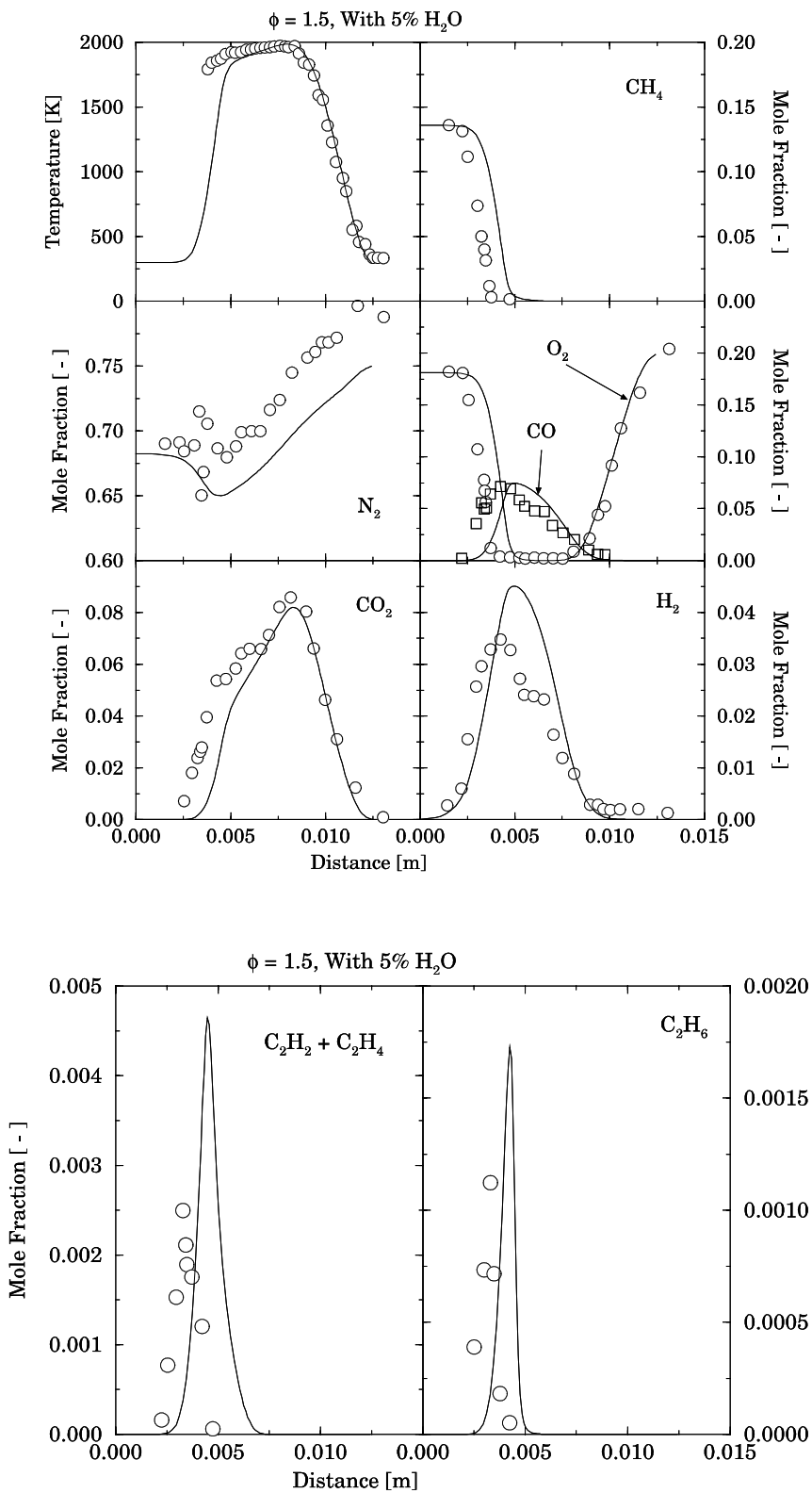


Fig. 4. Flame Structure for the Partially Premixed ( $\phi=1.5$ ;  $a = 50$  /s;  $\beta = 0.04$ ) Flame of Li & Williams (1999). Mechanism of Lindstedt & Skevis (1997) and Juchmann *et al.* (1998).

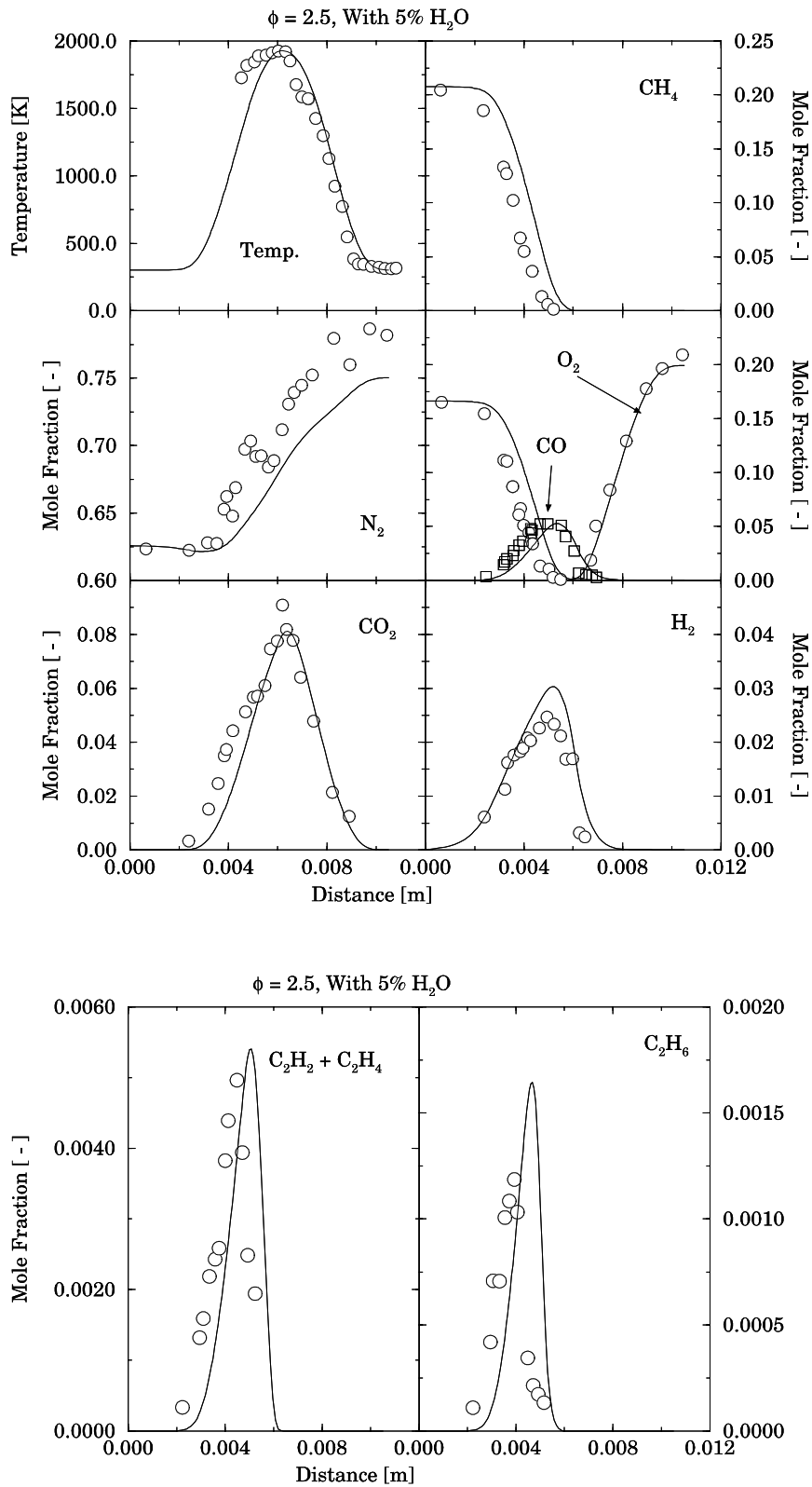


Fig. 5. Flame Structure for the Partially Premixed ( $\phi=2.5$ ;  $a = 50$  /s;  $\beta = 0.04$ ) Flame of Li & Williams (1999). Mechanism of Lindstedt & Skevis (1997) and Juchmann *et al.* (1998).

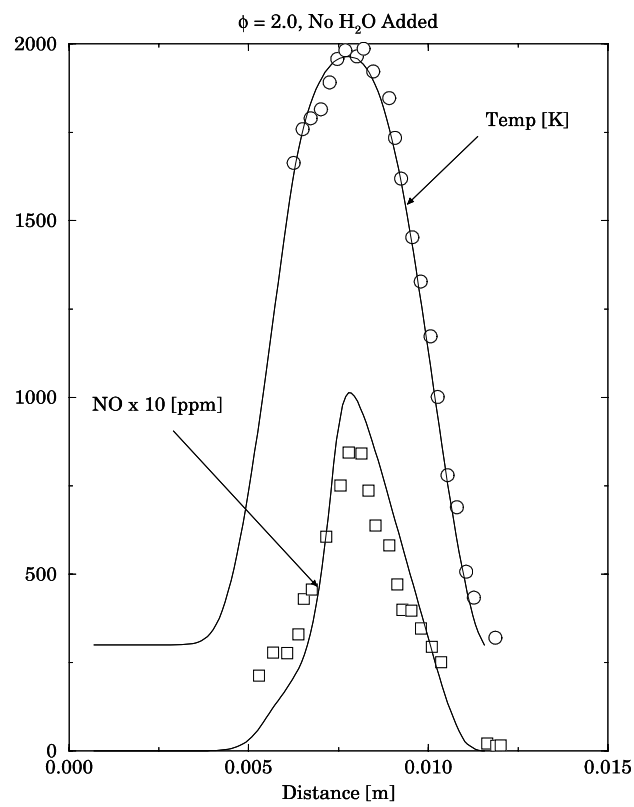
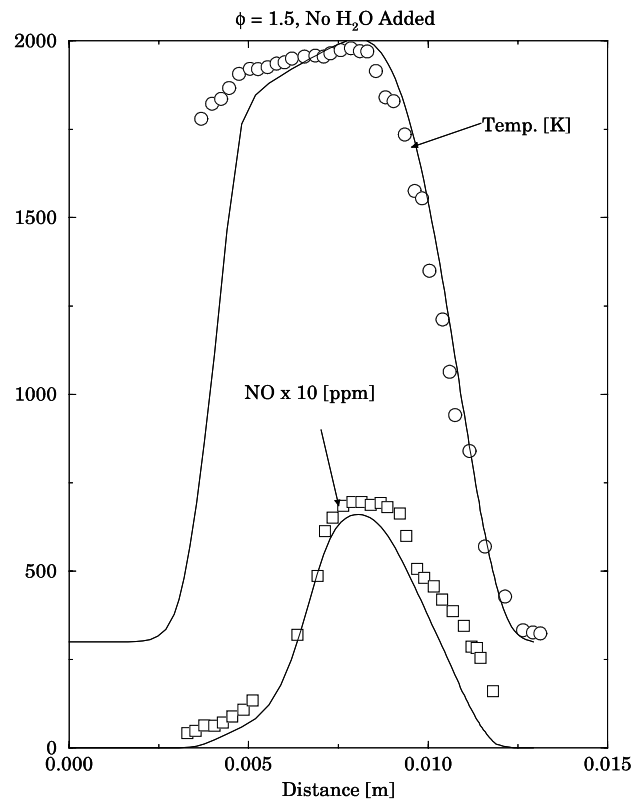


Fig. 6. Flame Structure for the Partially Premixed ( $\phi=1.5$  and  $2.0$ ;  $a = 50$  /s;  $\beta = 0.04$ ) Flame of Li & Williams (1999). Mechanism of Lindstedt & Skevis (1997) and Juchmann *et al.* (1998).

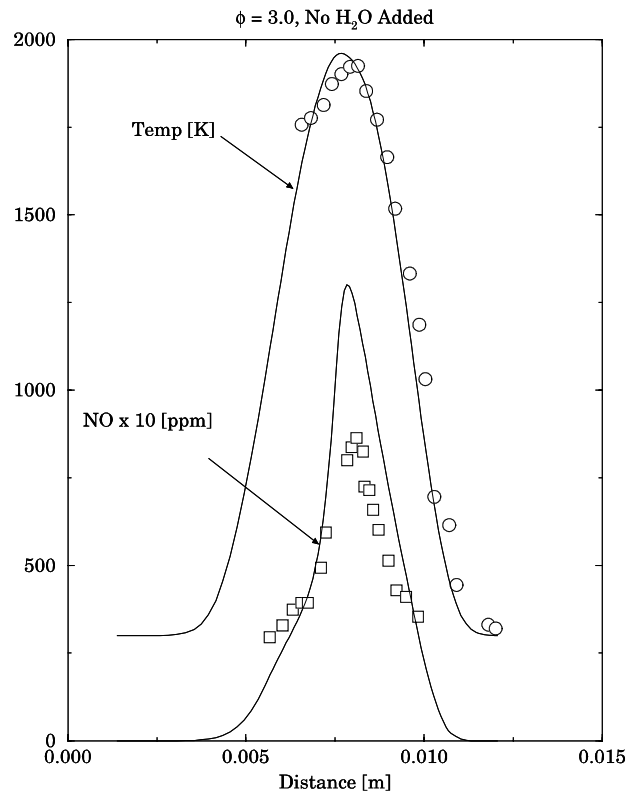
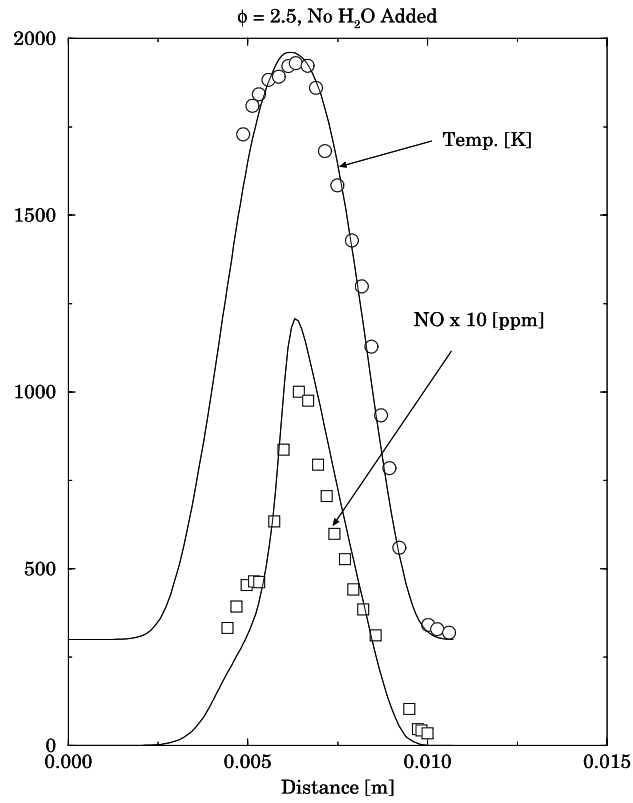


Fig. 7. Flame Structure for the Partially Premixed ( $\phi=2.5$  and  $3.0$ ;  $a = 50$  /s;  $\beta = 0.04$ ) Flame of Li & Williams (1999). Mechanism of Lindstedt & Skevis (1997) and Juchmann *et al.* (1998).

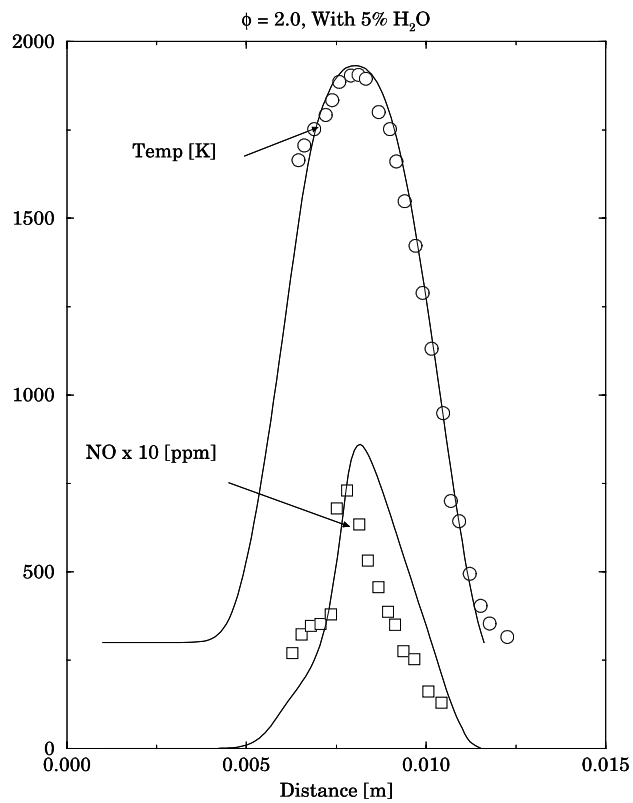
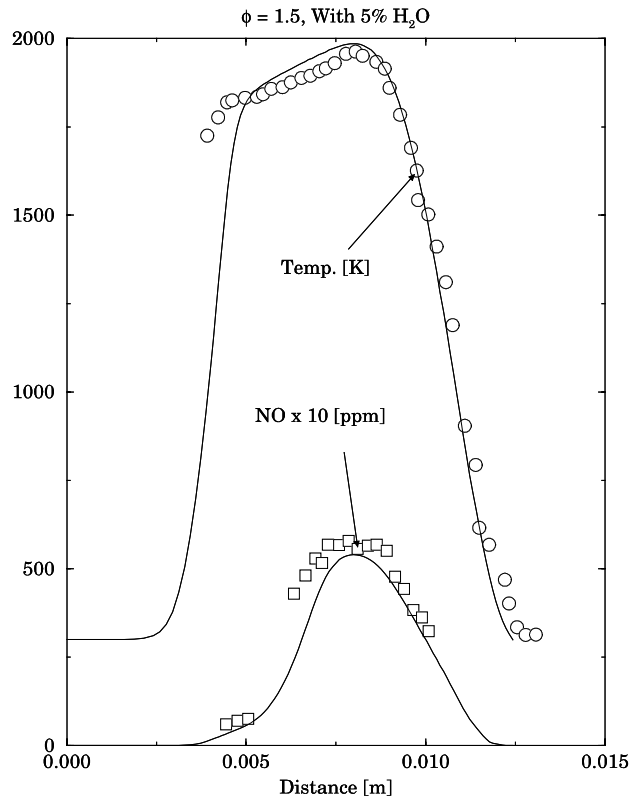


Fig. 8. Flame Structure for the Partially Premixed ( $\phi=1.5$  and  $2.0$ ;  $a = 50$  /s;  $\beta = 0.04$ ) Flame of Li & Williams (1999). Mechanism of Lindstedt & Skevis (1997) and Juchmann *et al.* (1998).

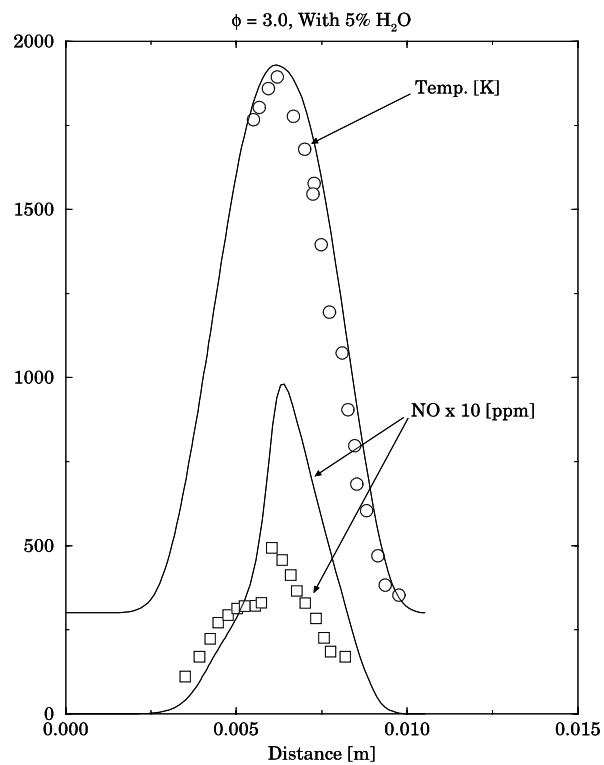
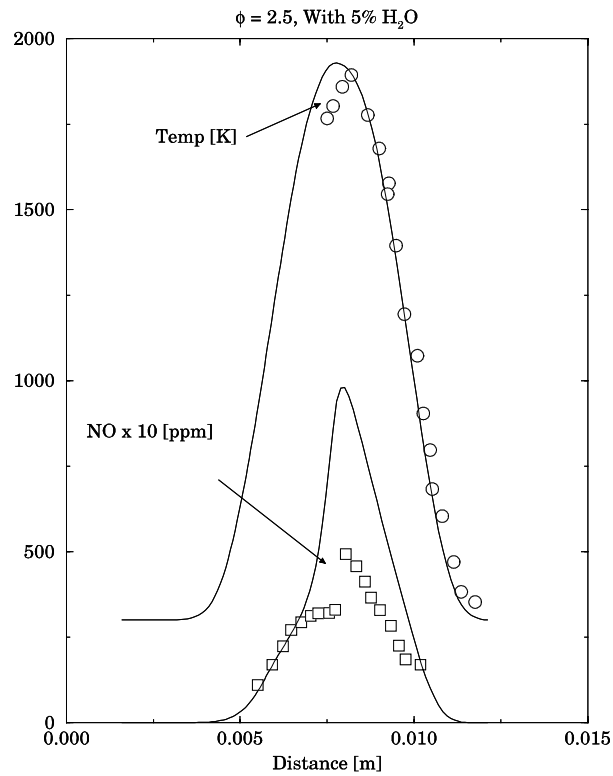


Fig. 9. Flame Structure for the Partially Premixed ( $\phi=2.5$  and  $3.0$ ;  $a = 50$  /s;  $\beta = 0.04$ ) Flame of Li & Williams (1999). Mechanism of Lindstedt & Skevis (1997) and Juchmann *et al.* (1998).

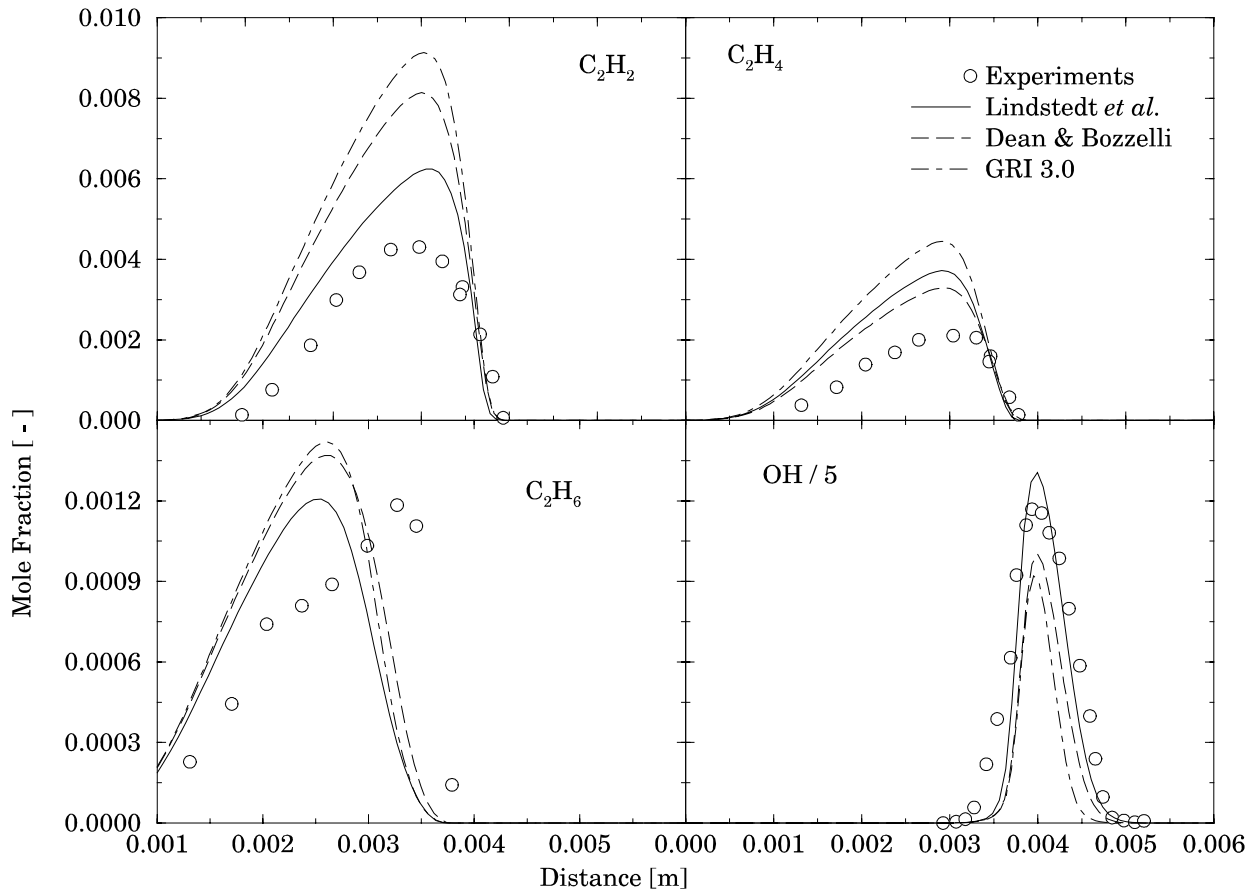


Fig. 10. Flame Structure for the Diffusion Flame ( $a = 100$  /s;  $\beta = 0.00$ ) Flame Tsuji and Yamaoka (1971). Mechanisms of Lindstedt & Skevis (1997), Bozzelli & Dean (1999) and GRI Mech. 3.0 (1999).

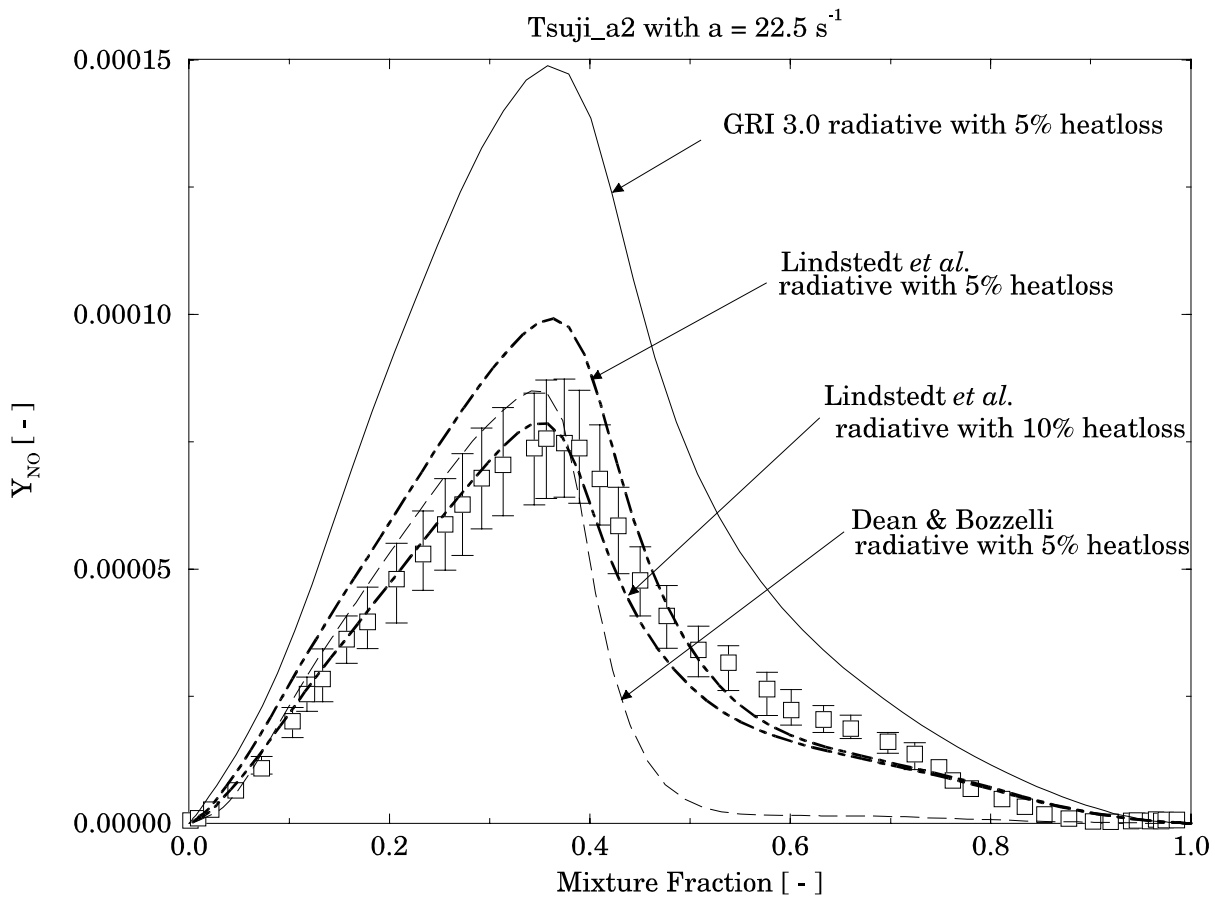


Fig. 11. Flame Structure for the Partially Premixed ( $\phi=2.2$ ;  $\beta = 0.05$  and  $0.10$ ;  $a = 22.5 \text{ /s}$ ) Flame of Barlow & Frank (2000). Mechanism of Lindstedt & Skevis (1997) and Juchmann *et al.* (1998), Bozzelli & Dean (1999) and GRI Mech. 3.0 (1999).



## **Chemistry Issues in the C/H/N/O System for C<sub>1</sub>/C<sub>2</sub> Fuels**

TNF 5 Workshop, Delft, Holland, July 26 - 28, 2000.

Peter Lindstedt, Department of Mechanical Engineering, Imperial College, London.

Part of the current presentation is based on joint work with PCI Heidelberg [1,2] and University of Michigan [2].

[1] Juchmann *et al.*, 27<sup>th</sup> Symp. (Int.) on Combust 1998/pp. 469-476.

[2] Sick *et al.* 27<sup>th</sup> Symp. (Int.) on Combust. 1998/pp. 1401-1409.

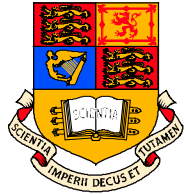


## Background

During successive TNF Workshops the issue of what constitutes an appropriate approximation of the chemistry for diffusion flames and rich partially premixed flames has arisen.

The current presentation describes a set of computations performed in order to ascertain the performance of mechanisms for a wide range of conditions.

Some key differences between mechanisms are outlined and examples are given for mechanisms from GRI (2.11 and 3.0), Bozzelli & Dean, Warnatz and Lindstedt & co-workers.



## Chemistry Background

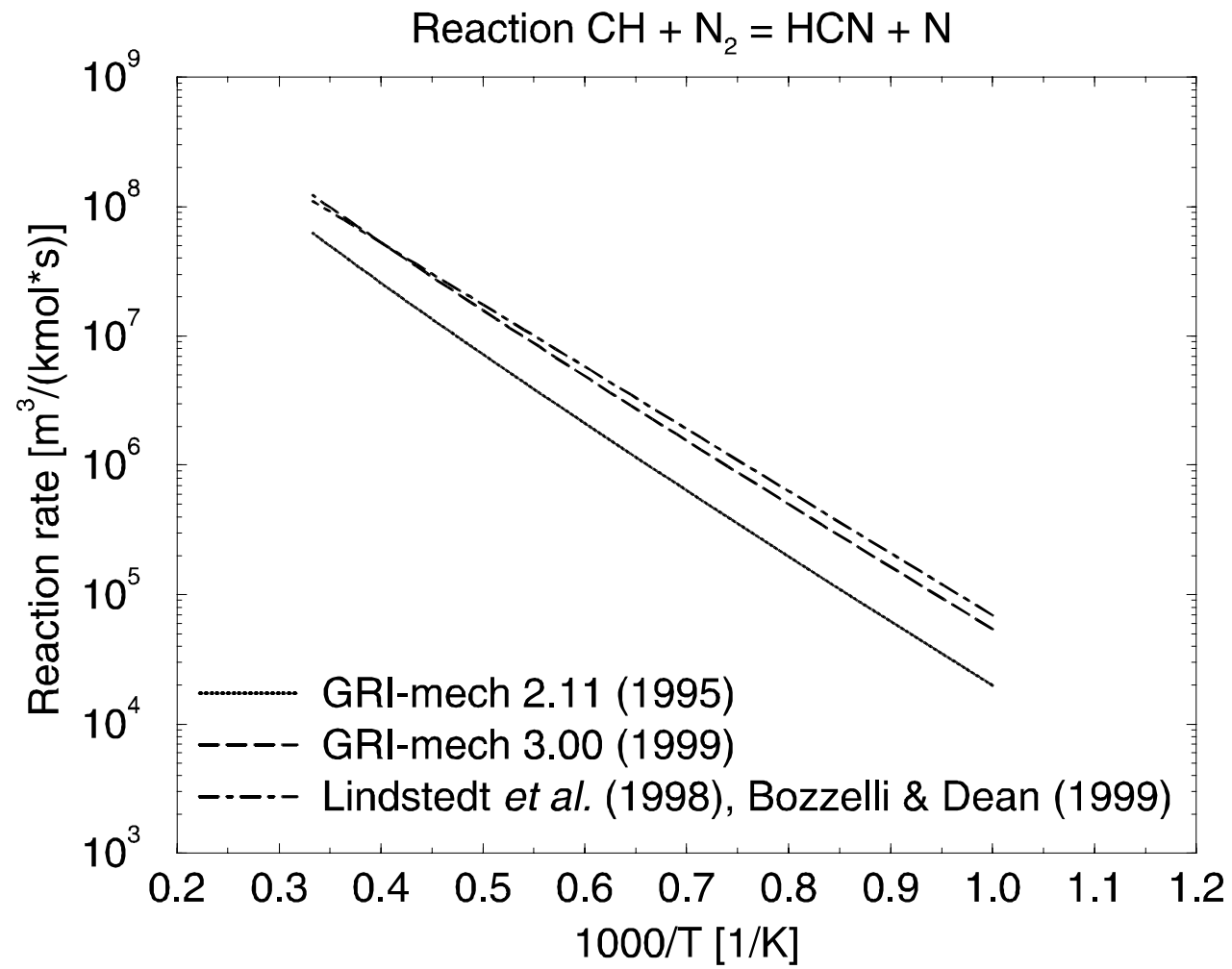
Particular issues include the balancing of abstraction, addition, and addition/decomposition reactions. The formation/destruction of oxides of nitrogen will also be covered and along with the coupling to the CH and C chemistry.

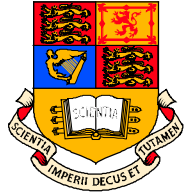
The base case mechanism is that by Lindstedt and Skevis (1997) with the modifications outlined by Lindstedt (1998) and Lindstedt & co-workers (1998).

From a TNF perspective it may be noted that the mechanism has been comprehensively validated covering both premixed and diffusion flame conditions.

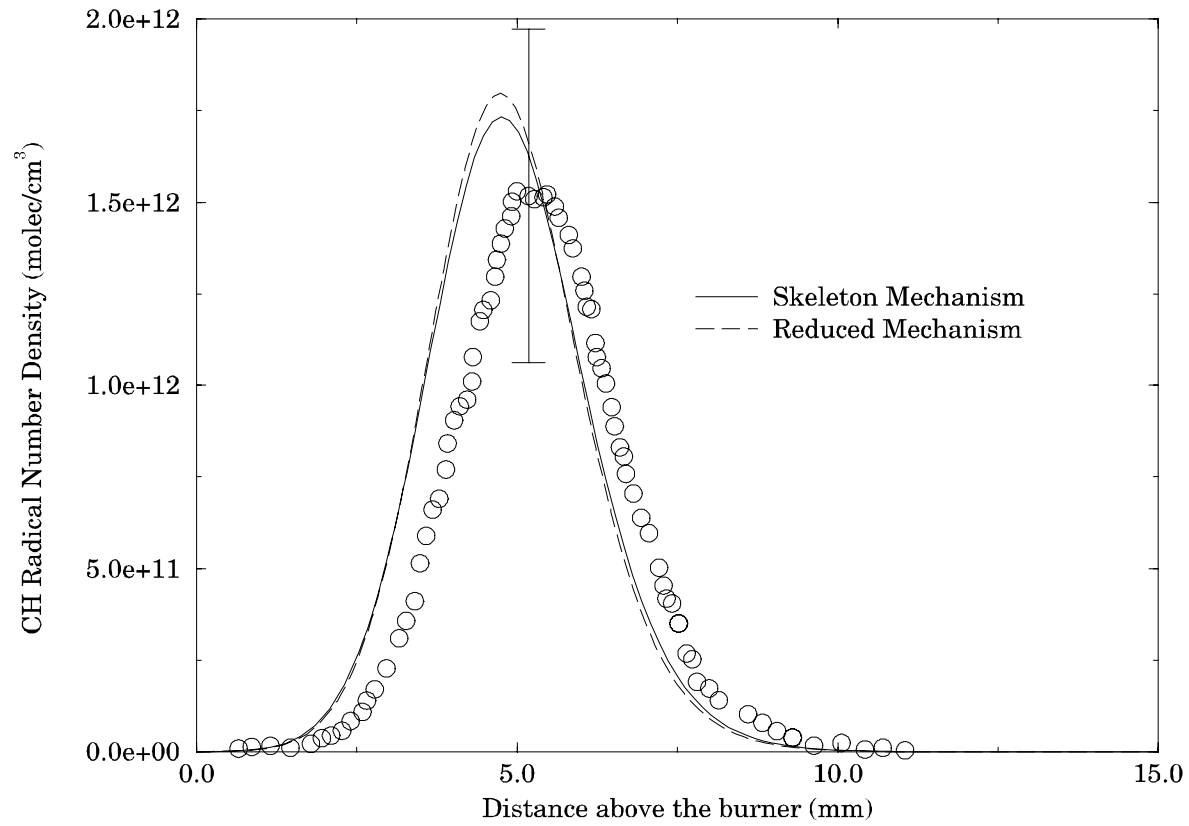


# Prompt Channel



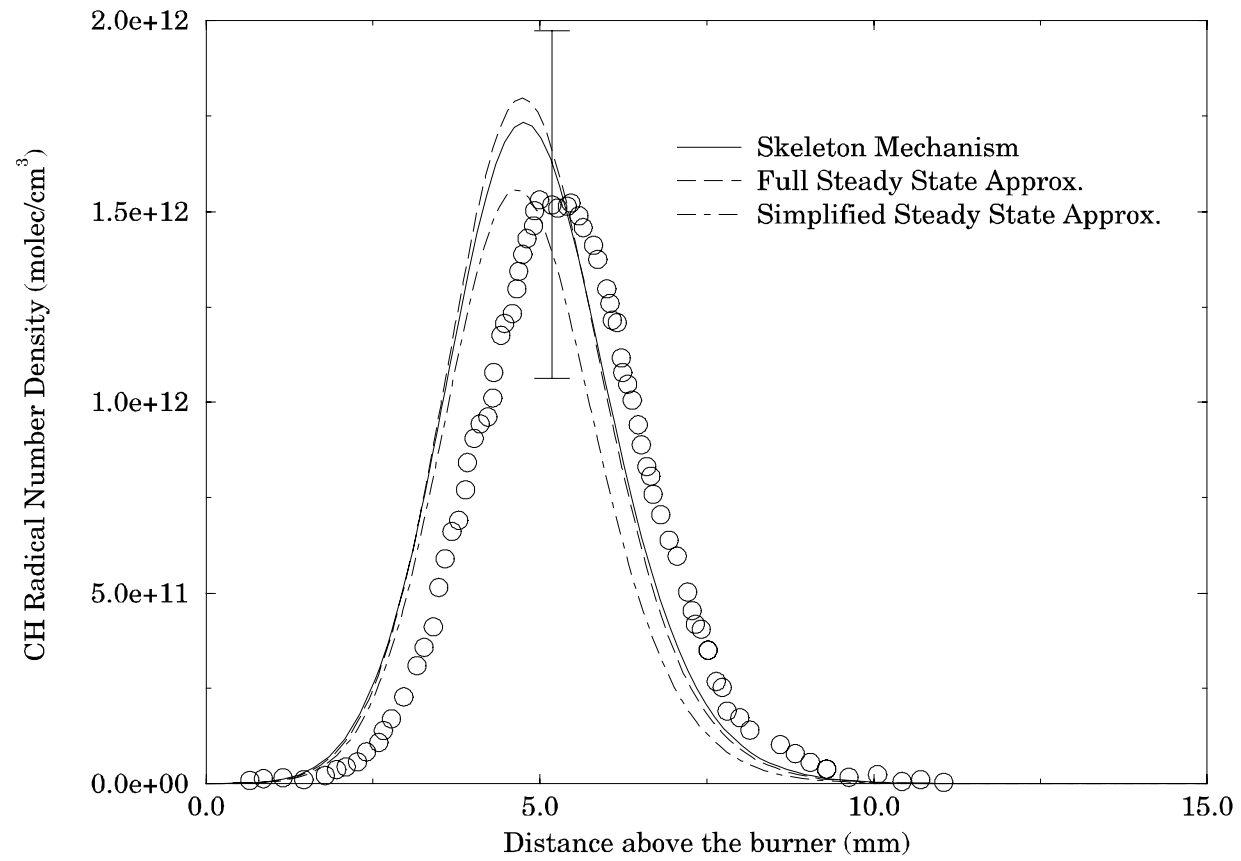


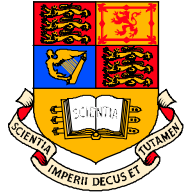
# Flame investigated by Luque *et al.* (1996)



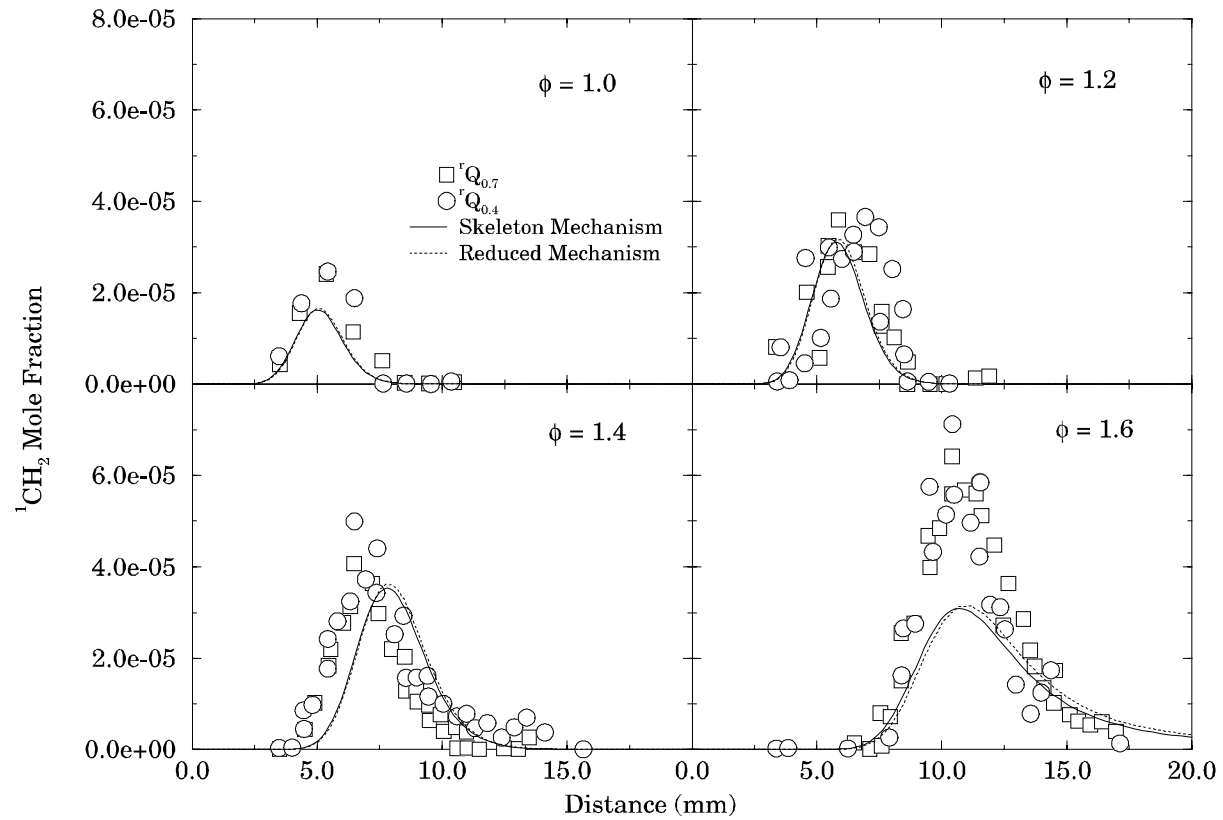


# Flame investigated by Luque *et al.* (1996)



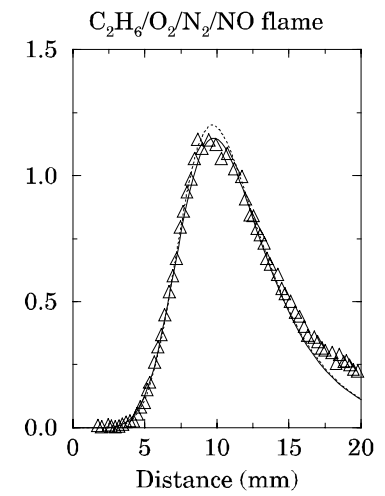
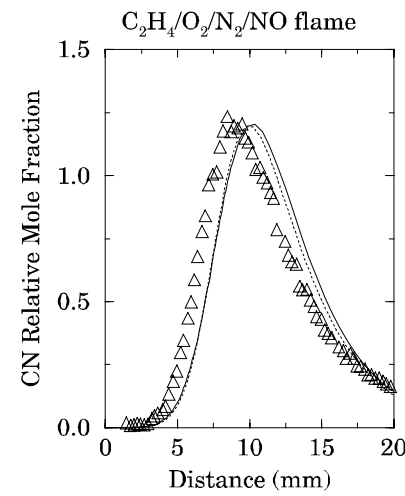
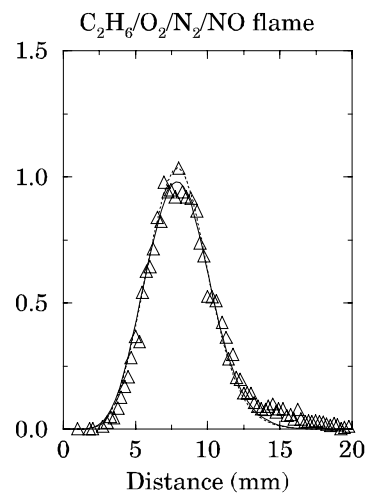
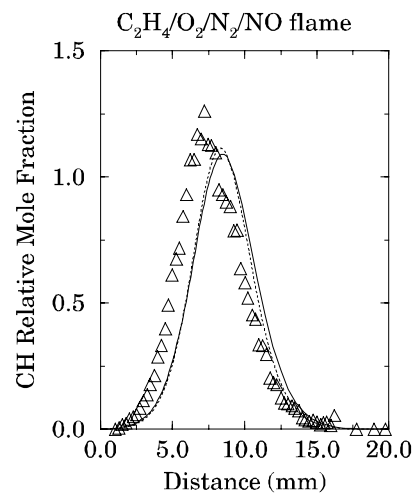
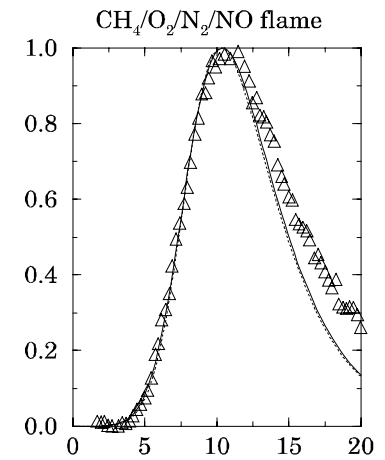
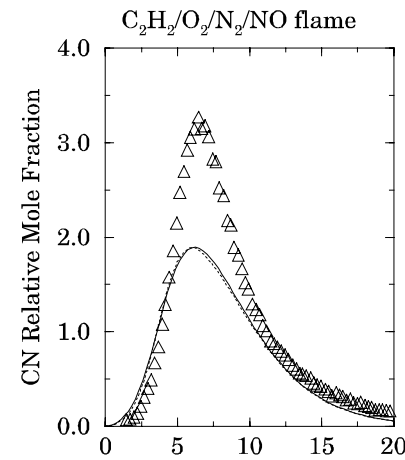
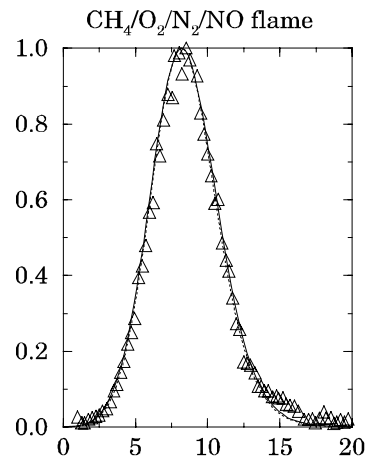
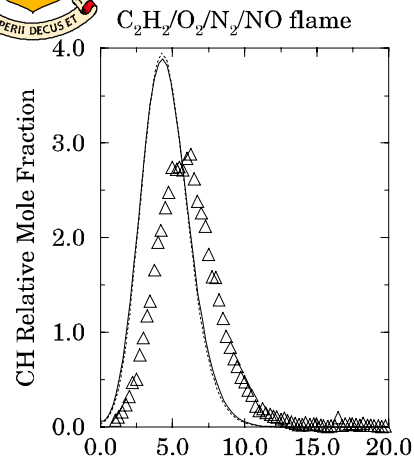


# CH<sub>4</sub> Flames Investigated by Mclroy (1998)



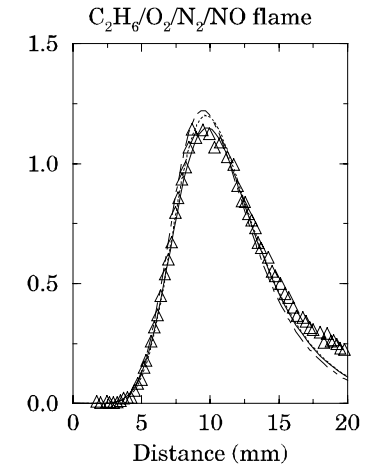
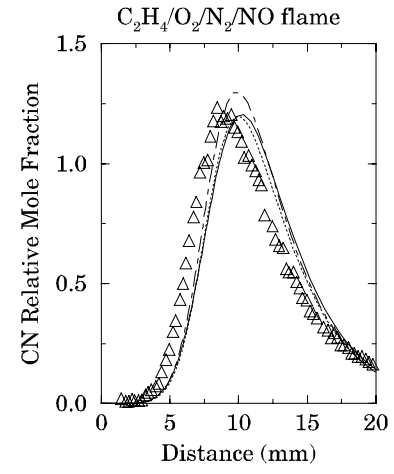
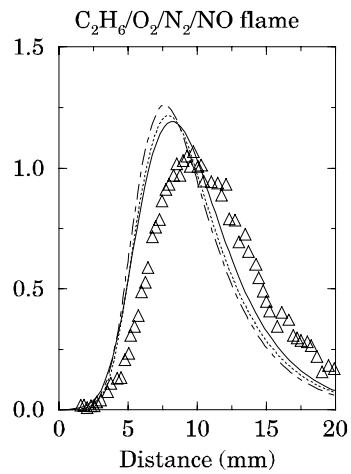
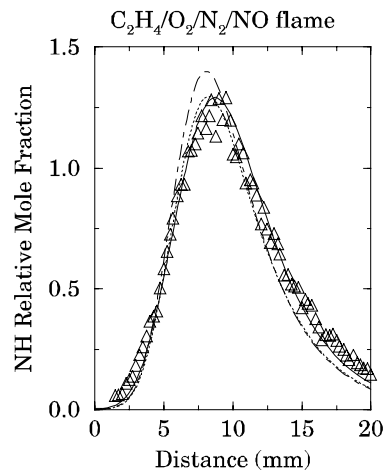
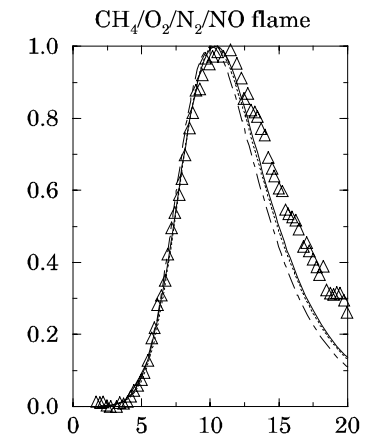
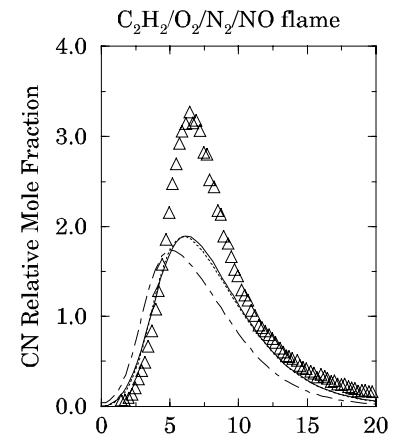
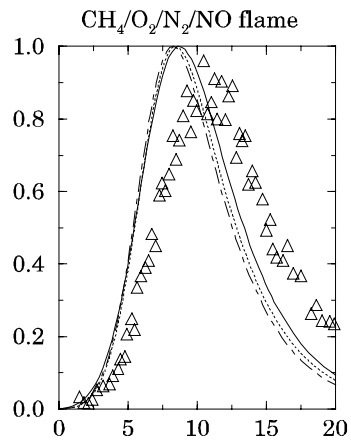
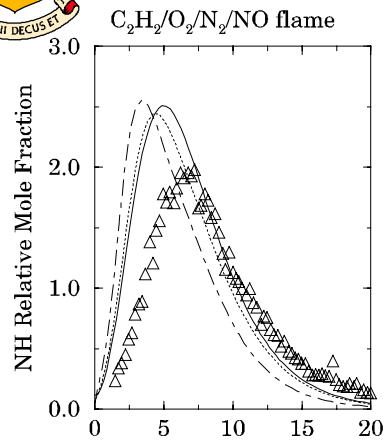


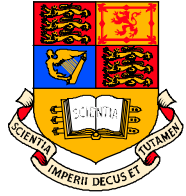
# Flames from Williams and Pasternack (1997)



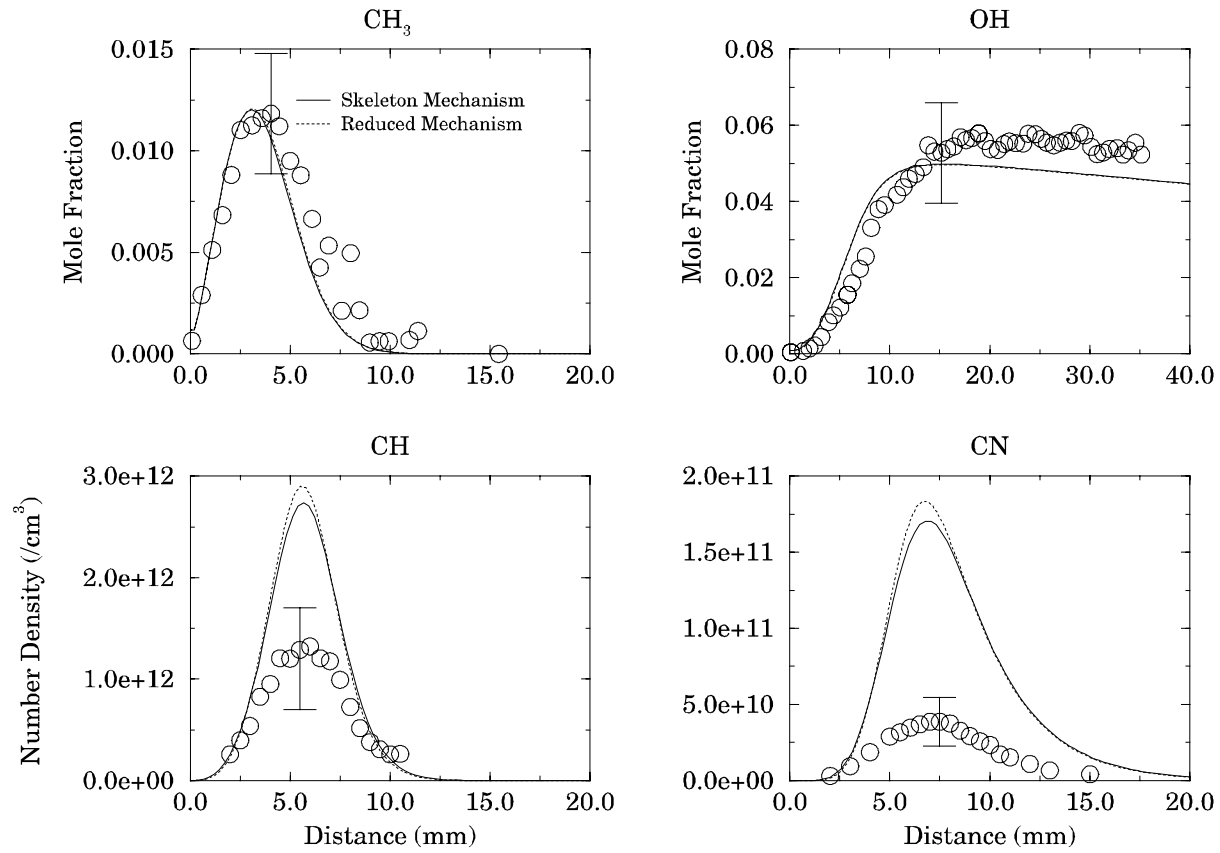


# Flames from Williams and Pasternack (1997)



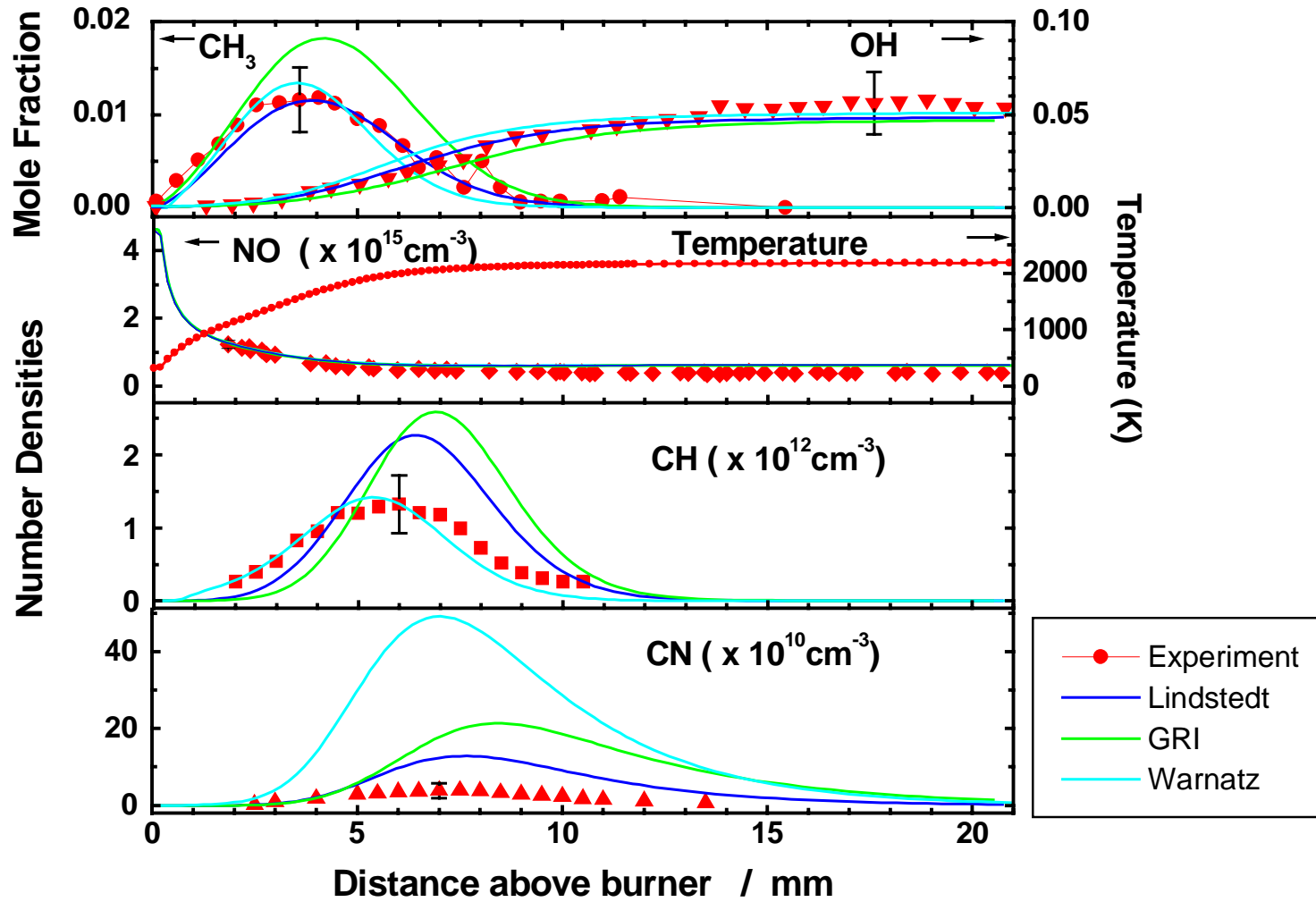


# Heidelberg Flame (Juchmann *et al.* 1998)



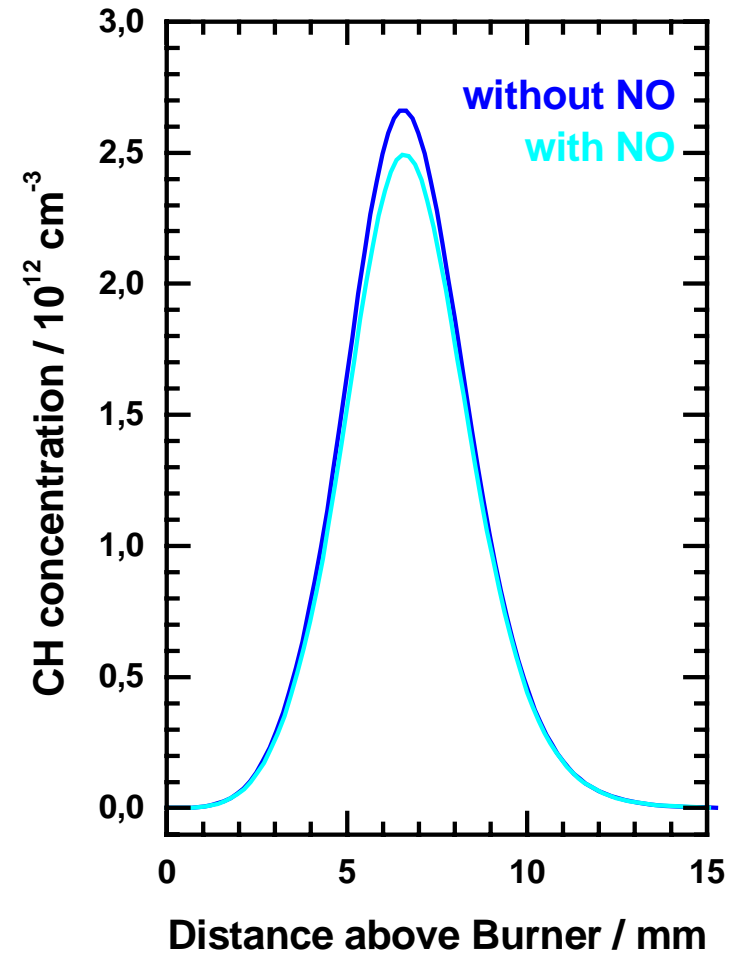
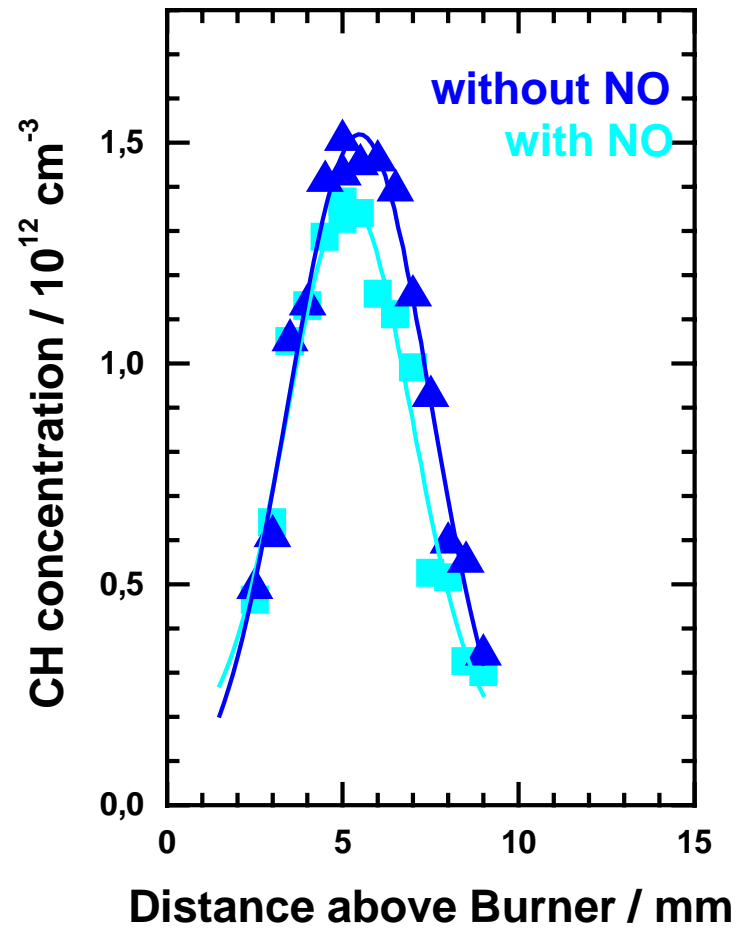


# Juchmann *et al.* 1998; Sick *et al.* 1998



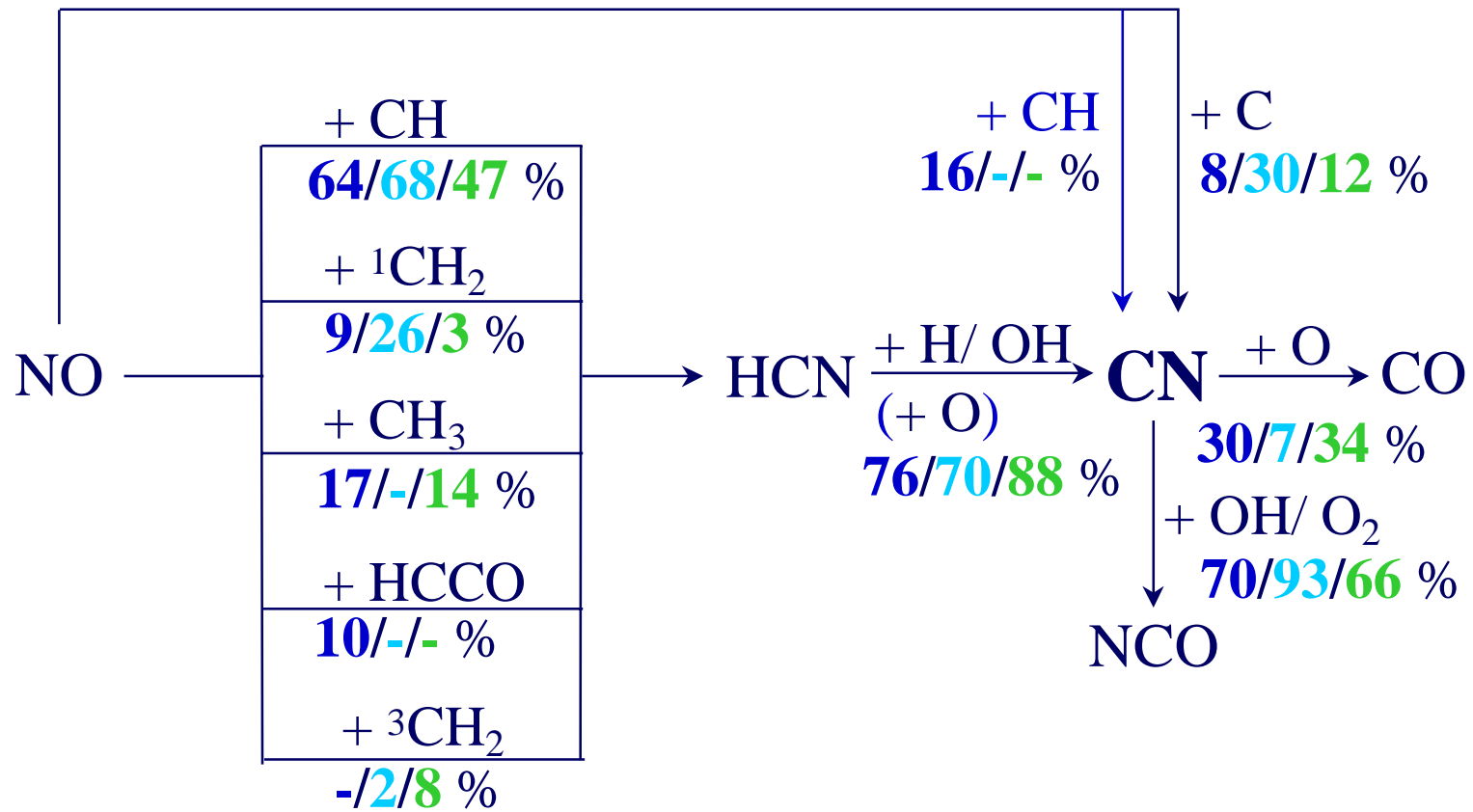


# Chemistry of Flames





# Chemistry of Flames





# Chemistry of Flames



All three mechanism adopt a similar total rate expression.

**Lindstedt** : Branching of the products

**HCN:CHO:NCO:NH:CN**

is **48:26:18:5:3** % (*cf.* Dean and Bozzelli).

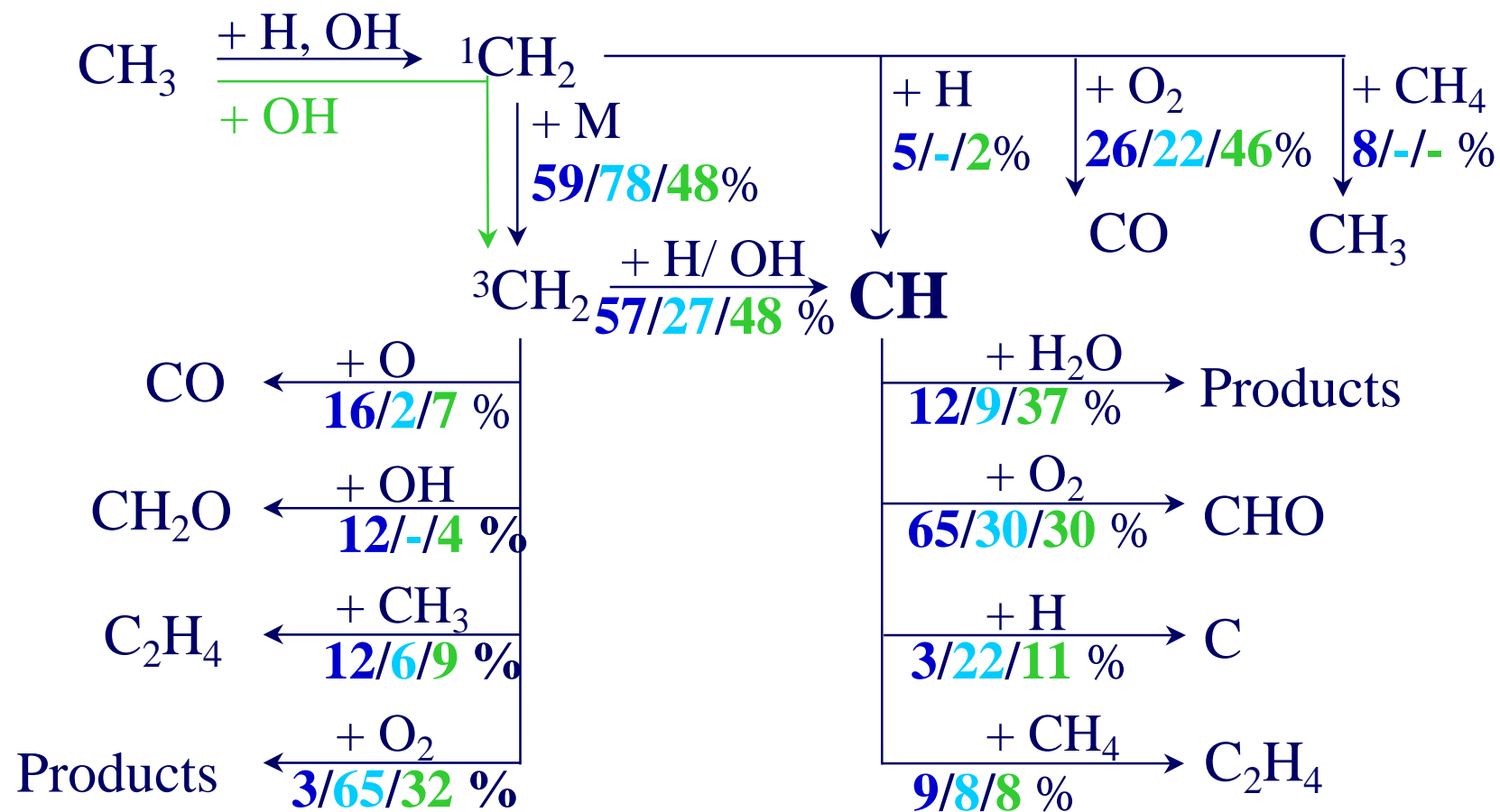
**GRI-Mech** : Branching of the products **HCN:CHO:NCO**

is **50:30:20** %.

**Warnatz** : Only **HCN + O** is assigned as a product channel.  
(**100** %)



# Chemistry of Flames





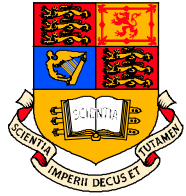
# Chemistry of Flames



**Lindstedt** : Mechanism features the experimental determination by Dombrowsky and Wagner (1992) obtained in the temperature range 1000 to 1800 K.

**GRI-Mech. 2.11** and **Warnatz** : Mechanisms features a rate expression determined by Vinckier and Debruyne (1979) in the temperature range 295 to 600 K.

The former determination is in excess of one order of magnitude slower at 1800 K than that of Vinckier and Debruyne (1979).



# Chemistry of Flames

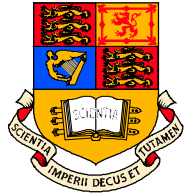


All three mechanism feature rate expressions based on the work by Zabarnick *et al.* (1986) in the temperature range 297 - 670 K.

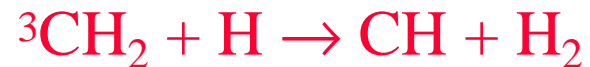
**Lindstedt** : The product is specified as an adduct ( $\text{CH}_2\text{OH}$ ).

**GRI-Mech** : The rate constant is assigned a value 3 times higher than that measured. Products are specified as  $\text{CH}_2\text{O} + \text{H}$ .

**Warnatz** : Two product channels ( $\text{CH}_2\text{O} + \text{H}$  and  ${}^3\text{CH}_2 + \text{OH}$ ) are specified with a branching ratio of 4:1.



# Chemistry of Flames



**Lindstedt** : Adopted a temperature independent rate from Böhland and Temps (1984).

**GRI-Mech**: Features a rate based on the upper limit expression of Zabarnick *et al.* (1986), which was subsequently reduced by a factor of 3. The final expression gives a rate similar to that used by Lindstedt.

**Warnatz** : Adopted a rate constant (CEC) which is a factor of 10 slower than those used in the other mechanisms.



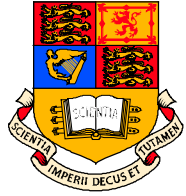
# Chemistry of Flames



**Lindstedt:** Adopted rate expression from the high temperature measurements of Markus *et al.* (1996).

**GRI-Mech. 2.11** and **Warnatz:** Adopted a rate constant from the room temperature measurements of Berman *et al.* (1982). This rate is a factor of 2 slower than that used by Lindstedt.

Recent experimental work of Röhrig *et al.* (1997) at high temperatures (2200 - 2600 K) supports the determination of Markus *et al.* (1996).



# Chemistry of Flames



**Lindstedt** adopted a rate expression from Grebe and Homann (1982) which is a factor of 3 slower than that used by **GRI-Mech. 2.11** and **Warnatz**.

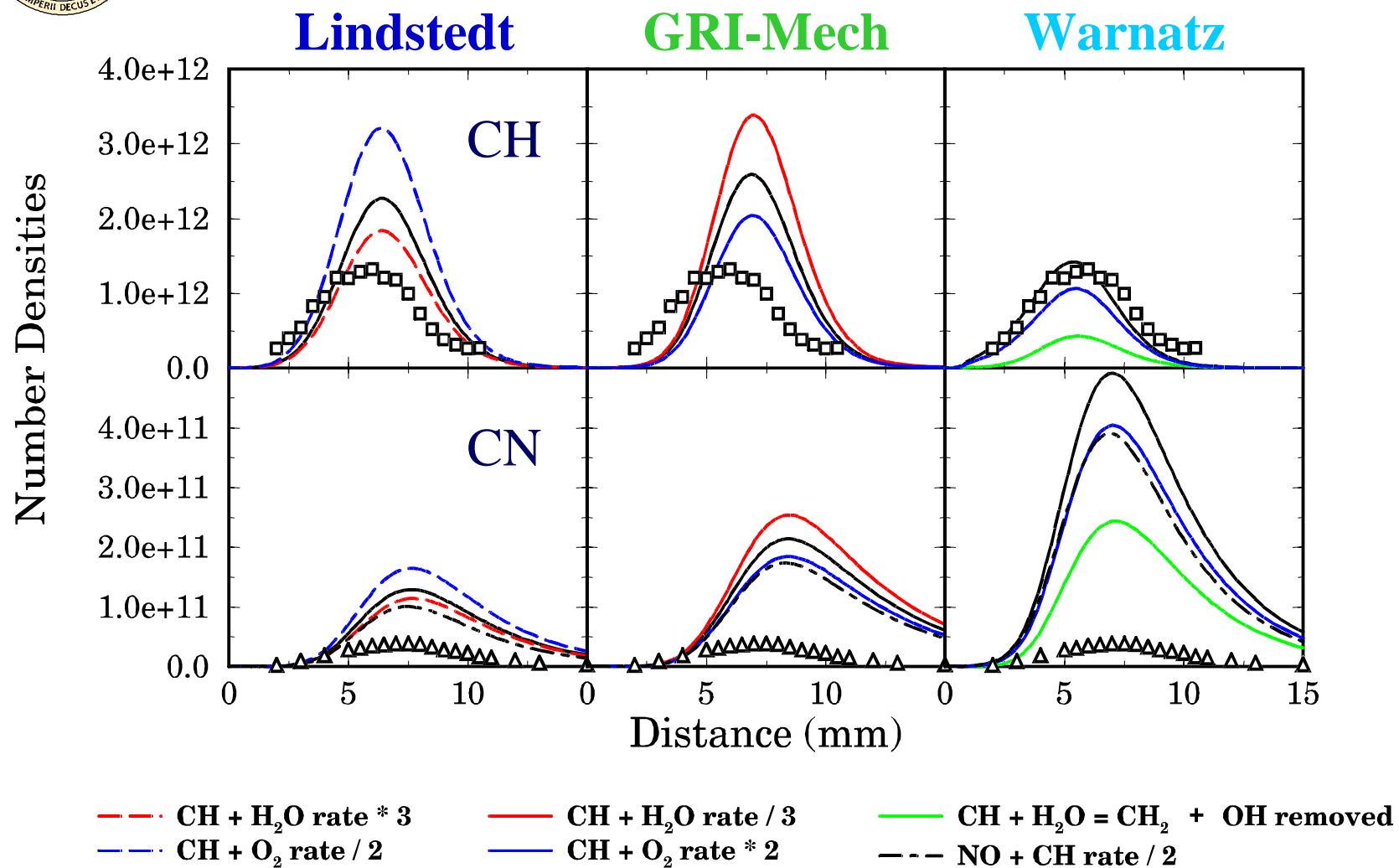


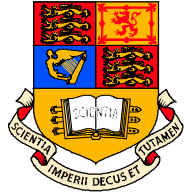
**GRI-Mech** and **Lindstedt** : Adopted rate constants from the work of Dean *et al.* (1991) with two product channels (CN + O and N + CO) specified.

**Warnatz** : Specified CN + O as the only channel.



# Chemistry of Flames





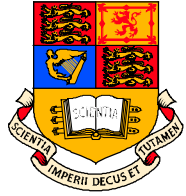
# Diffusion and Partially Premixed Flames

The partially premixed flames of Tsuji and Yamaoka (1976).

The data sets produced by Li and Williams (1999).

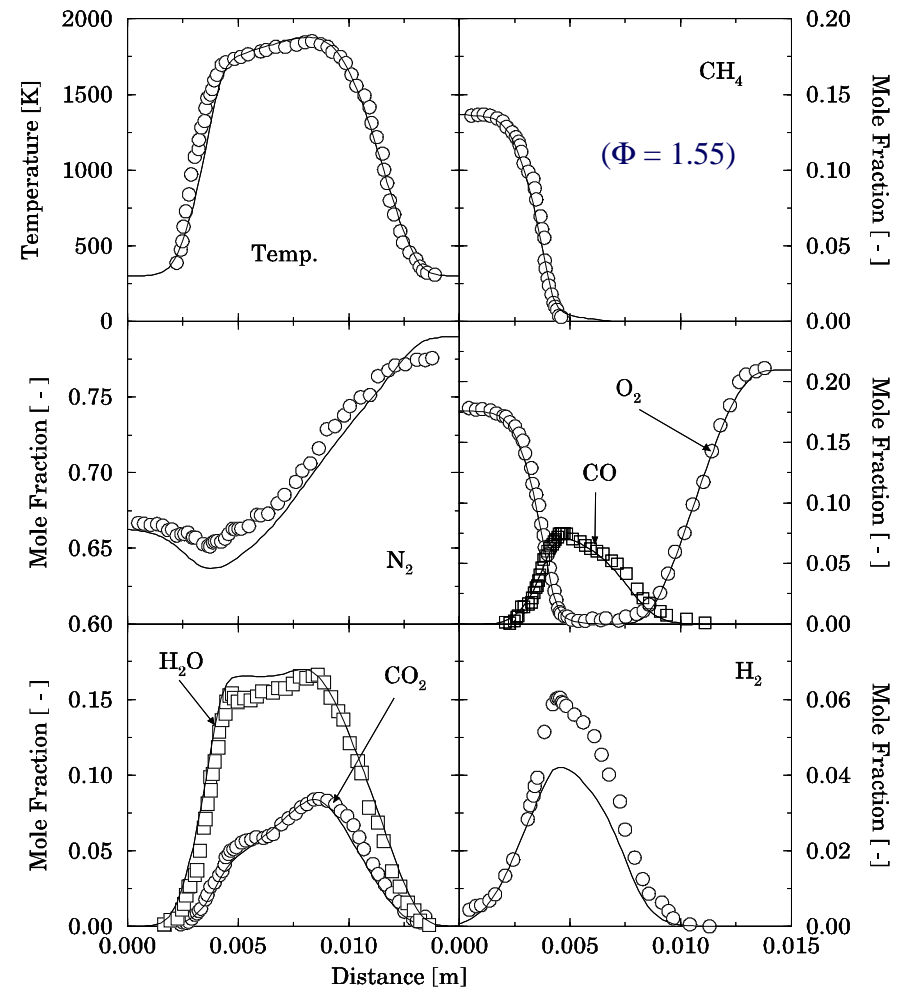
The diffusion flame of Tsuji and Yamaoka (1971).

The data sets of Barlow and Frank (2000).



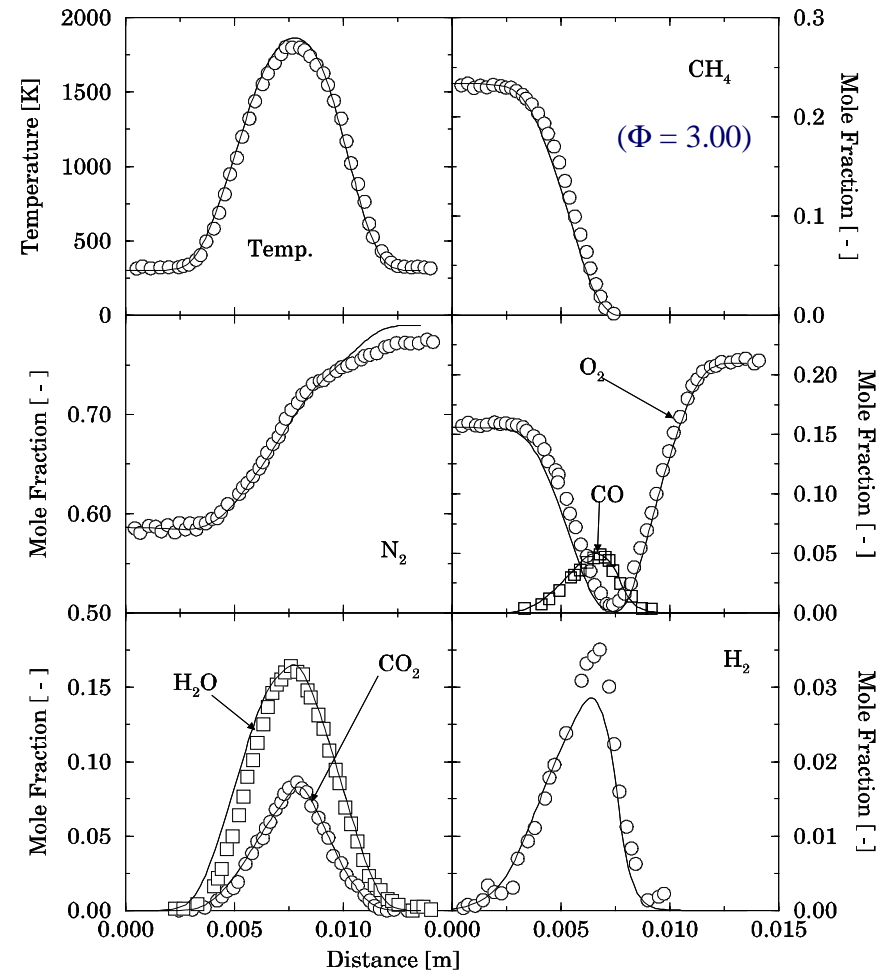
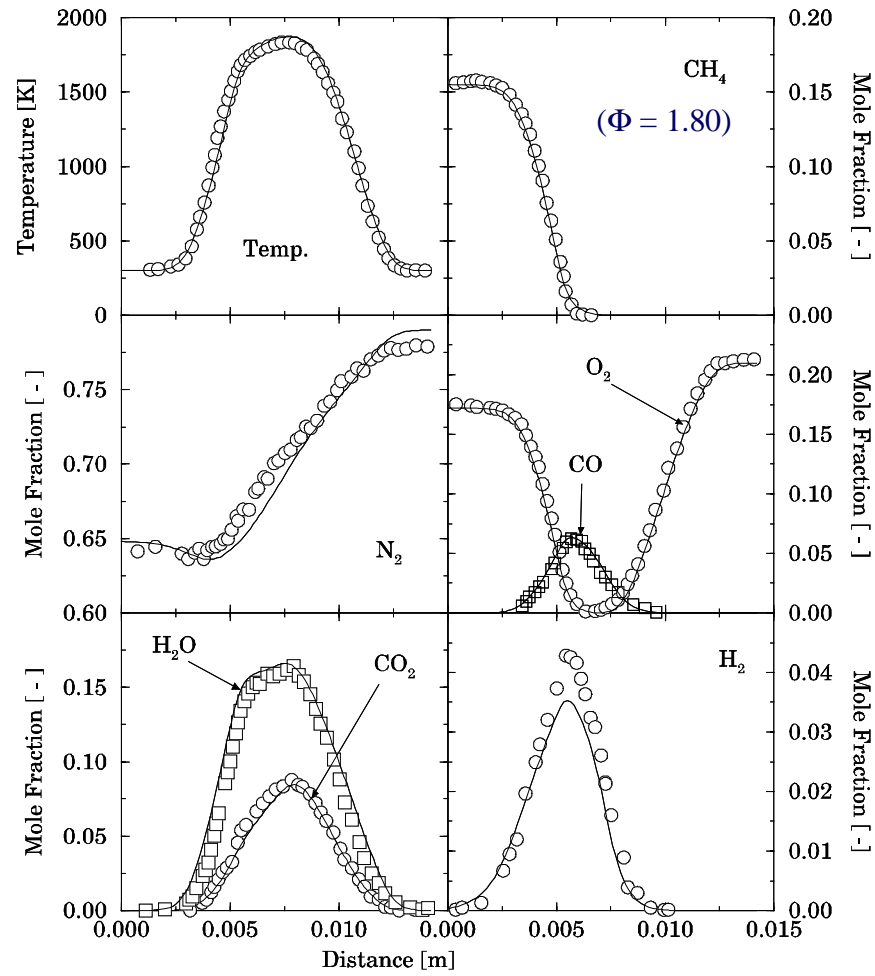
# Partially Premixed Flames ( $\Phi = 1.55, 1.80$ & $3.00$ )

## Tsuji & Yamaoka (1976)



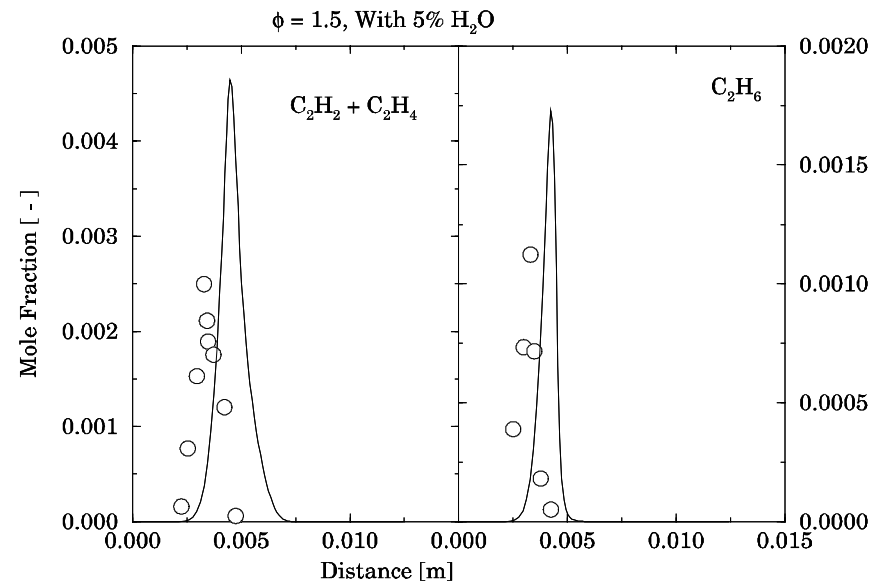
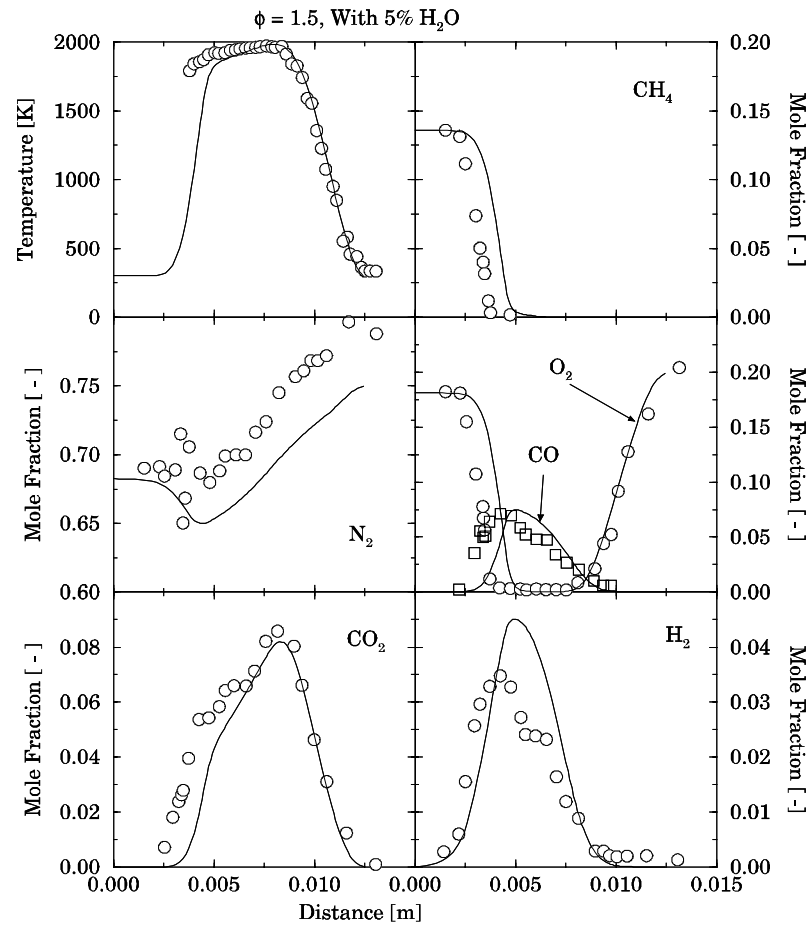


# Tsuji & Yamaoka (1976)



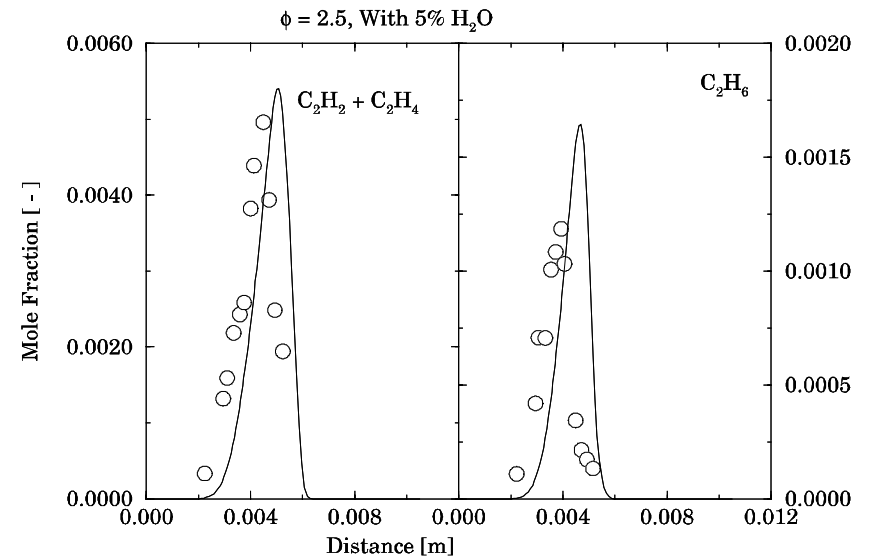
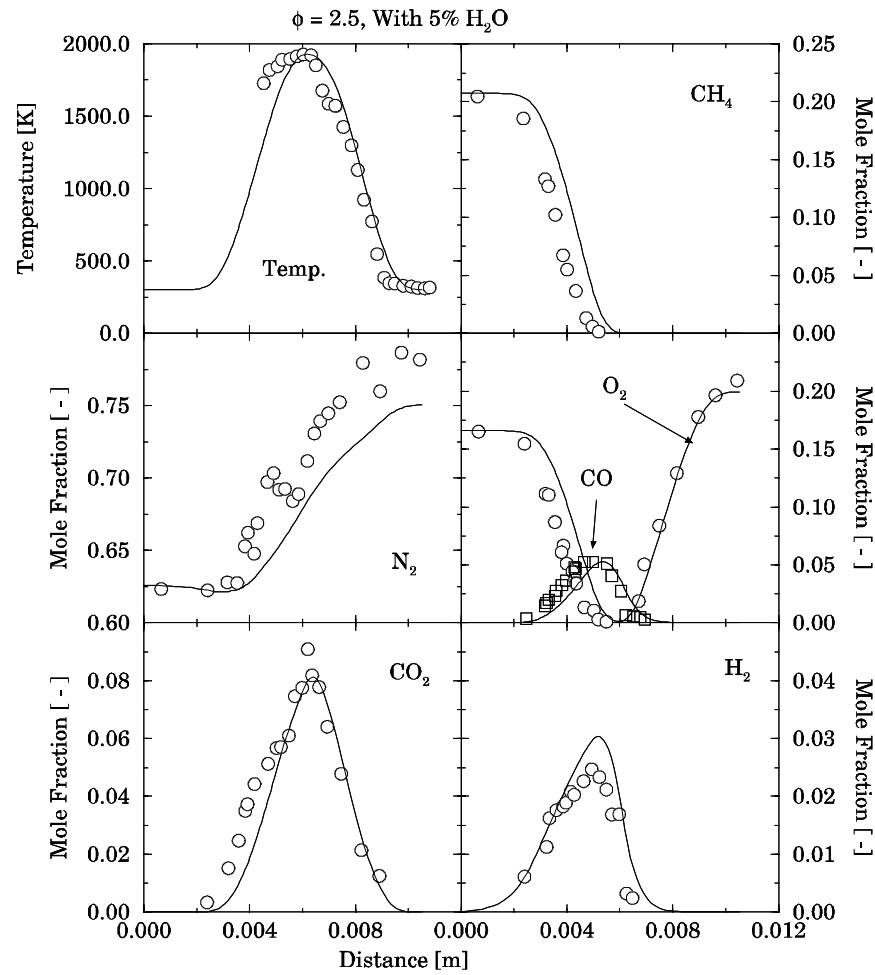


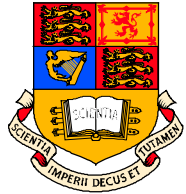
# Li & Williams (1999)



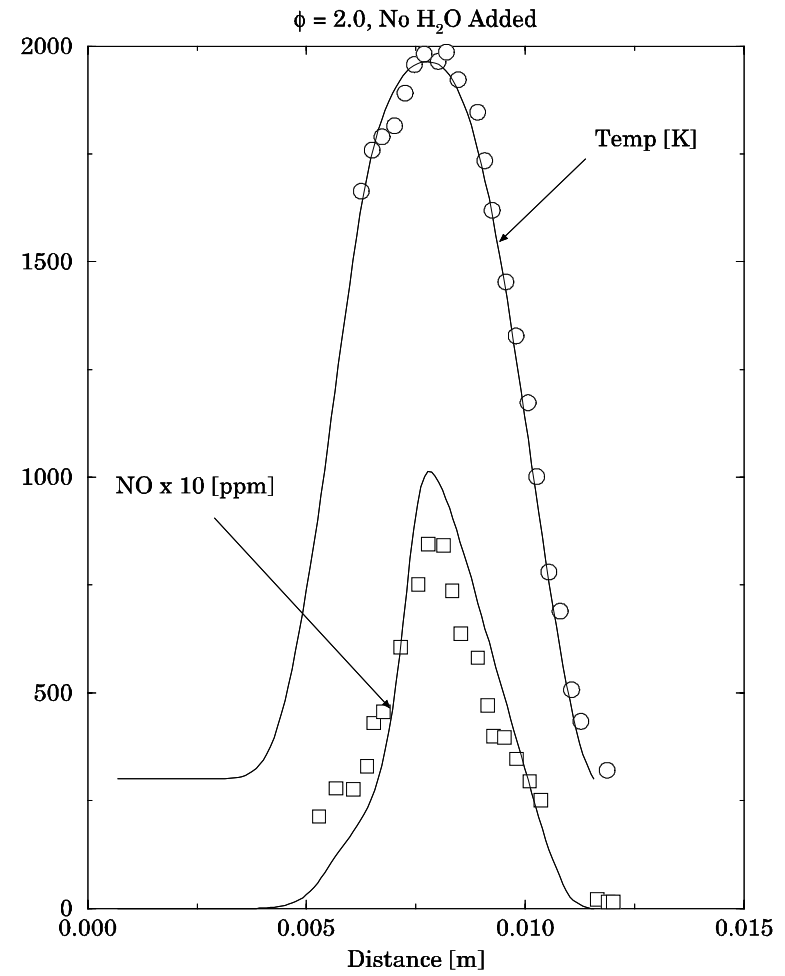
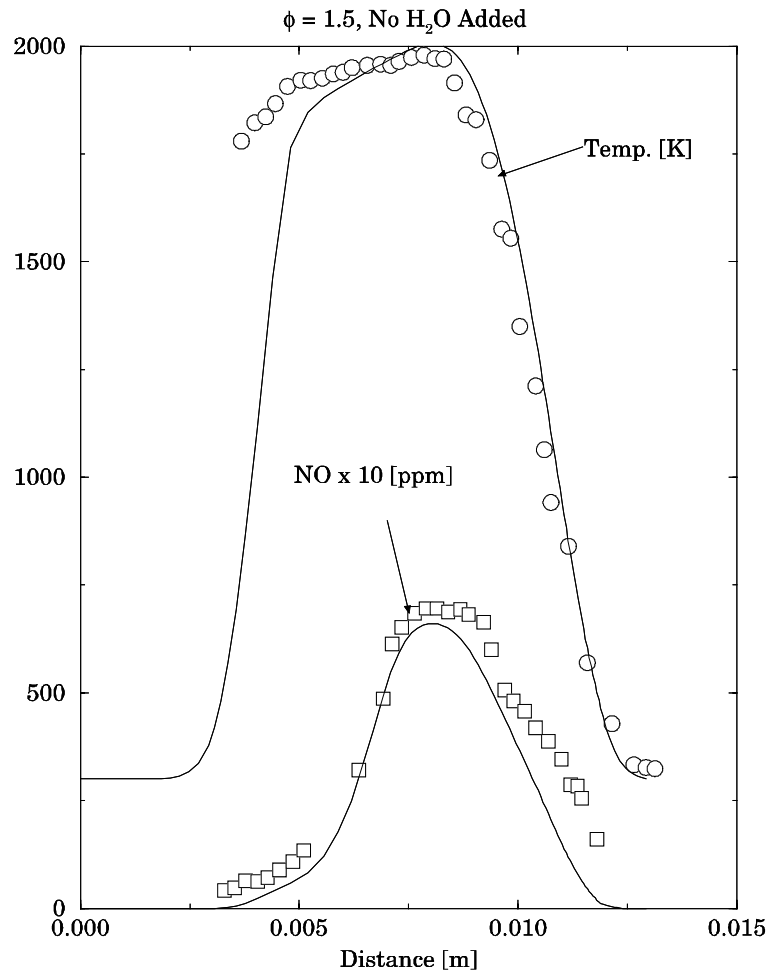


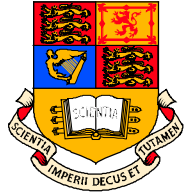
# Li & Williams (1999)



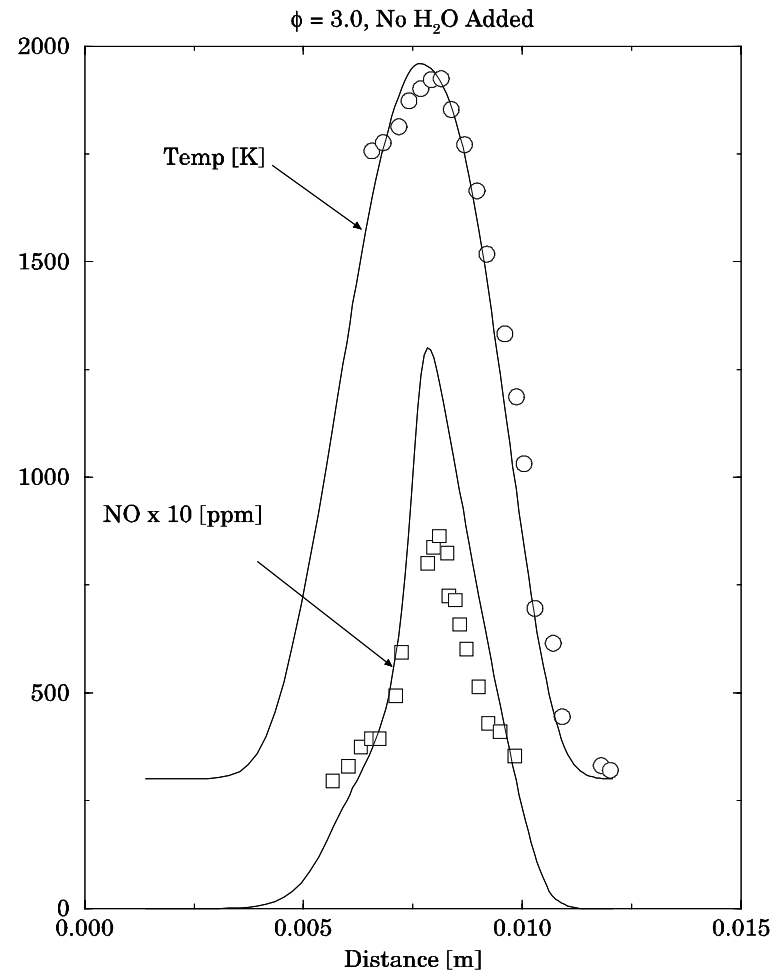
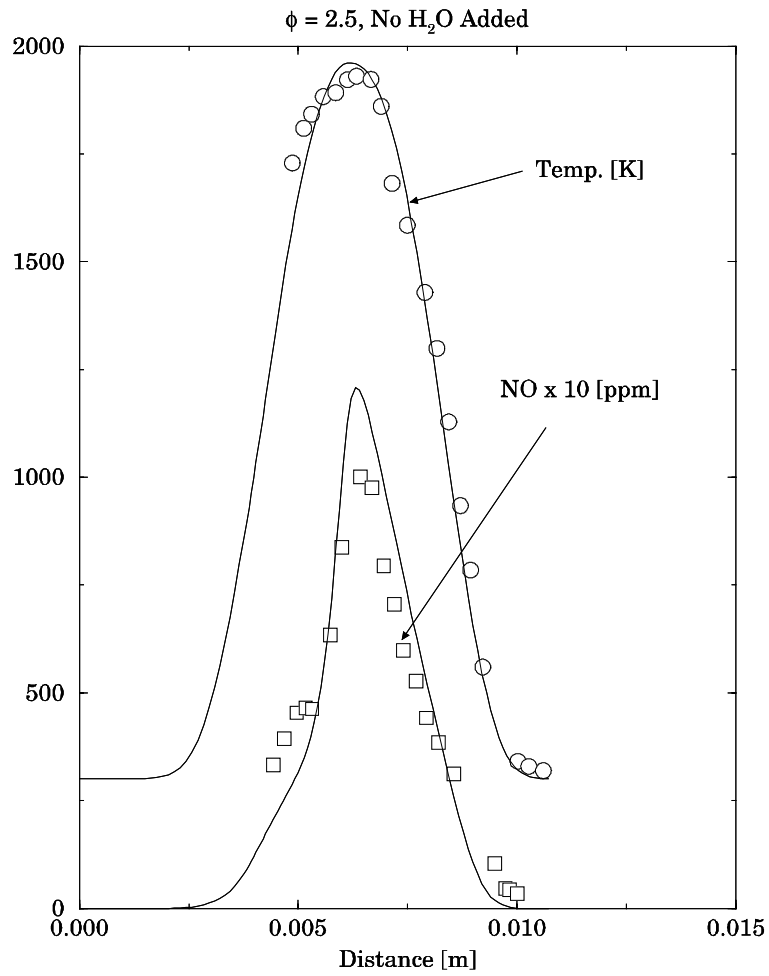


# Li & Williams (1999)



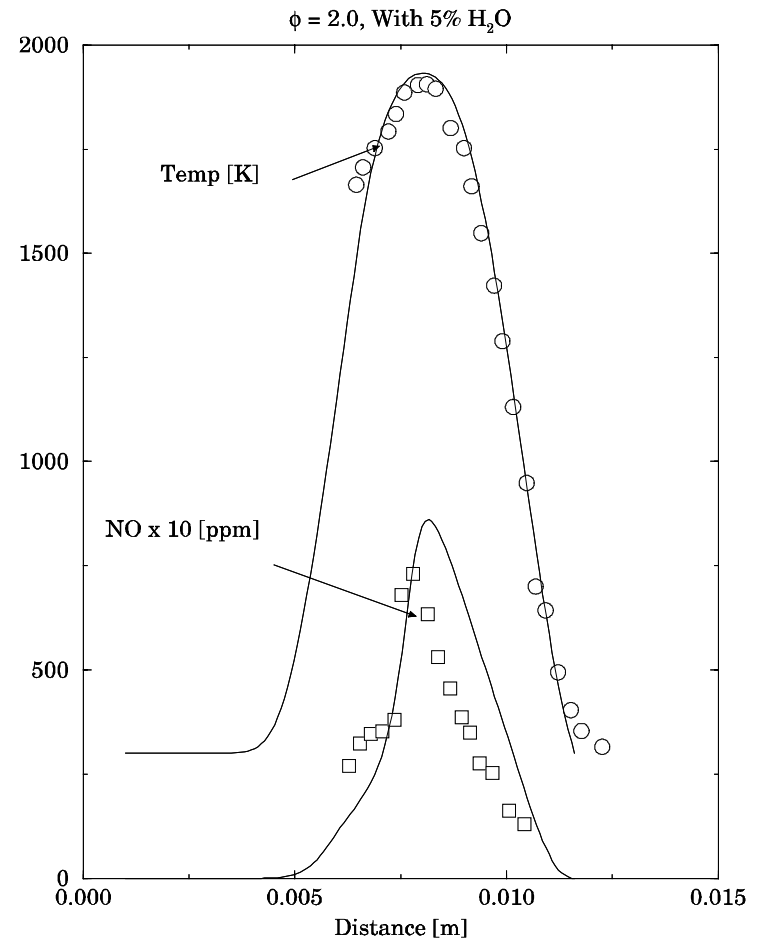
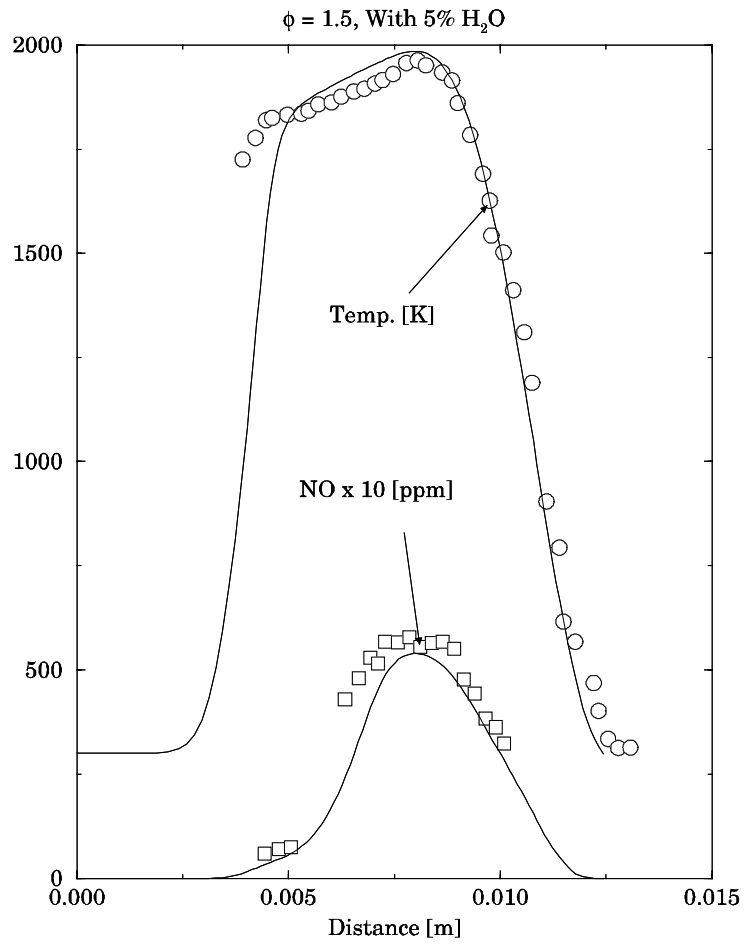


# Li & Williams (1999)



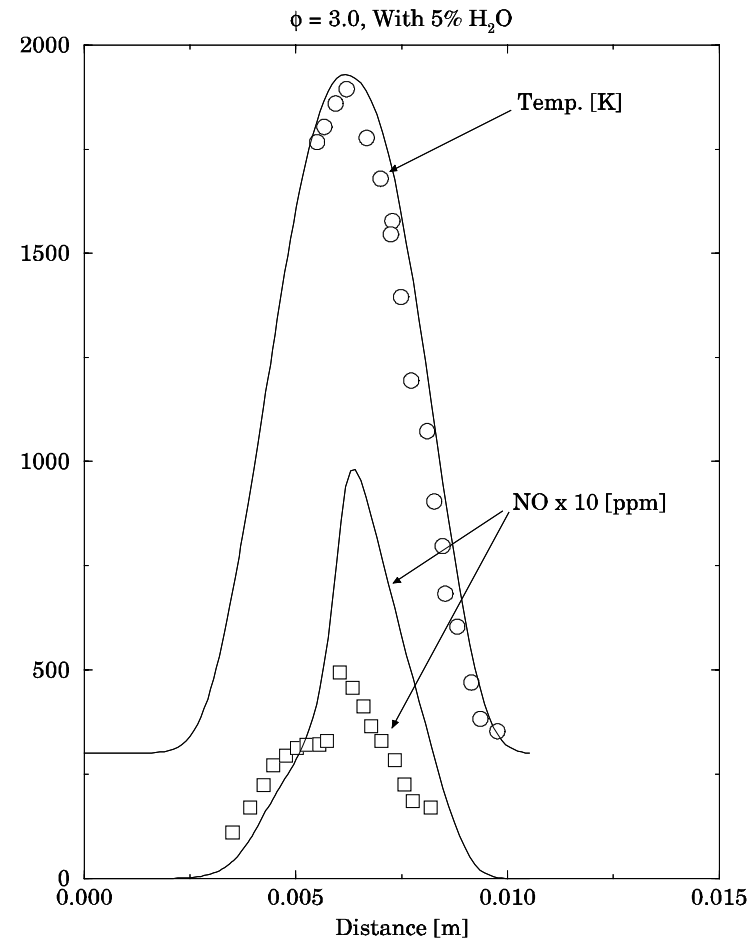
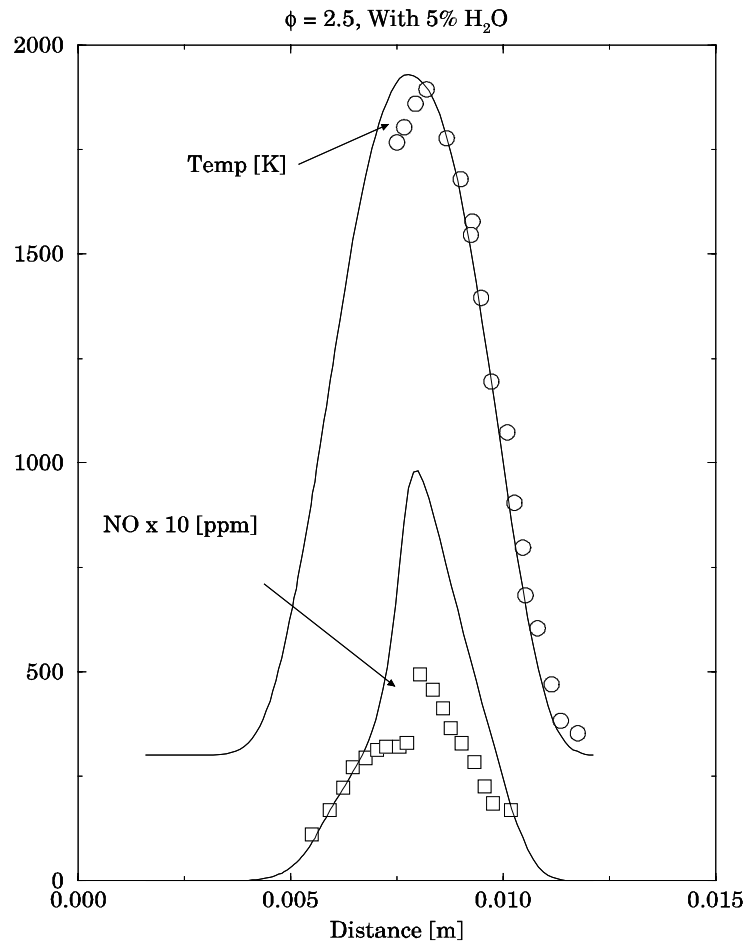


# Li & Williams (1999)



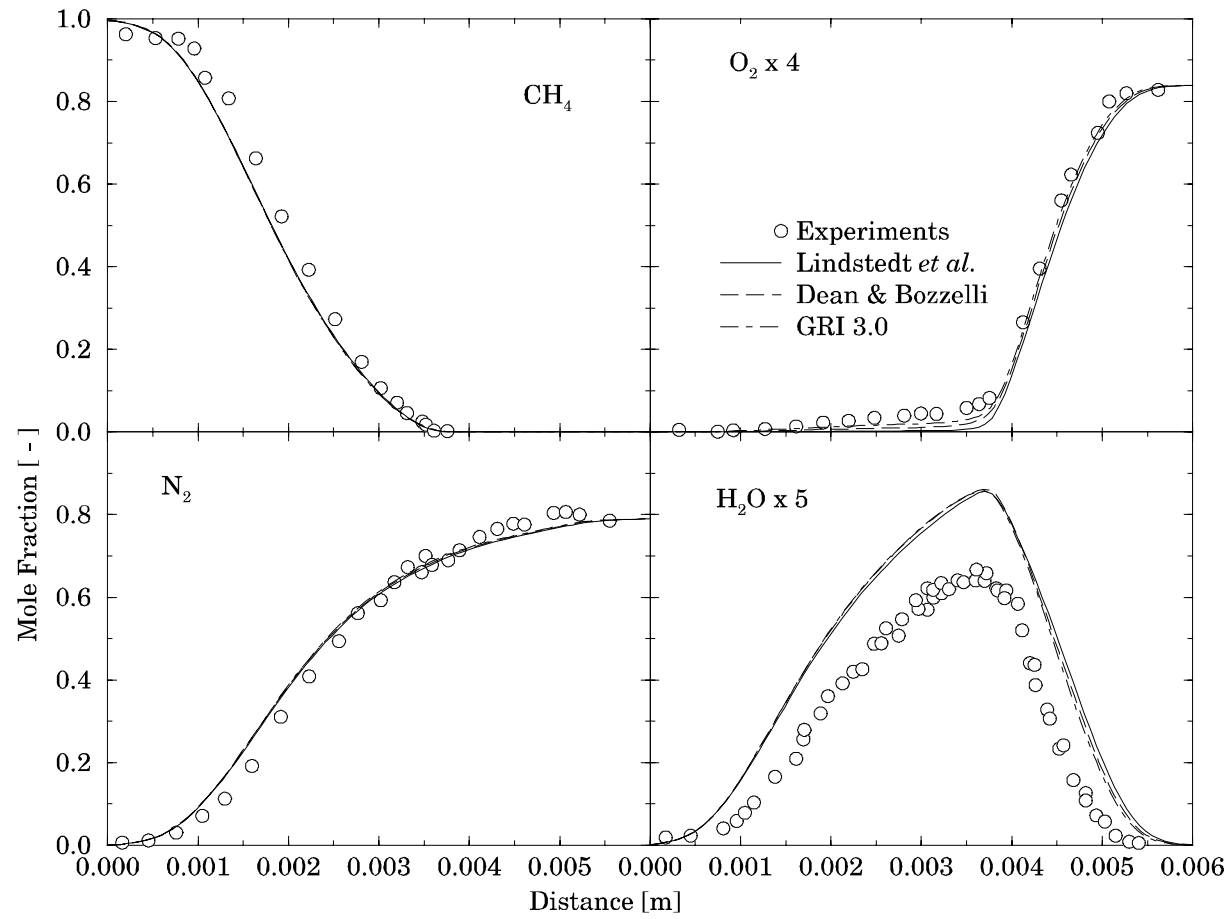


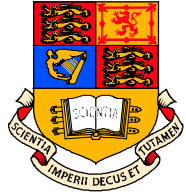
# Li & Williams (1999)



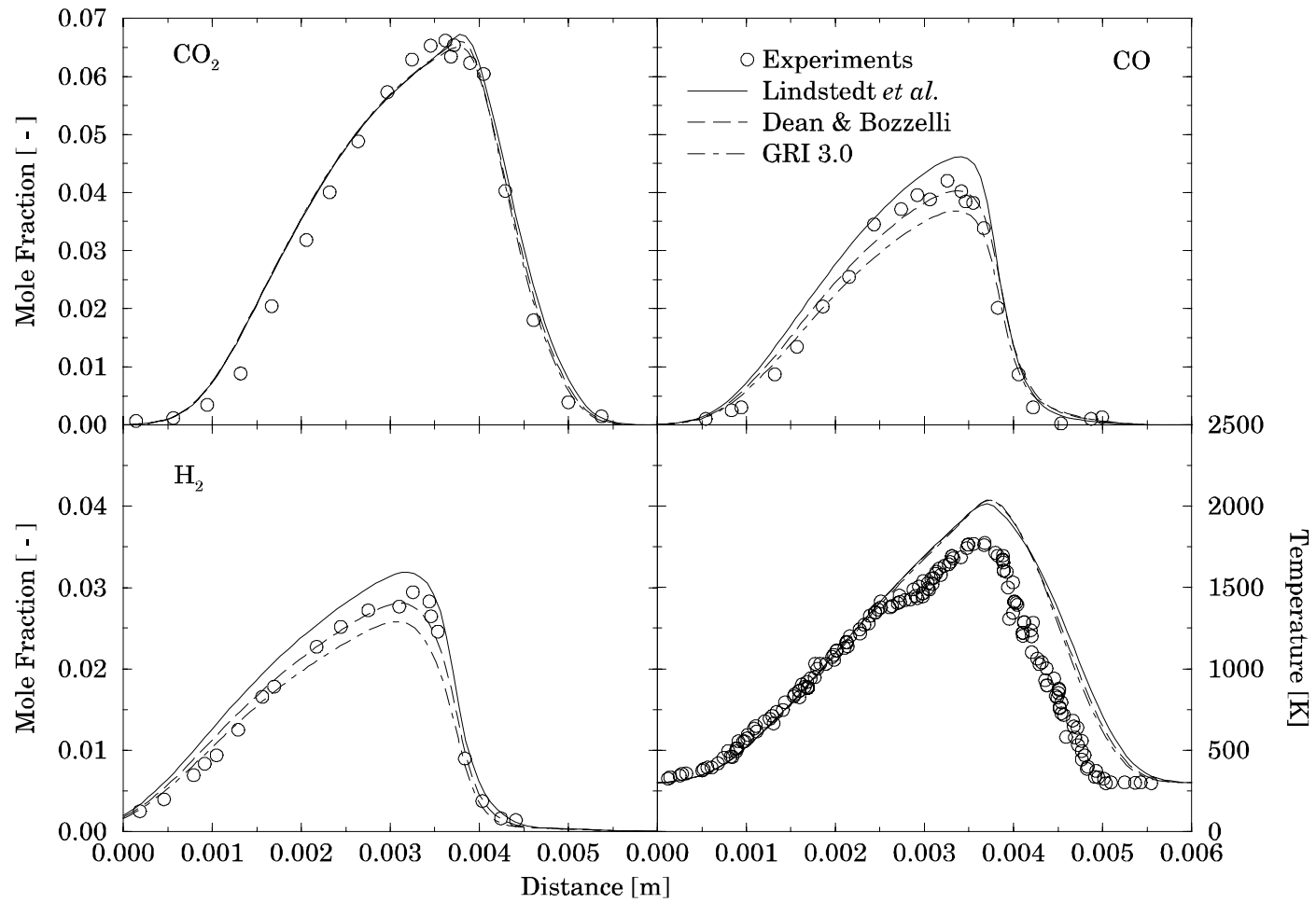


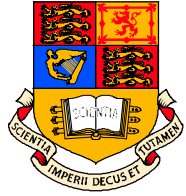
# Tsuji & Yamaoka (1971)



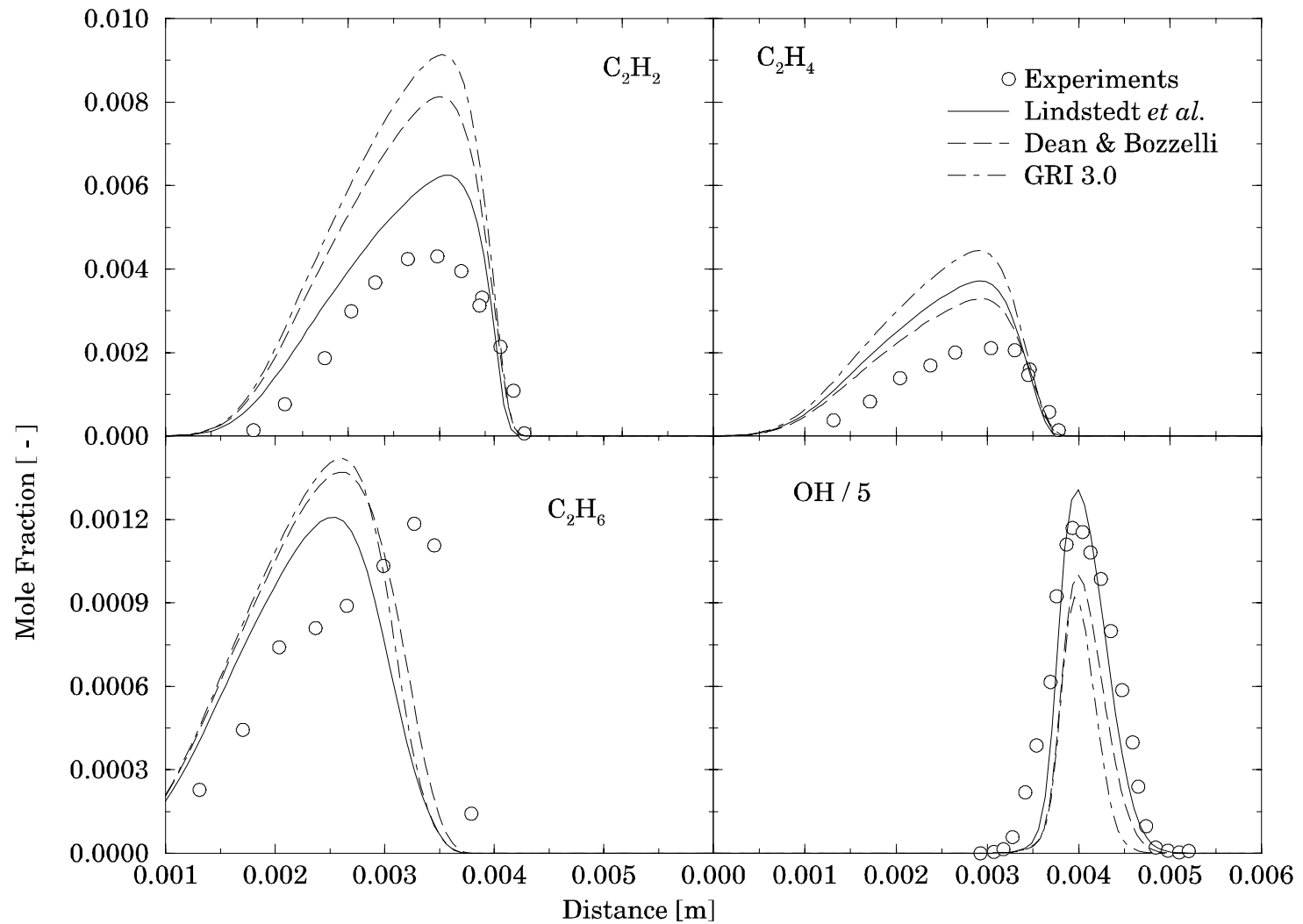


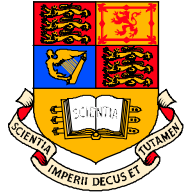
# Tsuji & Yamaoka (1971)



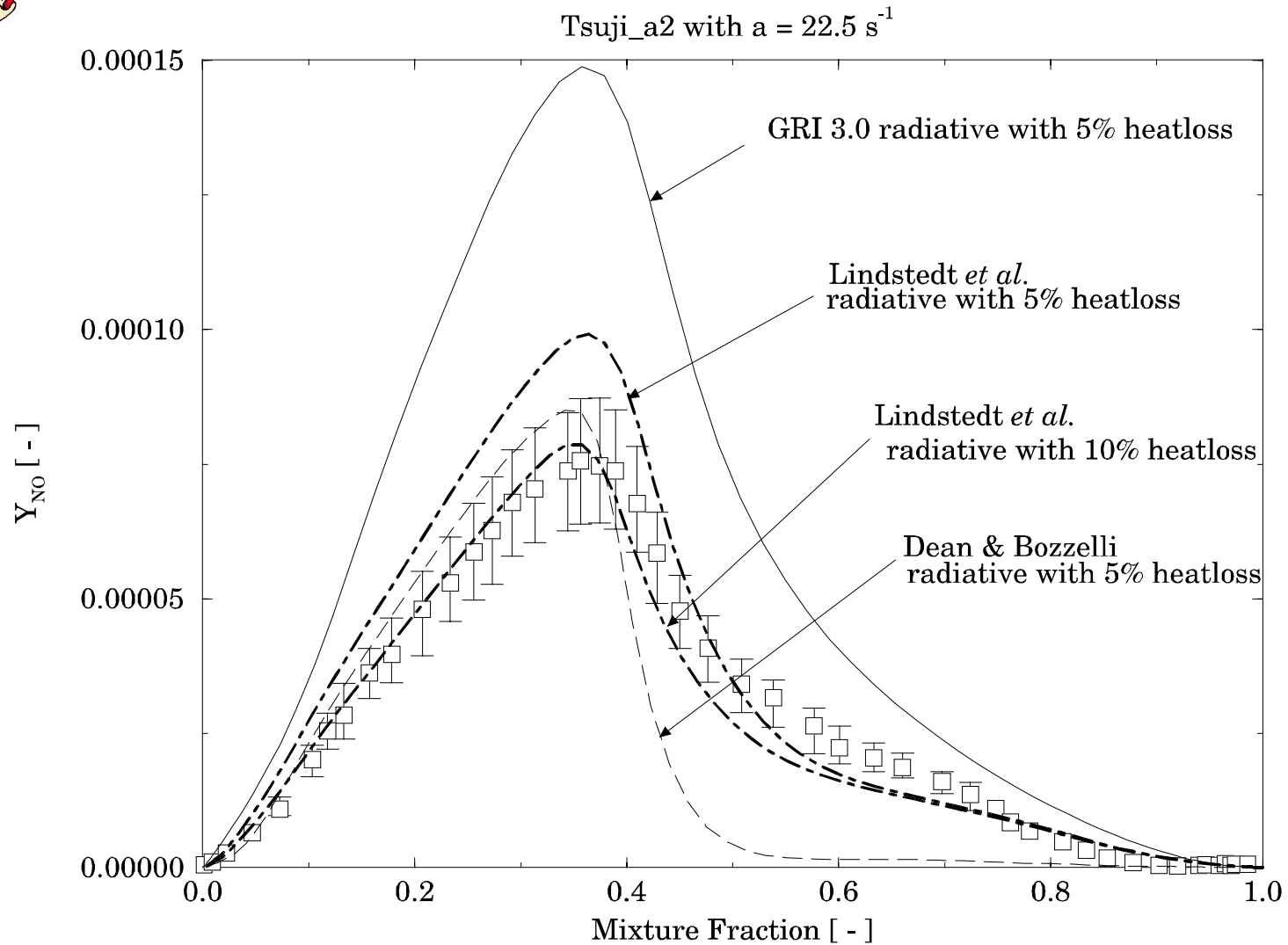


# Tsuji & Yamaoka (1971)





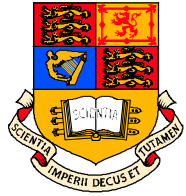
# Barlow & Frank (2000)





## Conclusions

- The key uncertainties in relation to CH predictions have been shown to relate to the  ${}^3\text{CH}_2 + \text{O}_2$ ,  ${}^3\text{CH}_2 + \text{H}$  and  $\text{CH} + \text{H}_2\text{O}$  reactions.
- The current work shows that rate expressions measured at combustion temperatures for the  ${}^3\text{CH}_2 + \text{O}_2$  and  $\text{CH} + \text{O}_2$  reactions are consistent with the present validation data.
- An additional uncertainty arises for the  $\text{CH} + \text{H} = \text{C} + \text{H}_2$  reaction which has a direct influence on the role of C + NO reburn channel.



## Conclusions

- The computational results show that with GRI Mech. 2.11 and the mechanism of Lindstedt the quality of predictions for the CN radical are linked to accurate predictions of the CH radical.
- The quantitative CN measurements obtained in the present work also indicates that uncertainties still prevail in the absolute rate and branching of the NO + CH reaction.
- The present analysis does not suggest a major inconsistency between data sets for NO obtained at SANDIA (Barlow & Frank) and UCSD (Li & Williams).

## Acknowledgements

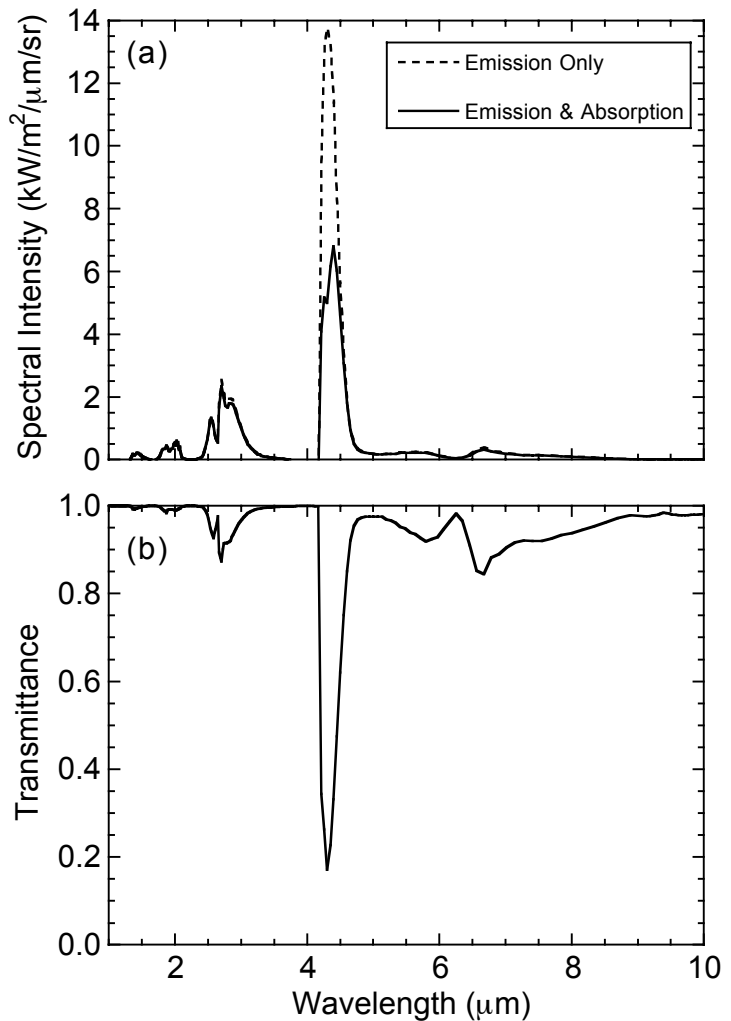
*The financial support of a number of organisations and the comments by staff and students at PCI Heidelberg, Imperial College and University of Michigan is gratefully acknowledged.*

## Update on Radiation Issues

Radiation can have a strong influence on NO formation, even in the non-sooting flames considered by the TNF Workshop. For example, NO levels in the adiabatic and radiative calculations of flame D by Roomina and Bilger, presented at TNF3, differ by roughly a factor of two. Radiative calculations of the TNF target flames have used an optically thin radiation model with Planck mean absorption coefficients based on the RADCAL code. To provide a check on the radiation calculation, measurements of total radiant fraction were obtained at Sandia for several TNF target flames. At TNF4 the point was made that calculated radiant fractions from CMC (Roomina and Bilger) and pdf (J-Y Chen) models were higher than the measurement by more than a factor of two. Questions were raised regarding both the accuracy of the radiation measurements and the validity of the optically thin model.

During the past year we completed experiments to confirm the accuracy of the radiation measurements and to determine radiant fractions for most of the simple and piloted jet flames in the TNF data archives. This work is reported by Frank et al. (28<sup>th</sup> Combustion Symposium).

Confirmation of the discrepancy between measured and predicted radiant fractions puts the optically thin model under greater suspicion. To gain some insight on this issue, we have used RADCAL to calculate spectral intensity and transmission for an optical path with temperature and species concentrations corresponding to the ensemble average profile through the flame diameter at  $x/d=45$  in piloted flame D. The figure shows that transmission drops below 20% at the peak of the 4.3-micron band of CO<sub>2</sub>, and the difference between emission-only results and emission/absorption results is significant for that band.



Summary of JY's parametric studies:

1) Parametric study of the effect of localness in the mixing model:

The influence of 'localness' in the mixing model on the predicted results is illustrated in the parametric studies. The equivalent 1-D flamelet model was done by arranging particles on an imaginary 1-D line (very much like that in the linear eddy model). The mixing is simulated by solving a 1-D diffusion equation with equal physical spacing. The spacing is assigned such that the amount of mixing (the decay of mixture fraction variance) is the same as in other mixing models, i.e., modified Curl's mixing model or the IEM model. The 1-D flamelet model is equivalent to the transient flamelet model with a flamelet assigned to every computational cell. This is much more expensive than the Lagrangian transient flamelet model which solves only one flamelet.

When turbulence intensity reaches a level the local flame structure starts to exhibit local extinction, the reactive fluids may be then mixed across the stoichiometric contours without reactions. Such a local extinction event is not intended for the presently available flamelet model. In the modified Curl's mixing model, random selections of pairs of particles to be mixed seem to be a reasonable representation for the situation of mixing without reactions. One may use the modified Curl's mixing model and the 1-D transient flamelet model as the two extremes. Past experiences indicated that the modified Curl's mixing model sometimes leads to 'premature' local flame extinction especially for flames with narrow reaction zones as in the case of pure methane-air combustion.

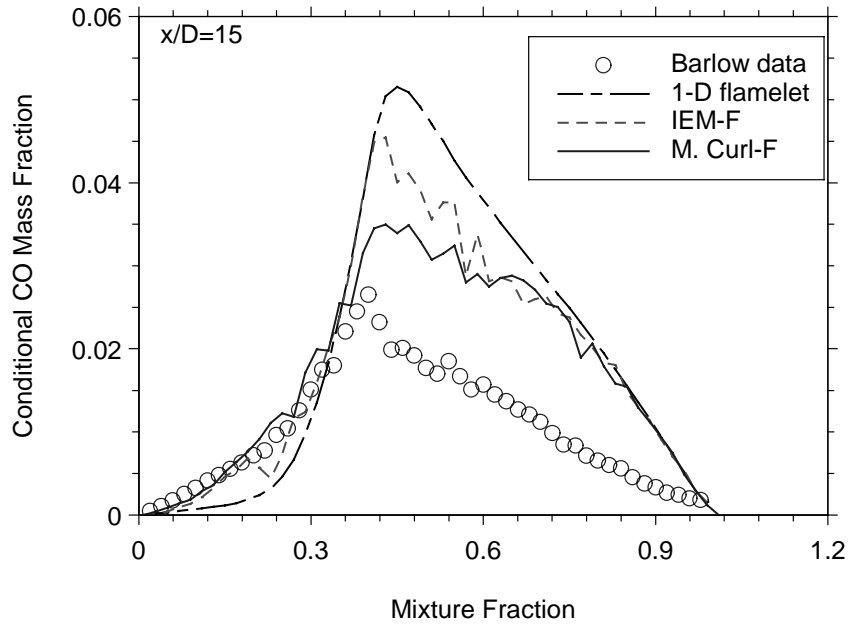
In the simulation of Flame F, the localness is shown to increase the degree of burning as conditional temperature increases. In the equivalent 1-D flamelet model, one notices that both the temperature and CO level are overpredicted. Consequently, the NO<sub>x</sub> levels are also overpredicted. In rich regions of the flame, the CO oxidation rate is expected to be slow and therefore turbulent mixing is faster than oxidation rate leading to a 'pure' mixing like behavior (a straight line in the mass fraction - mixture fraction space). As the jet flame slows down at  $x/D=45$ , the CO oxidation in rich side is evident in the experimental data. For the NO<sub>x</sub>, the trends are opposite to CO oxidation. The 're-burning' process in rich side of flame is seen to be comparable to turbulent mixing. This leads to a dip in the rich side of NO<sub>x</sub>. The chemical reaction of NO<sub>x</sub> in lean side of the flame is negligible and we expect a pure mixing behavior of NO<sub>x</sub> on lean side of the flame. Compared to the data, the predictions using a 13-step reduced chemistry based on GRI30 are too high by a factor of two or more. This is believed to be caused by the chemical mechanism as seen in the laminar flame comparisons.

2) Sensitivity of mixing frequency (or the adjustable parameter)

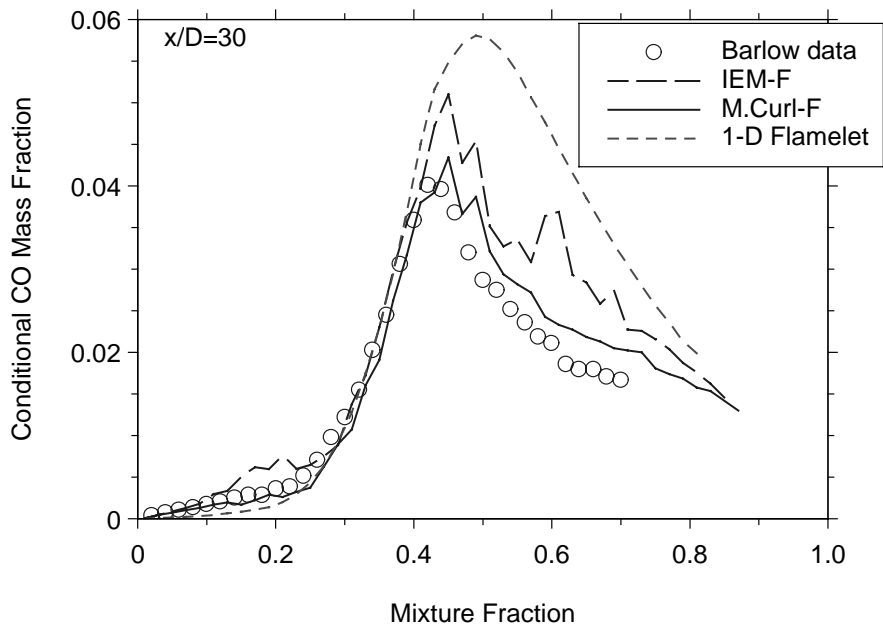
For Flame F with high probability of local flame extinction, the predictions are seen quite sensitive to the mixing frequency using the joint scalar PDF approach. When the mixing

frequency is reduced by 20%, the numerical model with the modified Curl's mixing model gives a nearly totally extinguished flame as seen in the centerline temperature profile. It is interesting to note that even under this severe condition, the flame re-ignites further downstream. As the mixing frequency is currently modeled by setting the ratio of time scales between turbulence and mixing, one expects a variable time scale ratio perhaps would be better. Modeling of mixing frequency by directly solving a modeled scalar dissipation rate equation also involves many uncertainties.

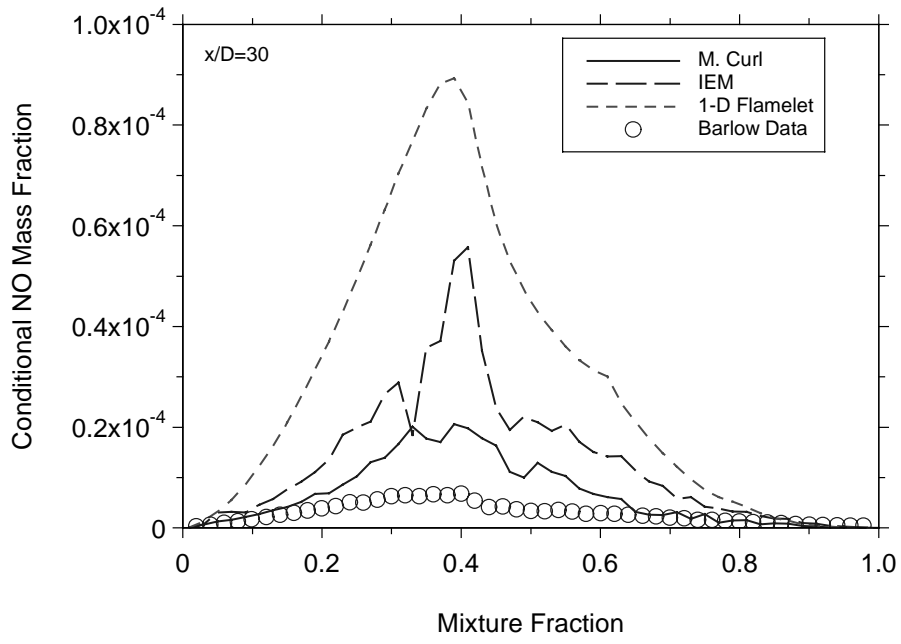
Piloted Jet Flame F: 13step Reduced Chemistry based on GRI30



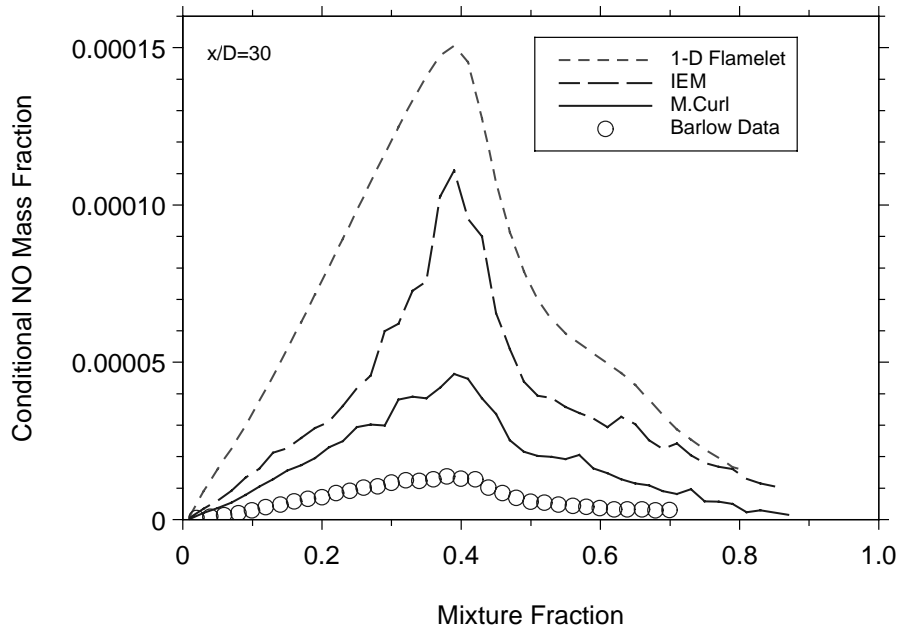
Piloted Jet Flame F: 13step Reduced Chemistry based on GRI30



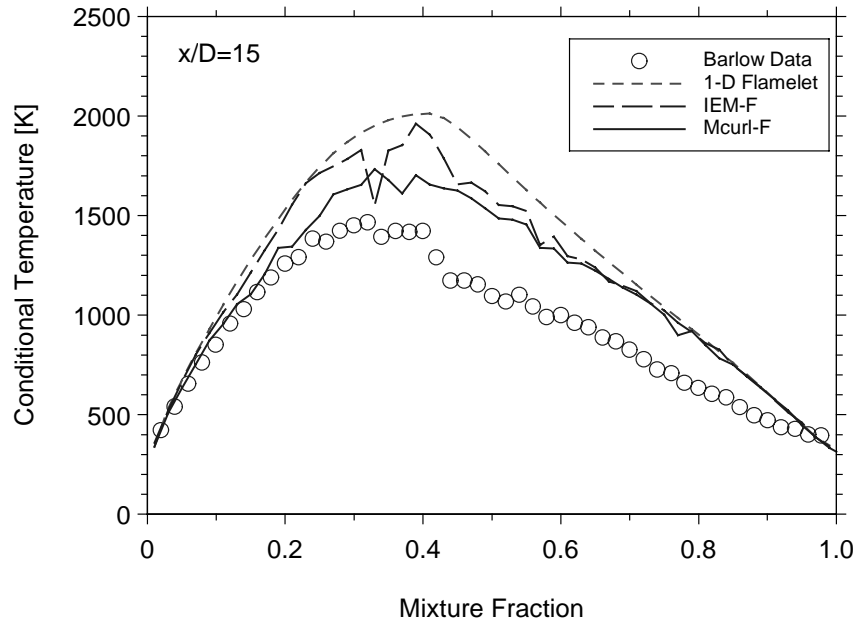
Piloted Jet Flame F:



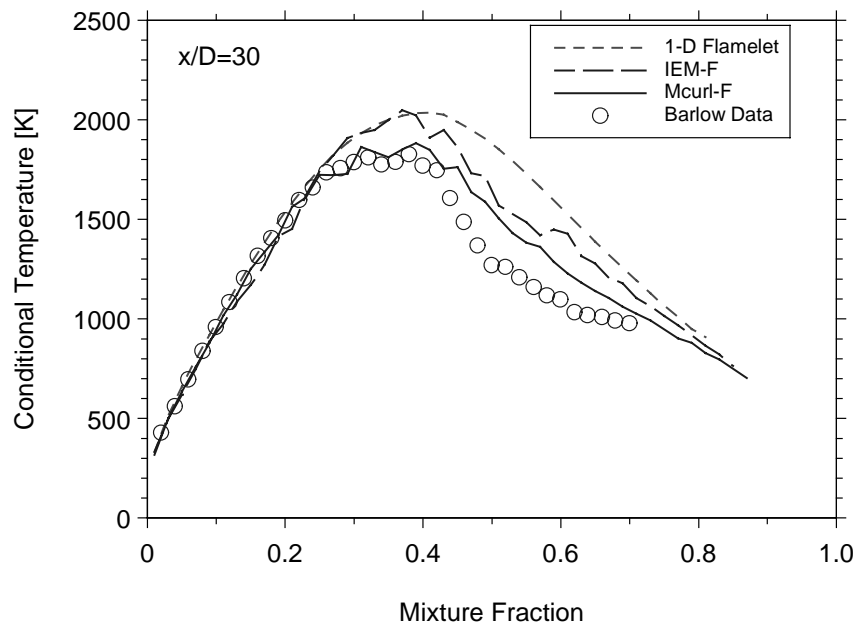
Piloted Jet Flame F:



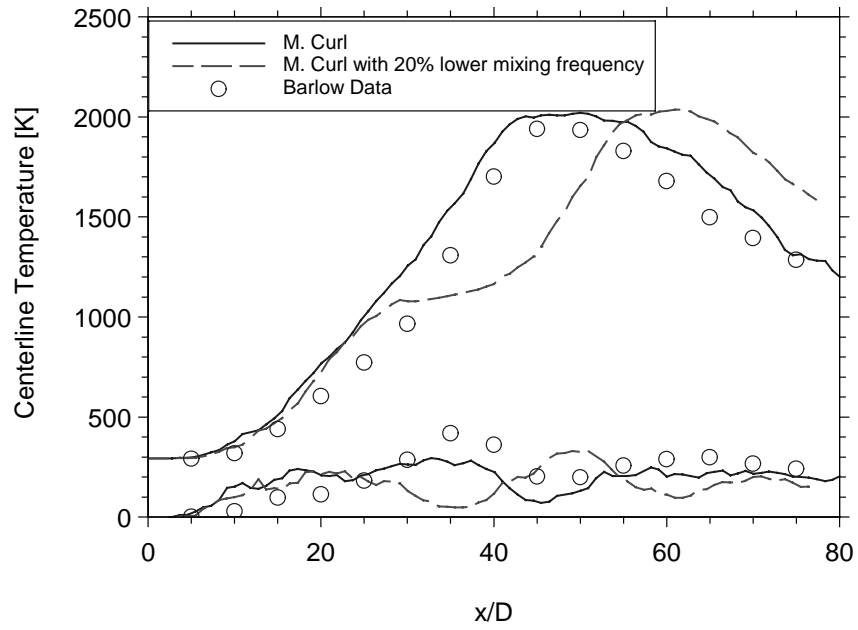
**Piloted Jet Flame F: 13-step reduced chemistry (GRI30)**



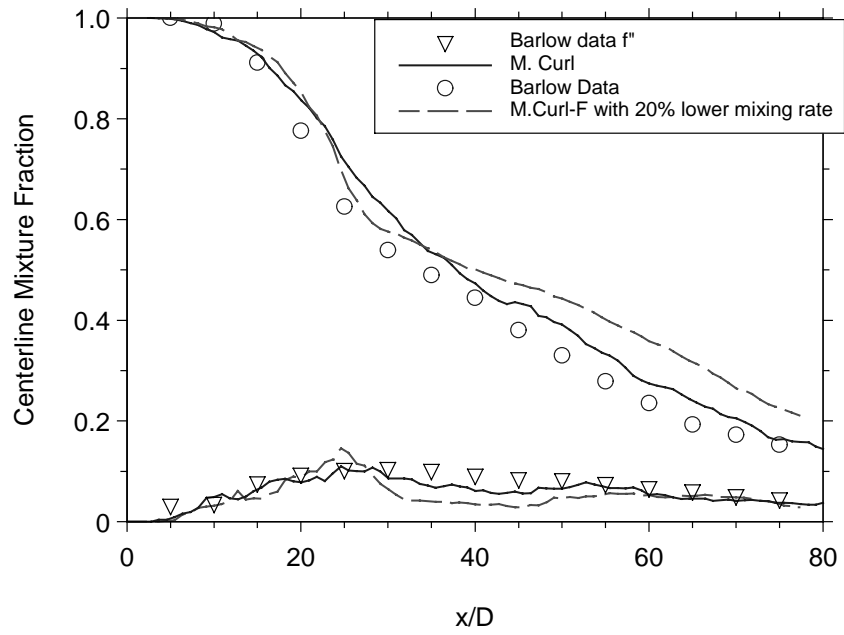
**Piloted Jet Flame F**



Flame F: 13step Reduced Chemistry based on GRI30



Flame F: 13step Reduced Chemistry based on GRI30



# NUMERICAL ERRORS IN PDF METHODS

Only when numerical (and other) errors are known to be small can firm conclusions be drawn about the accuracy of physical and chemical models.

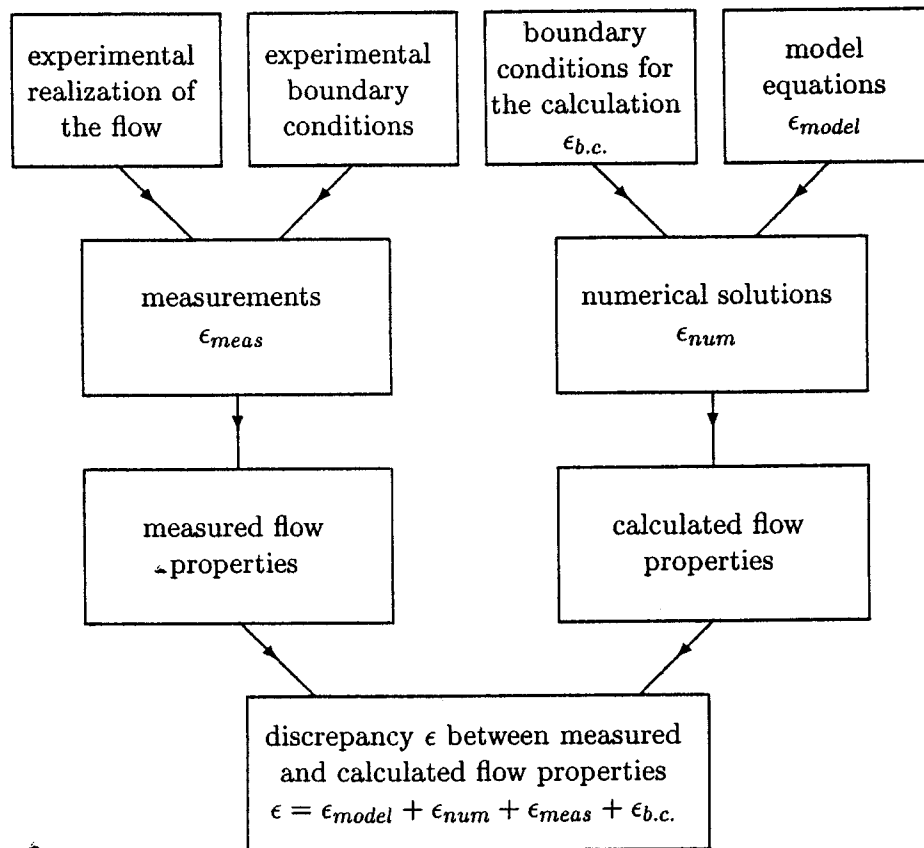


Figure 8.2: Chart illustrating that the discrepancy  $\epsilon$  between measured and calculated flow properties stem from: model inaccuracies,  $\epsilon_{model}$ ; numerical errors,  $\epsilon_{num}$ ; measurement errors  $\epsilon_{meas}$ ; and from discrepancies in the boundary conditions,  $\epsilon_{b.c.}$ . (The equation given for  $\epsilon$  is merely suggestive: the errors do not add linearly.)

# NUMERICAL ERRORS IN PDF METHODS

- all numerical methods involve numerical errors
- understand the nature of the errors
- quantify the errors
- adapt method to reduce errors
- choose numerical parameters so that errors are below an acceptable level (error tolerance)
- demonstrate that calculations are acceptably accurate

## GENERAL CONSIDERATIONS

- numerical parameters

$$\Delta t, \Delta x, N, \varepsilon_{\text{tol}}, \dots$$

- numerical errors

time stepping ( $\Delta t$ )

spatial truncation ( $\Delta x$ )

statistical (random, zero mean) ( $N$ )

bias (non-random) ( $N$ )

interpolation ( $\varepsilon_{\text{tol}}$ )

- local and global errors,  $\varepsilon_{\text{local}}, \varepsilon_{\text{global}}$

- consistency:  $\varepsilon_{\text{local}} \rightarrow 0$  as

$$\{\Delta t, \Delta x, N^{-1}, \varepsilon_{\text{tol}}\} \rightarrow 0$$

- convergence:  $\varepsilon_{\text{global}} \rightarrow 0$  as

$$\{\Delta t, \Delta x, N^{-1}, \varepsilon_{\text{tol}}\} \rightarrow 0$$

- stability: e.g.,  $U_{\text{ref}} \Delta t / \Delta x < 1$  (Lax)

- asymptotic behavior of local errors

$$\varepsilon_{\text{local}} \sim \{\Delta t^2, \Delta x^2, N^{-\frac{1}{2}}, N^{-1}, \varepsilon_{\text{tol}}\}$$

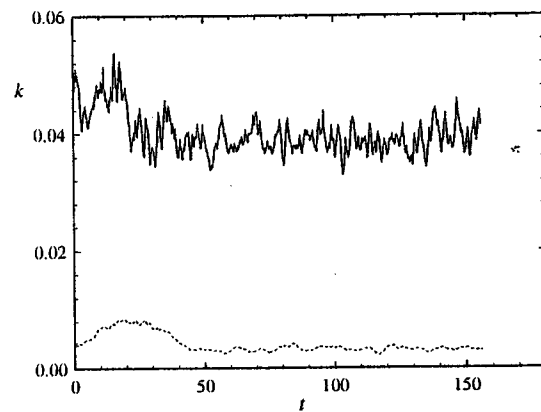
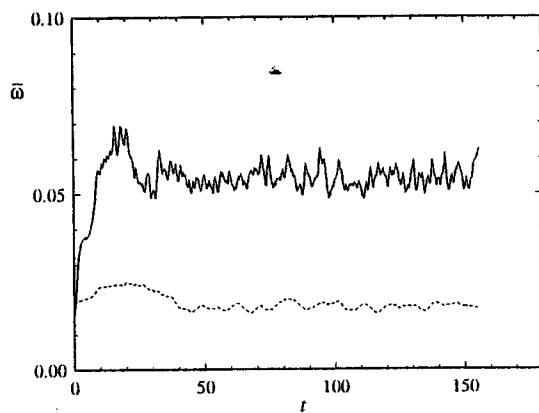
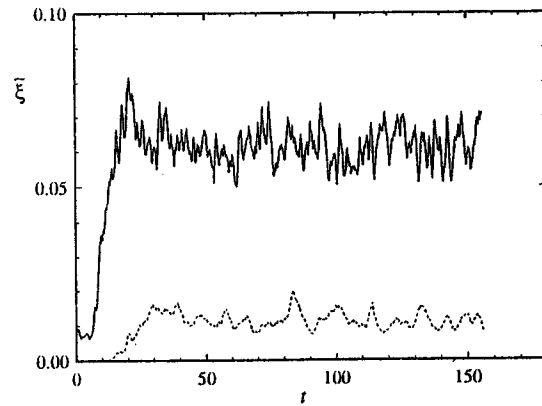
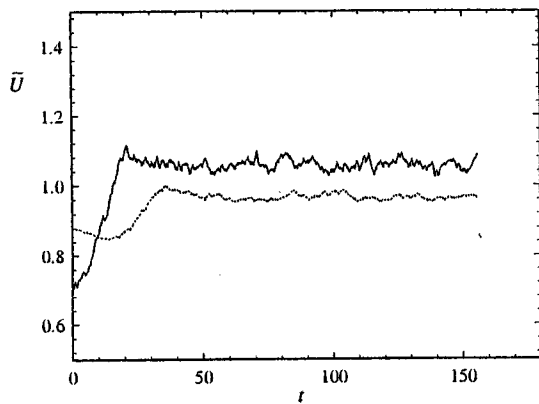
# ISAT

- $\varepsilon_{\text{tol}}$  controls local interpolation error
- Perform computational tests
  - directly measure  $\varepsilon_{\text{global}}$  as a function of  $\varepsilon_{\text{tol}}$
- Example: PMSR, ARM1

# STATISTICAL STATIONARITY

(Xu & Pope, JCP, 1999)

Time series of reference mean quantities



# STATISTICAL ERROR

- $\langle Q \rangle_N$ —estimate of mean of
- $Q$  based on  $N$  particles
- $\sigma_u^2 \equiv \text{var}(\langle Q \rangle_N)$
- $\sigma_u \sim N^{-\frac{1}{2}}$

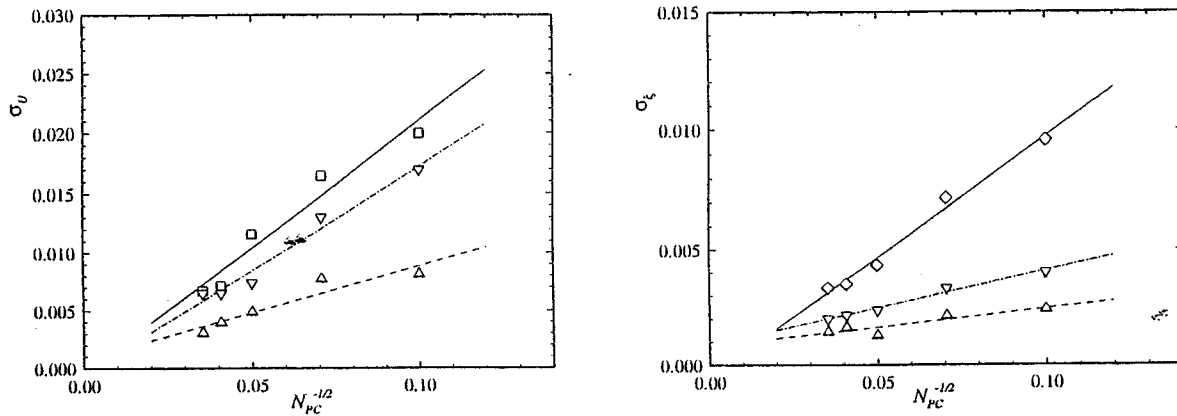
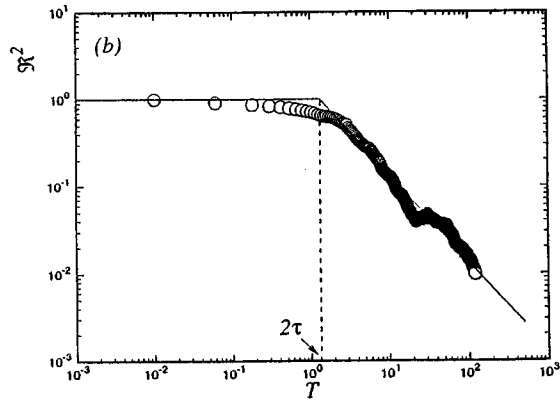
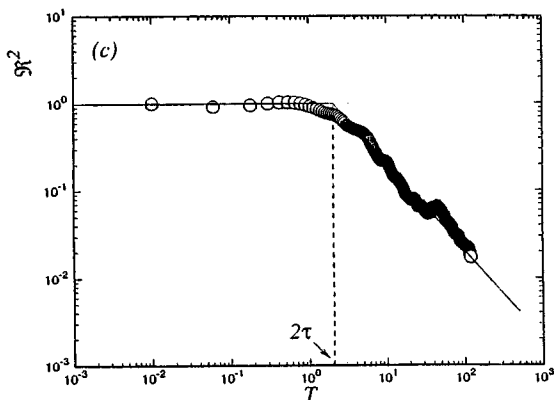
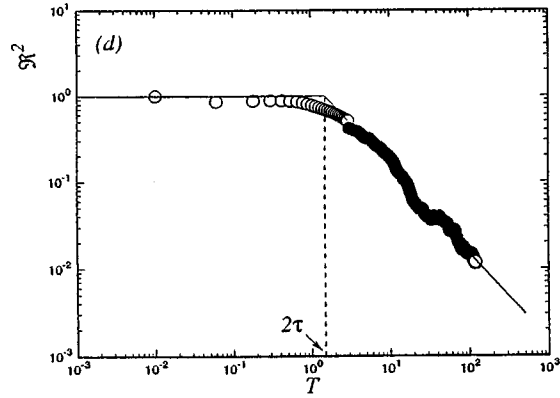
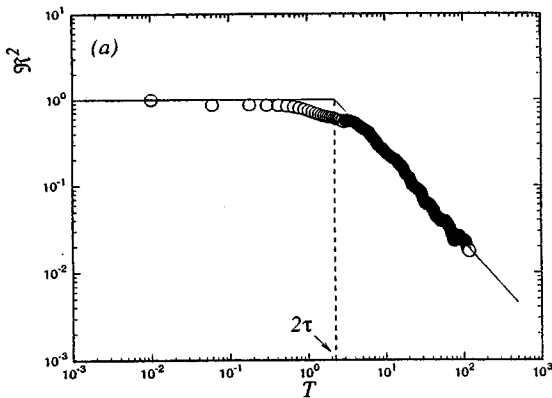


Figure 5: Statistical error in mean velocity and mixture fraction. Solid line and  $\square$ : point (40,2.5); Dashed line and  $\triangle$ : point (40,5); Dashed-dotted line and  $\nabla$ : point (60,5). Cells:  $30 \times 30$ . The lines are the least-squares fits to the data.

# TIME AVERAGING

- Reduce statistical error by time averaging over time  $T$
- $\sigma_Q \sim (NT/\tau)^{-\frac{1}{2}}$  for  $T/\tau \gg 1$
- Reduction factor for  $\sigma_Q^2$  vs.  $T$



## BIAS: TELLING EXAMPLE

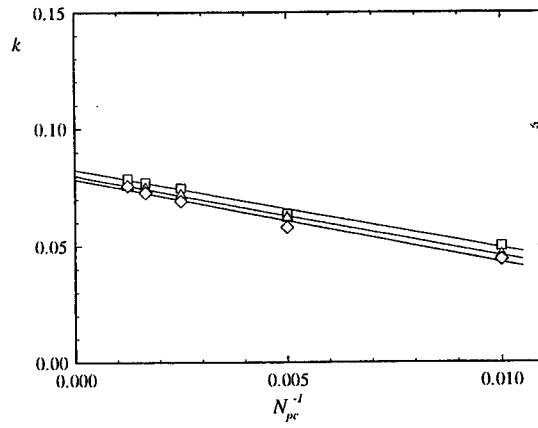
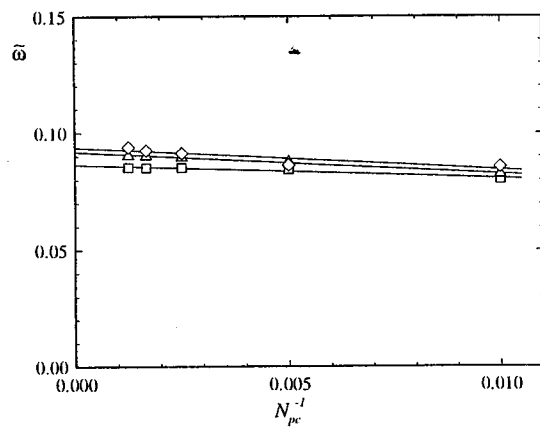
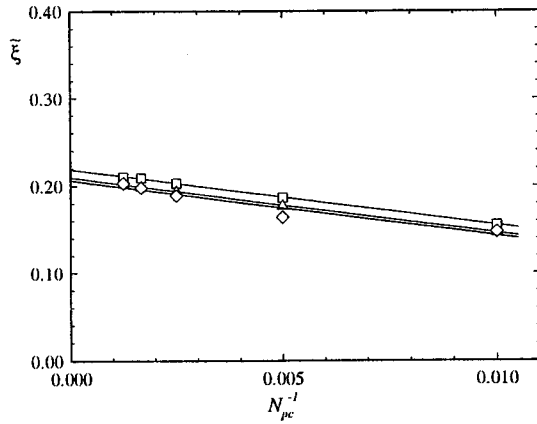
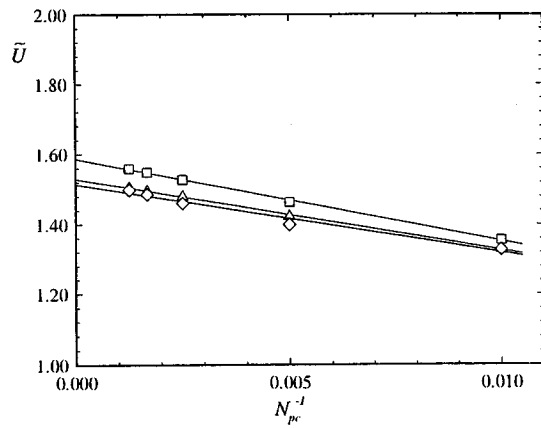
- $Q \equiv \left( \frac{\partial \langle U \rangle}{\partial y} \right)^2$
- estimate by central difference and  $N$ -particle ensemble mean
- $N$  particles at  $y + \Delta y$ ;  $N$  particles at  $y - \Delta y$
- $Q_{N,\Delta y} \equiv \left[ \frac{\langle U \rangle_{N,y+\Delta y} - \langle U \rangle_{N,y-\Delta y}}{2\Delta y} \right]^2$
- leading order bias:

$$B_Q \equiv \langle Q_{N,\Delta y} \rangle - \langle Q \rangle$$
$$\sim \frac{1}{3} \Delta y^2 \frac{\partial \langle U \rangle}{\partial y} \frac{\partial^3 \langle U \rangle}{\partial y^3} + \frac{\langle u^2 \rangle}{4N \Delta y^2}$$

- conditional convergence

# BIAS IN PDF2DV

Plots of  $\langle Q \rangle_N$  vs.  $1/N$



# EXTENDED RICHARDSON EXTRAPOLATION

- leading order spatial truncation error  
 $\sim \Delta x^2$
- leading order bias  $\sim N^{-1}$  (independent of  $\Delta x$ )

$$\varepsilon \approx a\Delta x^2 + bN^{-1}$$

- two calculations
  - $\Delta x_1, N_1 \rightarrow Q_1 = Q + \varepsilon_1$
  - $\Delta x_2, N_2 \rightarrow Q_2 = Q + \varepsilon_2$
  - choose  $\Delta x_2 = \Delta x_1/\alpha, N_2 = \alpha^2 N_1$   
(e.g.  $\alpha = \sqrt{2}$ )
  - then  $\varepsilon_2 = \varepsilon_1/\alpha^2$
- leading order errors eliminated in extrapolated value

$$Q_E \equiv \frac{\alpha^2 Q_2 - Q_1}{\alpha^2 - 1}$$

# EXTENDED RICHARDSON EXTRAPOLATION

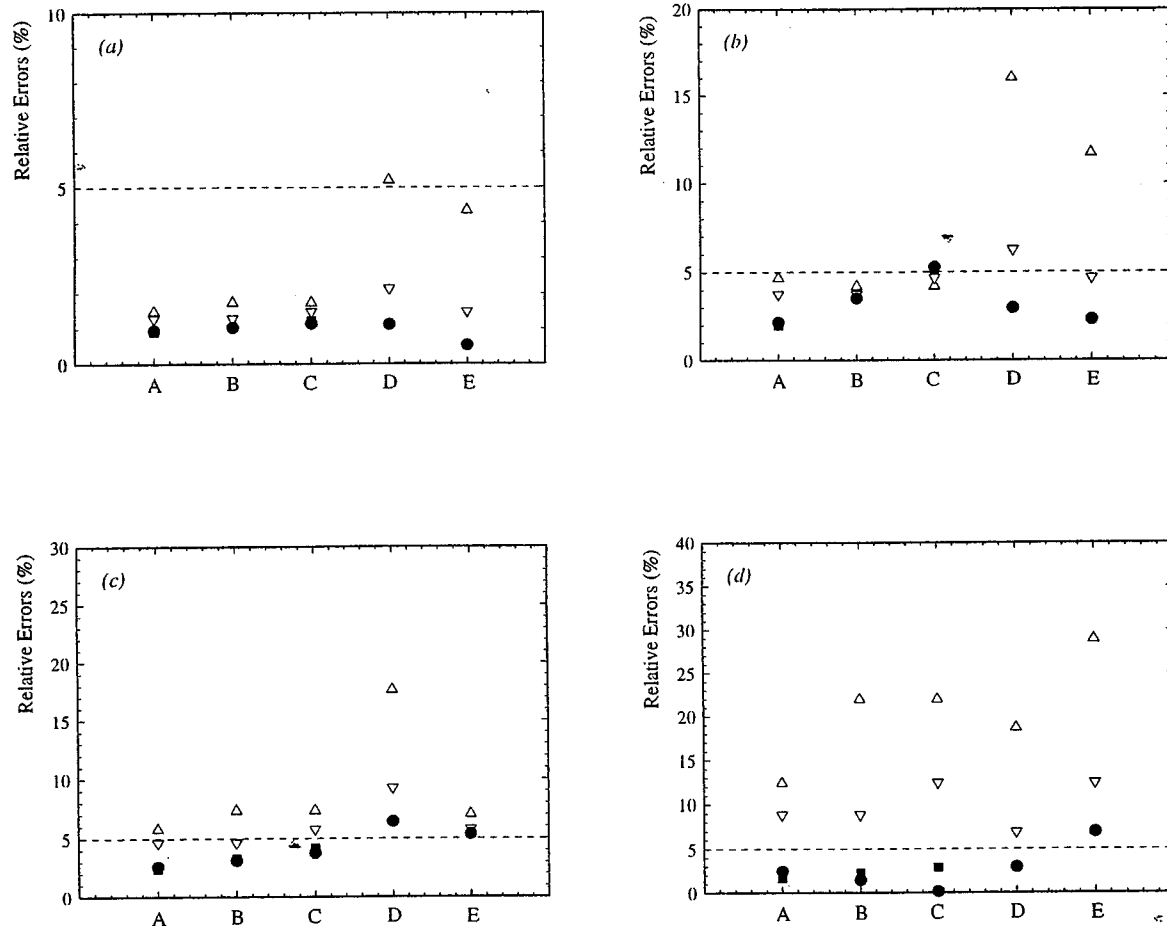
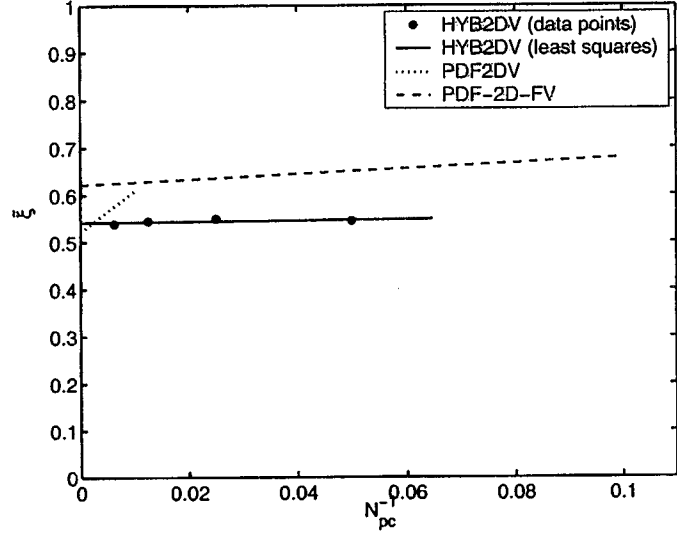
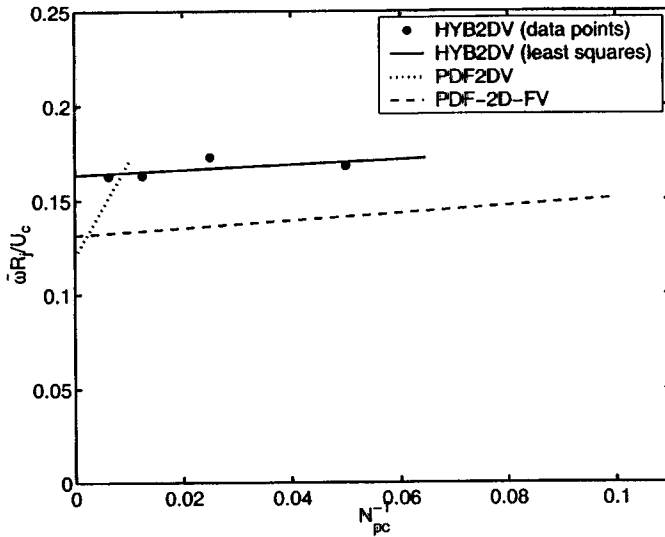
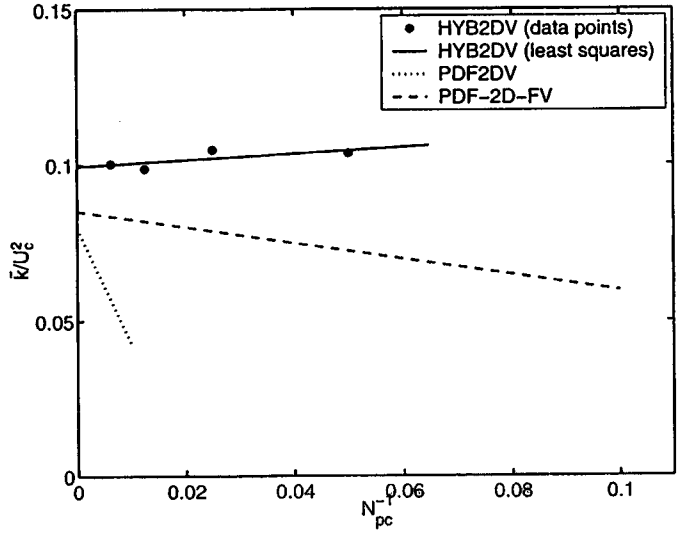
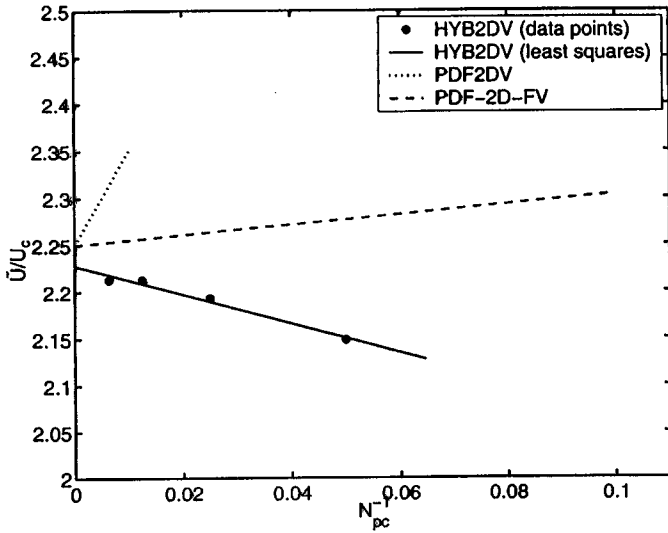


Figure 19: Relative errors of mean quantities at point (40, 1.0) for the calculations given in Table 9.  $\Delta$ , condition 1;  $\nabla$ , condition 2;  $\bullet$ , extrapolating using  $\alpha_1$ ; Boxes, extrapolating using  $\alpha_2$ . Dashed lines shows 5% error. (a) Mean velocity; (b) Mean mixture fraction; (c) Mean frequency; (d) Turbulence energy.

BIAS ERROR  $(x/R_j, r/R_j) = (40.0, 1.0)$

---

● Grid:  $48 \times 48$        $N_{pc} = 20, 40, 80, 160$



# CONCLUSIONS

- numerical accuracy essential to model testing and development
- accurate calculations have been demonstrated with PDF particle methods
- *demonstrating* accuracy requires orders of magnitude more effort than *achieving* accuracy.
- techniques for reducing error
  - time averaging
  - variance reduction
  - extended Richardson extrapolation
- beware of bias!

## **Fifth International Workshop on Measurement and Computation of Turbulent Nonpremixed flames**

### **Note in preparation of a discussion on the role of turbulence model and inlet profiles in computations of piloted jet flame D**

Dirk Roekaerts<sup>1</sup> and Joan Teerling

Thermal and Fluids Sciences, Department of Applied Physics, Faculty of Applied Sciences, Delft  
University of Technology, Lorentzweg, 1, 2628 CJ Delft, The Netherlands

Bart Merci

<sup>2</sup>Dept. Of Flow Heat and Combustion Mechanics, Ghent University, Belgium

In this note we present some results of a parametric study on the role of turbulence model and inlet profiles on predictions of piloted jet flame D. First the motivation for this study is explained by reviewing some relevant recommendations of previous TNF workshops. Then results are presented in the form of plots. At the workshop conclusions will have to be formulated on the basis of a discussion of these and related results.

After the Naples TNF workshop a webpage on computational submodels for the TNF workshops was prepared. (<http://www.ca.sandia.gov/tdf/Workshop/Submodels.html>) There one can find the statement that reference predictions shall be provided and that these calculations will be carried out with recommended turbulence models. For jets, the recommendations are: standard  $k-\varepsilon$  with  $C_{\varepsilon 1} = 1.60$  and Jones-Musonge Reynolds stress model. (Recall that the default values of the model constants in the  $\varepsilon$  equation are  $C_{\varepsilon 1}=1.44$  and  $C_{\varepsilon 2} = 1.92$ .) In practice at the TNF3 and TNF4 workshops none of the computations has been explicitly called the reference calculation. Most participants have adjusted model constants in their favourite turbulence model.

The "flame D" calculations most in line with the original proposal for reference calculation are the calculations submitted by Alexander Hinz, Egon P. Hassel and Johannes Janicka at TNF3 and TNF4. In TNF3 they presented results using  $k-\varepsilon$  model modified according to Launder (1972), and at TNF4 they presented results using Jones-Musonge model. So, it is observed that for the  $k-\varepsilon$  model a modification was chosen different from the original recommendation. In fact there are many different modifications of the  $k-\varepsilon$  model presented in the literature to reproduce the spreading rate of a round jet. The modification  $C_{\varepsilon 1}=1.60$  being one of the oldest ones. The question arises whether or not its use in a reference calculation of flame D has any special value. The answer depends on its performance in predicting the correct spreading rate (or axial profile of mean axial velocity), which however in principle will also be influenced by the chemical model and the turbulence-chemistry interaction model.

Of at least equal importance is the correct prediction of the axial profile of the mean mixture fraction, and in the webpage documenting the flame D this is boiled down to correct prediction of the axial location where the mixture fraction reaches its stoichiometric value:  $L_{\text{stoich}} = 47d$  (33.8 cm) (<http://www.ca.sandia.gov/tdf/Workshop>). The prediction of this feature is also directly influenced by the value for the turbulent Prandtl number and the mechanical to scalar time-scale ratio.

---

<sup>1</sup> Also at Shell Global Solutions International BV, Amsterdam, The Netherlands

It can be concluded that in the proceedings of the workshops no evidence is found that the choice  $C_{\varepsilon 1}=1.6$  in combination with a preferably not too complicated chemistry model satisfies the requirements of predicting the axial profiles of mean axial velocity and mean mixture fraction correctly. Therefore the test has been made.

In fact, looking at the proceedings of previous workshops, it can be seen that among the contributors to the TNF5 workshop it is more popular to decrease the value of  $C_{\varepsilon 2}$  than to increase the value of  $C_{\varepsilon 1}$  (which should be almost equivalent). P. Lindstedt uses  $C_{\varepsilon 2} = 1.8$  in the frame of SSG second moment closure (private communication). J.-Y. Chen used  $C_{\varepsilon 2} = 1.7$  with k- $\varepsilon$  model and,  $C_{\varepsilon 2} = 2.1$  and/or Pope's correction with a Reynolds stress model (private communication). Therefore the effectiveness of the suggested simple change  $C_{\varepsilon 2}=1.8$  has also been tested for flame D.

While analysing the result of the parametric study it became clear that the inlet profile of turbulence dissipation rate  $\varepsilon$  at the inlet also plays a role. (See also the poster by Merci et al.) In general profiles used by workshop participants differ in the radial profile of mixing length scale  $L_m$  used in the calculation of the boundary layer profile for used for  $\varepsilon$  using  $\varepsilon=C_{\mu}^{3/4} k^{3/2}/L_m$ . In the plots shown below "low  $\varepsilon$ " refers to calculation of  $\varepsilon$  from the experimental data for kinetic energy  $k$  via  $\varepsilon = \rho C_{\mu} k^2 / \mu_T$  with  $\mu_T$  a constant turbulent viscosity, and "high  $\varepsilon$ " refers to the calculation of  $\varepsilon$  by solving the nonlinear low Reynolds number k- $\varepsilon$  model at the inlet, using the measured data on  $U$  and  $k$  and assuming vanishing axial gradients.

In the plots shown below, a set of results are presented which all have been obtained using simple chemical models and the same numerical grid. They show the influence of changes in  $\varepsilon$  inlet profile and of turbulence model and values of model constants. The calculations were contributed by Bart Merci, University Gent, and by a team of Delft University (Joan Teerling, Bertrand Naud, Denis Krasinsky, Aristide Mbiock, Dirk Roekaerts). The nonlinear k- $\varepsilon$  has not been tuned for application to flame D.

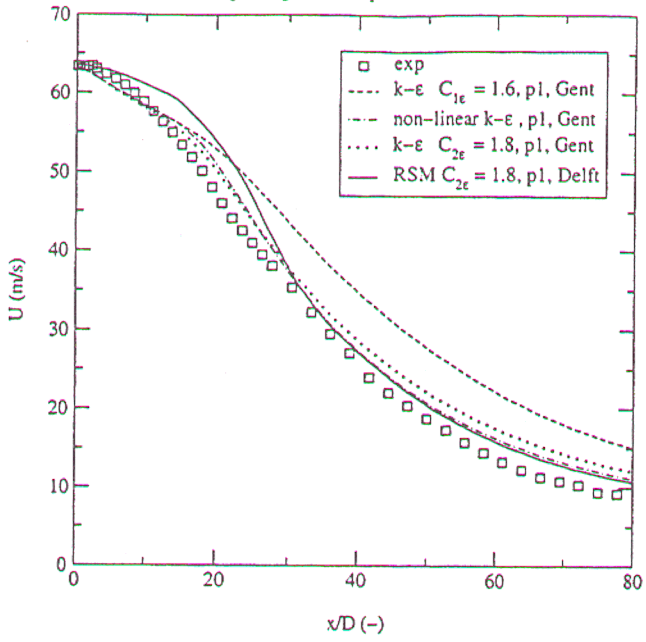
For comparison these results should also be compared with results by other contributors to this workshop (for more details see overview of new contributions by R. Barlow) and previous workshops. In the plots one contribution from TNF4 (Hinz et al) has been included. The calculation by Hinz et al used Jones and Musonge Reynolds stress model in combination with ILDM reduced chemistry.

#### NOTE ADDED AFTER THE WORKSHOP

The two assumed profiles for  $\varepsilon$  for which results are presented are extremes. The most realistic profile presumably is in between. The "high  $\varepsilon$ " inlet profile shown in the bottom right figure is in fact not a grid independent result. The grid independent result obtained by the same method on a finer grid has a near wall peak which is only 30 % as high. This comes closer to the fully developed pipe profile with length scale proportional to the distance to the wall. I.e. the formula  $\varepsilon=C_{\mu}^{3/4} k^{3/2}/L_m$  with  $L_m=0.4y$ , where  $y$  is the distance to the wall. When using this profile, the highest value is reached at the grid point closest to the wall, which should be sufficiently far from the wall in the logarithmic layer.

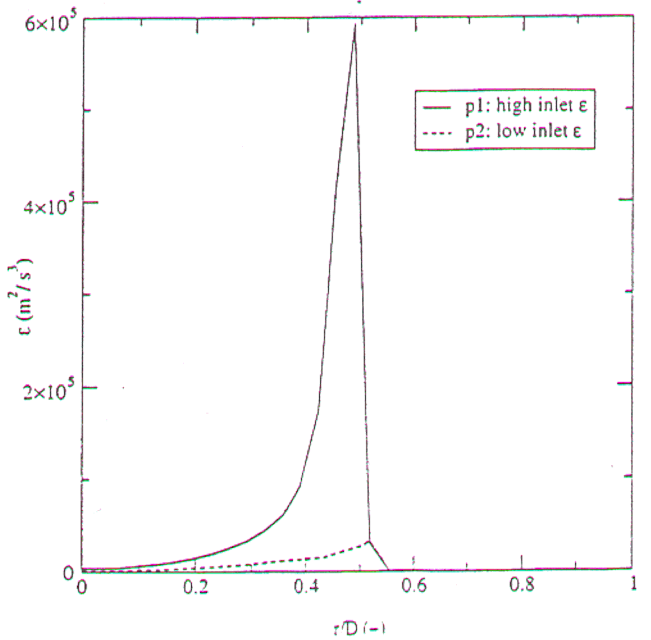
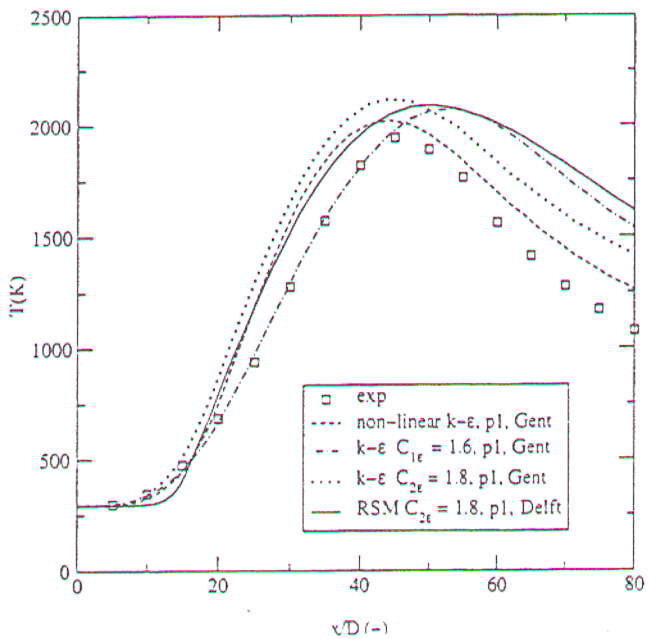
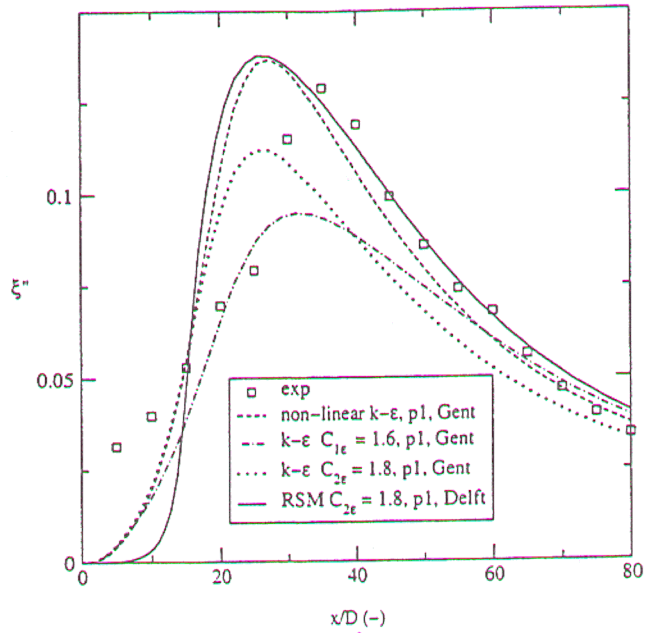
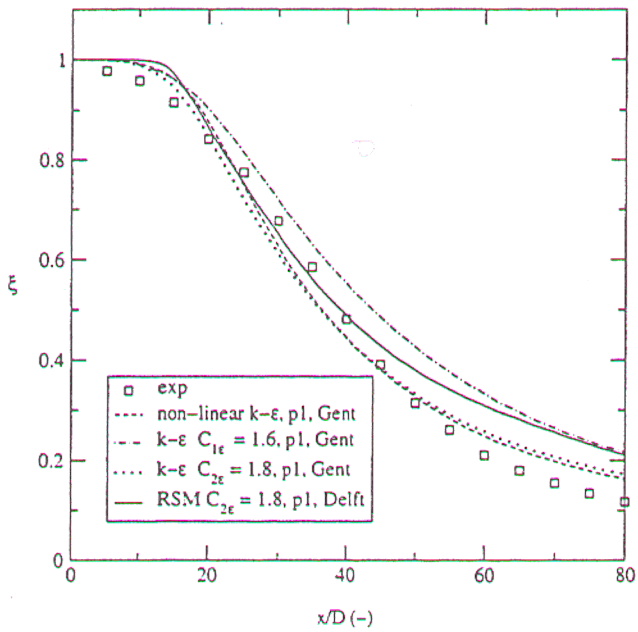
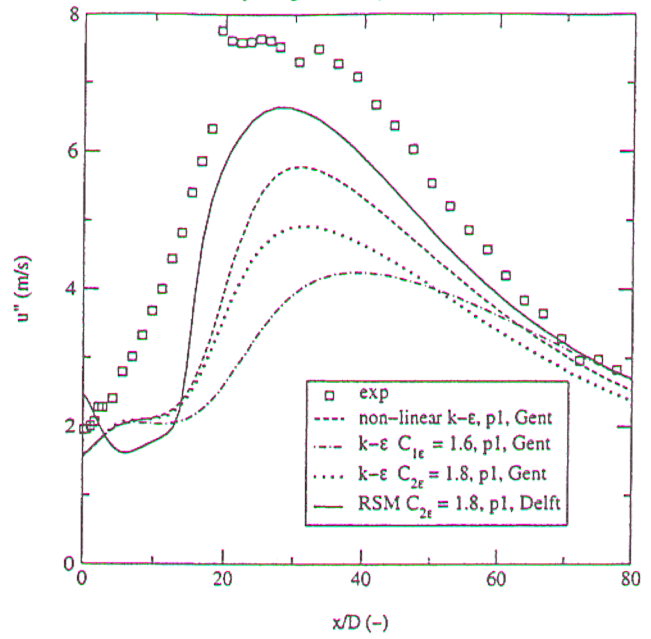
### flame D

p1: high inlet  $\epsilon$ ; p2: low inlet  $\epsilon$



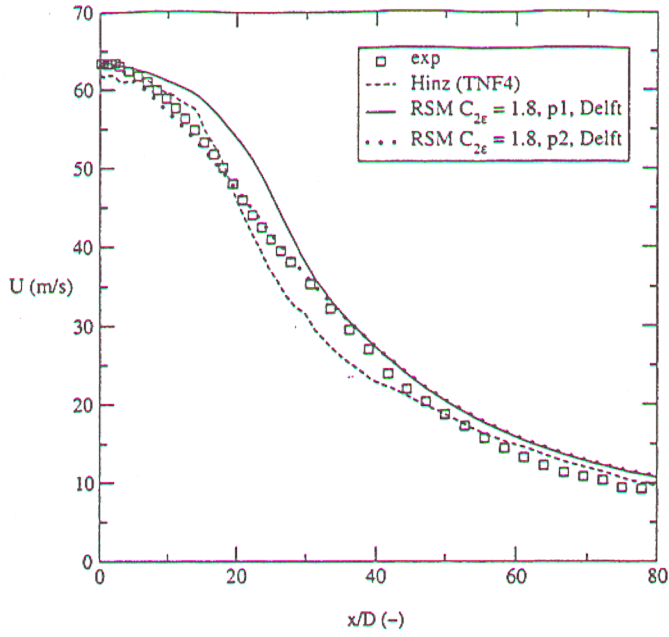
### flame D

p1: high inlet  $\epsilon$ ; p2 low inlet  $\epsilon$



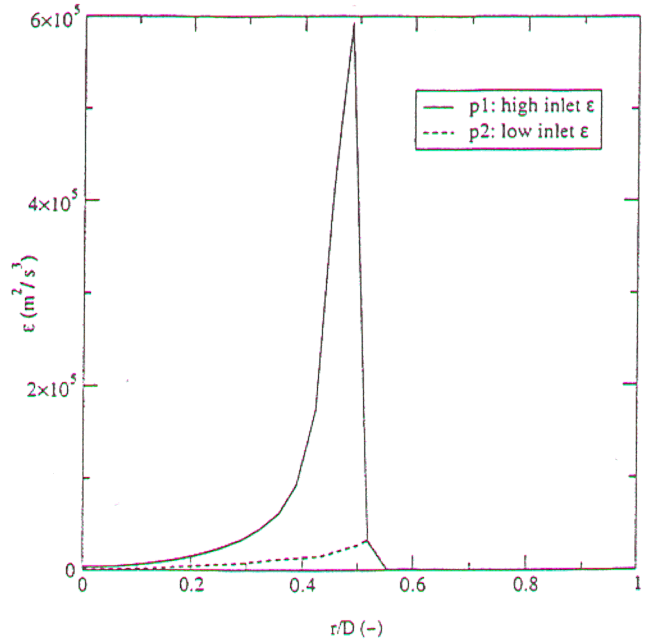
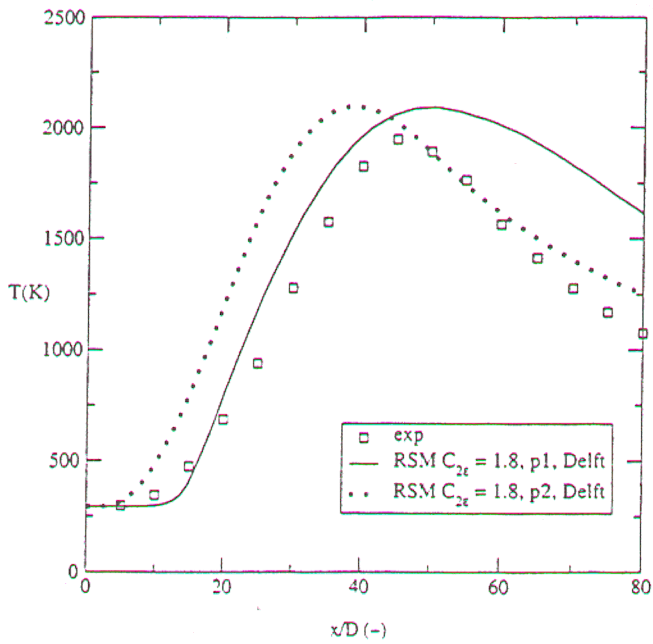
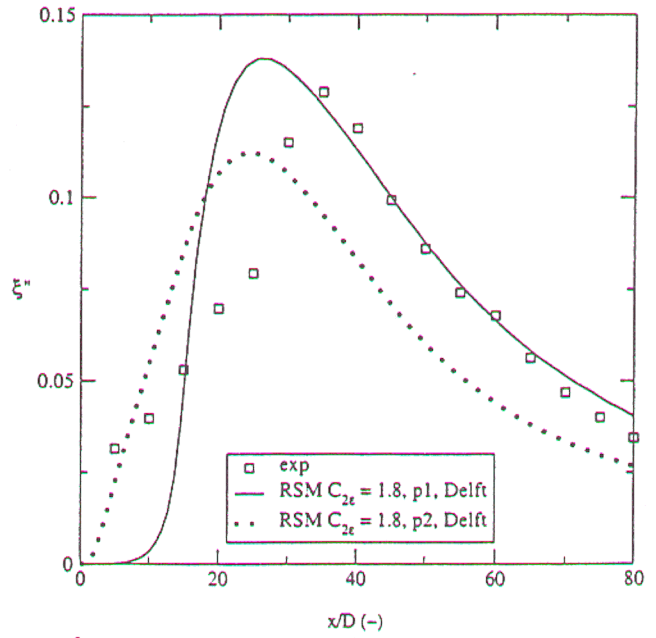
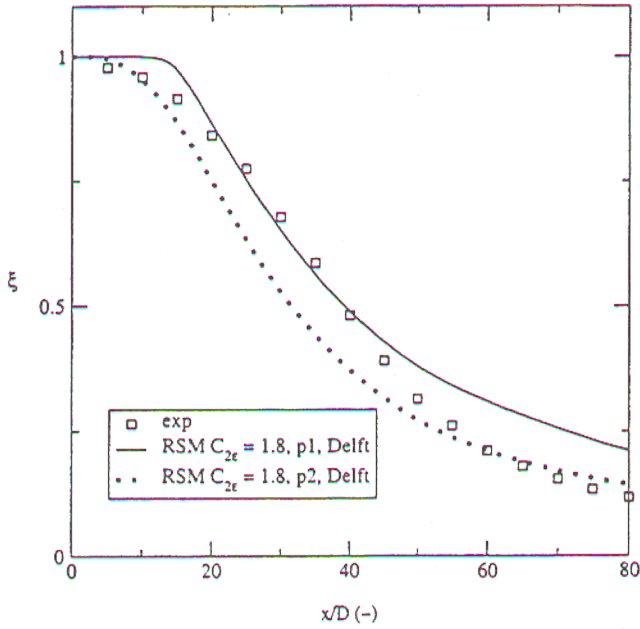
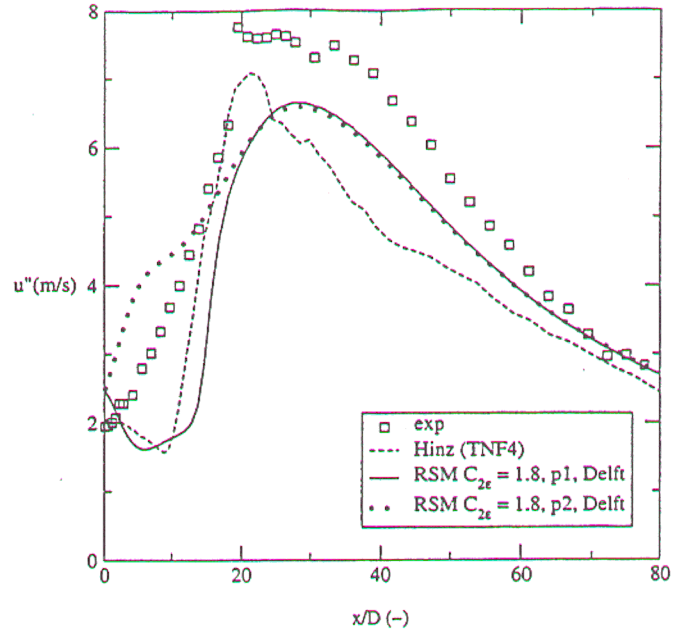
### flame D

p1: high inlet  $\epsilon$ ; p2: low inlet  $\epsilon$



### flame D

p1: high inlet  $\epsilon$ ; p2: low inlet  $\epsilon$



# SECTION 2

## Computations of Bluff-Body Stabilized Jets and Flames

# Fifth International Workshop on Measurement and Computation of Turbulent Nonpremixed Flames

TU Delft, Holland

July 27-28, 2000

## Computation of Bluff-Body Stabilised Jets and Flames

Coordinator:

A.R. Masri

Department of Mechanical and Mechatronic Engineering

The University of Sydney

NSW, 2006, Australia

### Burner Geometry

The bluff-body stabilised burner is located in a coflowing stream of air. The flame is not enclosed. The face of the burner is made of ceramic. The diameter of the bluff-body is 50mm and the central fuel jet diameter is 3.6mm. The burner assembly is located in a wind tunnel with an exit plane of 305x305mm.

### Computed Cases

#### Non-Reacting (NR)

- Jet: air in air
- Coflow air velocity = 20 m/s
- Bulk jet velocity = 62 m/s

Submitted comparisons: mean and rms velocity fluctuations for the axial and radial velocities.

#### Reacting (RX)

- HM1 flame
- Fuel Mixture: CH<sub>4</sub>/H<sub>2</sub> = 1/1 (by volume)
- Bulk jet velocity = 118 m/s
- Coflow air velocity = 40 m/s

Submitted comparisons: mean temperature and the mass fractions of OH and NO.

## Submissions

Computations were received from the following research groups

### Non-Reacting (NR)

Code	Approach	Authors	Institution
NR-01	k-e (modified)	Bart Merci and Erik Dick Dirk Roekaerts	University of Gent, Belgium Delft University of Technology
NR-02	Reynolds Stress	Bertrand Naud Dirk Roekaerts	Delft University of Technology Delft University of Technology
NR-03	Full-PDF	Kai Liu, Metin Muradglu Steve Pope and Dave Caughey	Mechanical and Aerospace, Cornell University, USA
NR-04	Hybrid-PDF	Metin Muradglu, Kai Liu Steve Pope and Dave Caughey	Mechanical and Aerospace, Cornell University, USA

### Reacting (RX)

Code	Approach	Authors	Institution
RX-01	k-e (modified)	Bart Merci and Erik Dick Dirk Roekaerts	University of Gent, Belgium Delft University of Technology
RX-02	Reynolds Stress	Bertrand Naud Dirk Roekaerts	Delft University of Technology Delft University of Technology
RX-03	Full-PDF	Kai Liu, Metin Muradglu Steve Pope and Dave Caughey	Mechanical and Aerospace, Cornell University, USA
RX-04	k-e-flamelet	Mamdud Hussain and W. Malalasekera ,	Mechanical Engineering Loughborough University, UK
RX-05	k-e-CMC	S.H. Kim and K.Y.Huh	POSTECH, Korea

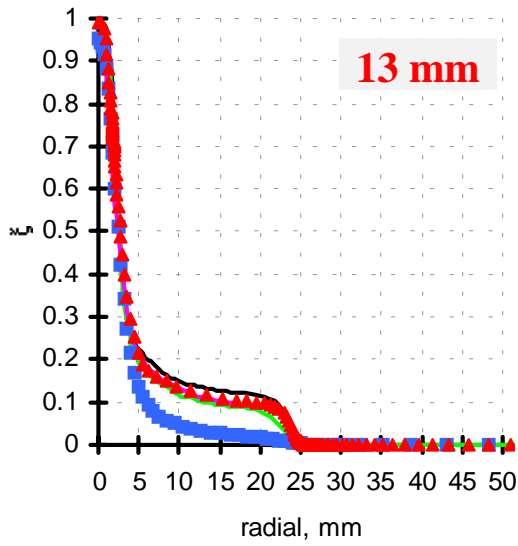
### Numerical information:

#### Non-Reacting (NR)

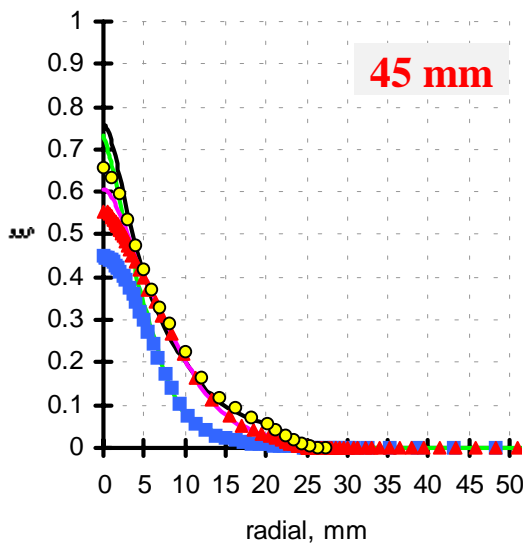
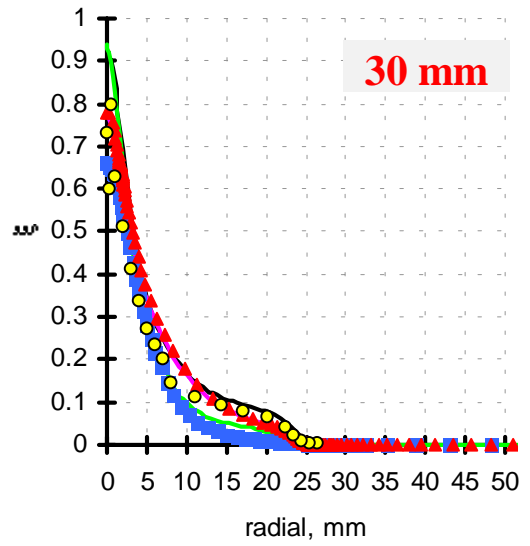
Code	C-e1	Grid Size	Sol'n Domain	Start Comp.	Assumed PDF	Chemistry
NR-01	1.44	105x141	500x100mm	-12.5mm	n/a	n/a
NR-02	1.6	104x144	200x100mm	-100mm	n/a	n/a
NR-03	PDF	65x65	300x150mm	0mm	(SLM, JPM and IEM models)	
NR-04	Hybrid	65x65	300x150mm	0mm	(SLM, JPM and IEM models)	
RX-01	1.44	105x141	1000x100mm	-12.5mm	Beta	Constrained Eq.
RX-02	1.6	104x144	200x100mm	-100mm	Beta	Equilibrium
RX-03	PDF	65x65	300x150mm	0mm	(SLM, JPM and IEM)	Flamelet
RX-04	1.6	99x98	216x170mm	0mm	Beta	Flamelet+diffdiff
RX-05	1.6	70x50	200x50mm	0mm	Beta	Miller-Bowman

### Acknowledgement

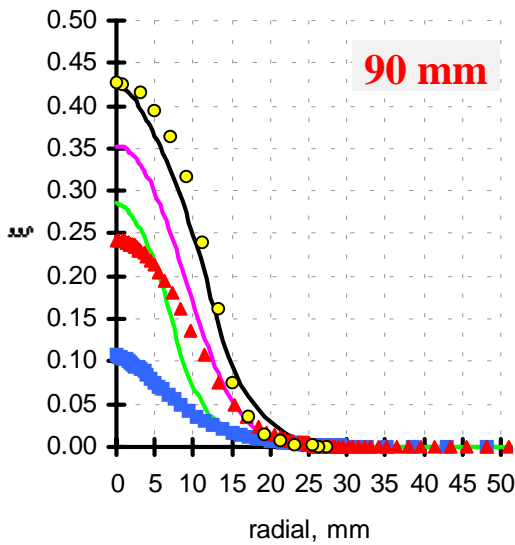
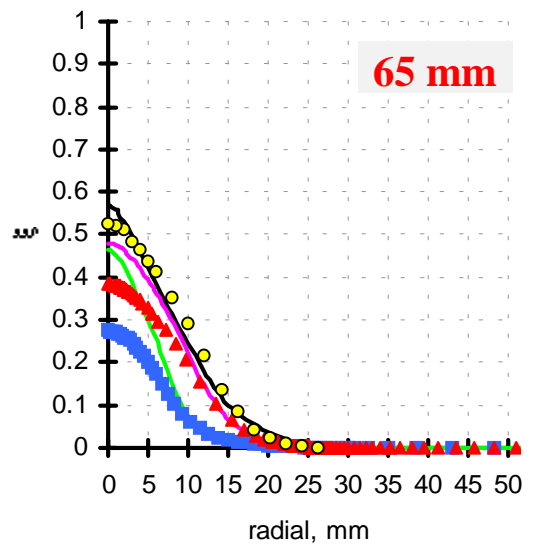
Thanks to all the groups who have contributed their computations for the comparisons presented here. Special thanks to Mr Yasir AlAbdeli for plotting the results.



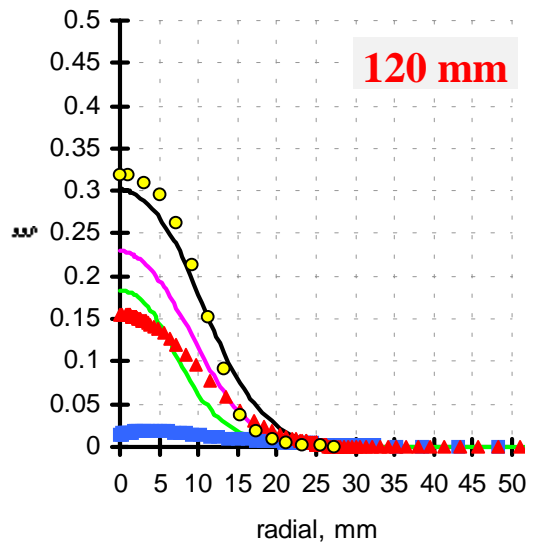
$u$



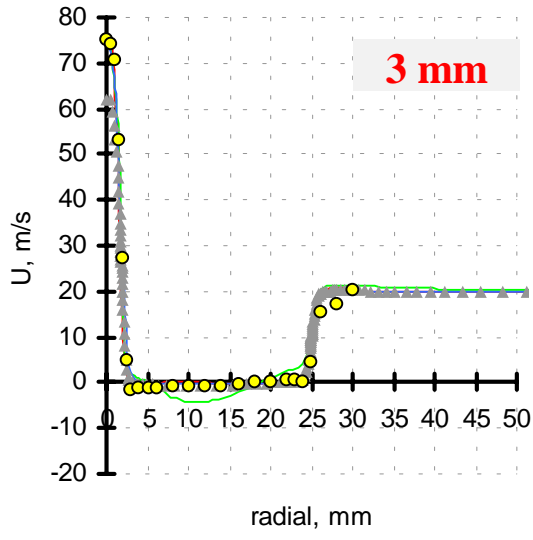
$u$



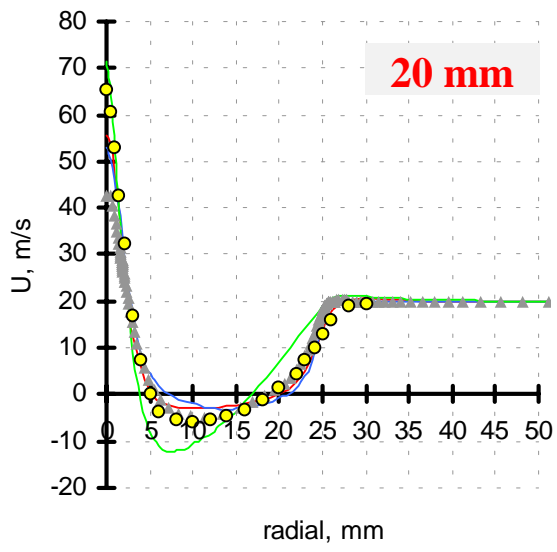
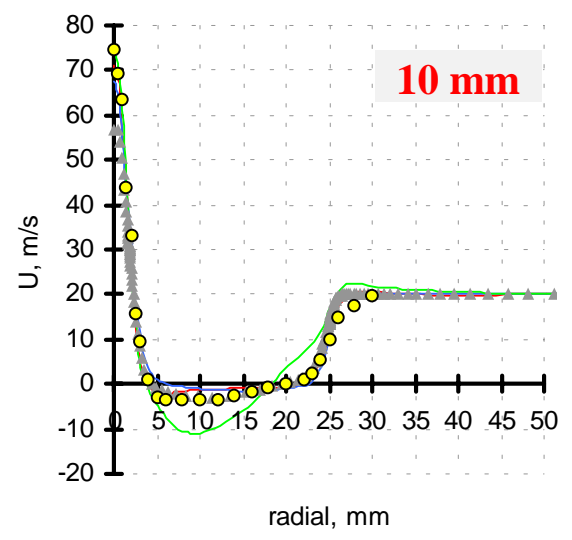
$u$



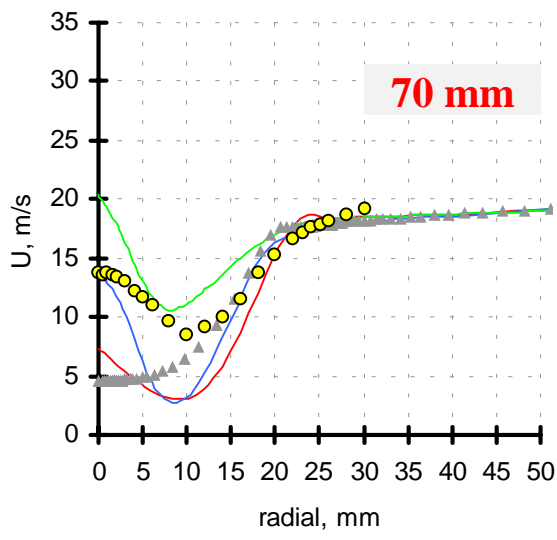
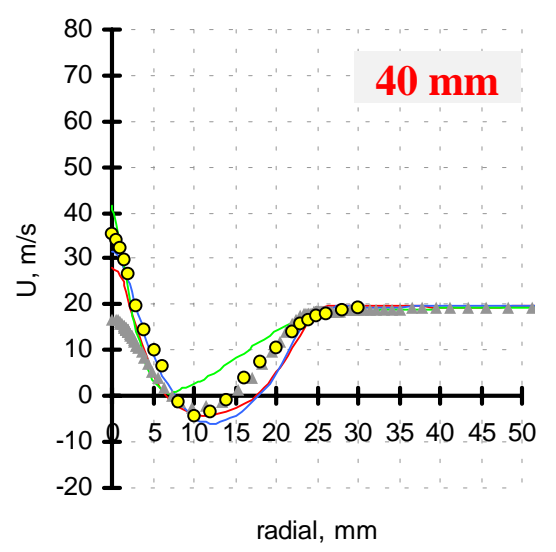
Key: Circles: Sydney experimental (reacting bluff body) data.  
Symbols & Lines **RED triangles** Merci & Dick (Gent / Belgium) **BLUE squares** Liu et al (Cornell / USA)  
**MAGENTA line** Hossain & Malalasekera (Nottingham / UK)  
**GREEN line** Naud (Delft / Netherlands) **BLACK line** Kim & Huh (Postech / Korea)



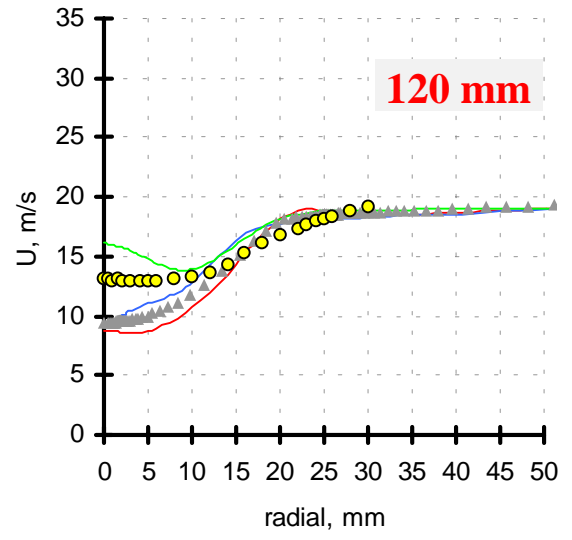
**U**



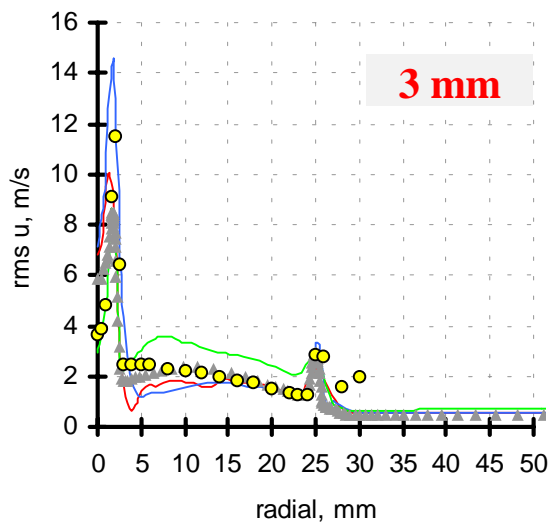
**U**



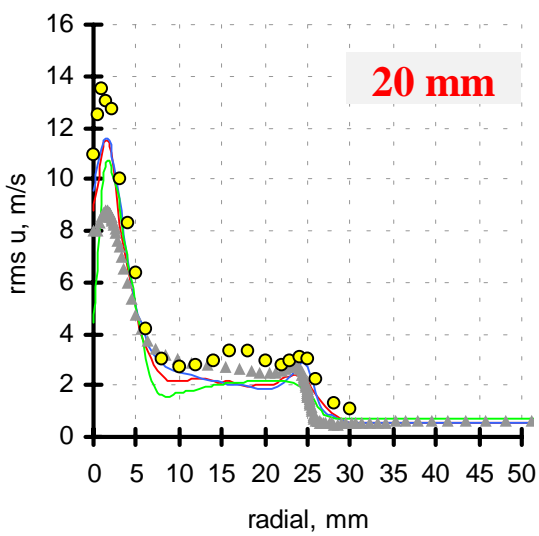
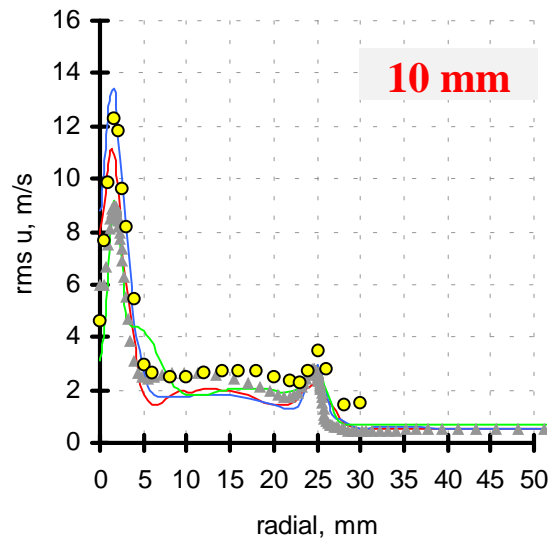
**U**



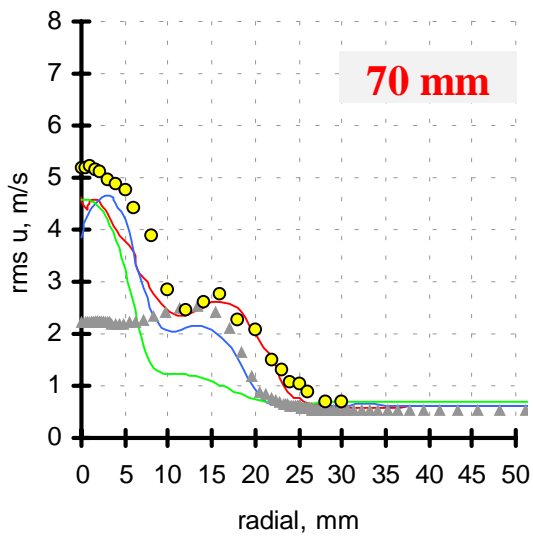
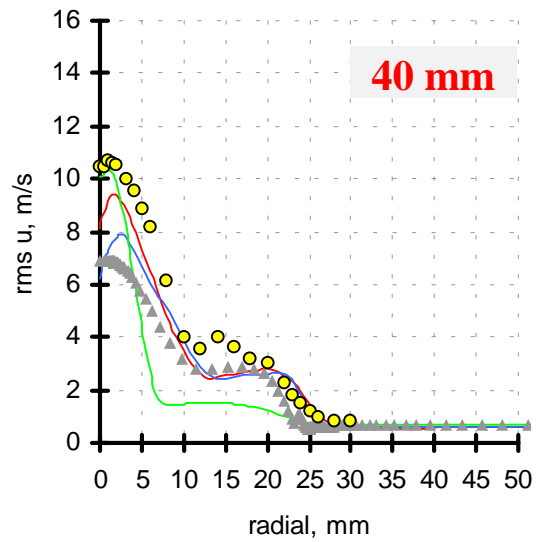
Key: **Circles:** Sydney experimental (non reacting bluff body) data.  
**Symbols & Lines** **GREY triangles** Merci & Dick (Gent / Belgium) **BLUE line** Liu et al (Cornell / USA)  
**GREEN line** Naud (Delft / Netherlands) **RED line** Muradoglu et al (Cornell / USA)



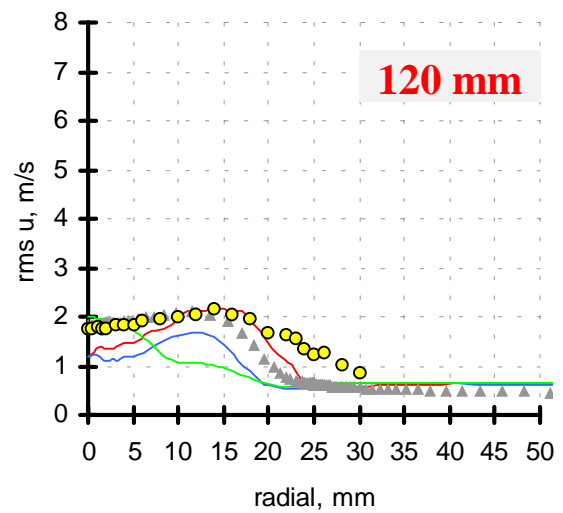
$u'$



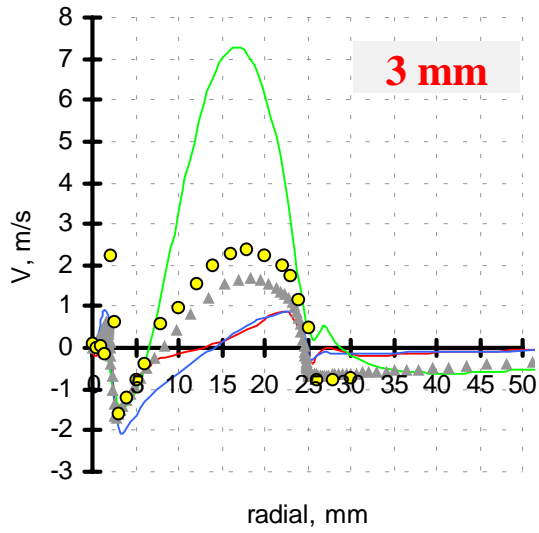
$u'$



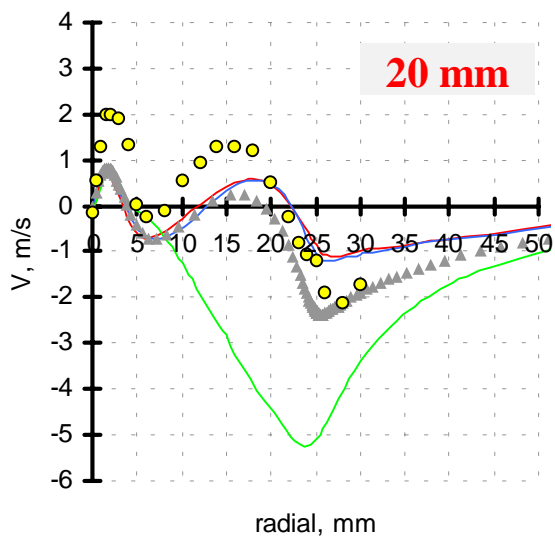
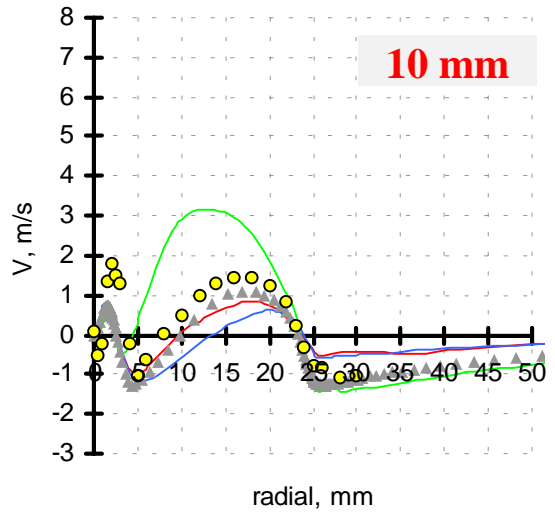
$u'$



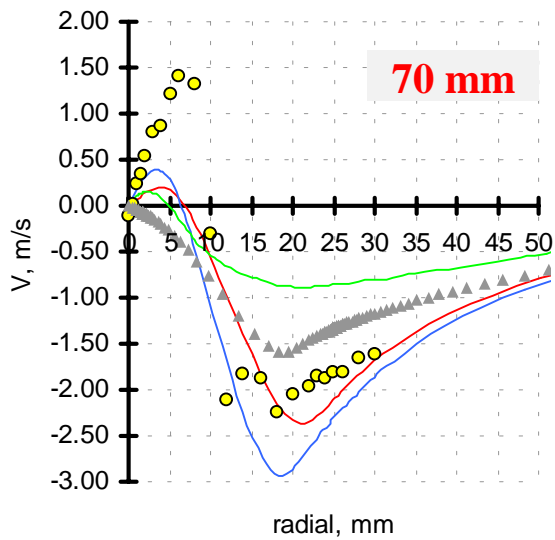
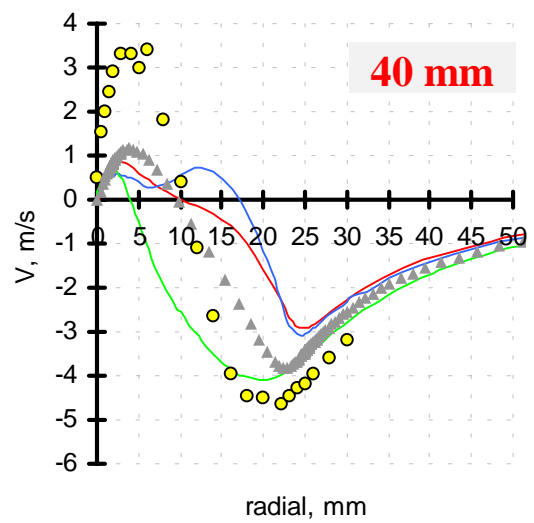
Key: Circles: Sydney experimental (non reacting bluff body) data.  
Symbols & Lines **GREY triangles** Merci & Dick (Gent / Belgium) **BLUE line** Liu et al (Cornell / USA)  
**GREEN line** Naud (Delft / Netherlands) **RED line** Muradoglu et al (Cornell / USA)



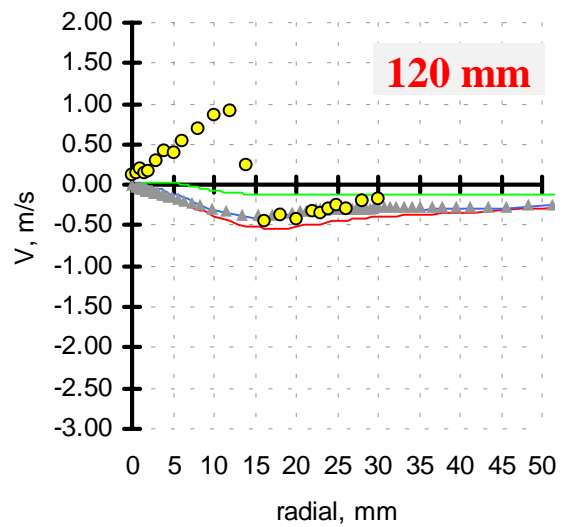
V



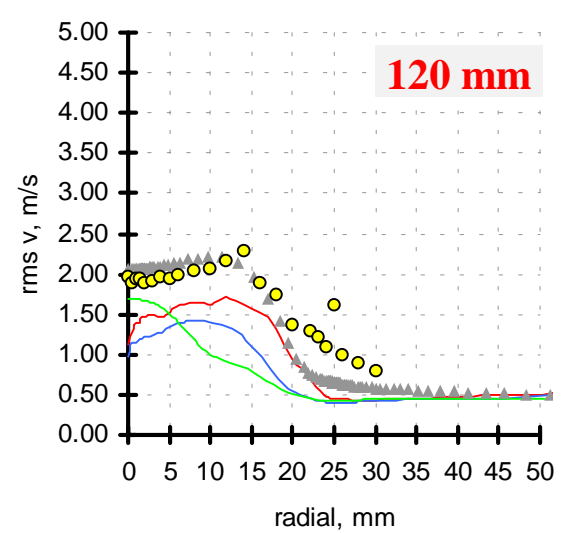
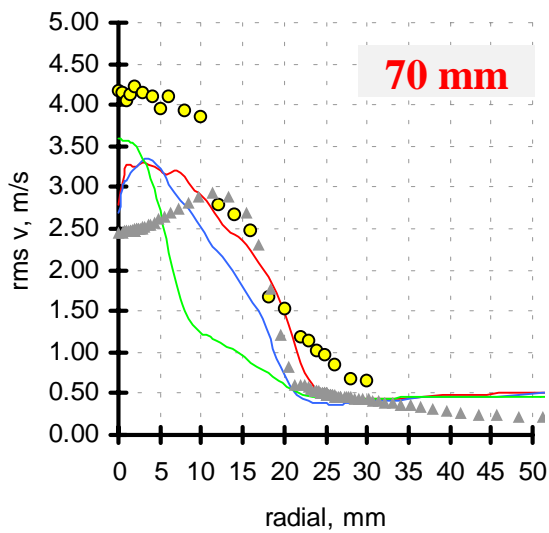
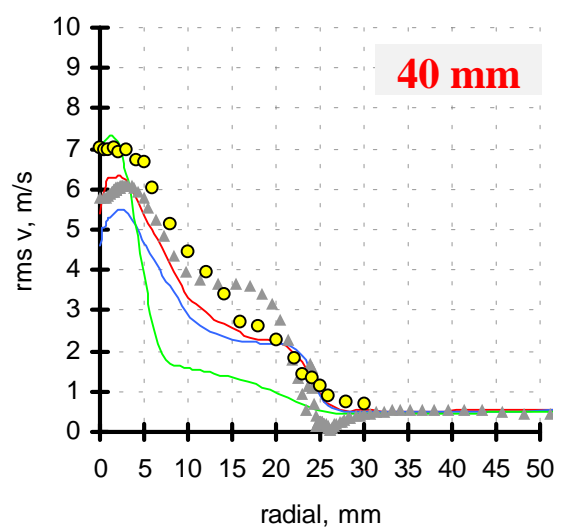
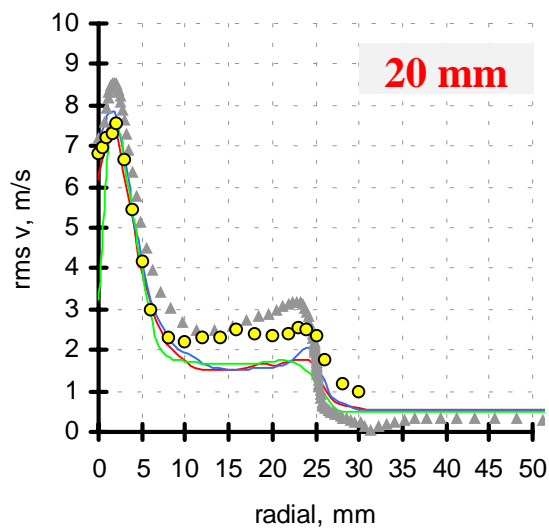
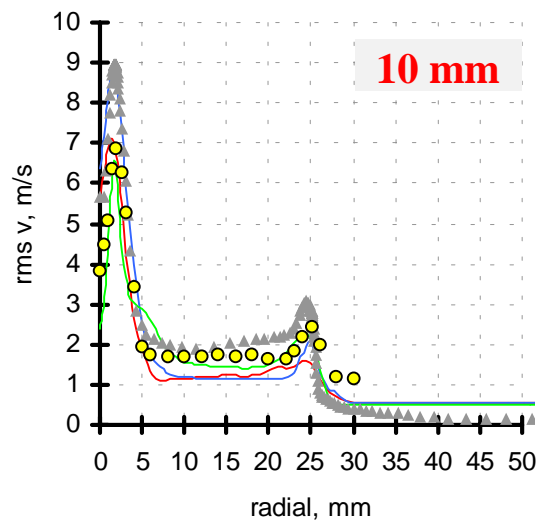
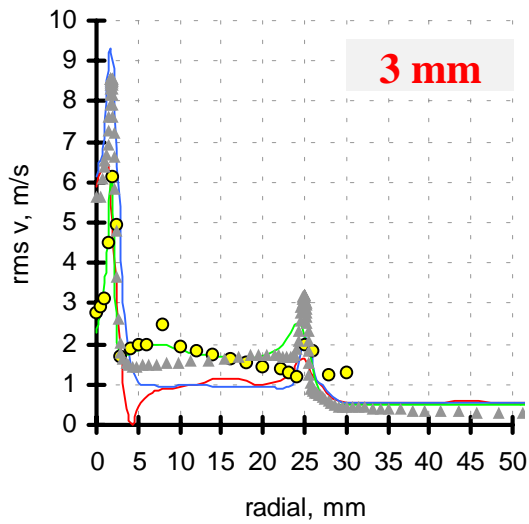
V



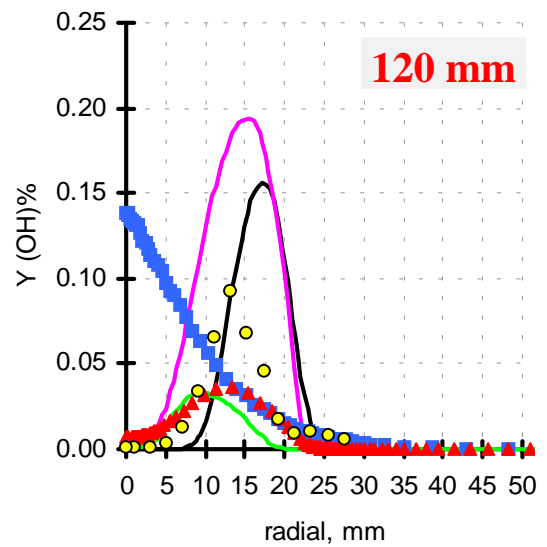
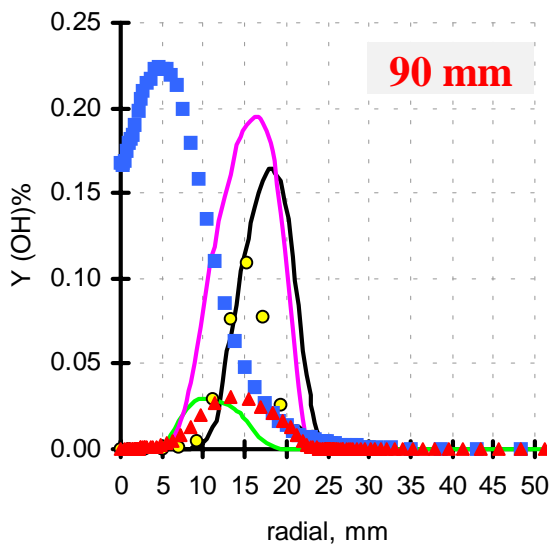
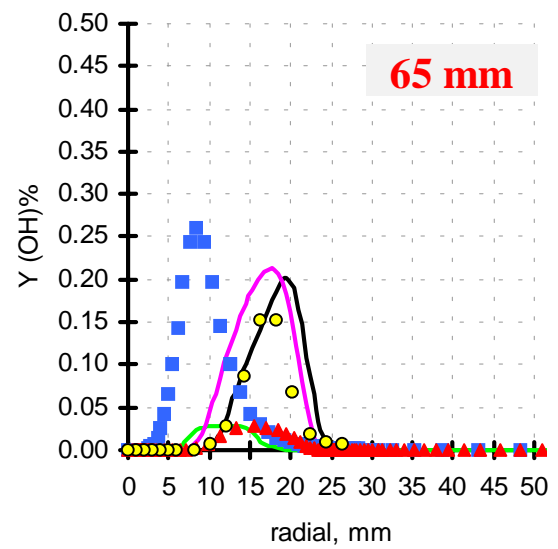
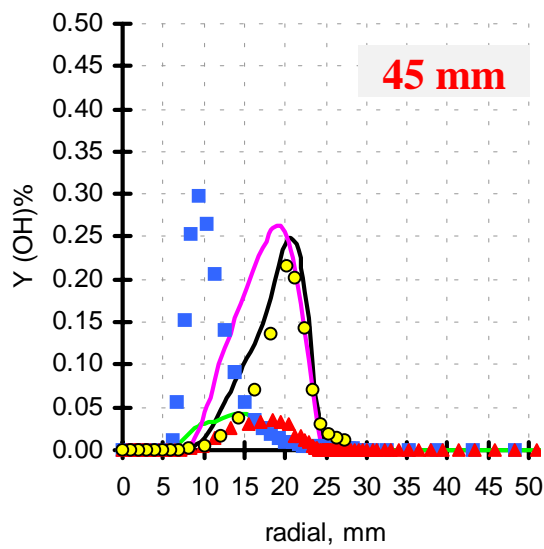
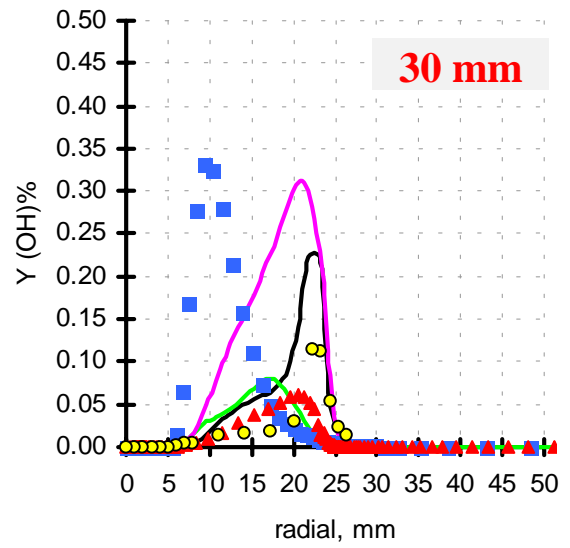
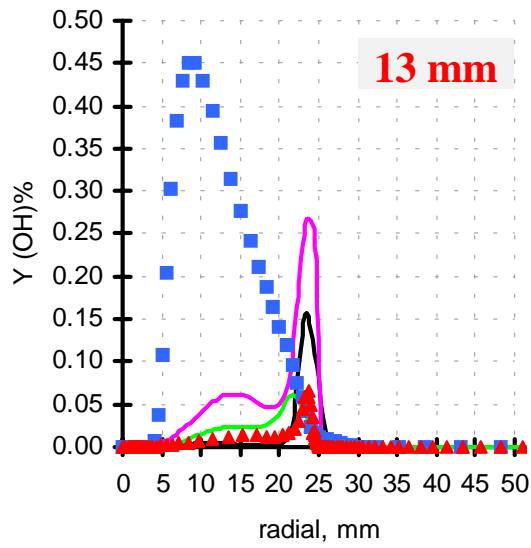
V



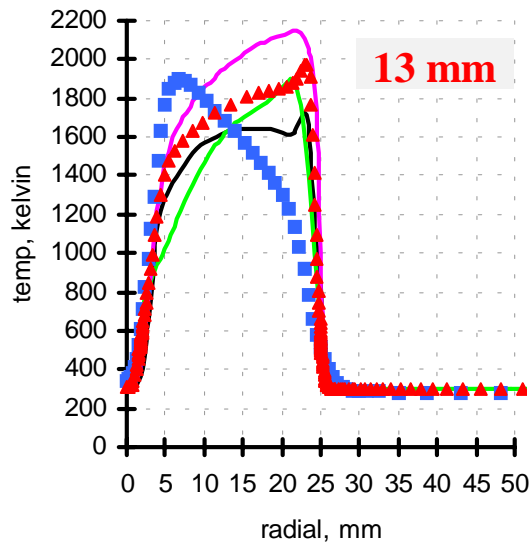
Key: **Circles:** Sydney experimental (non reacting bluff body) data.  
**Symbols & Lines** **GREY triangles** Merci & Dick (Gent / Belgium) **BLUE line** Liu et al (Cornell / USA)  
**GREEN line** Naud (Delft / Netherlands) **RED line** Muradoglu et al (Cornell / USA)



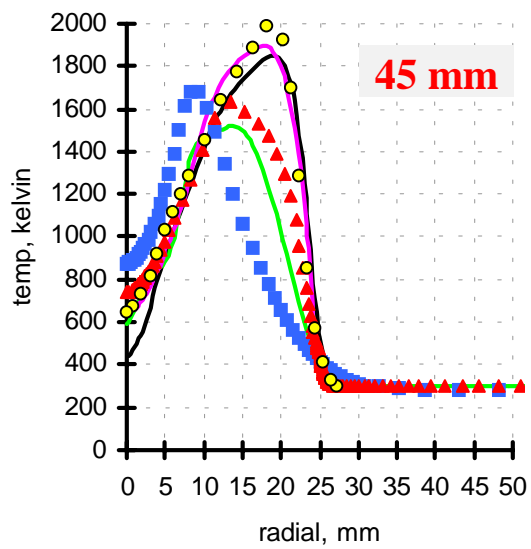
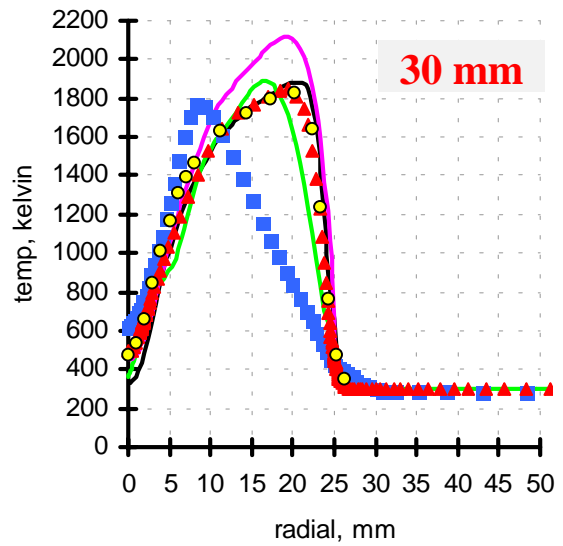
Key: **Circles:** Sydney experimental (non reacting bluff body) data.  
**Symbols & Lines** **GREY triangles** Merci & Dick (Gent / Belgium) **BLUE line** Liu et al (Cornell / USA)  
**GREEN line** Naud (Delft / Netherlands) **RED line** Muradoglu et al (Cornell / USA)



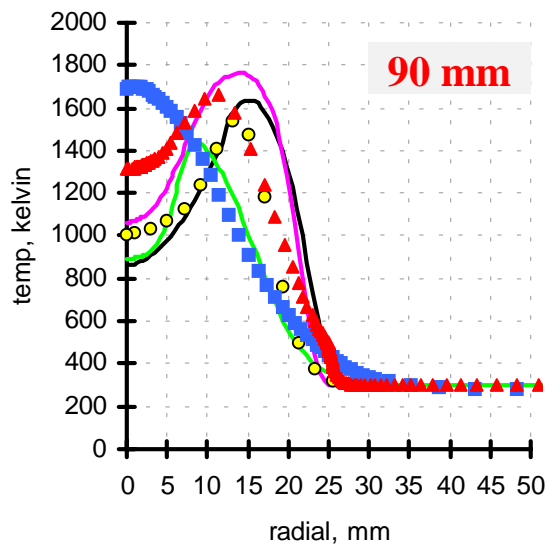
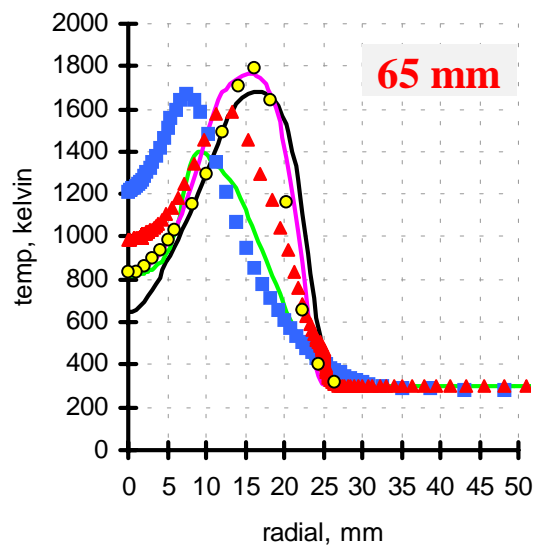
Key: Circles: Sydney experimental (reacting bluff body) data.  
Symbols & Lines **RED triangles** Merci & Dick (Gent / Belgium) **BLUE squares** Liu et al (Cornell / USA)  
**MAGENTA line** Hossain & Malalasekera (Nottingham / UK)  
**GREEN line** Naud (Delft / Netherlands) **BLACK line** Kim & Huh (Postech / Korea)



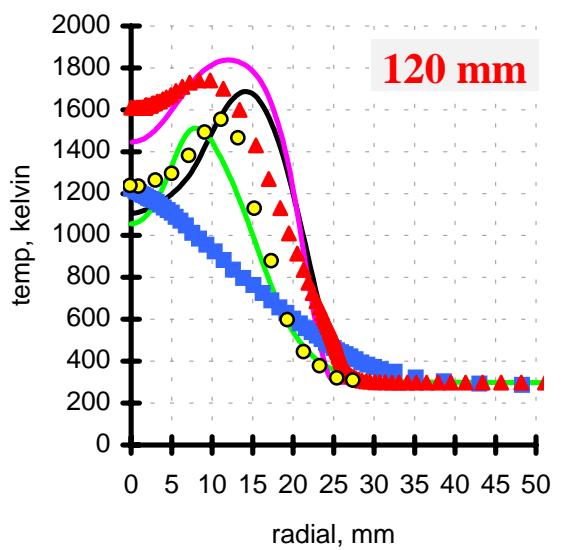
T



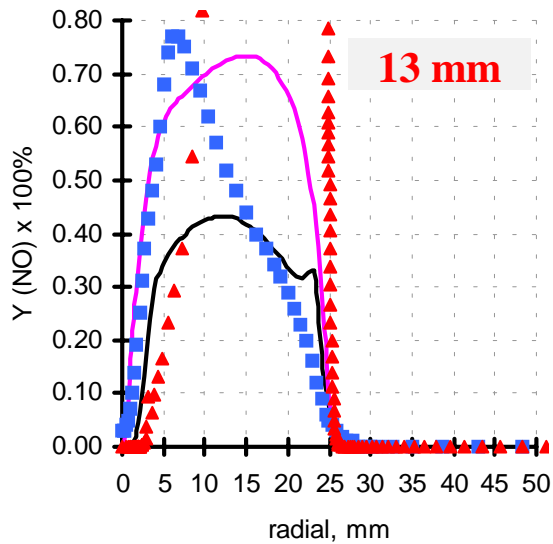
T



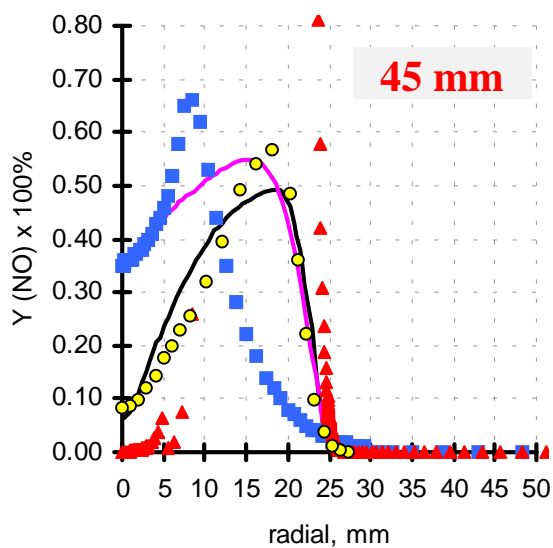
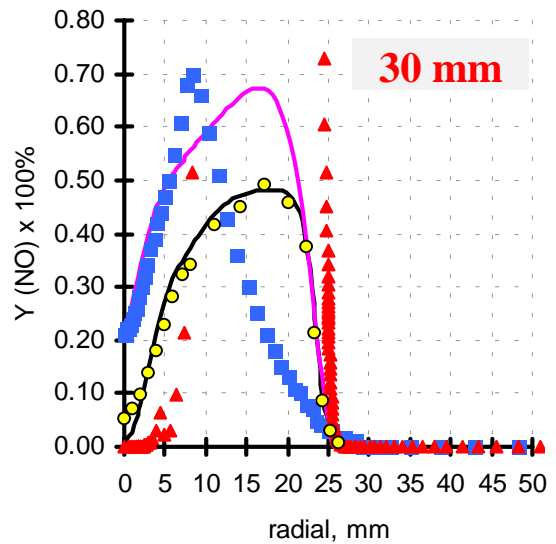
T



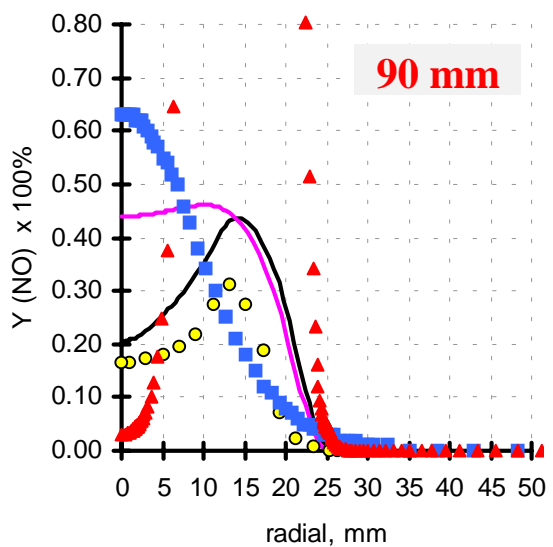
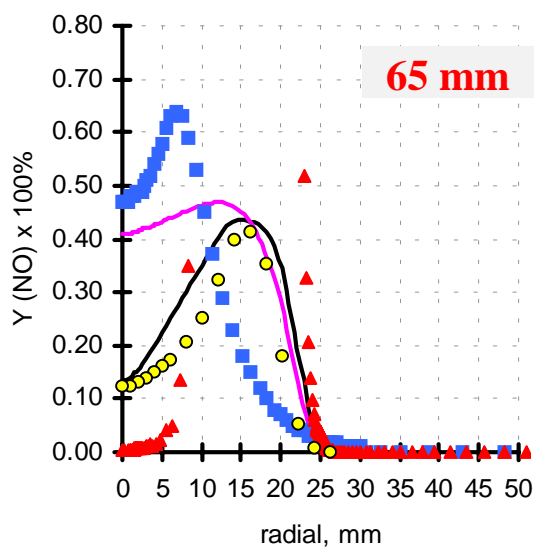
Key: Circles: Sydney experimental (reacting bluff body) data.  
Symbols & Lines **RED triangles** Merci & Dick (Gent / Belgium) **BLUE squares** Liu et al (Cornell / USA)  
**MAGENTA line** Hossain & Malalasekera (Nottingham / UK)  
**GREEN line** Naud (Delft / Netherlands) **BLACK line** Kim & Huh (Postech / Korea)



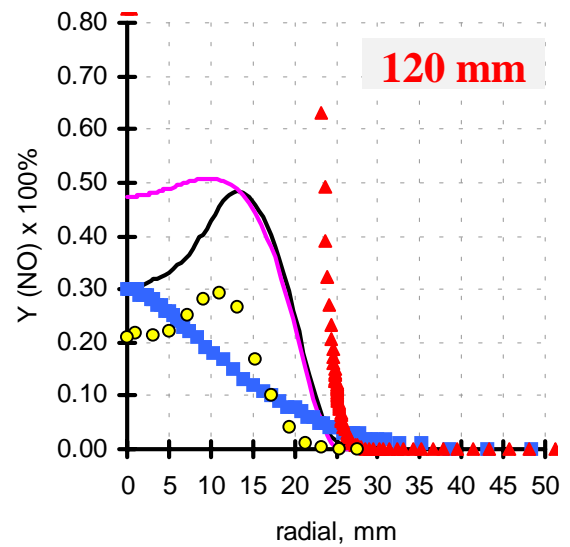
NO



NO



NO



Key: Circles: Sydney experimental (reacting bluff body) data.  
 Symbols & Lines **RED triangles** Merci & Dick (Gent / Belgium) **BLUE squares** Liu et al (Cornell / USA)  
**MAGENTA line** Hossain & Malalasekera (Nottingham / UK)  
**BLACK line** Kim & Huh (Postech / Korea)

# SECTION 3

## Confined TECFLAM Swirl Burner

# **Confined TECFLAM swirl burner: Experimental investigations and numerical simulations**

C. Schneider, S. Repp, A. Sadiki, A. Dreizler<sup>1</sup>, J. Janicka  
Energie- und Kraftwerkstechnik, TU Darmstadt  
Petersenstrasse 30, D-64287 Darmstadt

W. Meier, B. Noll  
Institut für Verbrennungstechnik, DLR Stuttgart  
Pfaffenwaldring 38, D-70569 Stuttgart

H. Bockhorn, W. Leuckel, B. Lenze, P. Schmittel  
Engler-Bunte-Institut, Bereich Verbrennungstechnik, Universität Karlsruhe  
Engler-Bunte-Ring 1, D-76128 Karlsruhe

C. Schulz, J. Wolfrum  
Physikalisch Chemisches Institut, Universität Heidelberg  
INF 253, D-69120 Heidelberg

## **Introduction**

A standard burner for confined swirling natural gas flames is presented which was developed within the German TECFLAM cooperation. The aims of the TECFLAM research program are the establishment of an extensive experimental database from selective flames and the validation and improvement of mathematical combustion models. Within this contribution, experimental as well as numerical results are presented and compared to each other.

Selected experimental results are obtained from non-intrusive laser based techniques and probe measurements, respectively. These data comprise joint PDF measurements of temperature, mixture fraction, and major species concentrations obtained by use of the Raman technique, elaborate velocity measurements performed with LDV, simultaneous two-dimensional Rayleigh/PLIF measurements as well as results from probe sample and thermocouple measurements. The data has been recorded in a turbulent diffusion flame with 150 kW thermal load, equivalence ratio 0.833, and swirl number 0.9. Major aspects of the investigation are the general quantitative characterization of the flame and the study of the thermochemical state, e.g. effects of turbulence-chemistry interactions. Also the consistency of the TECFLAM data is addressed in this presentation.

Furthermore, CFD calculations have been performed using different turbulence and chemistry models. In this context calculated results of the EKT Darmstadt are presented only. However, similar simulations were performed at the Engler-Bunte-Institut, Karlsruhe, and by the DLR Stuttgart. Approaches using LES for open (unconfined) TECFLAM burner are performed by Imperial College, UK.

In the following, some details are presented concerning the experiment as well as the laser based techniques. Figures including results and discussion are attached at the end of the text.

---

<sup>1</sup> Corresponding author: Andreas Dreizler, Energie- und Kraftwerkstechnik, TU Darmstadt, Petersenstrasse 30, 64287 Darmstadt, e-mail: dreizler@hrz2.hrz.tu-darmstadt.de, Tel.: +49 6151 16 2257, fax: +49 6151 16 6555

## Experiment

### Swirl burner

The swirl burner consists of a central bluff body, surrounded by one annulus of 3 mm width for the fuel (natural gas) and a second annulus (15 mm width) for the combustion air (<http://www.tu-darmstadt.de/fb/mb/ekt/>). The air flow is swirled by a moveable block with a variable intensity between  $S=0$  and 2.0 in terms of a theoretical swirl number. The thermal load amounts 150 kW. The corresponding Reynolds numbers are 42900 at the air flow inlet and 7900 at the (non-swirled) fuel flow inlet. The chamber walls are water-cooled with 60% of the thermal power transferred to the cooling water. Geometry of the chamber is as follows: Height  $H_c=1200$  mm, Diameter,  $D_c=500$ mm. The combustion chamber allows optical access by four quartz windows. An annular slit for the exhaust gas is placed at the top. The burner can be moved vertically within the chamber like a piston by 500 mm in order to change the relative measuring height. Note that it is experimentally checked that the height of the combustion chamber is of no significant importance for the flow field. The axial symmetry of the flame was experimentally checked and confirmed. The features of the overall flow field can be divided into three regimes: (1) the mixing zone between the fuel and air streams where combustion takes place predominantly, (2) the inner recirculation zone around the flame axis, and (3) the outer recirculation zone (compare transparency “General Features III” in the attached result section).

### LDV measurements (EKT Darmstadt and EBI Karlsruhe (similar set-up))

A two-component fiber optic Laser-Doppler-Anemometer (Dantec) was used to determine the velocity characteristics of the flow field. A 4 W argon-ion laser served as light source. The laser beam was submitted to a transmitter box. A Bragg cell divided the incoming beam into different colours. Two beam pairs of the wavelengths  $\lambda_g = 514.5$  nm (green) and  $\lambda_b=488$  nm (blue) were selected to survey the axial and the radial/circumferential velocity component, depending on the traversing direction. The first order beam of each colour was frequency shifted at 40 MHz. The laser beams (diameter of 2.2 mm) were then coupled into a fiber optic probe and collimated in the measurement volume with a front lens of  $f_1 = 500$  mm focal length. A beam expander ( $m = 1.9$ ) was applied to reduce the size of the measurement volume to allow analysis of regions of high velocity gradients in the flow. The distance between the beam pairs was  $D_s = 72$  mm. With these values, the size of the probe volume could be calculated to a length of  $I_m = 0.780$  mm and to a diameter of  $d_m = 0.094$  mm. Photomultipliers observed the measurement volume through interference filters in backward scatter mode. The signal was electronically down mixed depending on the measured Doppler frequency. A digital auto-correlator evaluated the Doppler signals. Statistical averaging was transit time weighted to minimize velocity bias. An estimate of the statistical error concerning mean velocity was 5%, whereas fluctuations were accurate within 10%. Data obtained from the shear zone were even more accurate.

### Raman measurements (DLR Stuttgart)

The Raman system, described in detail in [1, 2], is based on a flashlamp pumped dye laser ( $\lambda=489$  nm, 2  $\mu$ s pulse duration, 3 J pulse energy) whose beam is focused into the combustion chamber by a lens and retroreflected on the other side by a spherical mirror. The scattered light from the focal region is collected at 90° by an achromatic lens ( $\varnothing=100$  mm,  $f=300$  mm) and relayed to the entrance slit of a spectrograph. After spectral separation, the Raman signals from the major species  $\text{CH}_4$ ,  $\text{H}_2$ ,  $\text{O}_2$ ,  $\text{N}_2$ ,  $\text{H}_2\text{O}$ ,  $\text{CO}_2$ , and  $\text{CO}$  are detected simultaneously by

photomultiplier tubes, transferred to gated integrators, and finally stored and processed in a PC. The spatial resolution of the measurement is determined by the focal diameter of the laser beam and the slit width of the spectrograph and is 0.6 mm in each dimension.

In order to determine the number density of each species, the Raman signals are calibrated in cold and heated flows and in the exhaust gas of premixed laminar flames [2, 3]. The temperature is determined from the total number density via the ideal gas law, and the mixture fraction  $f$  is calculated using Bilger's definition [4], which is based on the measured atomic mass fractions of O, H, and C. The data evaluation includes corrections for cross talk between different Raman channels and background from laser induced fluorescence from water and polycyclic hydrocarbons (PAHs). The background from laser excited PAH emissions is corrected for by using the signals from additional photomultiplier tubes installed in Raman-free regions of the spectrum [2]. In the flame investigated the PAH concentrations are significantly smaller than in fuel-rich regions of jet diffusion flames [2], probably due to fast and efficient mixing of fuel and air by the swirling flow field which diminishes the formation of (large) PAHs. The accuracy achieved for the mean values is typically 2-3% for the temperature, 2% for  $N_2$ , 4% for  $CO_2$  and decreases for smaller mole fractions. The accuracy of a single-pulse measurement is reduced due to photon statistics and is on the order of 5% for the temperature, 5-7% for  $H_2O$  (with a mole fraction of 0.2 at 2000 K), 12-15% for  $O_2$  (mole fraction 0.03,  $T \approx 2000$  K), and 2% for  $CH_4$  (mole fraction 1,  $T \approx 1000$  K). The accuracy of the CO detection is lower than for the other species because of corrections for cross talk and interferences stemming from PAHs. For a CO mole fraction of 0.06 the accuracy of the measurements is 20%, for a mole fraction of 0.02 it is 50%. The investigation of the swirling flame is performed by recording series of 300 single-pulse measurements at eight different heights above the nozzle ( $h=10$  to 300 mm) and at radial locations ranging from -10 to 150 mm.

- [1] W. Meier, S. Prucker, M.-H. Cao, W. Stricker: *Combust. Sci. Technol.* **118**, 293 (1996)
- [2] V. Bergmann, W. Meier, D. Wolff, W. Stricker: *Appl. Phys. B* **66**, 489 (1998)
- [3] S. Prucker, W. Meier, W. Stricker: *Rev. Sci. Instrum.* **65**, 2908 (1994)
- [4] R.W. Bilger: *22nd Symposium (Int'l) on Combustion* (The Combustion Institute, Pittsburgh, 1988) p. 475

### **Rayleigh/PLIF measurements (PCI Heidelberg)**

#### *Temperature:*

Rayleigh imaging is used for thermometry. For excitation a KrF excimer laser @248nm is employed. The calibration is based on measurements in cold ambient air and on measurements in a calibration flame.

#### *NO concentration:*

NO concentration fields are measured by laser-induced fluorescence (LIF) imaging. For the excitation of NO the A-X(0,0)  $R_1(21.5)$  transition at 225.2 nm is used. Laser light of this wavelength is generated by  $H_2$ -Raman-shifting of a tunable KrF excimer laser. Fluorescence is detected in a range from 230 – 255nm. Calibration is performed by using a lean calibration flame doped with different concentrations of NO. The correction for quenching is based on the assumption of a gas composition according to completely burned gases. Simultaneously measured local temperatures are used to correct for temperature-dependent effects (absorption and fluorescence quantum yield)

#### *OH concentration:*

OH concentration fields are recorded by laser-induced fluorescence imaging. OH is excited at the A-X(3,0) P<sub>2</sub>(8) transition at 248 nm by use of a tunable KrF excimer laser. Detection of fluorescence is performed at 295 ± 5 nm. For calibration a calibration flame and literature data of OH concentrations is used.

#### *CH<sub>2</sub>O distribution:*

Qualitative CH<sub>2</sub>O distributions are measured by laser-induced fluorescence imaging using an excitation wavelength of 353.2 nm. For this purpose a tunable XeF excimer laser is used. Fluorescence is detected from 295 to 450 nm. Measurements are showing qualitative CH<sub>2</sub>O-LIF-intensity distributions only.

- [1] T. Landefeld, A., Kremer, E.P. Hassel, J. Janicka, T. Schäfer, J. Kazenwadel, C. Schulz, J. Wolfrum, *Laserdiagnostic and numerical studies of strongly swirling natural-gas flames*, Proc. Combust. Inst. 27, 1023-1030 (1998).
- [2] S. Böckle, J. Kazenwadel, T. Kunzelmann, D.-I. Shin, C. Schulz, *Single-shot laser-induced fluorescence imaging of formaldehyde with XeF excimer excitation*, Applied Physics B 70, 733-735 (2000).
- [3] S. Böckle, J. Kazenwadel, T. Kunzelmann, D.-I. Shin, C. Schulz, J. Wolfrum, *Simultaneous single-shot laser-based imaging of formaldehyde, OH and temperature in turbulent flames*, Proc. Combust. Inst. 28, in press (2000).
- [4] S. Böckle, J. Kazenwadel, C. Schulz, *Laser-diagnostic multi-species imaging in strongly swirling natural gas flames*, Appl. Phys. B, in press (2000).

## **Results**

Selected results are presented in the following figures including comparisons to results of numerical simulations.

## Confined TECFLAM swirl burner: experimental investigations and numerical simulations

W. Meier, B. Noll

Institut für Verbrennungstechnik, DLR Stuttgart

H. Bockhorn, W. Leuckel

Engler-Bunte-Institut, Universität Karlsruhe

C. Schulz, J. Wolfrum

Physikalisch Chemisches Institut, Universität Heidelberg

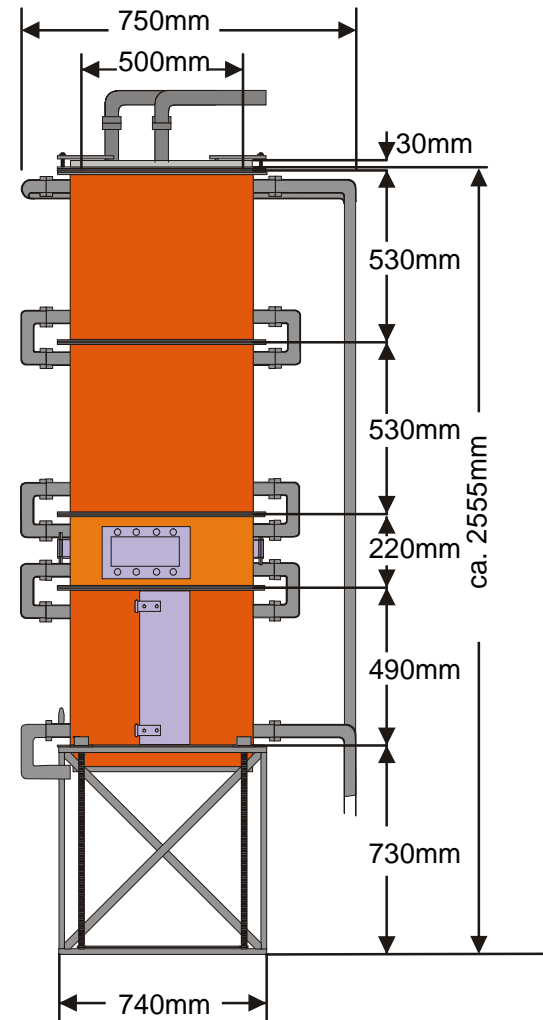
C. Schneider, S. Repp, A. Sadiki, **A. Dreizler**, J. Janicka

Energie- und Kraftwerkstechnik, TU Darmstadt

- General features of the swirl burner and burning chamber
- Experimental investigations
  - Survey of methods
  - Consistency
  - Selected results
- Numerical investigations
  - Survey of numerical approaches
  - Numerical set-up
- Comparisons of experimental and numerical data
- Conclusions

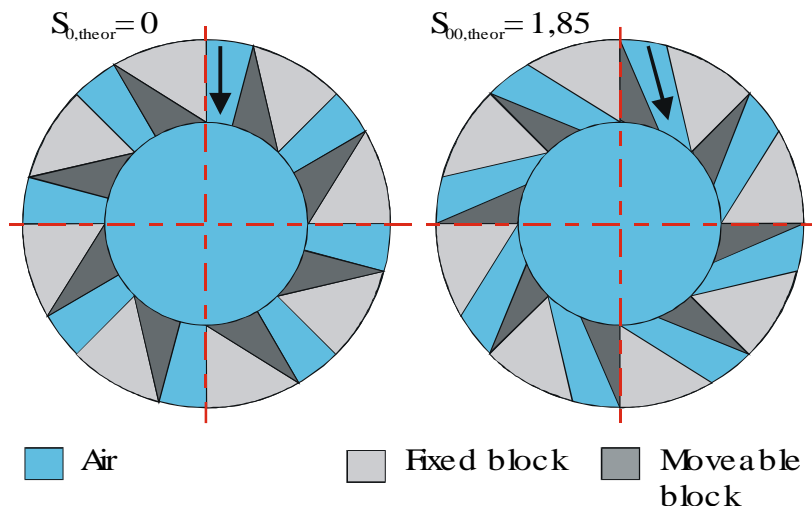
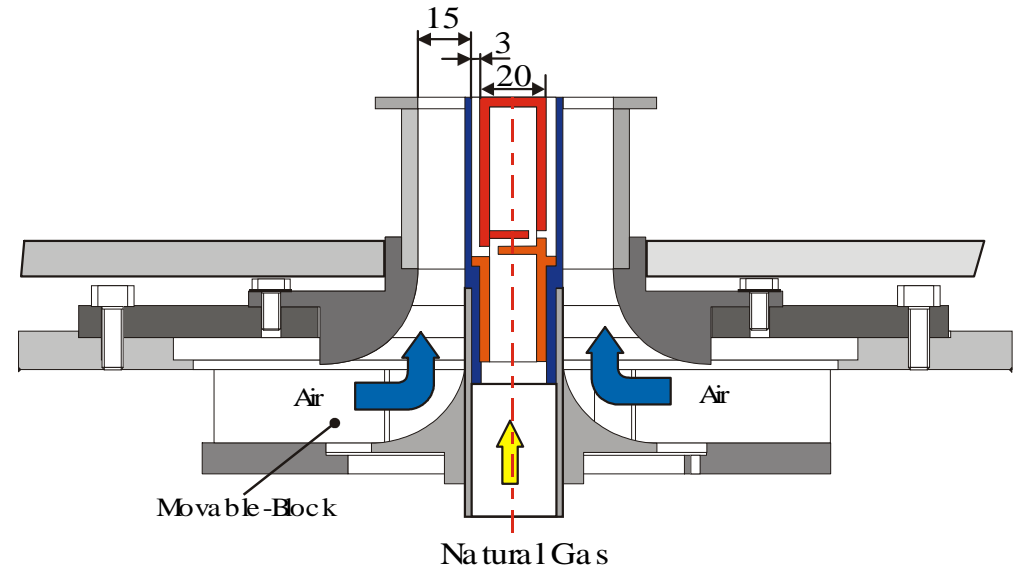
## Combustion chamber

- Height 1200 mm
- Inner diameter 500 mm
- Double walled
- Water cooled (80°C)

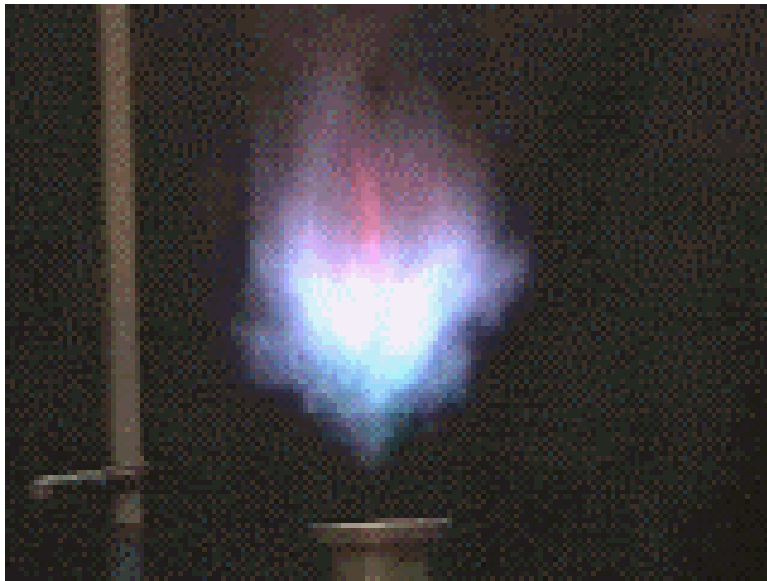


## Swirl burner

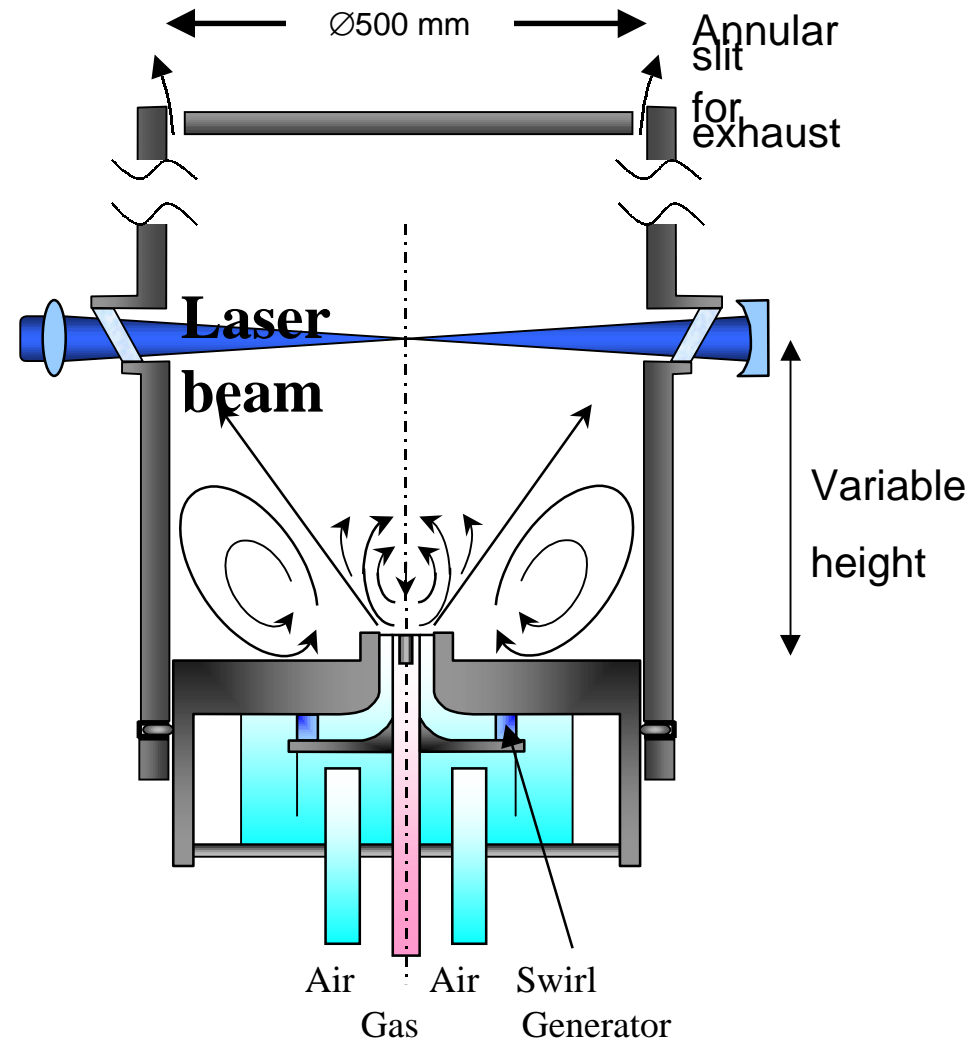
- Central bluff body
- Airflow swirled only
- Variable swirl number ( $S_{theo} = 0 - 2$ )
- Variable thermal load (50 - 350 kW)
- Fuel: natural gas



# General features III



Snap shot of the swirl flame



Sketch of the burner

## TECFLAM test cases:

**S09C**

**S14C**

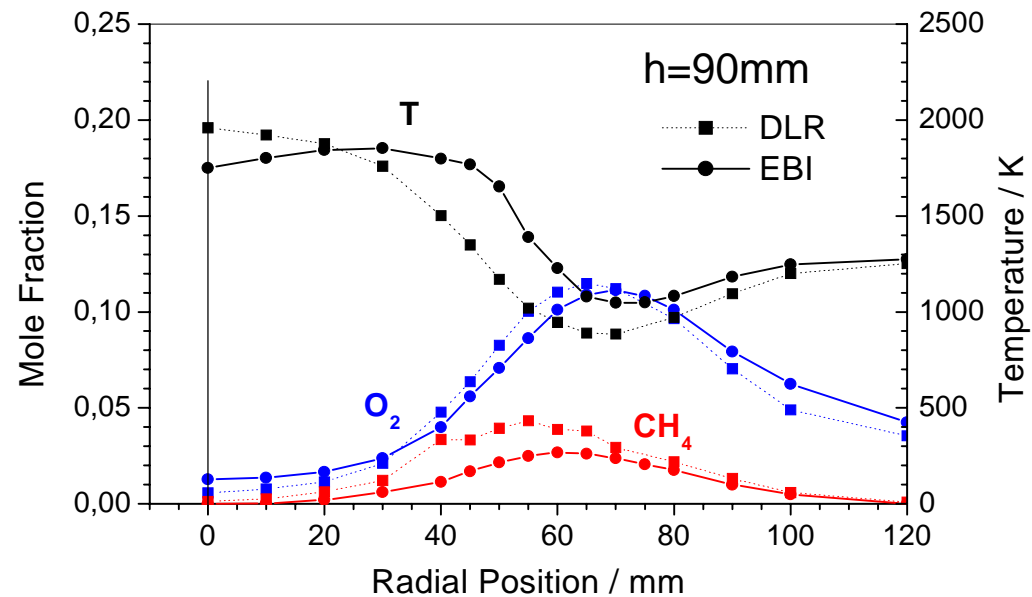
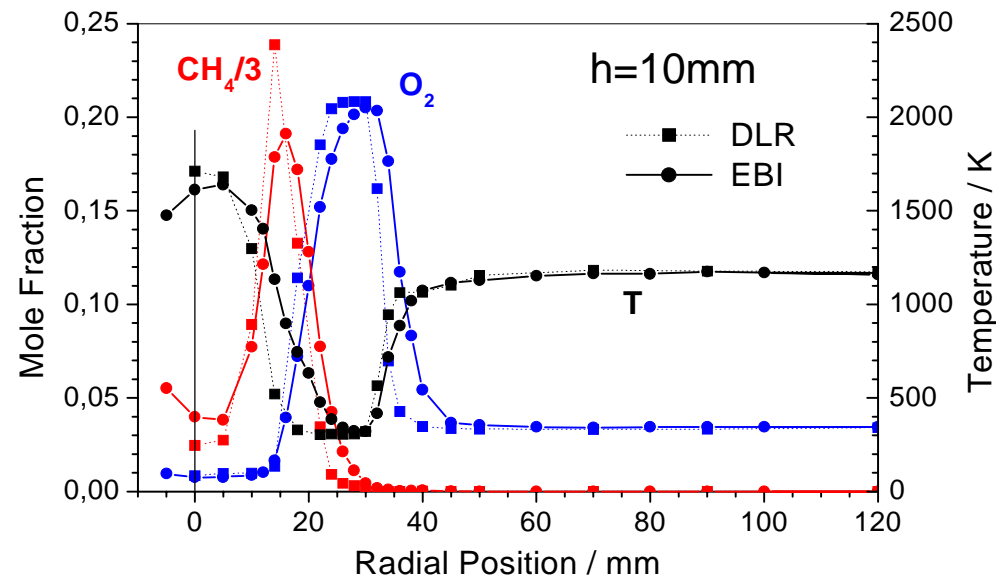
- Thermal power: 150 kW
- Swirl number S: 0.9 **1.4**
- Equivalence ratio: 0.833
- Fuel: natural gas
- Chamber pressure: ambient pressure
- Exit bulk velocity air: 23 ms<sup>-1</sup>
- Exit bulk velocity natural gas: 21 ms<sup>-1</sup>
- Re-number air: 42900
- Re-number natural gas: 7900
- Temperature cooling water: 80°C

## Experimental techniques

Quantity	Method	Executors
Velocity	Laser Doppler Velocimetry	EKT, EBI
Temp., main species	Raman scattering	DLR
Stable species	Probe sampling	EBI
2D temp. distribution	Rayleigh	PCI
Temperature	Thermocouple	EBI
Intermediates (OH, NO, CH <sub>2</sub> O)	Planar LIF	PCI

EBI, Karlsruhe; EKT, Darmstadt; DLR, Stuttgart; PCI, Heidelberg

## Consistency of temperature and species measurements Favre averaged

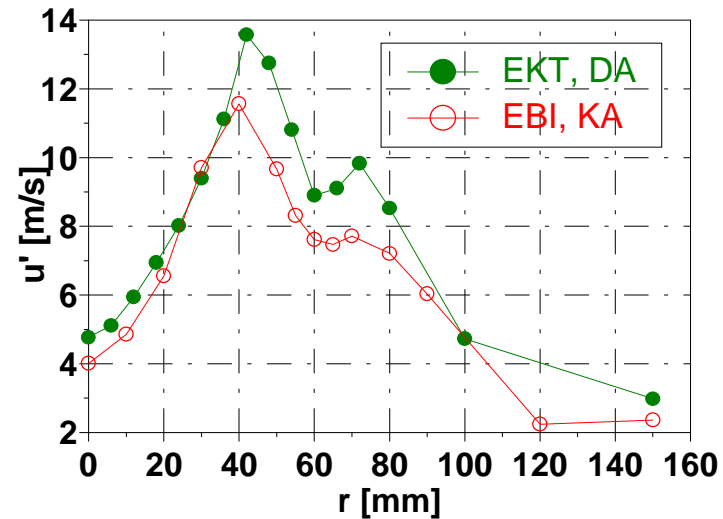
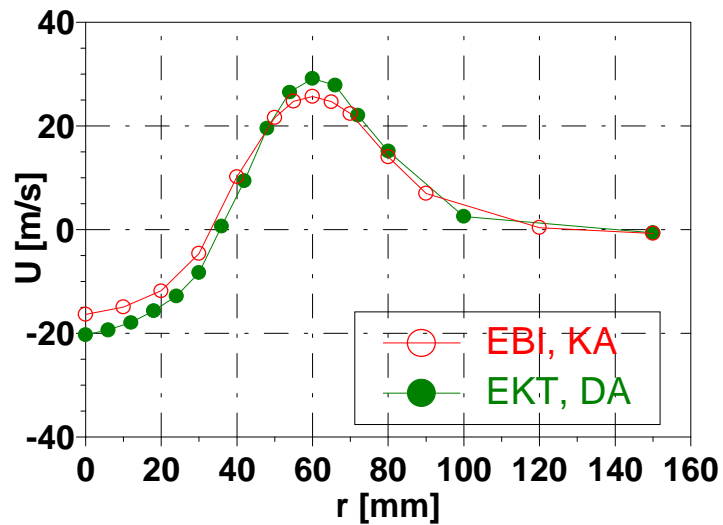


DLR - Raman measurement

EBI - Probe measurement

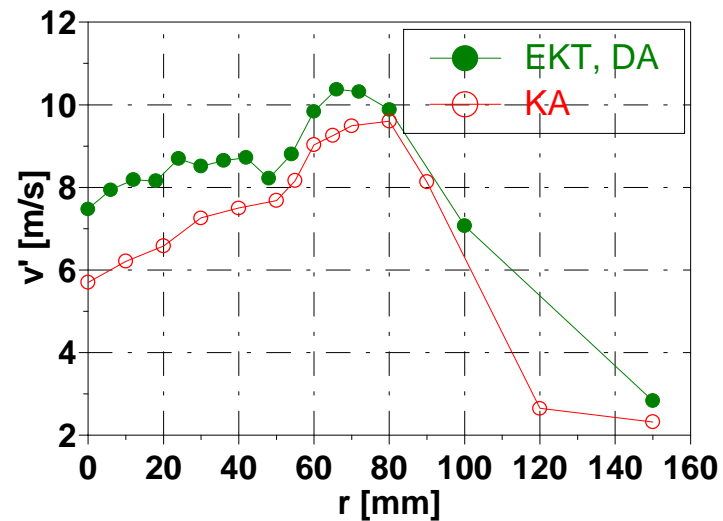
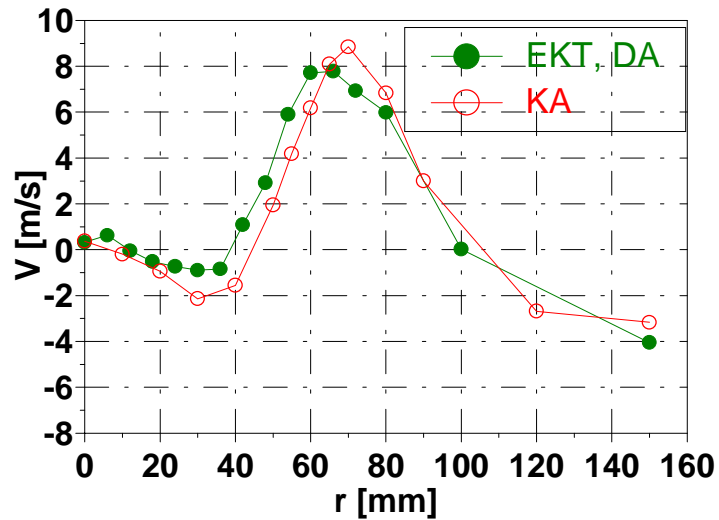
## Consistency of flow field measurements, LDV

Axial position  $h = 90$  mm



## Consistency of flow field measurements, LDV

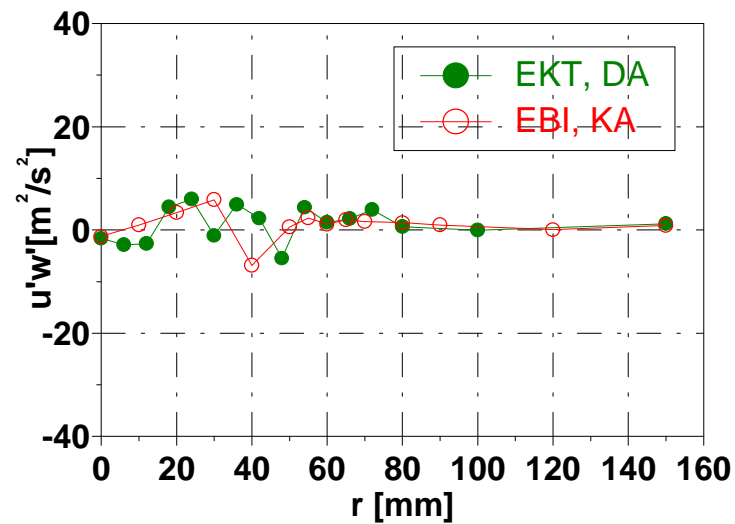
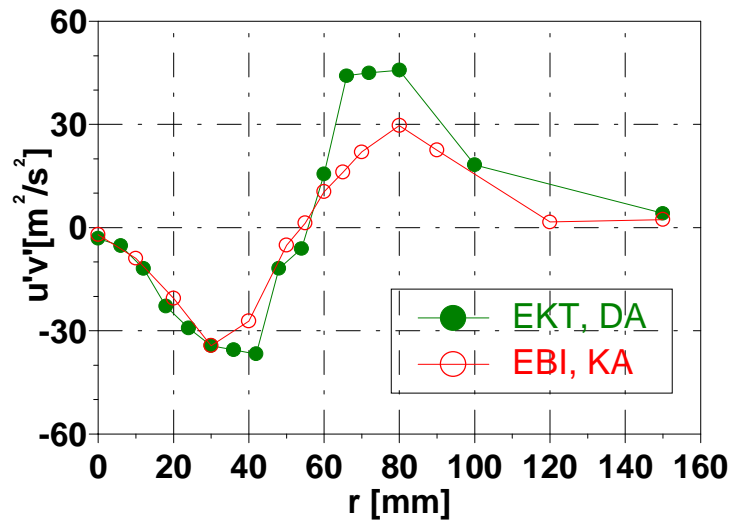
Axial position  $h = 90$  mm



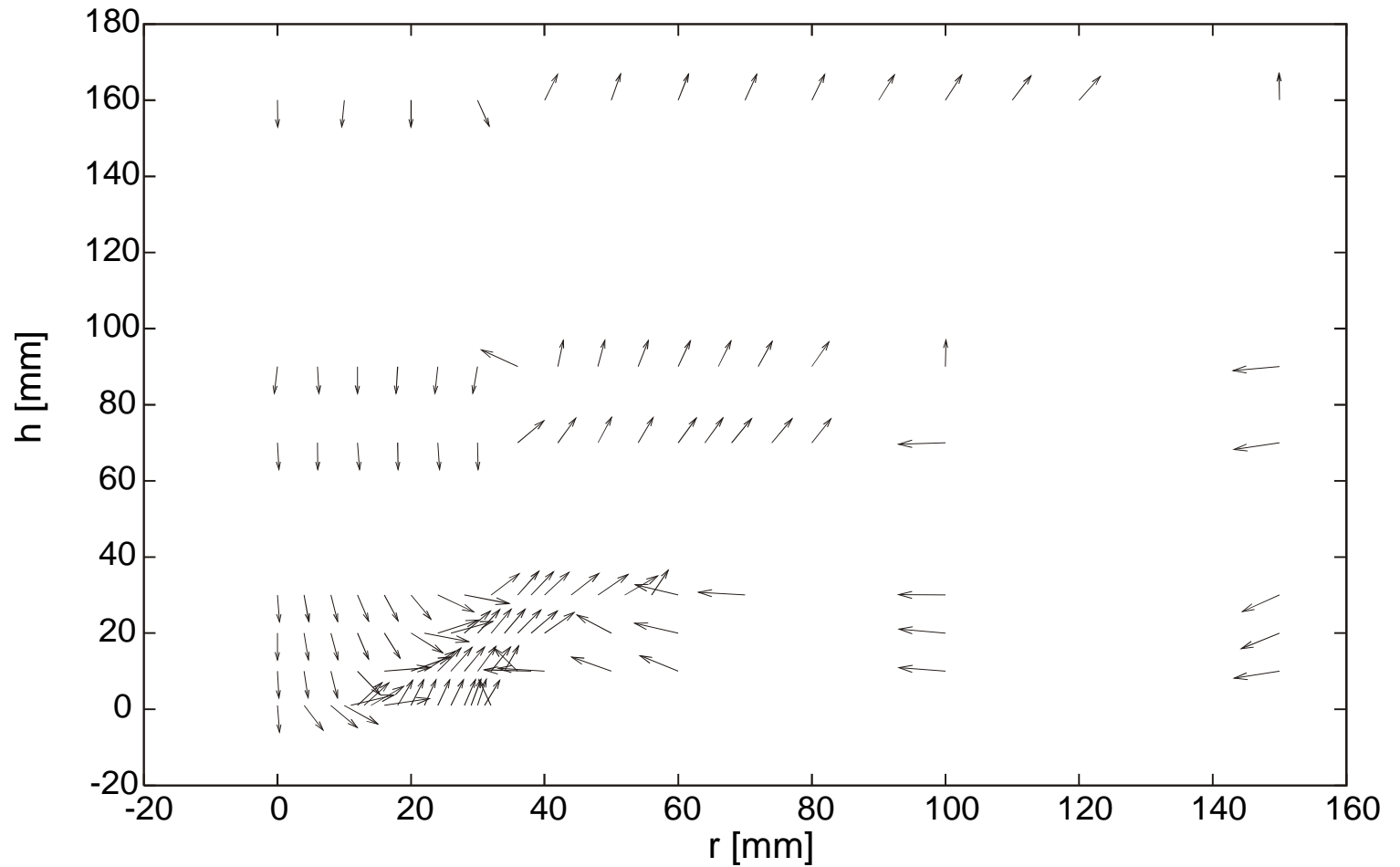
Comparable consistency for w-component, too (not shown)

## Consistency of flow field measurements, LDV

Axial position  $h = 90$  mm



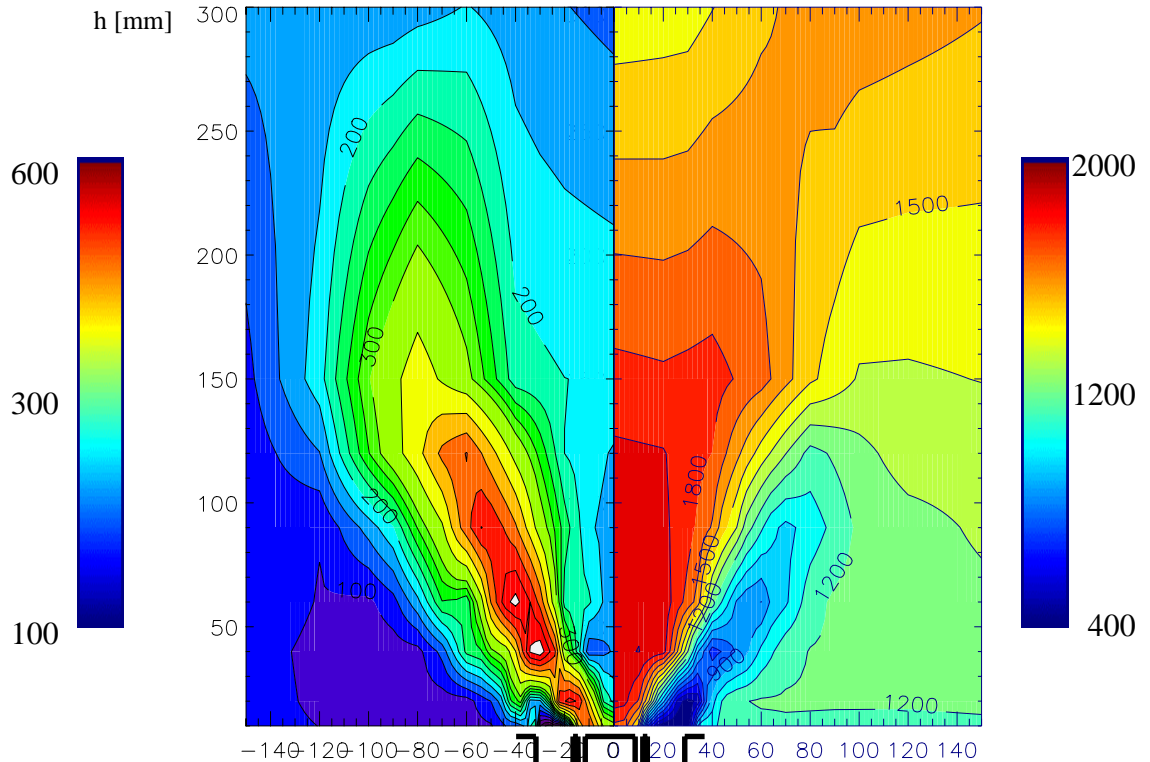
## Vectorplot Normalized (EKT)





# Temperature field

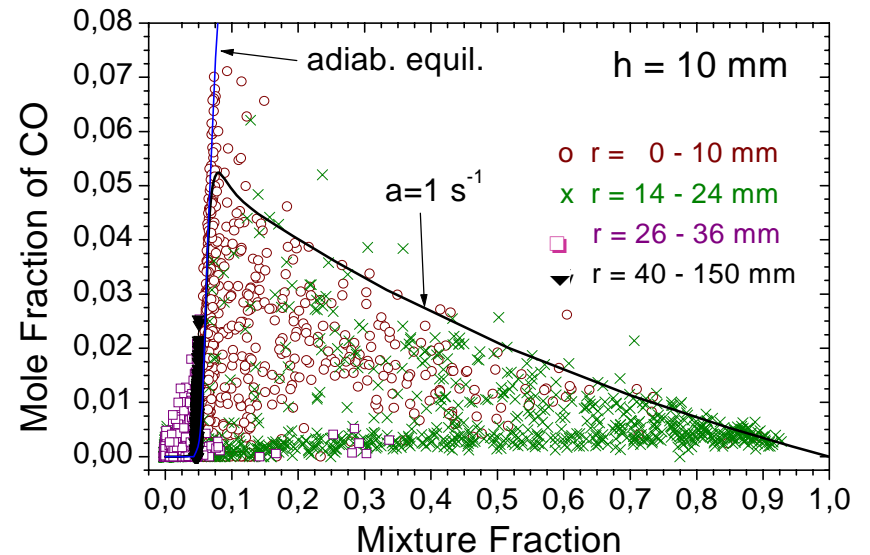
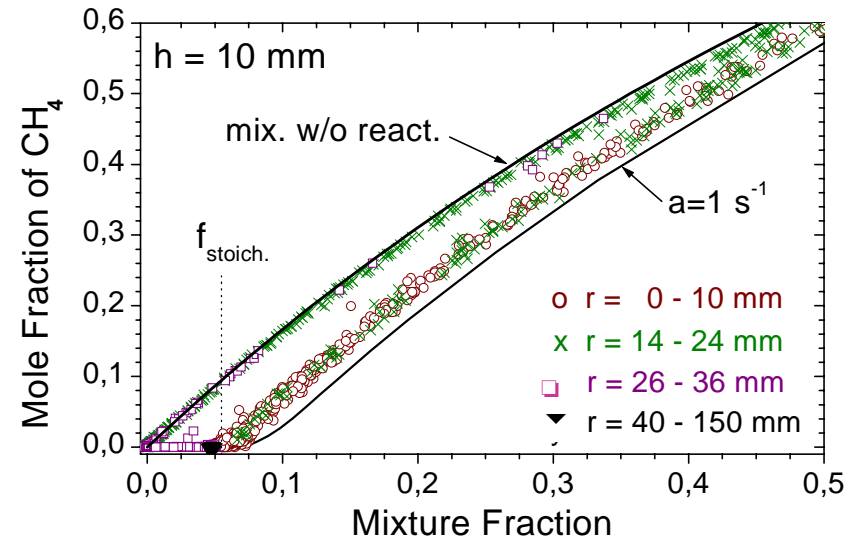
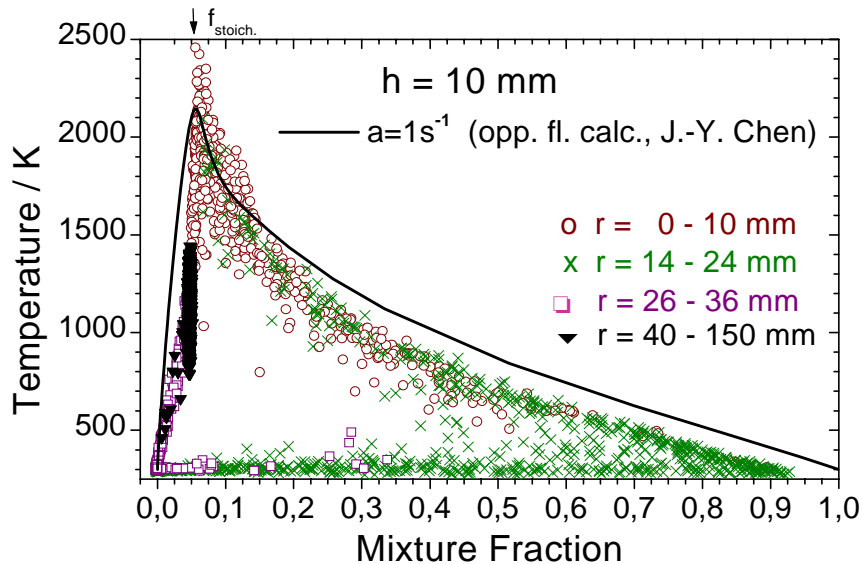
Constructed from point  
Raman scattering  
measurements  
(DLR)



rms fluctuations

averaged

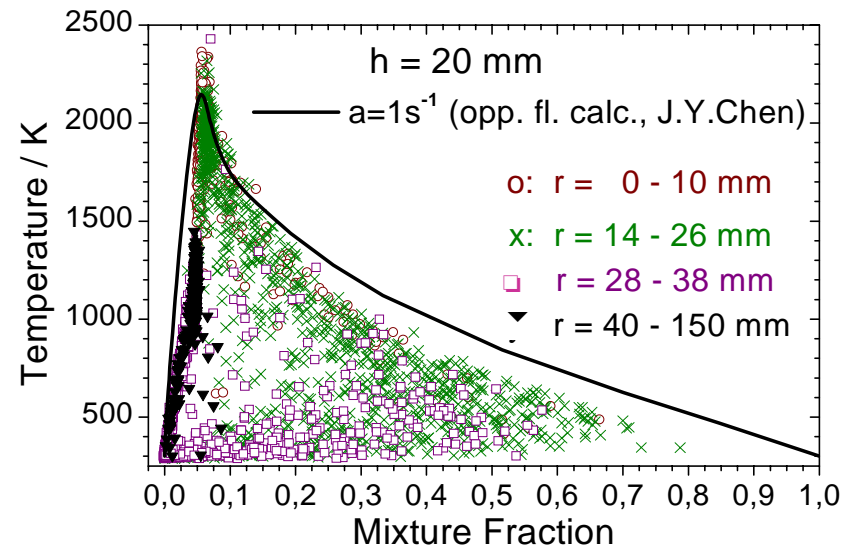
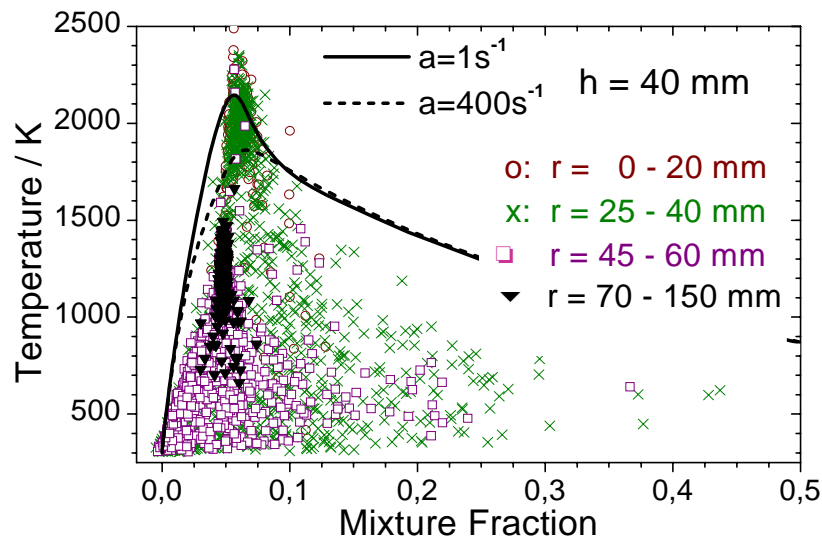
**Scatterplots of temperature, CH<sub>4</sub> and CO**  
**h = 10 mm, Raman scattering**  
**different symbols represent different radial**  
**regions**  
**(DLR)**



## Main findings, $h = 10$ mm

- **$r = 0 - 10$  mm** (inner recirculation zone)
  - ⊖ temperatures close to flamelet calculations
  - ⊖ only marginal heat losses in this region
- **$r = 14 - 24$  mm** (zone above fuel and air nozzle, mixing zone)
  - ⊖ wide spread of mixture fraction
  - ⊖ two branches of temperature
    - Unreacted,  $T = 300 - 400$  K (even for stoichiometric mixtures)
    - Fully reacted,  $T$  close to adiabatic flame temperature
      - ⊖ Influence of turbulence-chemistry interaction
- **$r = 26 - 36$  mm** (above air nozzle)
  - ⊖ mixture of cold air and hot combustion products
- **$r > 40$  mm** (outer recirculation zone)
  - ⊖ burnt gas with mixture fraction  $f = 0.047$  (equivalence ratio = 0.833)
  - ⊖ measured flame temperature below adiabatic flame temperature
    - Severe heat losses

## Scatterplots of temperature h = 20 mm and 40 mm, Raman scattering different symbols represent different radial regions



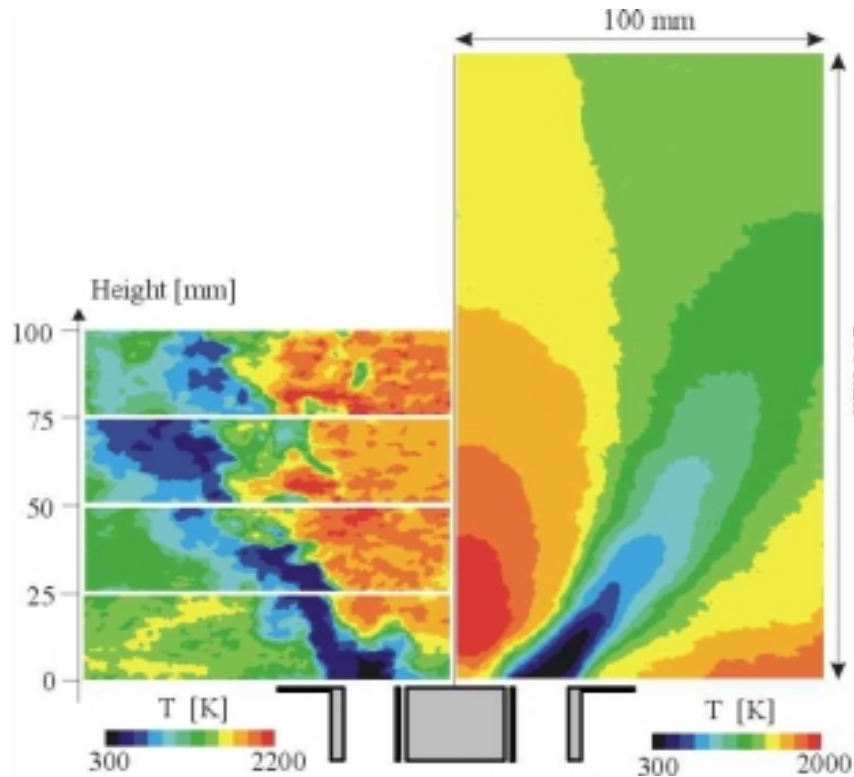
## Main findings, $h = 20$ and $40$ mm

- Scatterplots are more narrow in mixture fraction space compared to  $h = 10$  mm
  - ω rapid mixing of the flow
- **$r = 14 - 16$  mm** (mixing region)
  - ω temperatures from 300 to 2300 K observable
    - ω local extinction
  - ω Coexistence of oxygen and hydrocarbons
    - ω mixing of hot combustion products with cold fuel/air mixture?
- **$r > 70$  mm** (outer recirculation zone)
  - ω burnt gas with mixture fraction  $f = 0.047$  (equivalence ratio = 0.833)
  - ω measured flame temperature below adiabatic flame temperature
    - ω Severe heat losses

## Temperature field, Rayleigh (PCI)

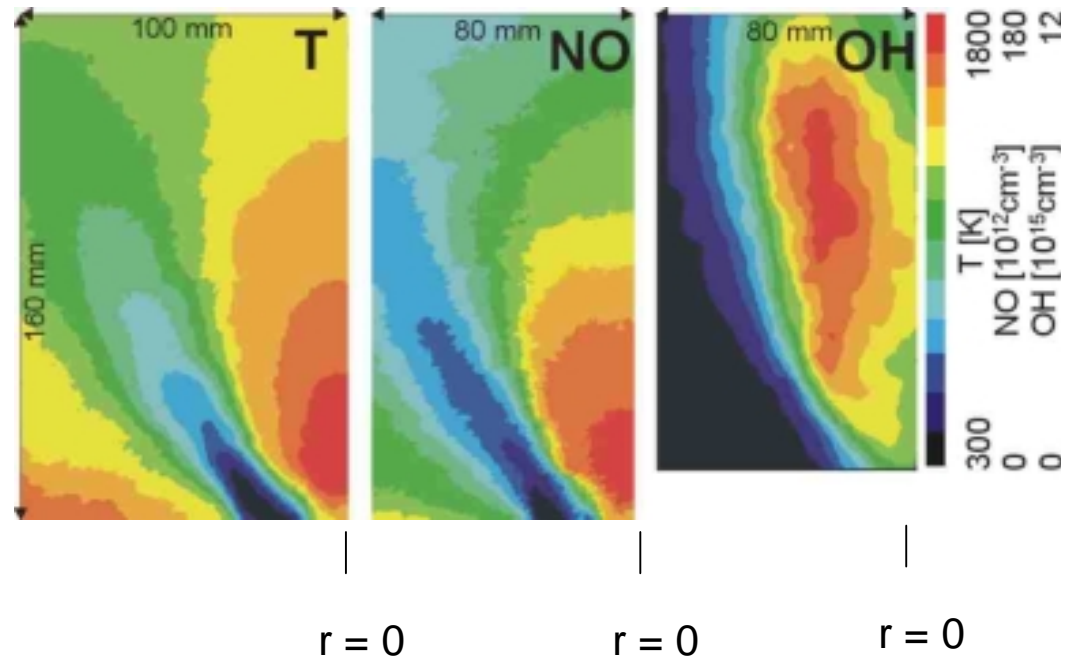
Single shots

Averaged

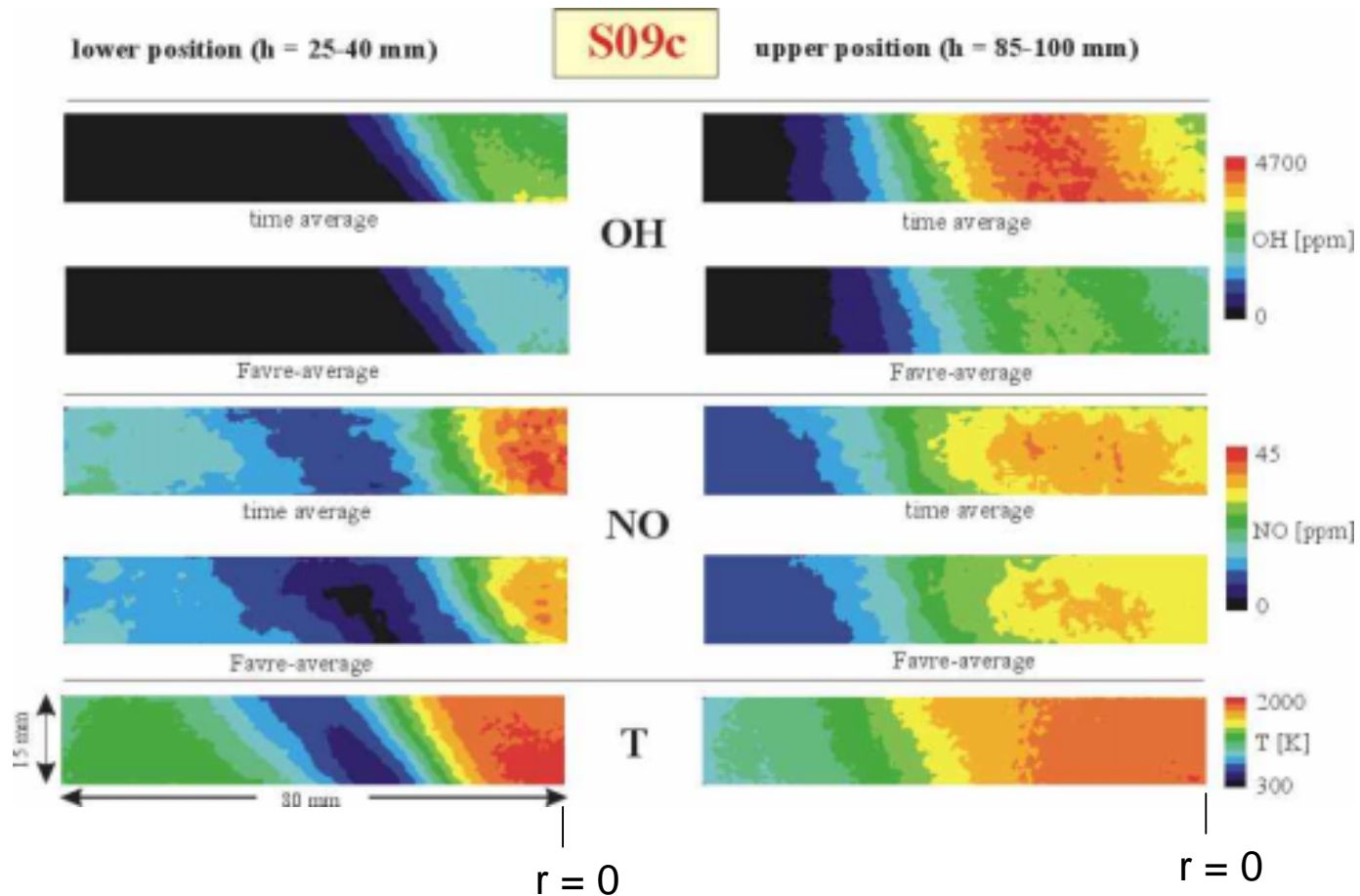


## Temperature, NO and OH field Rayleigh, PLIF (PCI)

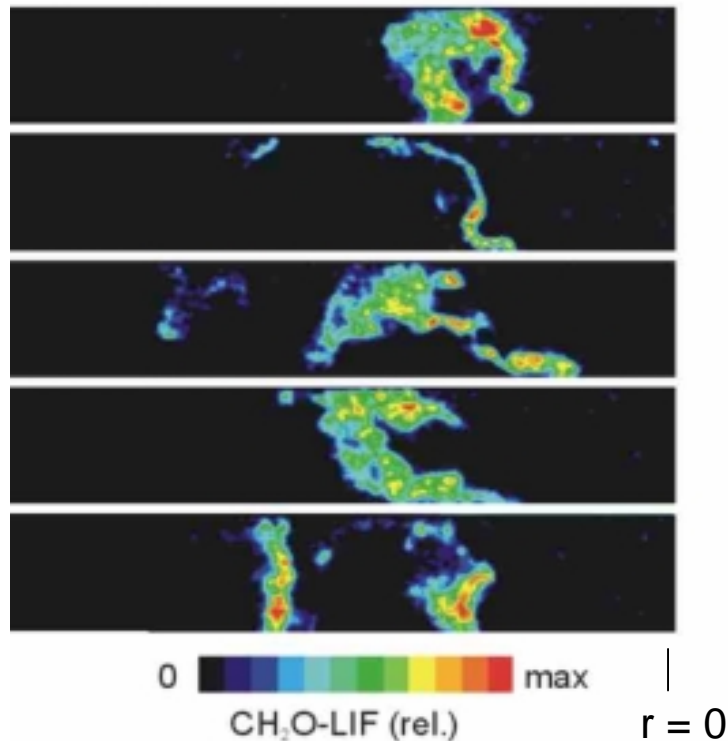
Averaged



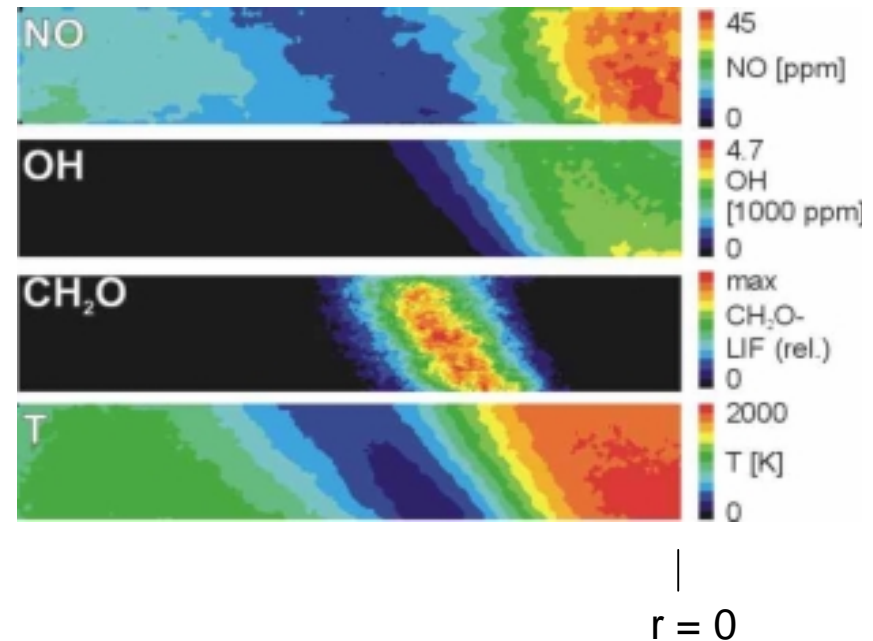
## Simultaneous 2D temperature, NO and OH measurements Rayleigh, PLIF (PCI)



Single-shot images of CH<sub>2</sub>O  
PLIF  
(lower position, h = 25-40 mm)  
PCI



Averaged distribution of T, NO, OH, CH<sub>2</sub>O  
Rayleigh, PLIF  
(lower position, h = 25-40 mm)



## Survey of numerical approaches

<p>k-<math>\epsilon</math> model Jones &amp; Launder (Int. J. Heat Mass Trans. 1972)</p>		<p>Equilibrium chemistry, <math>\beta</math>-PDF, adiabatic</p>	<p>EKT, Darmstadt</p>
		<p>ILDLM (CO<sub>2</sub>, H<sub>2</sub>O), <math>\beta</math>-PDF, adiabatic</p>	<p>EBI, Karlsruhe EKT, Darmstadt</p>
<p>Second moment closure Jones-Musonge (Phys. Fluids 1988)</p>		<p>Equilibrium chemistry, <math>\beta</math>-PDF, adiabatic</p>	<p>EKT, Darmstadt</p>
		<p>ILDLM (CO<sub>2</sub>, H<sub>2</sub>O), <math>\beta</math>-PDF, adiabatic</p>	<p>EKT, Darmstadt</p>
		<p>ILDLM (CO<sub>2</sub>, H<sub>2</sub>O), Monte Carlo PDF adiabatic</p>	<p>EKT, Darmstadt</p>
<p>Second moment closure Launder, Reece, Rodi (J. Fluid Mech 1975)</p>		<p>Equilibrium chemistry, <math>\beta</math>-PDF, adiabatic</p>	<p>DLR, Stuttgart</p>
<p>Large Eddy Simulation</p>		<p>Open TECFLAM burner</p>	<p>Imperial College, UK</p>
<p>Large Eddy Simulation</p>		<p>Confined TECFLAM burner (in progress)</p>	<p>Imperial College, EKT, ... ??</p>

## CFD code

- Two-dimensional elliptic *Finite Volume Method* (FVM)
- Pressure correction via SIMPLEC, TDMA-solver

## Specific information

- Resolution: 80 \* 60 grid points (axial \* radial), condensed around reaction zone
- Iterative information exchange between CFD and chemistry
- Monte Carlo method: 100 particles/cell
- CPU time
  - ILDM/ $\beta$ -PDF: 10 hours on DEC-alpha 533 workstation
  - ILDM/MC: 140 DEC- $\alpha$  workstation

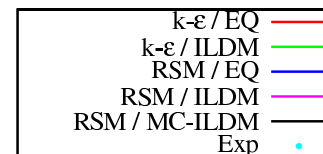
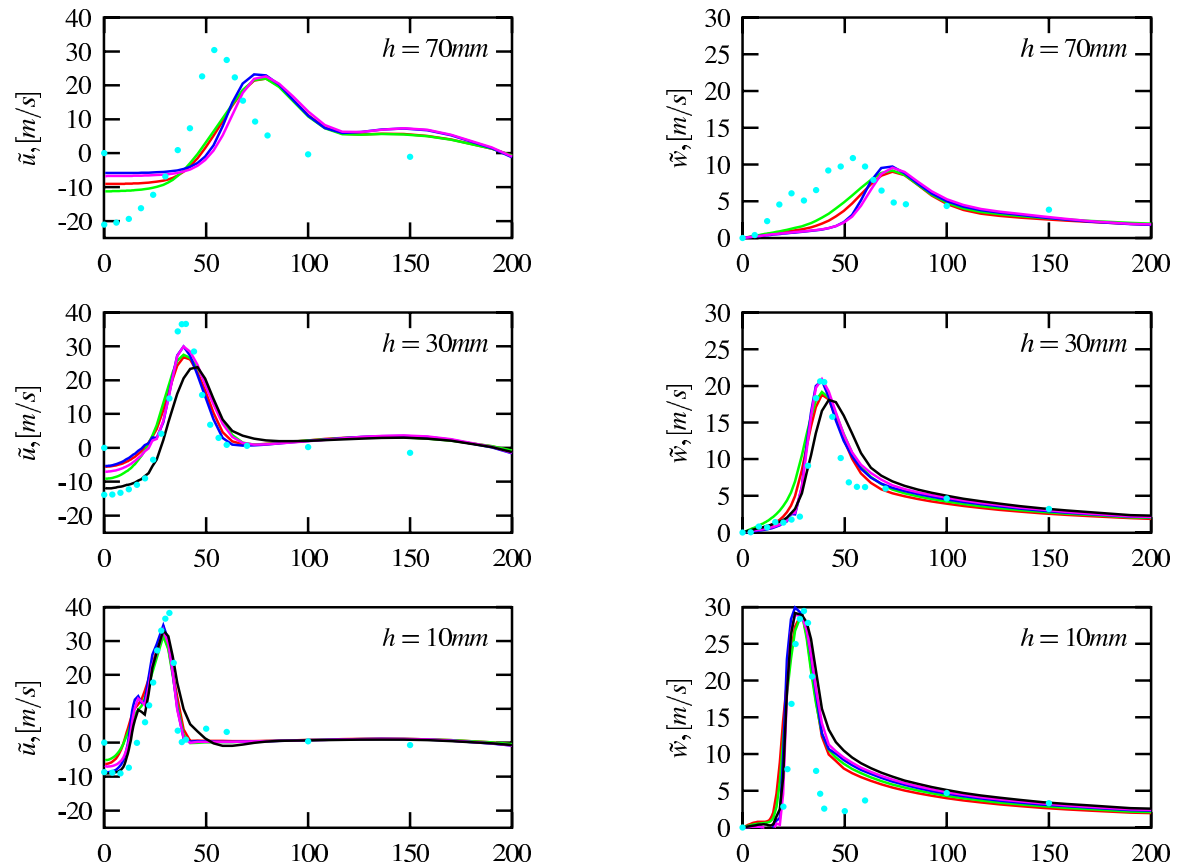
## Boundary conditions

- Adiabatic
- Wall: Logarithmic wall function
- Inflow:
  - Velocity and turbulent quantities from LDV measurements near the nozzle
  - Flow rate adjustments of fuel and air to match experimental values at  $h = 1\text{mm}$
  - Dissipation rate based on integral length scale
- Outflow: parabolic character
- Centre line: symmetry line

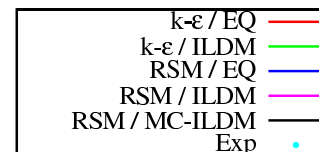
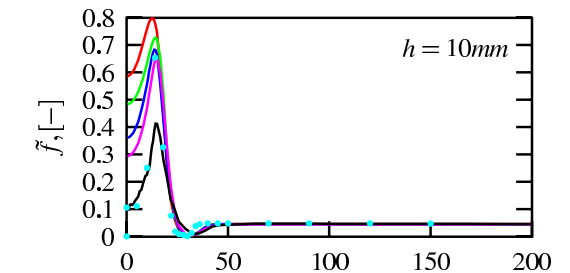
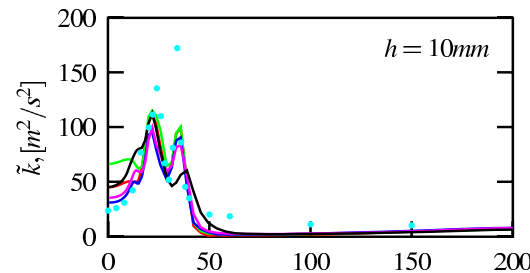
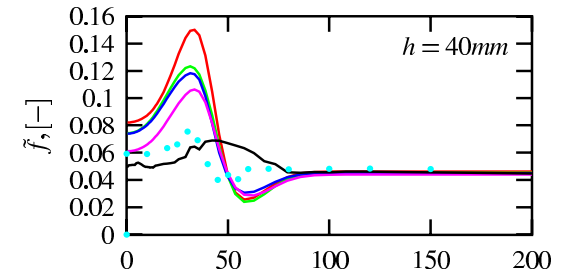
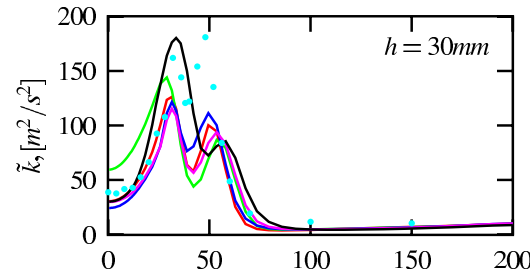
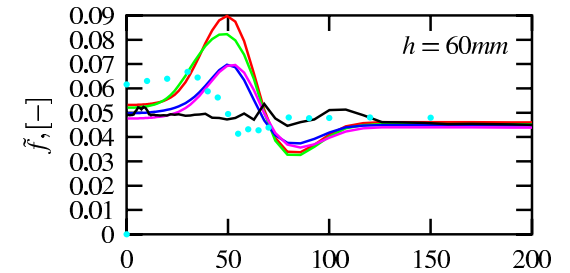
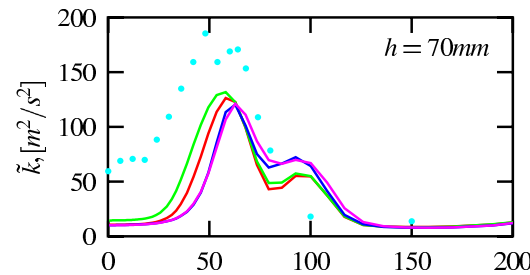
**! Kinetically controlled region:**

**between burner nozzle and ~100 mm downstream**

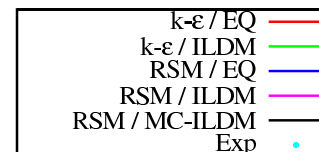
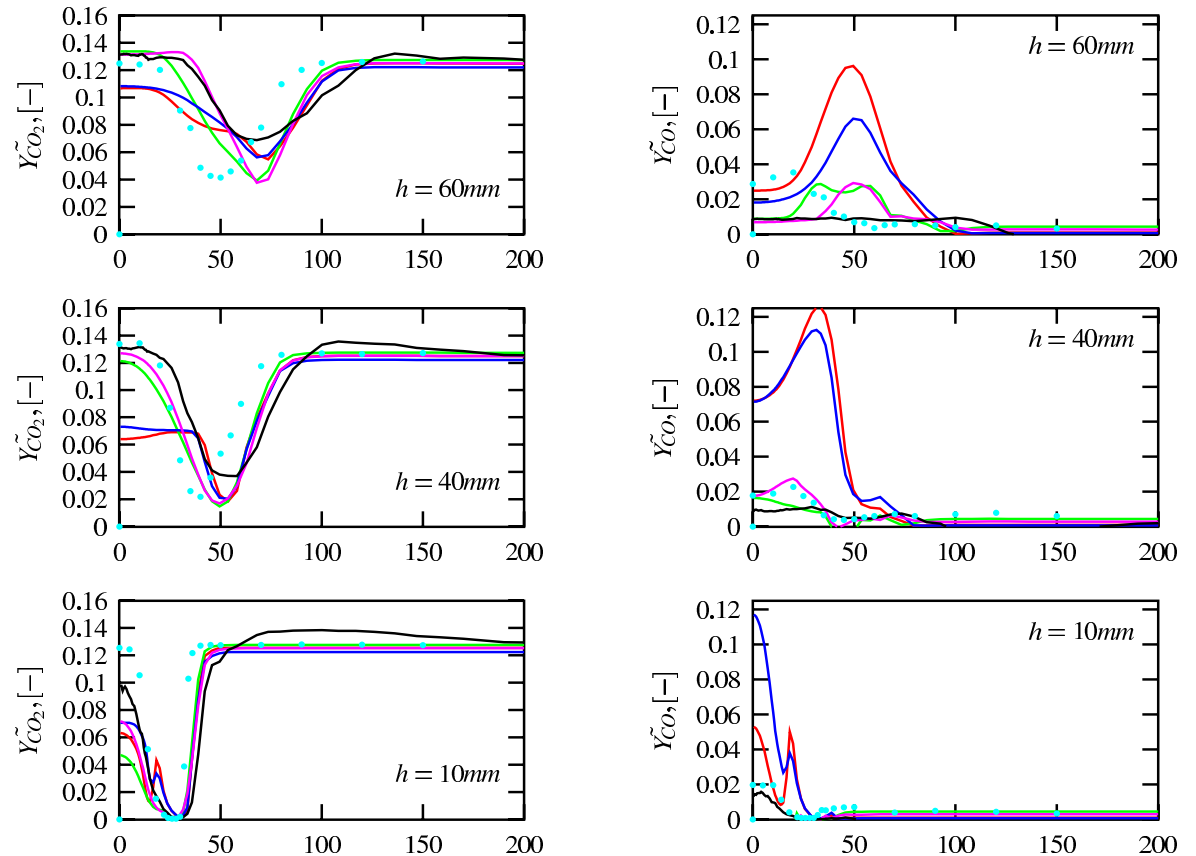
## Comparison of axial velocity $u$ and circumferential velocity $w$



## Comparison of turbulent kinetic energy $k$ and mixture fraction $f$



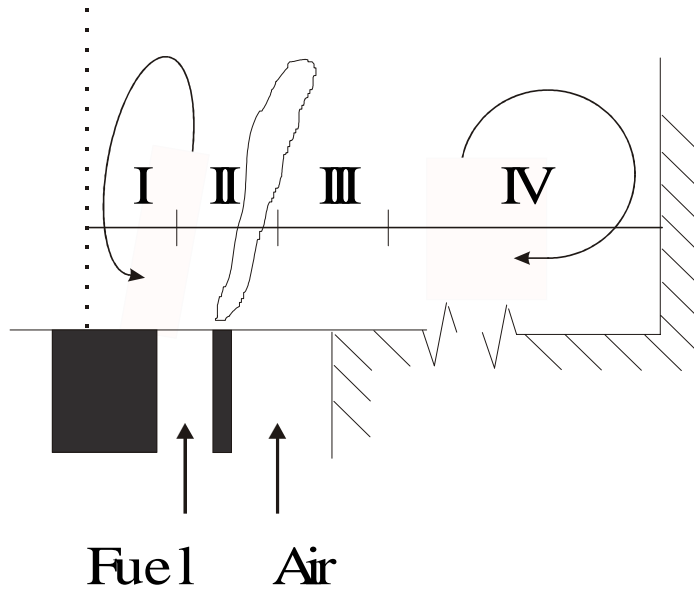
## Comparison of mass fractions of CO<sub>2</sub> and CO



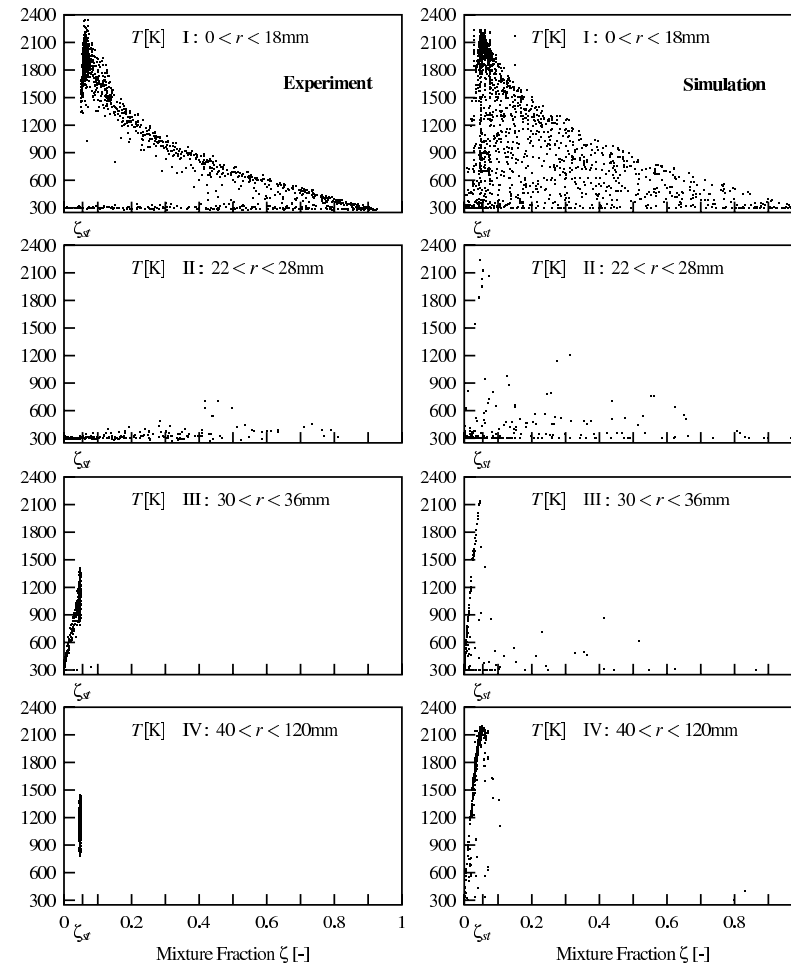
## Main findings

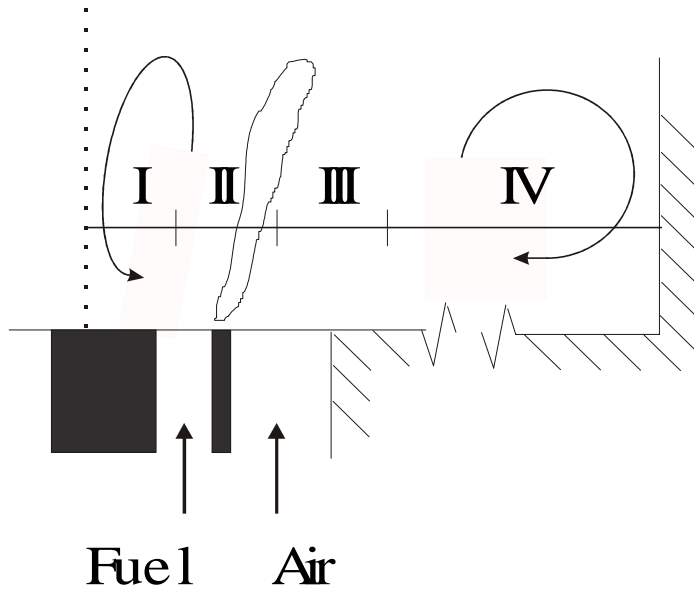
- Flow field is well predicted up to axial positions of 30 mm
- For axial positions further downstream ( $h \geq 70$  mm) spreading of the central recirculation zone is over estimated
- Computed distributions of major species as well as their variances are in reasonable agreement to experimental values
- CO representing minor species sensitive to finite chemistry effects is predicted fairly well using an ILDM which is spanned by two progress variables
- Retroactive effect of chemistry model on flow field is marginal
- Differences of presumed  $\beta$ -PDF compared to Monte Carlo method are observable but not crucial

## Scatter Plots of Temperature $x = 10\text{mm}$



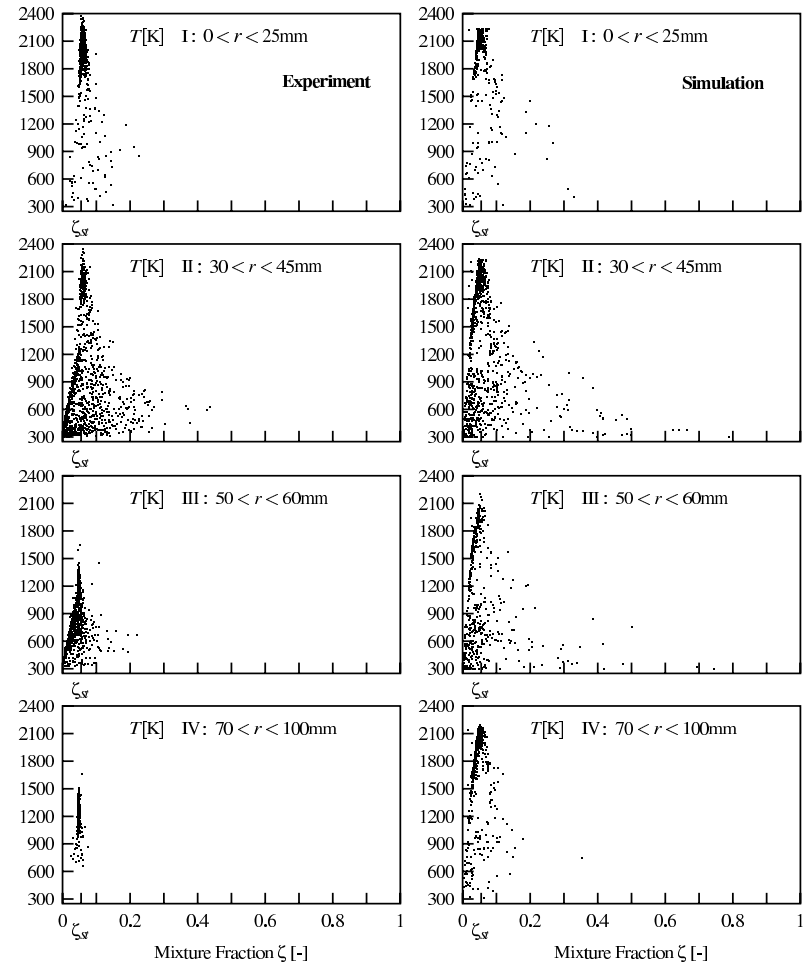
	$x = 10\text{ mm}$	Region
I	$0 < r < 18\text{ mm}$	Central recirculation
II	$22 < r < 28\text{ mm}$	Mixing zone, fuel
III	$30 < r < 36\text{ mm}$	Mixing zone, air
IV	$40 < r < 120\text{ mm}$	Outer recirculation





Scatter Plots of Temperature  
 $x = 40\text{mm}$

	$x = 40\text{ mm}$	Region
I	$0 < r < 25\text{ mm}$	Central recirculation
II	$30 < r < 45\text{ mm}$	Mixing zone, fuel
III	$50 < r < 60\text{ mm}$	Mixing zone, air
IV	$70 < r < 100\text{ mm}$	Outer recirculation



## In general promising agreement

### **h = 10 mm**

- Turbulence-chemistry interaction are obvious in the regions I and II
- Ignitable mixtures are apparent especially in region II
  - ω fast mixing
- In region I simulation and experiments show comparable high temperatures
  - ω heat losses (radiation, convection) can be neglected in this region
  - ω for simulation of central parts of the flame adiabatic boundary conditions are reasonable

### **h = 40 mm**

- Mixture fraction is concentrated on a more narrow region compared to h=10 mm
- Especially for region II temperatures are significantly higher compared to h=10mm
- For region IV too high temperatures are predicted
  - ω heat losses (radiation, convection) are of significance in this region

## Most critical points for a successful simulation

- Accurate boundary conditions from experiment
- Accurate prediction of mixture fraction and CO
- ...

## What do we need for further progress?

- Radiation included to calculations
  - ω reliable radiation models suitable for CFD
- More advanced chemistry models
  - ω reduced chemical reaction mechanisms with more than 3 progress variables (ILDM, ...)
- More information concerning the boundary conditions
  - ω Calculation of flow field inside the burner nozzle by LES?
- For one target flame identical boundary conditions used by the different groups of the numerical combustion community

## **Acknowledgements**

Financial support of the TECFLAM project by the BMBF and the Land Baden-Württemberg

# SECTION 4

## Poster Abstracts

## List of Posters Presented at TNF5

**Pankaj Bajaj, Jurg Gass, Dimos Poulidakos**

Numerical investigation of several methane/air reaction mechanisms in rich partially premixed laminar flames

**R.S. Barlow, J.H. Frank and J.Y. Chen**

Scalar profiles and NO formation in laminar methane/air flames

**S. Böckle, A. Hoffmann, J. Kazenwadel, T. Kunzelmann, C. Schulz, J. Wolfrum**

Laser-diagnostic investigation of NO and H<sub>2</sub>CO formation in strongly swirling natural gas flames

**B.B. Dally**

Laminar Nonpremixed Flame Calculations of Methane with Highly-Preheated Air

**B. B. Dally, A. R. Masri, R. S. Barlow and G. J. Fiechtner**

Measurement of Carbon Monoxide in Turbulent Nonpremixed Bluff Body Flames using Two Photon Laser Induced Fluorescence Technique

**L. Demiraydin, J. Gass**

Numerical modeling of non-premixed turbulent flames in opposed jet flows with PDF transport equations

**L. Demiraydin, J. Gass**

Numerical simulation of a piloted methane/air flame using PDF transport equation model

**Jeffrey M. Donbar, Campbell D. Carter, Kyle A. Watson and Kevin M. Lyons**

**James F. Driscoll, Werner J.A. Dahm, and A. Ratner**

Multi-Diagnostic Imaging For the Study of Turbulent and Unsteady Flames

**D. Geyer, D. Sauer, A. Dreizler, E.P. Hassel, J. Janicka**

Investigation of temperature, species and their gradients in a turbulent methane/air opposed jet flame by 1-D Raman/Rayleigh scattering

**John C. Hewson and Alan R. Kerstein**

Near-Nozzle Phenomena in a Nonpremixed CO/H<sub>2</sub>/N<sub>2</sub> Jet Diffusion Flame:  
Modeling Extinction/Reignition, Differential Diffusion, and Initial Condition Sensitivities

**Werner Hübner and Mike Golombok**

Experimental Study of a new Rotating Swirl Burner

**Olaf Keck, Wolfgang Meier, Winfried Stricker**

Characterization of the TECFLAM swirling diffusion flames  
by laser Raman measurements

**A. Kempf, A. Sadiki, J. Janicka and J.Y. Chen**

Large eddy simulation of a turbulent diffusion flame using flamelet modeling

**A. Kempf, H. Farkel, A. Sadiki, J. Janicka and J.Y. Chen**

Large eddy simulation of a non-reactive counter flow configuration

**Seung Hyun Kim and Kang Y. Huh**

Prediction of NO formation in a bluff-body CH<sub>4</sub>/H<sub>2</sub> flame by the conditional moment closure model

**Yongmo Kim**

Effects of differential diffusion and radiation on NO<sub>x</sub> formation characteristics of the turbulent CO/H<sub>2</sub>/N<sub>2</sub> jet flames

**P.A.M. Kalt, R.S. Barlow and A.R. Masri**

Scalar measurements in turbulent swirling flames

**Denis Krasinsky, Theo H. van der Meer, Dirk Roekaerts, Baifang Zuo**

Flamelet modeling for 3-D simulation of high-temperature gas-fired furnaces

**Oliver Kunz, Peter Gerlinger, Berthold Noll, Manfred Aigner**

TECFLAM swirl flame: Comparison of different turbulence and chemistry models

**R.P. Lindstedt, S.A. Louloudi and E.M. Vaos**

Joint scalar PDF Monte Carlo simulations of methanol turbulent jet diffusion flames with Comprehensive chemistry

**K. Liu, P. Jenny, M. Muradoglu, S. B. Pope and D. A. Caughey**

JPDF Calculations of Bluff-Body Stabilized Flames

**C. Y. Ma, T. Mahmud, M. Fairweather, P. H. Gaskell and E. Hampartsoumian**

Calculations of Turbulent Non-Premixed Jet Flames Using a Laminar Flamelet Model with Radiative Heat Transfer

**P.Martinelli, M.Nutini**

Numerical and experimental investigation of turbulent non-premixed flames of industrial interest

**Aristide Mbiok, Joan Teerling, and Dirk Roekaerts**

Application of BEM and Analysis of the Role of Radiation Effects in Labscale Turbulent Diffusion Flames

**Wolfgang Meier, Robert S. Barlow, Jyh-Yuan Chen**

Measurements and Simulations of the Turbulent DLR CH<sub>4</sub>/H<sub>2</sub>/N<sub>2</sub> Jet Diffusion Flame

**B. Merci, D. Roekaerts, T.W.J. Peeters and E. Dick**

The impact of the turbulence model and inlet boundary conditions on Calculation results for reacting flows

**Michael W. Renfro, Galen B. King, and Normand M. Laurendeau**

Time-Series Measurements of Scalars in H<sub>2</sub>/CH<sub>4</sub>/N<sub>2</sub> Jet Flames

**Christoph Schneider, Andreas Dreizler, Johannes Janicka, Egon Hassel**

Experimental investigation of a confined swirling natural gas flame (TECFLAM)

**Szasz Robert, Laszlo Fuchs**

Numerical Simulation of the Piloted Flame Type D

**Qing Tang, Jun Xu, Stephen B. Pope**

PDF Calculations of NO Production in Piloted-Jet Turbulent Methane/Air Flame (Flame F)

# NUMERICAL INVESTIGATION OF SEVERAL METHANE/AIR REACTION MECHANISMS IN RICH PARTIALLY PREMIXED LAMINAR FLAMES

**Pankaj Bajaj, Jurg Gass, Dimos Poulidakos**

Laboratory for Thermodynamics in Emerging Technologies  
Swiss Federal Institute of Technology,  
CH - 8092 Zurich  
Tel. No. 0041 1 632 6913  
Fax No. 0041 1 632 1023

and

**Ishwar K. Puri**

Department of Mechanical Engineering  
University of Illinois at Chicago, IL 60607-7022  
Tel. No. 001 312 413 7560  
Fax. No. 001 312 413 0447

In the present work, the performance of the several detailed methane/air reaction mechanisms is investigated with respect to the rich laminar flame structure and the NO<sub>x</sub> production. Different reaction mechanisms, namely GRI 2.11, GRI 3.0 [1], Warnatz [2], are implemented in the one-dimensional computer code [3]. This code is used to solve the velocity, temperature and species concentrations in the flames. The inflow axial velocities and the stoichiometry of both the rich and lean inlet streams are parametrically varied, and the consequent effects on the NO<sub>x</sub> production are studied.

The one-dimensional simulation results are compared with the experimental data [4] [5] available from the literature for the laminar partially premixed counter flow flames. The flame structure is discussed with respect to the NO<sub>x</sub> production. It was found that all the tested reaction mechanisms behave in a similar manner with respect to the flame structure for the present configurations. However, certain differences are found for the NO formation using these chemical reaction mechanisms (cf. Fig.1, Fig. 2). It has also been found that the computed flame shows differences on the rich side for a particular configuration, as compared with the experimental data. The chemical reaction mechanisms are unable to predict a region, where the flame separates into a twin flame structure. It may be due to the underprediction of the laminar burning speed for this configuration on the rich side. This leads to incorrect prediction of the stable species structure on the rich side.

A kinetic analysis of the chemical mechanism is performed using a sensitivity code [6] in order to identify the discrepancies in the flame chemistry on the rich side. The obtained results are to be discussed in the poster presentation.

Reference:

[1] [http://www.me.berkeley.edu/gri\\_mech/](http://www.me.berkeley.edu/gri_mech/)

[2] <http://www.ca.sandia.gov/tdf/3rdWorkshop/ch4mech.html>

[3] Lutz, A. E., Kee, R. J., Grcar, J. F., and Rupley, F. M., 1997, "A Fortran Program for Computing Opposed Flow Diffusion Flames", Report, SAND96-8243, Sandia National Laboratories, Livermore.

[4] Williams, F. A., and Li, S. C., 1999, "NO<sub>x</sub> Formation in Two-Stage Methane-Air Flames", *Combustion and Flame*, Vol. 118, pp. 399-414.

[5] Williams, F. A., Iiincic, N., and Li, S. C., 1997, "Reduction of NO<sub>x</sub> Formation by Water Sprays in Strained Two-Stage Flames", *Journal of Engin. Gas Turbines Power*, Vol. 119, pp. 836-843.

[6] Turanyi, T., "KINALC", URL: <http://chem.leeds.ac.uk/Combustion/Combustion.html>.

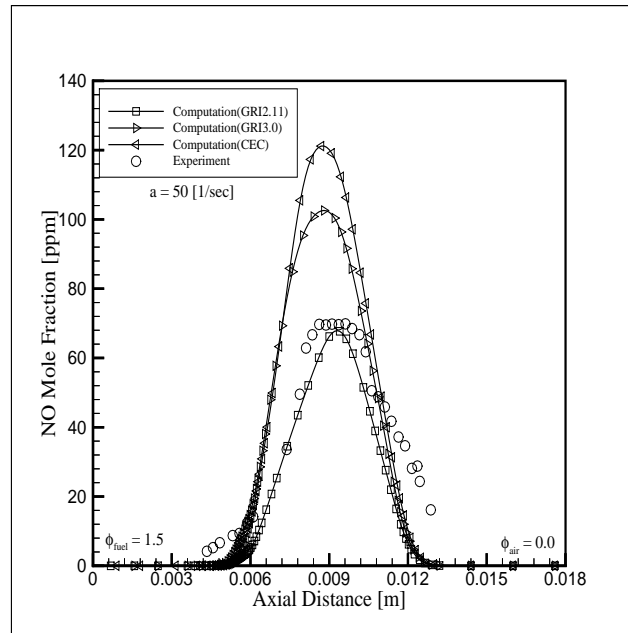


Figure 1: Comparison of the experimental data and the computational results in the physical space for the NO mole fraction profiles for the configuration  $\phi_{\text{air}} = 0.0$  and  $\phi_{\text{fuel}} = 1.5$ .

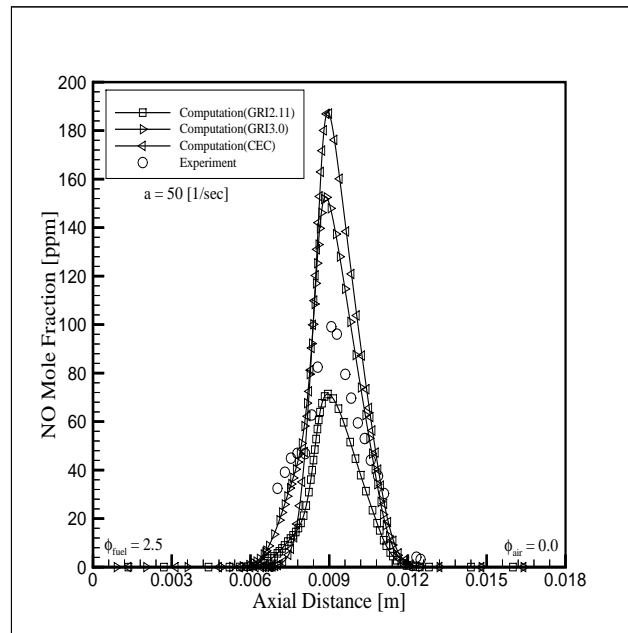


Figure 2: Comparison of the experimental data and the computational results in the physical space for the NO mole fraction profiles for the configuration  $\phi_{\text{air}} = 0.0$  and  $\phi_{\text{fuel}} = 2.5$ .

## Scalar Profiles and NO Formation in Laminar Methane/Air Flames

R. S. Barlow\*, J. H. Frank\*, and J.-Y. Chen\*\*

\*Sandia National Laboratories, Livermore, CA 94550

\*\*Mechanical Engineering Dept., University of California, Berkeley, CA 94720

Measurements of temperature, the major species ( $N_2$ ,  $O_2$ ,  $CH_4$ ,  $CO_2$ ,  $CO$ ,  $H_2O$ ,  $H_2$ ),  $OH$ , and  $NO$  are obtained in steady, laminar, partially-premixed methane/air flames, using simultaneous Rayleigh/Raman/LIF techniques. Flames are stabilized on a porous cylinder in a low-velocity flow of air (Tsuji geometry) and operated at relatively low strain rates. Flames having fuel-side equivalence ratios of  $\phi=2.17$  and  $\phi=3.17$  are considered, with the latter being the same composition used in experiments on piloted turbulent jet flames [1]. The experimental objective is to provide detailed scalar data that may be used to validate chemical mechanisms, at least for steady combustion. Nitric oxide formation and the progress of partial oxidation of  $CH_4$  in fuel-rich conditions to form  $CO$  and  $H_2$  are of primary interest, as these are the areas where comparisons of turbulent flame results have shown significant differences [2].

Measurements are compared with calculations, which use a version of the Sandia flame code for the Tsuji flame geometry that includes optically-thin treatment of molecular radiation. Calculations, based on RADCAL, of emission and absorption in these flames show small effects of absorption and support the optically-thin assumption. Strain rates have not been measured. Therefore, the strain rate in the calculation is selected to match the measured profile of mixture fraction in each flame. Calculations are performed using GRI Mech versions 2.11 and 3.0, which differ significantly in their predictions of  $NO$  formation. Adiabatic and radiative calculations are performed using each version of the mechanism.

This abstract includes results for one flame with 25%  $CH_4$  and 75% air in the fuel stream ( $\phi=3.17$ ). Figure 1 shows that measured and calculated mixture fraction profiles are well matched for a strain parameter of  $a=25\text{ s}^{-1}$  in the calculation. The scalar dissipation rate in this laminar flame is comparable to the conditional mean scalar dissipation at the stoichiometric value of mixture fraction at  $x/d=30$  in the Flame D calculations of Pitch [3] and Roomina [4]. Measured temperatures are between the adiabatic (solid) and radiative (dashed) calculations, with estimated experimental uncertainties being comparable to the difference between the two calculations. Measurements of  $O_2$ ,  $CH_4$ ,  $CO_2$ , and  $H_2O$  (Figs. 2 and 3) are in good agreement with the radiative calculation. Measured  $CO$  levels (based on two-photon LIF) in Fig. 2 are somewhat higher on the fuel-rich side those from the radiative calculation. However, agreement is still reasonably good (within 15-20%). Measured  $H_2$  levels on the fuel-rich side in Fig. 4 appear to be in good agreement with the adiabatic calculation. The estimated uncertainty in  $H_2$  is  $\pm 10\%$  at the highest temperatures and up to  $\pm 20\%$  at intermediate temperatures, where the calibration curve is interpolated [1]. However, error bars are not plotted because we are still investigating a possible bias in the  $H_2$  data resulting from our inability to fully correct for effects of broadband hydrocarbon fluorescence interference in these flames. All calculated curves in Figs. 1-6 are from GRI 3.0, except for those labeled GRI 2.11 in the graph of  $Y_{NO}$ . In Fig. 5 the maximum measured  $NO$  mass fraction is best matched by the radiative calculation using GRI 2.11, while GRI 3.0 appears to significantly over predict the peak  $NO$  level in this flame. It is also apparent that the effects of reburn are greater in the calculations than in the measurements. Similar results are obtained in other flames, which are included on the poster. Figure 6 shows that radiation has a significant influence on the calculated results for several major species, not just  $T$  and  $NO$ , in these flames.

### References:

1. Barlow, R.S., and Frank, J.H., *Proc. Combust. Inst.* 27:1087-1095 (1998).
2. TNF3 Proceedings, 1998 and TNF4 Proceedings 1999, <http://www.ca.sandia.gov/tdf/Workshop>
3. H. Pitsch, personal communication 1999.
4. Roomina, M., Ph.D Thesis, University of Sydney, 1999.

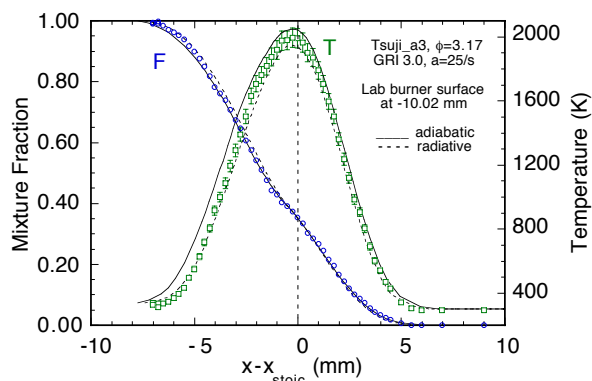


Fig. 1 Measured and calculated profiles of mixture fraction and temperature in a laminar Tsuji flame with 25% CH<sub>4</sub> and 75% air ( $\phi=3.17$ ) in the fuel stream.

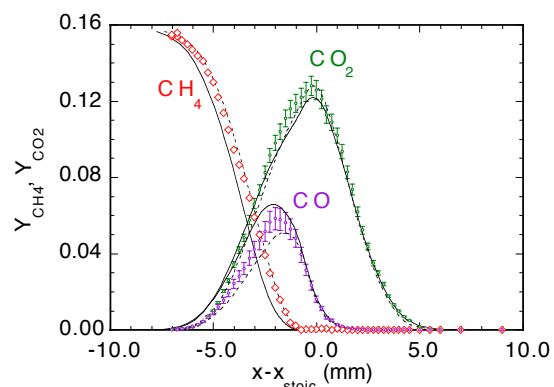


Fig. 2 Measured and calculated profiles of CH<sub>4</sub>, CO<sub>2</sub> and CO. The high values of CO<sub>2</sub> near -2 mm are believed to result from undercorrection of C<sub>2</sub> interferences.

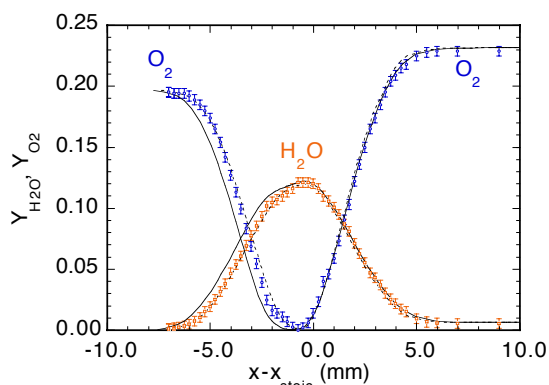


Fig. 3 Measured and calculated profiles of H<sub>2</sub>O and O<sub>2</sub>.

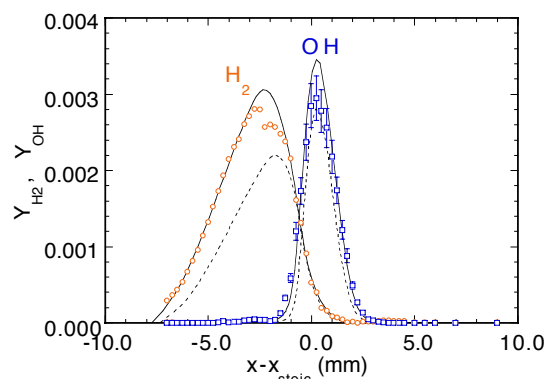


Fig. 4 Measured and calculated profiles of H<sub>2</sub> and OH. H<sub>2</sub> measurements may be biased by broadband hydrocarbon fluorescence interference, so error bars are not plotted.

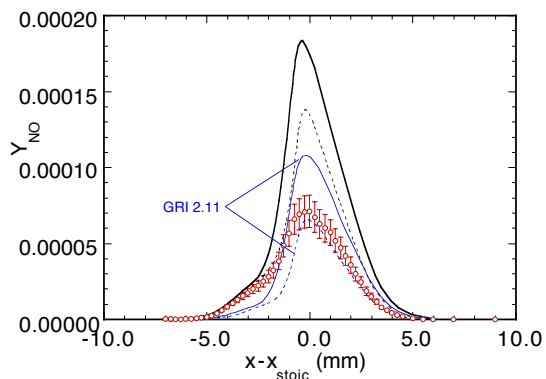


Fig. 5 Measured and calculated profiles of NO, including radiative and adiabatic calculations using GRI Mech 2.11 and 3.0.

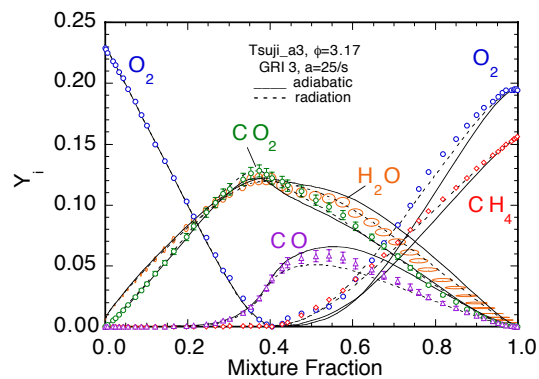


Fig. 6 Major species mass fractions plotted vs. mixture fraction. Apparent deviations in the measurements of O<sub>2</sub>, H<sub>2</sub>O, and CO<sub>2</sub> near  $\xi=0.8$  are caused by errors in mixture fraction that result from uncertainty in the calibration curve for CH<sub>4</sub> at corresponding temperatures.

# Laser-diagnostic investigation of NO and H<sub>2</sub>CO formation in strongly swirling natural gas flames

S. Böckle, A. Hoffmann, J. Kazenwadel, T. Kunzelmann, C. Schulz, J. Wolfrum

PCI, Physikalisch-Chemisches Institut, Ruprecht-Karls-Universität Heidelberg  
Im Neuenheimer Feld 253, 69120 Heidelberg, Germany  
tkunzelm@ix.urz.uni-heidelberg.de

Within the TECFLAM group a standard swirl burner [1] is investigated both, experimentally using optical and probe measurements and by simulations using different modeling attempts. The present study is focused on the laser-based investigation of the NO distribution within the reacting flow field of a strongly swirling, confined 150 kW natural gas flame (swirl number  $S = 0.9$ , equivalence ratio  $\phi = 0.83$ ). Simultaneous quantitative measurements of NO- and OH-concentration fields (using laser-induced fluorescence imaging, LIF) and temperature distribution (by Rayleigh scattering) allow the determination of concentration distributions as well as the analysis of correlation between all three scalars, respectively.

Up to now only a limited amount of temperature and species distribution data are available for swirling flames [2- 4]. Especially the NO distribution is difficult to observe due to the intrinsically low levels of NO produced in this flame type. Whereas for comparison with computational fluid dynamics simulations (CFD) temporally averaged information about temperature and species concentrations are sufficient, for probability density function approaches (PDF) correlations between different scalars are of interest. Simultaneous two-dimensional measurements of these scalars by laser-based imaging techniques allow to assess the necessary information.

Simultaneous measurements are carried out with NO A-X(0,0) excitation. Using published quenching cross sections [5] quantification of signal intensities is feasible as long as information about local gas composition is available. For detecting OH, rotational transitions in the A-X(3,0) band can be excited around 248 nm readily available from tunable KrF excimer lasers. Rayleigh temperature imaging is performed using the same laser beam in areas where variations in local Rayleigh cross-sections  $s_{Ray}$  are known from additional mixing experiments [6].

Both, time- and Favre averaged concentration fields are obtained from the simultaneous measurements. Correlations between all three simultaneously measured scalars are presented showing significant differences in the different parts of the reactive turbulent flow. Whereas the overall correlation of NO concentration and temperature shows a linear trend no correlation between NO and OH was found in the observed area. Independent experiments assessing the mean fields of temperature, NO- and OH-concentration throughout the whole reaction zone were carried out. Maximum NO concentrations are localized in the lower part of the inner recirculation zone. In contrast, maximum average OH concentrations are found close to the shear layer near the path of the injected fresh gases. These global scalar fields will be used to validate simulation calculations within the TECFLAM project.

Single-shot formaldehyde laser-induced fluorescence (LIF) imaging measurements in the same flame have been obtained using XeF excimer laser excitation in the  $\tilde{A}^1A_2 - \tilde{X}^1A_1$  transition at 353.2 nm [7]. Formaldehyde distribution fields have the potential, in combination with OH concentration fields, to visualize the heat release distribution and therefore give an optimal visualization of flame-front positions [8]. The extended areas where formaldehyde was detected in the swirl flame indicate the presence of low temperature chemistry in preheated gas pockets before ignition. Figure 1 shows averaged H<sub>2</sub>CO-LIF distributions compared with temperature, NO- and OH-concentrations. The imaged area is at 25 to 40 mm above the burner exit; the axis of symmetry of the burner corresponds to the right end of the images shown in figure 1.

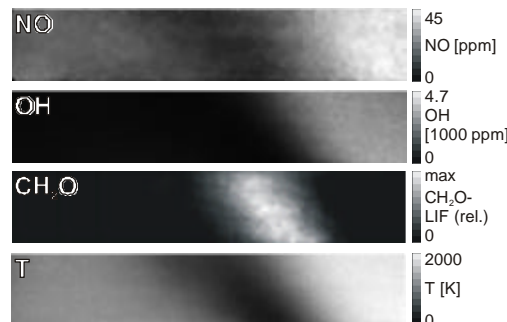


Figure 1: Averaged H<sub>2</sub>CO-LIF, NO, OH, and T distributions in the swirling flame. The imaged area is 15 x 80 mm.

Mixing properties of the unburned gases have been investigated for the isothermal and combusting flow using tetrahydrothiophene (THT) as a new fluorescing tracer. This compound is present at concentrations of  $10 \text{ mg/m}^3$  in the natural gas delivered by the gas supply network where it is added as an odor marker for safety reasons. Figure 2 shows the distribution of natural gas in the isothermal non-reactive and in the reactive flow directly above the exit of the swirl burner. The axis of symmetry of the burner lies in the middle of figure 2, whose width corresponds to 90 mm and whose height to 30 mm. For the non-reacting case three single shots are presented, showing, that the occurrence of high concentrations of natural gas is limited to a restricted area. The direction of the fresh gas flow after leaving the burner nozzle can be seen from the averaged distribution field. The relative standard deviation reveals the presence of two shear layers at both sides of the main gas flow where fluctuations are increased. In the reactive flow, THT-LIF still indicates the presence of unburned natural gas. However, the direction of the fresh gas flow is slightly changed as compared to the non-reactive case due to volumetric variation during the reaction and to variations in gas viscosity in the presence of temperature gradients.

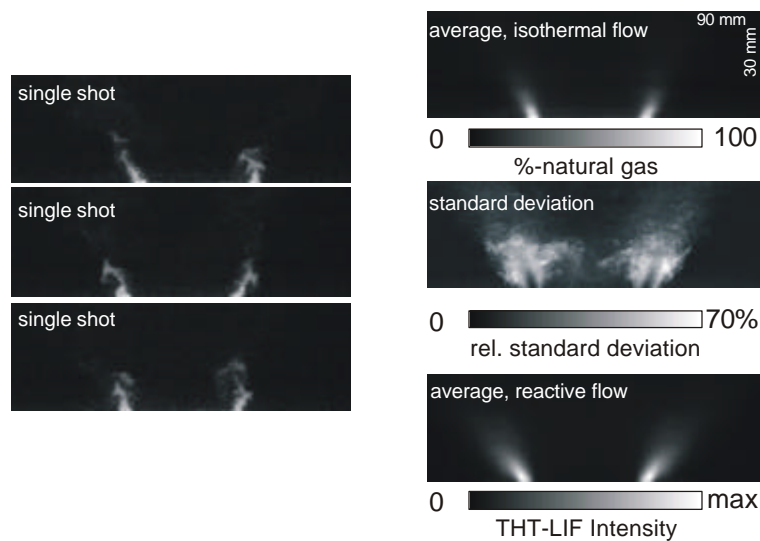


Figure 2: Distribution of natural gas in the non-reactive and reactive flow.

The financial support by the BMBF within the TECFLAM project (FKZ 0327059 L) is gratefully acknowledged by the authors.

- 1 Leuckel, W., Fricker, N., *Journal of the Institute of Fuel* 49:103-122 (1976).
- 2 Tacke, M.M., Hassel, E.P. and Janicka J., *Proc. Combust. Inst.* 26:75-82 (1996).
- 3 Landefeld, T., Kremer, A., Hassel, E.P., Janicka, J., Schäfer, T., Kazenwadel, J., Schulz, C., Wolfrum, J., *Proc. Combust. Inst.* 27:1023-1030 (1998).
- 4 Böckle, S., Kazenwadel, J., Kunzelmann, T., Shin, D.-I., Schulz, C., Wolfrum, J., Simultaneous single-shot laser-based imaging of formaldehyde, OH and temperature in turbulent flames, *Proc. Combust. Inst.* 28 (2000), in press.
- 5 Paul, P. H., Gray, J. A., Durant Jr., J. L., Thoman Jr., J. W., *Appl. Phys. B* 57:249-259 (1993).
- 6 Böckle, S., Kazenwadel, J., Schulz, C., *Laser-diagnostic multi-species imaging in strongly swirling natural gas flames*, *Appl. Phys. B*, in press.
- 7 Grebner, D., Hein, J., Triebel, W., Burkert, A., König, J. und Eigenbrod, C., in *Proceedings of the Joint Meeting of the British, German and French sections of the Combustion Institute*, 1999, pp. 485-487.
- 8 Paul, P.H. and Najm, H.B., *Twenty-Seventh Symposium (International) on Combustion*, The Combustion Institute, Pittsburgh, PA, 1998, pp. 43-50

# Laminar Nonpremixed Flame Calculations of Methane with Highly-Preheated Air

Dr. B.B. Dally

Department of Mechanical Engineering  
The University of Adelaide  
South Australia, Australia

Flameless Oxidation (FLOX) is a combustion regime which incorporates recirculation of hot combustion products to the oxidant stream (vitiation) to oxidise the fuel without having a flame. The concept is being implemented commercially on large and small scale facilities [1]. This regime achieves low emission of  $\text{NO}_x$  and CO pollutants and improved fuel savings. Its application can also be tailored to low calorific fuels, which are often produced in chemical processes or vented from coal mines. The combustion in these devices takes place at reduced temperature in the range of 1100-1700K. It is characterised by a flat thermal field, minor temperature fluctuations and when optimised, there are no visible or audible flame, hence the name [2].

Although this technology has been known for quite some time valuable information on the structure of these flames are yet to be explored. Issues such as the importance of mixing on the stability of the flame, the interaction between the turbulence and chemistry and modelling issues such as CO and  $\text{NO}_x$  predictions are yet to be investigated. In this poster the laminar nonpremixed flame is investigated computationally using the OPPDIF code. Methane is used as fuel, while the air was diluted with combustion products ( $\text{CO}_2$  and  $\text{H}_2\text{O}$ ) to alter the oxygen levels in the oxidant stream. The chemical kinetics mechanism used in the calculations has been optimized for low temperature methane oxidation [3]. It consists of 51 species and 200 reactions including nitrogen oxidation. It is worth mentioning that the GRI-2.1 mechanism do not sustain methane flames at temperatures lower than 1400K. Current investigation using the GRI-3.0 mechanism is underway.

Figure 1 contains methane nonpremixed laminar flame calculations under preheated oxidizer stream conditions and at low strain rate. These flames exhibit the following characteristics:

1. An increase in the oxidizer stream temperature broadens the reaction zone substantially and exhibits a distributed reaction regime;
2. At temperatures higher than 1200K and low oxygen levels ( <4% by volume) the combustion regime resembles that of the FLOX regime;
3. The OH radical at the FLOX conditions does not seem to be of importance while  $\text{CH}_2\text{O}$  species increases substantially under these conditions.

This work is a first in a series that aim at enhancing the understanding of FLOX combustion. In particular issues such as Damköhler number effects on the structure and stability of the flame will be explored. A burner is being built to investigate laminar and turbulent nonpremixed flames under the FLOX regime. This burner will be used to conduct

measurements or reactive scalars using single-point Raman-Rayleigh-LIF measurements at Sandia National Laboratory later in the year.

Reference:

1. Weber, R., Verlaan, Ad.L., Orsino, S., and Lallemand, N., *Journal of the Institute of Energy*, 77, pp. 77-83, 1992.
2. Wüning, J.A. and Wüning, J.G., *Progress in Energy and Combustion Science*, Vol. 23, pp. 81-94, 1997
3. Bromly, J.H., Barnes, F.J., Muris, S., You, X., and Haynes B.S., “Kinetic and Thermodynamic Sensitivity Analysis of the NO-sensitised Oxidation of Methane” *Combustion Science and Technology*, 115, 259-297 (1996).

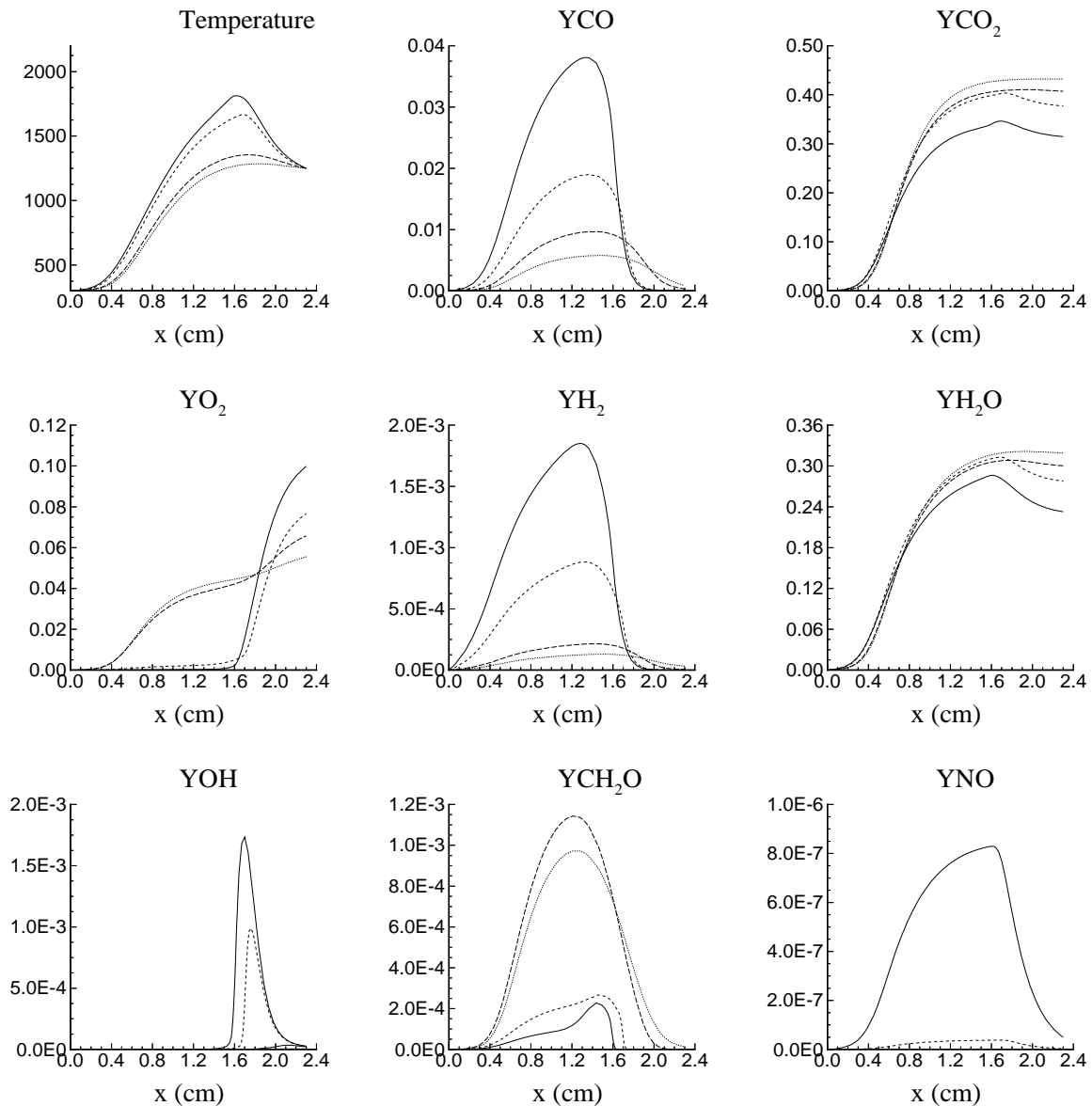


**Figure 1** Temperature and mass fraction profiles plotted against the axial distance  $x$  for methane laminar diffusion flame at a strain rate of  $a=20$  1/s.  
 Solid lines: YO<sub>2</sub>=10%, Dashed lines: YO<sub>2</sub>=7.7% , Long-dashed line: YO<sub>2</sub>=6.6%, Dotted line: YO<sub>2</sub>=5.5%

# Measurement of Carbon Monoxide in Turbulent Nonpremixed Bluff Body Flames using Two Photon Laser Induced Fluorescence Technique

B. B. Dally<sup>1</sup>, A. R. Masri<sup>2</sup>, R. S. Barlow<sup>3</sup> and G. J. Fiechtner<sup>3</sup>

<sup>1</sup>The University of Adelaide, <sup>2</sup>The University of Sydney, Australia

<sup>3</sup>Sandia National Laboratories, Livermore, CA

A study of turbulent nonpremixed flames of hydrocarbon fuels stabilised on a bluff-body burner is reported in this paper. Flame HM1, which uses a mixture of methane and hydrogen (1:1 by volume) have been chosen as a benchmark for modellers to the international workshop on turbulent nonpremixed flames. Previously published data [1] which is also available on the web [2] were collected using the Raman scattering technique for all major species including CO. This technique suffers from fluorescence and other Raman interference which contributes to reduced signal to noise ratio. In this study a new and more accurate technique was used to measure the CO mass fractions at different locations in the flame. This technique uses the Two-Photon Laser Induced Fluorescence (TPLIF), which was developed by Greg Fiechtner and Robert Barlow at the Combustion Research Facility, Sandia National Laboratories and was applied simultaneously with the Raman scattering technique. The setup at the TDF laboratory is used in this study and it was described extensively in the literature [3,4]. Only a brief description is given here. A laser beam with 700  $\mu$ s/pulse at 230.1 nm was focused down to a probe volume of 0.3 mm waist diameter and the CO emission was collected at 484 nm using a PMT. A reference cell at room temperature was used to tune the laser wavelength for maximum signal. The laser beam in the probe volume was tuned by a fixed amount to a position corresponding to a relatively flat region in the flame spectrum. The measurement were then linearly normalized with measured laser power on a shot to shot basis.

The results presented in Figure 1 show CO mass fractions measured in the HM1 flame using the Raman and TPLIF techniques. Measured scatter plots at different axial locations above the bluff-body burner are compared with laminar flame calculations with and without differential diffusion. The agreement with the calculations is quite good albeit of slightly higher values of the measured CO mass fraction at certain locations. It is also clear from the Fig. 1, that the TPLIF technique to measure CO is superior to the Raman technique and does not suffer from interference.

In conclusion it is clear that the new data will be a more accurate and reliable to use for the comparison with the models. This data will be available on the web [2] for modellers to use.

## References:

1. B.B. Dally, A.R. Masri, R.S. Barlow and G.J. Fiechtner, 'Instantaneous and Mean Compositional Structure of Bluff-Body Stabilised Nonpremixed Flames', *Combustion and Flame*, Vol 114/1-2, pp. 119-148, 1998.
2. Data-base available from Masri, A.R., Mechanical and Mechatronic Engineering, The University of Sydney, NSW, 2006, Australia. (<http://www.mech.eng.usyd.edu.au/research/energy/energy.html>)
3. B. S. Barlow and J. H. Frank, 'Effects of Turbulence on Species Mass Fractions In Methane Jet Fkames', *Twenty-Seventh Symposium on Combustion*, 1998, pp. 1087-1095
4. G. J. Fiechtner, C. D. Carter and R. S. Barlow, 'Quantitative Measurements of CO Concentrations in Laminar and Turbulent Flames Using Two-Photon Laser-Induced Fluorescence', *33<sup>rd</sup> National Heat Transfer Conference*, Albuquerque, New Mexico, 1999.

<sup>1</sup> Email: [bassam.dally@adelaide.edu.au](mailto:bassam.dally@adelaide.edu.au)

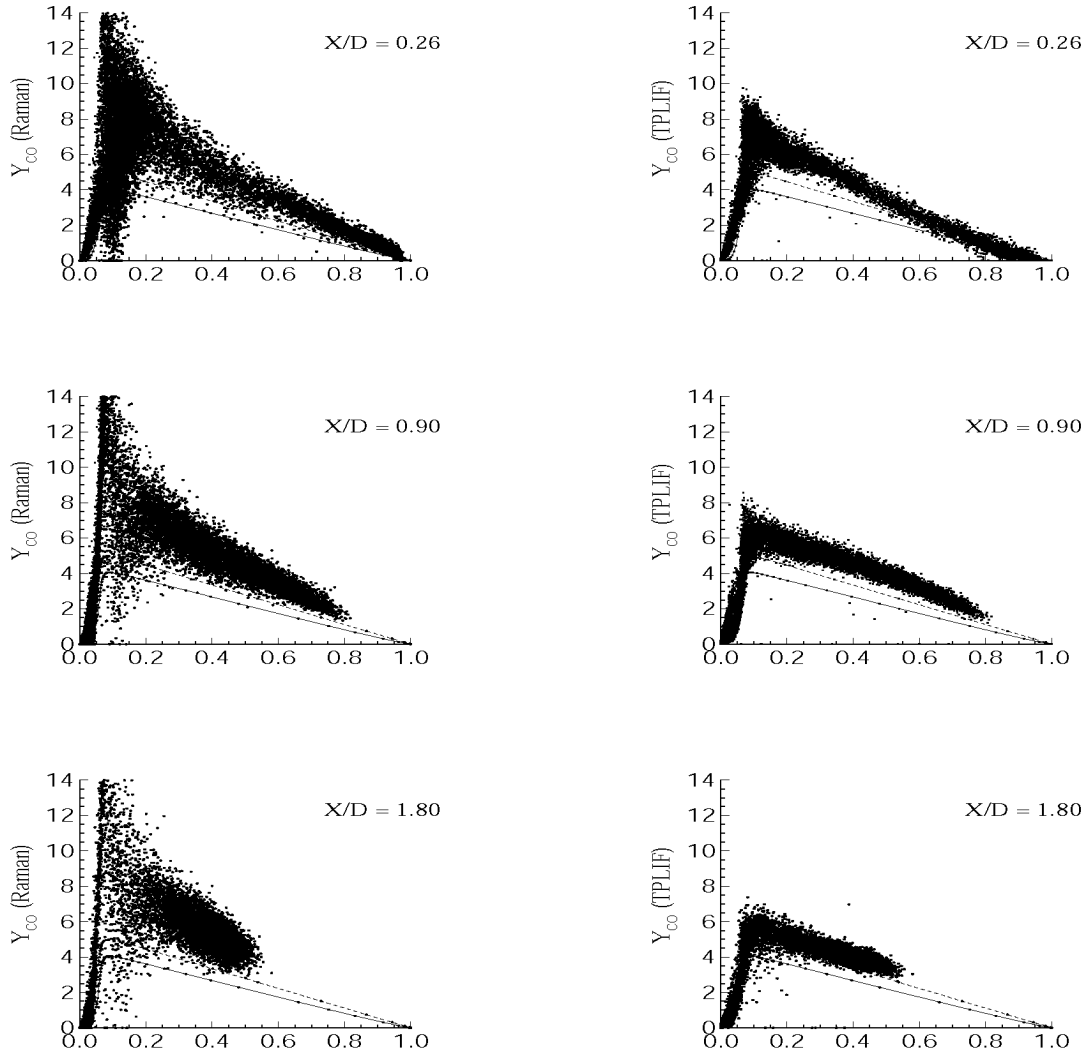


Figure 1: Scatter plots of measured CO mass fractions plotted against the mixture fraction for turbulent nonpremixed Flame of  $\text{CH}_4/\text{H}_2$  (1/1 by vol.) HM1, stabilized on a bluff-body. Each axial location plot contains data measured at different radial positions in the flame. Lines represent laminar flame calculations for standard case (solid-line) and equal diffusivity case (dashed line).

<sup>1</sup> Email: [bassam.dally@adelaide.edu.au](mailto:bassam.dally@adelaide.edu.au)

# NUMERICAL MODELING OF NON-PREMIXED TURBULENT FLAMES IN OPPOSED JET FLOWS WITH PDF TRANSPORT EQUATIONS

L. Demiraydın , J. Gass

Institute of Energy Technology, ETH Zurich  
Laboratory of Thermodynamics in Emerging Technologies  
LOW C1, ETH-ZENTRUM, CH-8092 Zurich Switzerland  
e-mail : [demiraydin@tnt.iet.mavt.ethz.ch](mailto:demiraydin@tnt.iet.mavt.ethz.ch)

The study of opposed-jet flames aroused the interest in the recent years because of their convenience either in experimental establishment or in description of the mathematical expressions related to flame stretching. By taking this recent interest into consideration, the present project aims the modeling of non-premixed flames in opposed turbulent flows.

For the numerical improvement and the comparison of this work, the geometrical configuration and non-premixed case experimental measurements are taken from the counterflow burner, which is built by Mastorakos [1]. Some salient comparisons are done for velocity, temperature, species and mixture fraction results. We have to note that; instead of nitrogen co-flow which is used in experiment, air co-flow is used in the numerical work. Numerical modeling is improved with a coupled code which consists of the commercial flow solver CFX-TASCflow and a Finite Difference method code which solves the PDF transport equations [2]. The flow field is solved with CFX-TASCflow by the help of  $k-\epsilon$  turbulence modeling and the information is given to PDF Code, which solves an ensemble of five variables consisting of  $\{Z_{mix}, n_{CH_4}, n_{CO}, n_{O_2}, n_H\}$ . The PDF equations are represented by an ensemble of statistical particles (Monte Carlo Method) in each computational cell which every element of particle is the instantaneous stochastic values in the thermochemical state vector.

Basically, PDF Transport Equations model comprises four basic processes, which two of them, -diffusion and convection-, are solved in physical space and the others, -reaction and mixing-, are solved in composition space. Of these four processes, only reaction is simulated deterministically. That means, chemical source term appears in closed form. For modeling the chemistry, a four-step reduced mechanism is used [3,4]. The modeling of turbulent transport is achieved by Gradient Diffusion Assumption and for the modeling of mixing term, IEM is preferred.

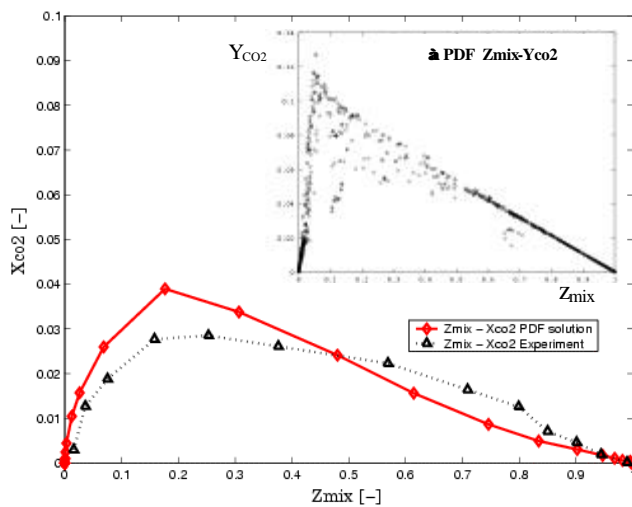


Fig 1. Mean value and scatter plot CO<sub>2</sub> - mixture fraction profiles along the centerline (H=20 mm.)

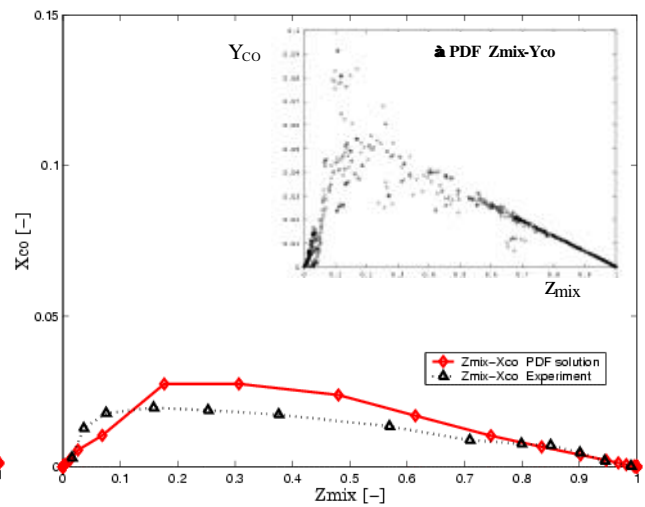


Fig 2. Mean value and scatter plot CO-mixture fraction profiles along the centerline (H=20 mm.)

In the numerical calculations, some problems in the flame location and flame width are observed. (Fig3) The short residence times cause some difficulties in the turbulent mixing of scalars and also to stabilize the flame. Results of the computations will be presented more detailed.

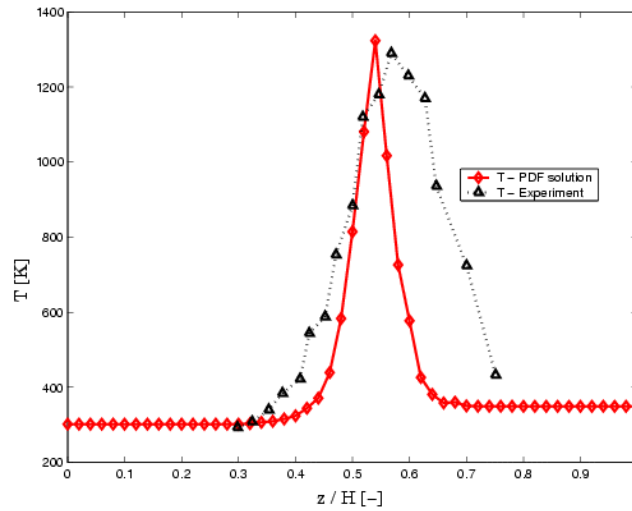


Fig 3. Temperature profiles along the centerline (H=20 mm.)

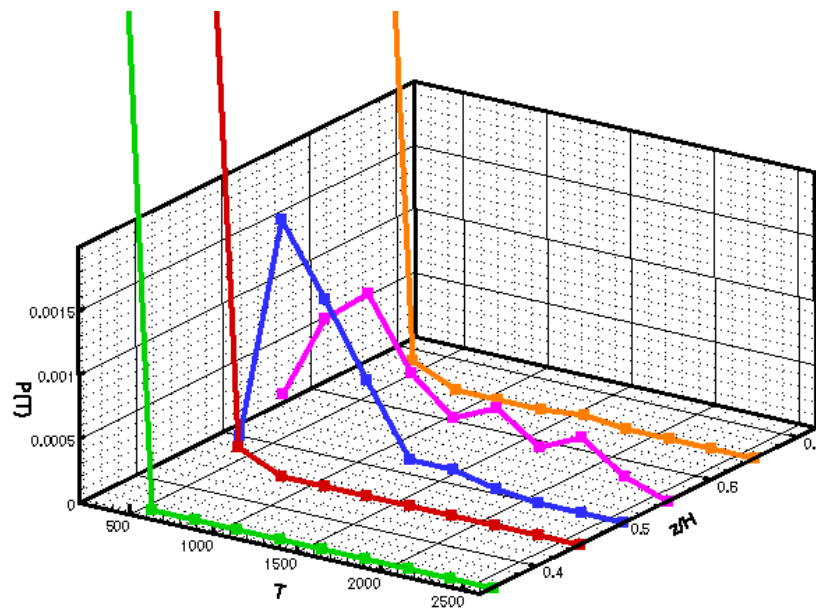


Fig 4. Numerical results of Probability Density Functions for the temperature (H=20 mm.)

- [1] E.Mastorakos, Turbulent combustion in opposed jet flows , Ph. D. Thesis Imperial College of Science, Technology and Medicine, July 1993
- [2] A. Laxander, Numerische Simulation von turbulenten Diffusionsflammen mit einem PDF-Transportgleichungsmodell, Ph. D. Thesis Universität Stuttgart, 1996
- [3] B. Rogg, Sensitivity Analysis of Laminar Premixed CH<sub>4</sub> – Air Flames using full and reduced Kinetic Mechanisms and Asymptotic Approximations for Methane – Air Flames, Volume 384 of Lecture Notes in Physics, page 159-192, Springer Verlag, 1991
- [4] N. Peters and R.J. Kee, The Computation of stretched laminar methane- air diffusion flames using a reduced four-step mechanism, Combustion and Flame, 68:17-29, 1987

# NUMERICAL SIMULATION OF A PILOTED METHANE/AIR FLAME USING PDF TRANSPORT EQUATION MODEL

L. Demiraydin, Dr. J. Gass

Institute of Energy Technology, ETH Zurich  
Laboratory of Thermodynamics in Emerging Technologies  
LOW C1, ETH-ZENTRUM, CH-8092 Zurich Switzerland  
e-mail : [demiraydin@tnt.iet.mavt.ethz.ch](mailto:demiraydin@tnt.iet.mavt.ethz.ch)

This work presents the modeling of the piloted methane/air flame (Flame E) with the Reynolds number 33,400. The calculations are based on a PDF Transport Equations Model where a 4-step reduced chemistry is used [2,3]. The flow field calculations are achieved with k- $\epsilon$  turbulence model by using a sophisticated Finite volume commercial code. For solving the composition space, an Eulerian composition Finite Difference PDF/Monte Carlo method is used. [1] An ensemble of  $\{Z_{\text{mix}}, n_{\text{CH}_4}, n_{\text{CO}}, n_{\text{tot}}, n_{\text{H}}\}$  is chosen for the description of the system. The mixing model is the IEM with 100 particles in each cell.

The grid consists of 120x90 nodes with an assumption of axisymmetry which has a grid-refinement in the nozzle-exit. The boundary conditions are taken from the documentation for Flame E.

Some results of the work are presented in Figure 2 for the radial direction at  $x/d=15$ . The calculations of temperature and species are resulted in a good agreement. Only the CO and H<sub>2</sub> calculations are overpredicted compared to the experiments. This overprediction is thought to be caused by 4-step reduced mechanism which is used. It is also observed that the extinction phenomena could not be predicted well with the model used. The results will be presented detailed.

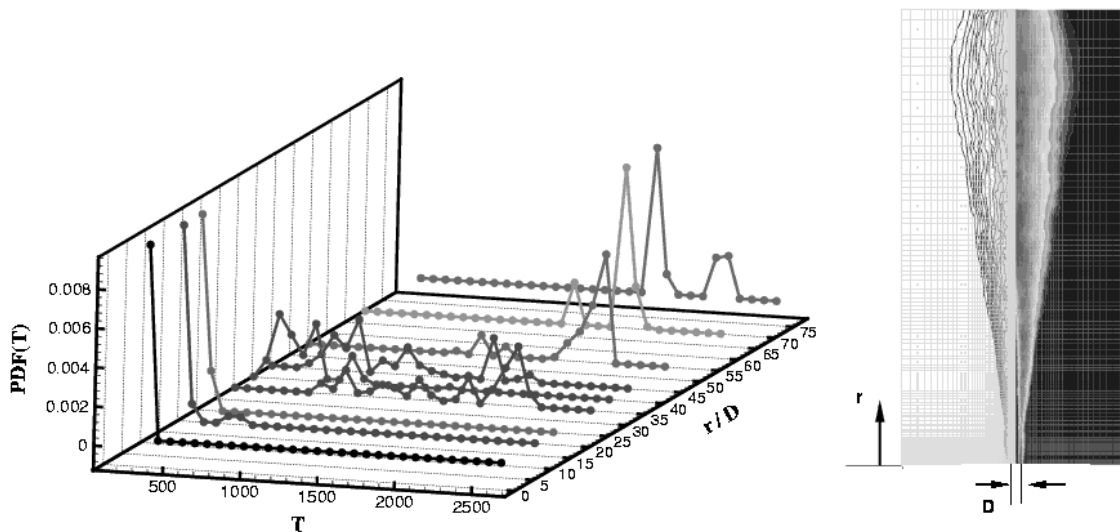
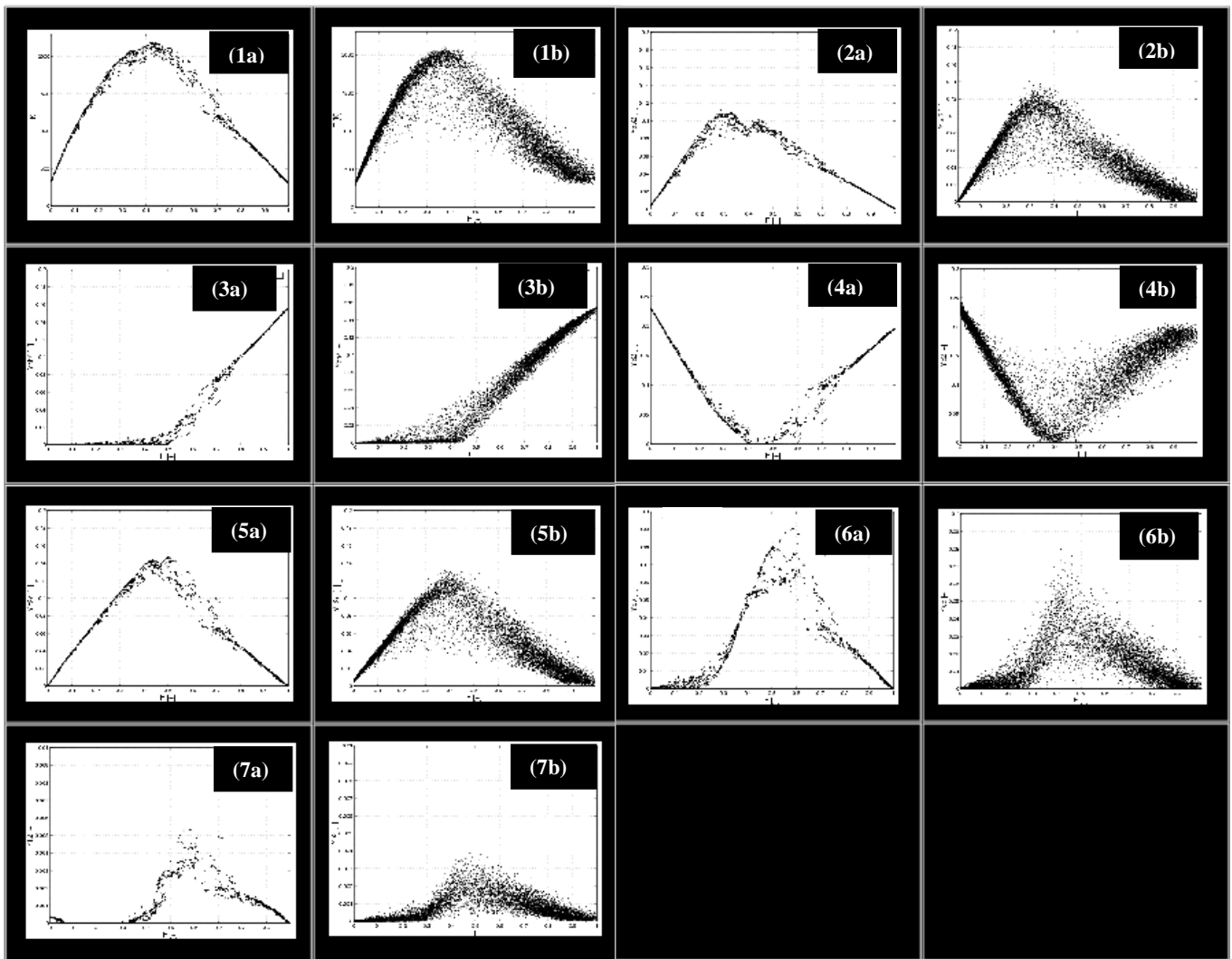


Figure 1 The Probability Density Function of Temperature in respect of normalized radial direction



**Figure 2** Scatter plots of Temperature and Mass Fractions of Species in respect of mixture fraction at  $x/d=15$   
 (a) denotes to modeling with PDF Transport Equations Model (b) denotes to experimental measurements.  
 1-Mixture Fraction – Temperature,  
 2-Mixture Fraction – Mass Fraction of  $\text{CO}_2$ ,  
 3-Mixture Fraction – Mass Fraction of  $\text{CH}_4$   
 4-Mixture Fraction – Mass Fraction of  $\text{O}_2$ ,  
 5-Mixture Fraction – Mass Fraction of  $\text{H}_2\text{O}$ ,  
 6-Mixture Fraction – Mass Fraction of  $\text{CO}$ ,  
 7- Mixture Fraction – Mass Fraction of  $\text{H}_2$

### **REFERENCES:**

- [1] A. Laxander, Numerische Simulation von turbulenten Diffusionsflammen mit einem PDF-Transportgleichungsmodell, Ph. D. Thesis Universität Stuttgart, 1996
- [2] B. Rogg, Sensitivity Analysis of Laminar Premixed  $\text{CH}_4$  – Air Flames using full and reduced Kinetic Mechanisms and Asymptotic Approximations for Methane – Air Flames, Volume 384 of Lecture Notes in Physics, page 159-192, Springer Verlag, 1991
- [3] N. Peters and R.J. Kee, The Computation of stretched laminar methane- air diffusion flames using a reduced four-step mechanism, Combustion and Flame, 68:17-29,1987

## Multi-Diagnostic Imaging For the Study of Turbulent and Unsteady Flames

Jeffrey M. Donbar  
Air Force Research Laboratory, AFRL/PRSC, WPAFB, OH 45433  
donbarjm@possum.appl.wpafb.af.mil

Campbell D. Carter  
Innovative Scientific Solutions, Inc., Beavercreek, OH 45440

Kyle A. Watson and Kevin M. Lyons  
North Carolina State University, Raleigh, NC 27695

James F. Driscoll, Werner J.A. Dahm, and A. Ratner  
University of Michigan, Ann Arbor, MI 48109

The combination of diagnostic methods such as CH/OH PLIF (planar laser-induced fluorescence)—which enables instantaneous imaging of the flamefront—and PIV (particle imaging velocimetry) or PRS (planar Rayleigh scattering) have proved very powerful in elucidating the underlying physics of reacting flows. Two examples from our studies of lifted jet flames are shown in Figs. 1 and 2. In Fig. 1 we show the interaction of the turbulent flowfield ( $Re_{jet} = 6600$ ) and the flamefront (derived from CH PLIF); here, the flame surface at the stabilization point has become engulfed by a vortex. In Fig. 2 we show local extinction of the lifted flame using the combined techniques of CH PLIF and PRS. Here, one can see that a finger of jet fluid ( $CH_4$  with some mixed air and products) has penetrated the flamefront, causing the flame to extinguish locally; below the flame one can clearly see the role of turbulence in creating flammable fuel-air mixtures. In Fig. 3 we show simultaneous CH/OH image pairs in a high-swirl burner. As CH peaks on the fuel-rich side and OH on the fuel-lean side, the combination of these radicals provides insight on fuel-air mixing in complicated flowfields. Ultimately, the leitmotif of these efforts is to provide data for the development of improved modeling methods for turbulent flames. Indeed, images such as these show the basic structure and evolution of the flamefront. Validation of new models such as the Large Eddy Simulation (LES) and the Linear Integral Moment methods will require that they adequately reproduce these features.

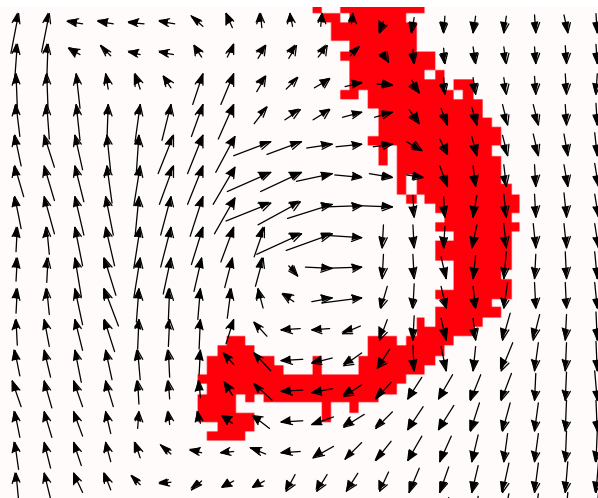
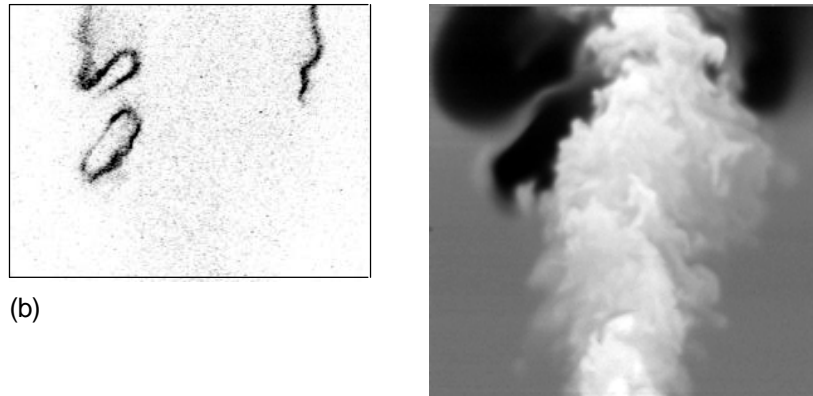


Fig. 1. Interaction of a vortex and the flame surface (denoted by the CH radical) at the stabilization point of a lifted  $CH_4$ -air jet flame. Here, the fuel side is the left-hand portion of the image, while the air side is the right-hand portion. Half of the mean fuel-jet centerline velocity has been subtracted from all the vectors to highlight the presence of the vortex. This  $6 \times 7.5$  mm *sub-image* was extracted from the original  $24 \times 36$  mm image.



(b)

Fig. 2. Extinction and stabilization of a lifted jet  $\text{CH}_4$ -air flame. Here, PLIF of the CH radical (left) marks the flamefront, while planar Rayleigh scattering (right) shows the fuel-mixing regions in relation to the burning regions. The highest scattering intensity (white) corresponds to fuel scattering, while the lowest intensity (black) corresponds to hot-gas (low-density) scattering. Note the presence of fuel enveloping the pocket of hot gas (on the left-hand side of the flame).

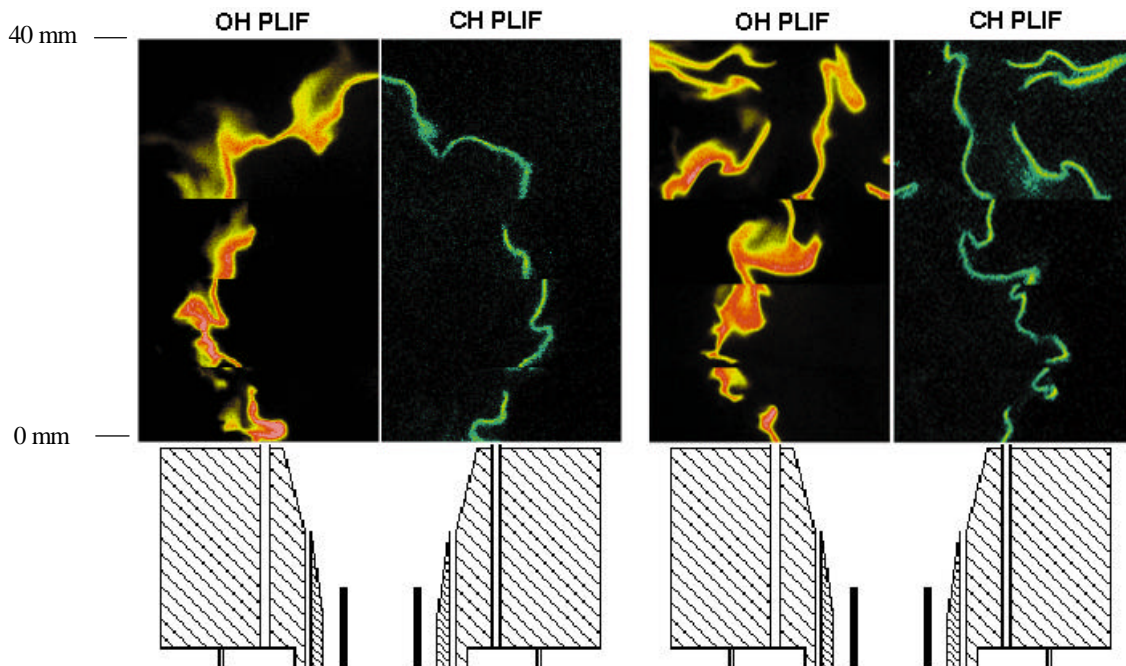


Fig. 3. Simultaneous CH/OH PLIF in a high-swirl burner. Four simultaneous image pairs (shown in mirror-image format) comprise each composite image. The utility of simultaneous imaging in a complex flowfield is the ability to distinguish between fuel (CH peak) and air side (OH peak) of the flamefront. Similar to what has been noted in jet flames, the CH layer remains thin throughout the flame length, while OH tends to thicken with increasing axial distance.

## Investigation of temperature, species and their gradients in a turbulent methane/air opposed jet flame by 1-D Raman/Rayleigh scattering

D. Geyer<sup>1</sup>, D. Sauer, A. Dreizler, E.P. Hassel, J. Janicka

Fachgebiet Energie- und Kraftwerkstechnik, Technische Universität Darmstadt, Petersenstrasse 30, 64287 Darmstadt, Germany

A new turbulent opposed jet burner for non-premixed and partially premixed methane flames was developed in cooperation between the TU Darmstadt, FORTH-ICEHT/Greece and Sandia National Labs/USA. The special attention of the design is directed to the application of laser diagnostic techniques, in particular Raman/Rayleigh scattering. In future, identical copies of the burner will be operated in all three labs. In order to allow measurements of temperature, species and the gradients of these scalars perpendicular to the stagnation plane access for the laser beam along the centerline of the burner is provided. An exhaust system in combination with water-cooling of sensitive burner parts ensures stable conditions even for longer operation times.

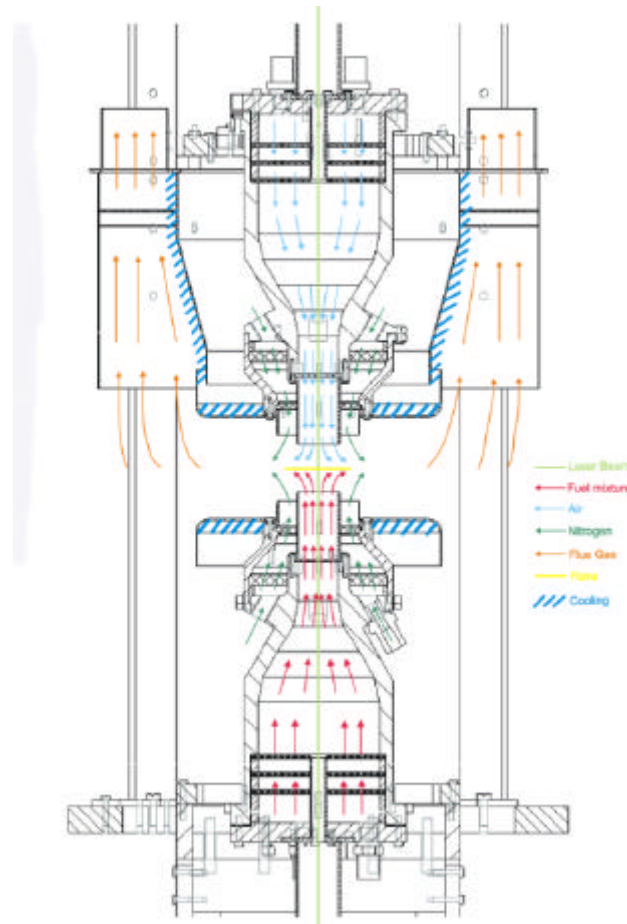


Fig 1 : Turbulent opposed-jet burner including path of laser beam

<sup>1</sup> corresponding author: Dirk Geyer, geyer@hrz2.hrz.tu-darmstadt.de

The requirements to achieve a flow with a sufficient high Re number on the one hand (large diameter of the jet nozzle) and on the other hand to produce a flame which is small enough to avoid a damage of the Raman out-couple optics resulted in a compromise for the jet nozzle diameter of 30 mm. These nozzles are enclosed by a concentric 60 mm co-flow of N<sub>2</sub>, which is operated at a comparatively high gas velocity of 0.8 ÷ 1.0 m/s. Lower co-flow velocities facilitate unburned fuel from the stagnation plane to wrap in an extended flame around the burner, which again was to avoided because of damage to the optics. Different flow stratifiers are inserted in each co-flow to generate a homogenous velocity profile.

Turbulence is enhanced by perforated plates that are placed downstream a contoured nozzle (contraction ratio 9:1). A straight tube with 50 mm length is located between the turbulence generator and the jet exit. Two different contoured nozzles and several perforated plates were tested in order to produce radial-symmetric flow profiles. The perforated plates employed had blockage ratios of 35% to 45% and hole diameters between 3.3 and 4.0 mm.

Velocity exit profiles of a single jet as well as of the opposed jets with and without perforated plates were measured by hot wire anemometry of a non-reacting flow for typical operation conditions. In addition the velocity profiles of the co-flow and the influence of the exhaust system on the exit profiles were explored. For a fuel consisting of 1 part methane and 3 parts air extinction limits of the flame were investigated for several perforated plates in order to determine the configuration, which is most suited for the Raman/Rayleigh experiments.

As light source for Raman/Rayleigh experiments a frequency doubled Nd:YAG laser is used. To inhibit gas breakdown in the measurement volume two pulse stretchers are employed. Raman scattering is collected perpendicular to the laser beam axis by a specially designed achromatic objective ( $f_{\#}=2.0$ ,  $f=275$  mm on object side) and directed onto the entrance slit of an imaging spectrometer ( $f_{\#}=4.1$ ,  $f=310$  mm). Raman signals are spectrally resolved and recorded by the use of an intensified CCD (ICCD) array detector selected for high quantum efficiency. Raman signals of different locations in the measurement volume are monitored on different parts of the CCD detector to enable one-dimensional spatially resolved measurements. Rayleigh signals are monitored by means of a second ICCD array.

## Near-Nozzle Phenomena in a Nonpremixed CO/H<sub>2</sub>/N<sub>2</sub> Jet Diffusion Flame: Modeling Extinction/Reignition, Differential Diffusion, and Initial Condition Sensitivities

John C. Hewson and Alan R. Kerstein  
Combustion Research Facility  
Sandia National Laboratories  
Livermore, CA 94551-0969

Using the one-dimensional turbulence (ODT) model (Kerstein, 1999), a number of phenomena that occur in the near-nozzle region of nonpremixed flames can be studied. These are studied in the context of the nonpremixed CO/H<sub>2</sub>/N<sub>2</sub> jet diffusion flame measured by Barlow *et al.* (2000).

The ODT model solves an unsteady reaction-diffusion equation to model diffusive scalar mixing. Concurrently, advective mixing is implemented through the use of triplet-maps occurring at a rate determined by the local velocity gradient. All chemically relevant length scales are resolved in one dimension along the ODT domain. The phenomena described here highlight some of the physics captured by the ODT model. Also, the sensitivity of the ODT model to certain initial conditions is examined.

There are two constants within the model that together determine the overall mixing rate and the magnitude of conserved scalar fluctuations. The same model constants are used for CO/H<sub>2</sub>/N<sub>2</sub> flames, CH<sub>4</sub>/air flames, H<sub>2</sub> flames and nonreacting temporally evolving shear layers. The ODT model adequately predicts the flowfield evolution except for the effects of dilatation on the mixing rate. Results presented at the previous TNF workshop and in a forthcoming paper indicate that the ODT model is able to predict the evolution of the first and second conditional moments of the temperature and reacting scalars with good accuracy. An example is provided in Fig. 1.

In the ODT simulation of this flame, regions of localized extinction and reignition occur in the first several diameters downstream, as implied by Figs. 1 and 2. Before the first measurement at  $x/d=20$ , all flamelets are reignited. It is significant that ODT captures not only localized extinction but also reignition. ODT is not able to capture any phenomena with unaligned relevant property gradients, so there is no triple flame propagation in the model. That is, reignition can not occur in the simulation through triple flame propagation. Reignition occurs by rapid relaxation of the scalar dissipation rate or by diffusive transport to quenched pockets from adjacent flamelets.

The sensitivity of the observed extinction and reignition to certain model parameters and initial conditions that affect the rate of development of turbulent fluctuations has been studied. Changes that slow the development of turbulence (the use of smooth nozzle outlet velocity profiles and changes in the model constants, for example) delay both extinction and reignition and may result in persistence of locally extinguished flamelets at  $x/d=20$ , contrary to the experiments. Broadening the initial flamelet between the fuel and oxidizer streams similarly delays the onset of extinction but did not affect reignition.

Because ODT combines both advective and diffusive transport mechanisms, ODT allows the study of differential diffusion in turbulent flows. In the present case the initial condition is a strained flamelet with differential diffusion effects included as calculated in the counterflow configuration. The evolution of the differential diffusion variable,  $Z_H - Z_C$ , where  $Z_i$  is the elemental mixture fraction of element  $i$ , is shown in Fig. 3. The initially strong correlation of  $Z_H - Z_C$  with mixture fraction disappears rapidly as turbulence crosses the flame. At  $x/d=2$ , eddies have acted on only about half of the flame centers (the stoichiometric mixture fraction is 0.3), but much of the deficit of  $Z_H - Z_C$  on the rich side has already been removed by turbulent mixing. By  $x/d=6$  the correlation between  $Z_H - Z_C$  and the mixture fraction is mostly removed. While turbulence tends to remove differential diffusion in the mean, it can promote fluctuations in  $Z_H - Z_C$ . Fluctuations in  $Z_H - Z_C$  are large relative to the means for  $x/d > 6$ .

### References:

- Barlow, R. S., Fiechtner, G. J., Carter, C. D., and Chen, J.-Y., *Combust. Flame* **120**, 549-569 (2000).
- Kerstein, A. R., *J. Fluid Mech.* **392**, 277-334 (1999).

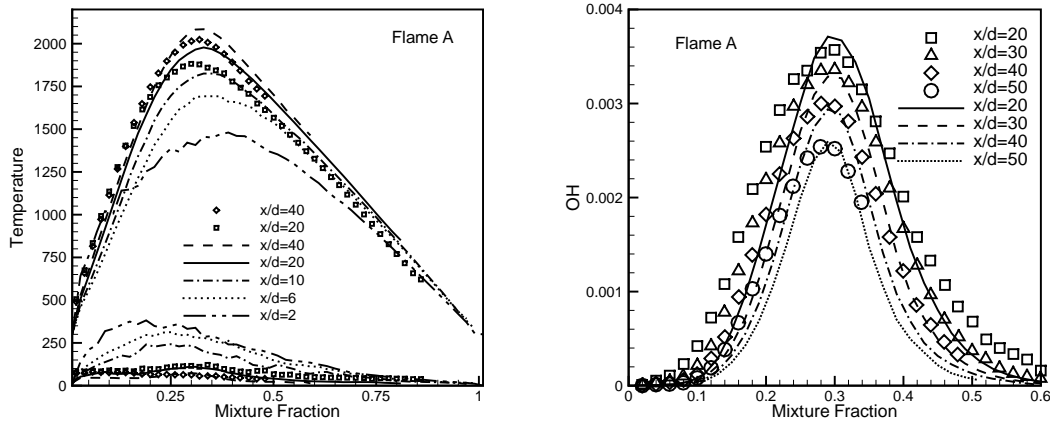


Figure 1: The evolution of the conditional mean temperature and OH mass fraction as predicted using the ODT model is shown. In the left figure, rms temperature fluctuations in the near-nozzle region are also shown. Symbols are measurements by Barlow *et al.*

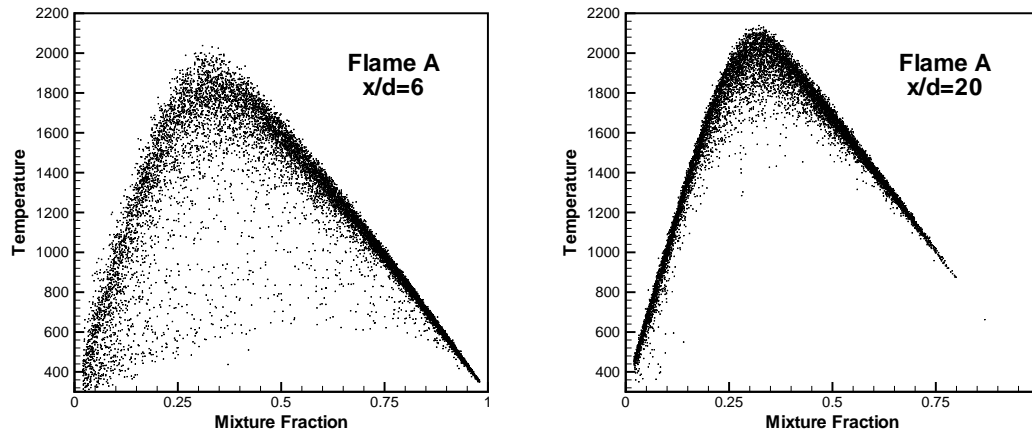


Figure 2: Scatter plots of the temperature conditioned on the local mixture fraction qualitatively show the extent of local extinction that occurs early in the flame and indicate complete reignition before  $x/d=20$ .

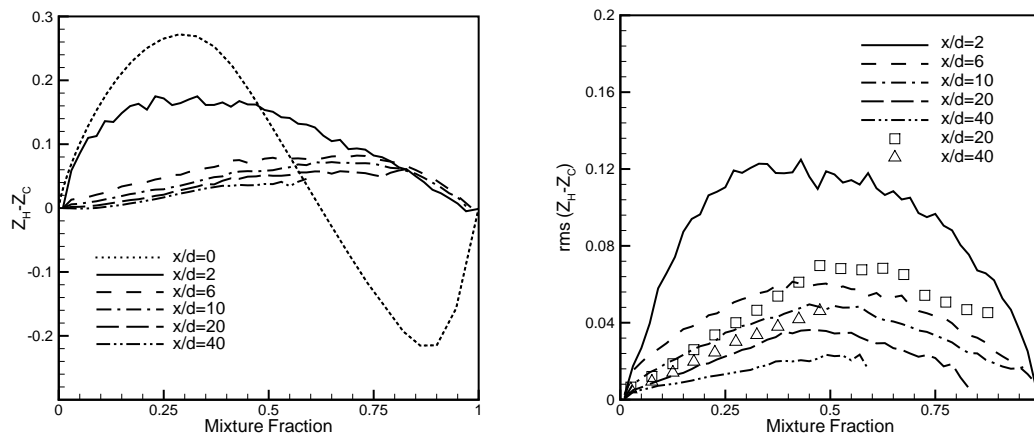


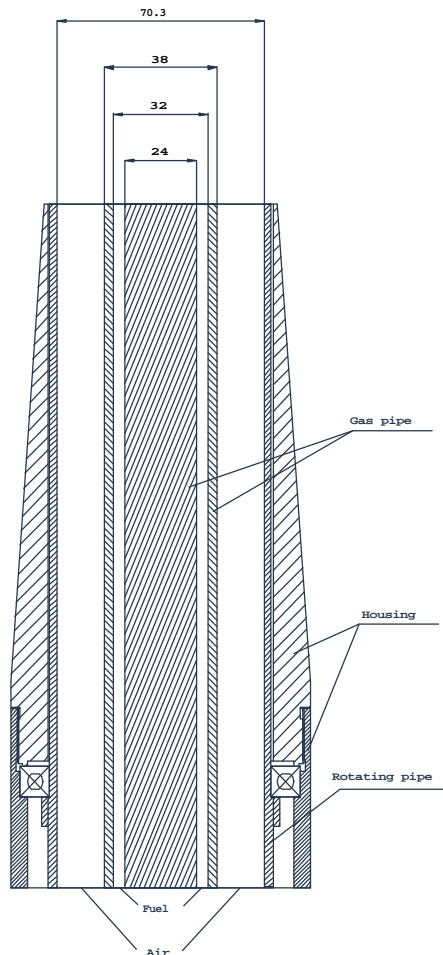
Figure 3: Conditional means (left) and rms fluctuations (right) for the differential diffusion variable  $Z_H - Z_C$ . Measured values are indicated with symbols.

# Experimental Study of a new Rotating Swirl Burner

Werner Hübner and Mike Golombok\*

*Delft University of Technology, Faculty of Applied Sciences  
Lorentzweg 1, 2628 CJ Delft*

In many industrial burners swirl is used to stabilize the flame. This swirl is usually generated by tangential inlets which results in a very complex flow field. Recently we developed a novel type of burner that uses a rotating pipe to swirl the primary air flow. For a sufficiently long rotating pipe this principle of swirl generation provides an almost developed air flow at the exit of the burner. Therefore it is possible to concentrate on turbulence chemistry interaction without variations in the flow field at the burner rim.



The burner basically consists of two concentric pipes. Through the inner pipe the fuel is provided as an annular jet. To generate a swirling airflow, the outer pipe of the burner rotates at up to 5000 rpm. The length of the rotating pipe is 1 m. Preliminary studies showed that this is sufficient to get close to the steady state of the tangential velocity profile at the upper end of the pipe. A frequency-controlled electric motor is used to drive the pipe. This motor allows variation of the rotation rate of the pipe continuously from less than 500 rpm to 5000 rpm. It is thus possible to study flames with a wide range of swirl numbers. Figure 1 shows the upper part of the burner and its main dimensions.

We first studied the influence of the rotation rate on the blow off limits for different air equivalence ratios  $\lambda$ , and Dutch natural gas as fuel. A number of interesting features are observed, e.g. for rotation rates up to 1500 rpm and an air equivalence ratio of  $\lambda=1.2$  the blow-off limit of the burner stays almost constant. For higher rotation rates, the blow off limit increases with the rotation rate of the air pipe (see figure 2). We also observed some interesting phenomena like flame transitions

Figure 1: Design of the burner  
(all dimensions in mm)

\* Also at Shell International Chemicals, Badhuisweg 3, 1031 CM Amsterdam, The Netherlands

and hysteresis effects. For example at 3000 rpm, when increasing flow, the transition from yellow to blue flame occurred at 4.7 m<sup>3</sup>/h. However when the flow is decreased, the reverse transition occurred at 2.2 m<sup>3</sup>/h. The

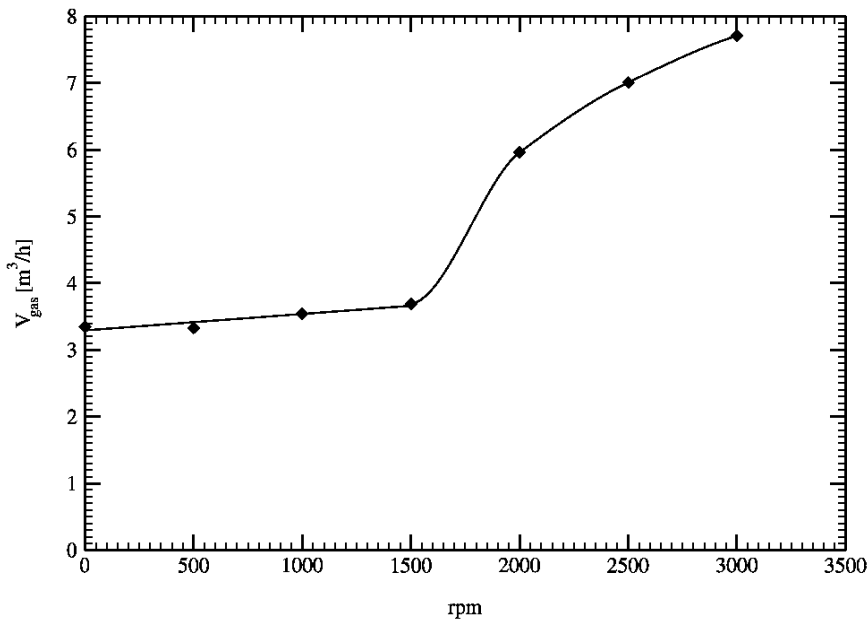


Figure 2: Blow-off limits for  $\lambda = 1.2$

difference between these two transition points, is a function of rotation rate. These phenomena are the subject of further studies.

Measurement techniques used in these studies are (1) laser doppler anemometry for point velocity mapping, (2) particle image velocimetry for flow field mapping, (3) coherent anti-stokes Raman spectroscopy for temperature measurement and (4) laser induced fluorescence for species concentration measurement.

### Corresponding author:

Dipl.-Ing. Werner Hübner  
Delft University of Technology - Faculty of Applied Sciences  
Department of Applied Physics - Thermal and Fluids Sciences  
Lorentzweg 1, 2628 CJ Delft  
The Netherlands  
P.O. Box 5046  
2600 GA Delft, The Netherlands  
Phone +31(0)15 278 2418  
Fax +31(0)15 278 1204  
E-mail [werner@ws.tn.tudelft.nl](mailto:werner@ws.tn.tudelft.nl)

# Characterization of the TECFLAM swirling diffusion flames by laser Raman measurements

**Olaf Keck, Wolfgang Meier, Winfried Stricker**

German Aerospace Center DLR, Institute of Combustion Technology,  
Pfaffenwaldring 38, 70569 Stuttgart, Germany  
e-mail: [olaf.keck@dlr.de](mailto:olaf.keck@dlr.de) or [wolfgang.meier@dlr.de](mailto:wolfgang.meier@dlr.de)

## Summary

Within the German TECFLAM cooperation, a burner for confined swirling natural gas flames with a thermal power of typically 150 kW was developed. A number of well-defined 'standard flames' has been investigated in order to improve the understanding of swirling flames and to establish a data base that can be used for the verification of CFD calculations. The data sets measured at the DLR consist mainly of the joint probability density functions (PDFs) of the temperature, the mixture fraction, and the major species concentrations determined by spontaneous Raman scattering. The mean values and rms fluctuations of the temperature and mixture fraction will be presented as (interpolated) two-dimensional distributions and give an overview of the general flame behavior. The thermochemical state of the flame and effects of turbulence-chemistry interactions will be discussed showing scatterplots of the correlations between various quantities.

## Burner and Flames

Swirling natural gas/air flames with a thermal load of 150 kW were stabilized in the confined TECFLAM swirl burner [1]. Natural gas and swirling air are supplied to the flame through annular nozzles with i.d. 20 mm, o.d. 26 mm, and i.d. 30 mm, o.d. 60 mm, respectively. The amount of swirl, i.e. the swirl number of the air stream, can be changed by a movable block inside the burner [2]. Flames with an overall air/fuel ratio of 1.2 and swirl numbers 0.9, 1.13, 1.4, and 1.8 have been investigated in detail. The water cooled burner housing has an inner diameter of 500 mm, a height of 1200 mm, and a top with an annular slit for the exhaust gas. The optical access is provided by four quartz windows.

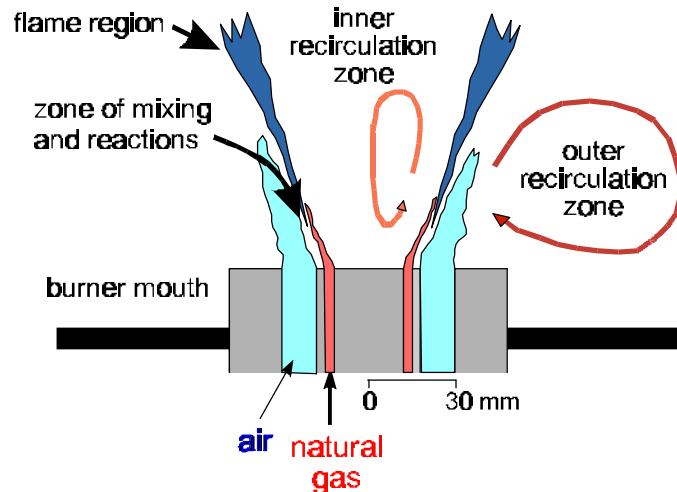
## Measuring Technique

Spontaneous Raman scattering has been applied to determine simultaneously the temperature, mixture fraction, and the species concentrations of CH<sub>4</sub>, H<sub>2</sub>, O<sub>2</sub>, N<sub>2</sub>, H<sub>2</sub>O, CO<sub>2</sub>, and CO in pointwise single shot measurements with a spatial resolution of 0.6 mm. A flashlamp pumped dye laser ( $\lambda=489$  nm, 2  $\mu$ s pulse duration, 3.5 J pulse energy) was used for the excitation, the scattered light was detected by an array of photomultiplier tubes after wavelenghts separation in a spectrograph [3]. The flames were investigated at typically 120 locations. At each location 300 single-pulse measurements were performed from which the joint PDFs were determined.

## Results

In order to yield a general quantitative characterization of the flames, two-dimensional distributions of the mean values and rms fluctuations of the temperature, concentrations, and mixture fractions were generated from the pointwise measurements by interpolation. These distributions reflect, for example, the position and downstream development of the mixing zone, the turbulent fluctuations, and the overall temperature level. The two recirculation zones of the flames, i.e. the inner one near the flame axis and the burner mouth and the outer one, which reaches from the flame region to the burner walls, can be clearly distinguished. Within the inner recirculation zone, hot near-stoichiometric combustion products ( $T \approx 1900\text{--}2000\text{ K}$ ) are transported to the flame root where they ignite and stabilize the flame.

A deeper insight into the turbulence-chemistry interaction and the thermochemical state of the flame was gained from the correlations between various quantities. The most interesting part of the flame is the flame root with the highest flow velocities and smallest turbulent structures. The ignition and stabilization of the flame takes place at a height of  $h \approx 20\text{ mm}$  above the burner mouth. Below  $20\text{ mm}$  stoichiometric (cold) compositions were also measured in the mixing zone of fuel and air, but reactions were not initiated there because the hot products from the inner recirculation zone were shielded from these mixtures by the inlet flow of natural gas (see figure). Above  $h \approx 20\text{ mm}$  the natural



Schematic drawing of the flows near the burner

gas flow is sufficiently dissolved by the turbulent flow field so that the ignition of reactive mixtures can occur. The scatter-plots also show that in the mixing layer between the inner recirculation zone and the natural gas flow the thermochemical state is governed by pyrolysis, e.g. the thermal decomposition of methane. In the region of fuel/air mixing and reactions, the thermochemical state including unreacted, partially reacted, and completely reacted mixtures, and a coexistence of fuel and oxygen is frequently observed. From the Raman data it cannot be decided whether the partially reacted mixtures stem from local flame extinction or whether these are mixtures of gases with different states of combustion (e.g. fuel/air/exhaust gas) which have not yet finished reactions. From the general experience with these flames we believe that both effects occur.

Simultaneous Raman and NO-LIF measurements are currently in progress and we hope to present some first results.

- [1] [www.tu-darmstadt.de/fb/mb/ekt/tecflam/](http://www.tu-darmstadt.de/fb/mb/ekt/tecflam/)
- [2] F. Holzäpfel, B. Lenze, W. Leuckel: Twenty-Sixth Symposium on Combustion/The Combustion Institute, p.187 (1996)
- [3] V. Bergmann, W. Meier, D. Wolff, W. Stricker: Appl.Phys. B 66, 489 (1998)

# Large Eddy Simulation of a Turbulent Diffusion Flame Using Flamelet Modeling

A. Kempf, A. Sadiki, J. Janicka, J.-Y. Chen\*

*Fachgebiet Energie- und Kraftwerkstechnik, TU-Darmstadt, Germany*

akempf@gmx.net

\* *UC-Berkeley, CA*

Large Eddy Simulation has a great potential for the simulation of turbulent flames, because fluctuations of velocity and chemical composition are resolved down to filter width. An accurate description of mixing, the driving mechanism of combustion, is therefore possible. This renders LES to be a very convenient tool to predict mixing-dominated combustion systems.

Only some recent publications show results of full 3d LES with varying density, combined with equilibrium chemistry [1] for the simulation of turbulent flames. Although a satisfying overall agreement to experimental results could be achieved, no reasonable information on coexistence, minor species or extinction-related phenomena can be derived. These shortenings can be overcome by switching to flamelet chemistry without introducing too much additional numerical effort. Thus, Flamelet chemistry appears perfectly suited

The aim of the present work is thus to merge a proven 3d LES-code for varying density flows [1] [3] with a Flamelet-Model. This combination promises great benefits since both models are perfectly suited for each other.

In this work, sub-grid fluctuations are modeled according to Smagorinsky. The model constant is determined dynamically by the well known Germano approach [2]. Because of low Mach numbers, the flow is considered incompressible, what greatly reduces numerical cost. The chemical composition of the flow is described by solving the filtered transport equation for the mixture fraction  $f$ . In this equation, the conserved scalar is  $\overline{\rho f}$ , not  $f$ . The splitting of  $\overline{\rho f}$  into mean density  $\bar{\rho}$  and Favre-averaged Mixture Fraction  $\tilde{f}$  is done according to a procedure established by [1].

As test-case, a Nitrogen diluted Hydrogen Jet-Flame defined by M. Tacke [5] was simulated. Figure 1 shows the Hydrogen-Massfraction plotted over Oxygen conditionally averaged. One clearly finds a significant coexistence of both Hydrogen and Oxygen. Flamelet chemistry appears well able to reproduce these experimental data, whereas equilibrium chemistry [6] does strongly deviate. Furthermore, Figure 2 shows the OH concentration plotted over the mixture-

fraction. Further computations are running, their results will be presented in the workshop.

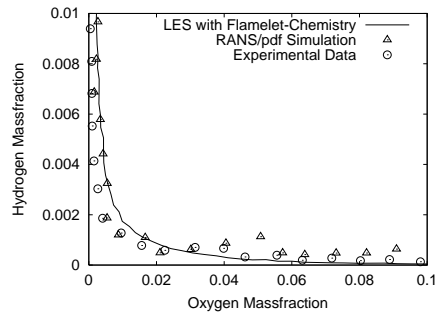


Figure 1

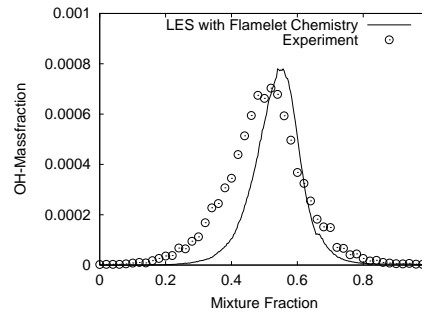


Figure 2

## References

- [1] H. Forkel, J. Janicka, *Large-Eddy Simulation of a turbulent Hydrogen Diffusion Flame*, 1st Symposium on Turbulent Shear Flow Phenomena (1999)
- [2] M. Germano, U. Piomelli, P. Moin and W.H. Cabot, *A dynamic subgrid-scale eddy viscosity model*, Phys. Fluids A, 3, S. 1760/1765 (1991)
- [3] A. Kempf, H. Forkel, J.-Y. Chen, A. Sadiki, J. Janicka, *Large Eddy Simulation of a Counterflow Configuration with and without Combustion*, accepted for Proc. Combust. Inst. 28: (2000)
- [4] J.S. Smagorinsky, *General circulation experiments with the primitive equations, 1. The basic experiment*, Monthly Weather Rev., 91, S. 99-164, (1963)
- [5] M.M. Tacke, S. Linow, S. Geiss, E.P. Hassel, J. Janicka, J.-Y. Chen, *Experimental and Numerical Study of a Highly Diluted Turbulent Diffusion Flame Close to Blowout*, Proc. Combust. Inst. 27: 1139-1148 (1998)
- [6] M.M. Tacke, *Zur Stabilität angehobener turbulenter Diffusionsflammen*, Dissertation, Technische Universität Darmstadt, (1998)

# Large Eddy Simulation of a Non-Reactive Counter Flow Configuration

A. Kempf, H. Forkel, A. Sadiki, J. Janicka, J.Y. Chen\*  
TU-Darmstadt, \* UC Berkeley  
akempf@gmx.net

LES has a great potential for the simulation of turbulent flames, because fluctuations of velocity and chemical composition are resolved down to filter width. An accurate description of mixing, the driving mechanism of combustion in such systems, is therefore possible. The aim of present work is to extend the possibilities of controlling turbulent activity and mixing in counter-flow burners. Such burners are well suited for the calibration and validation of combustion models. Because of their geometry, they allow simulations to be performed in only one dimension of space. This saves much computation time, rendering the simulation of detailed chemistry possible. Here, a three dimensional LES is applied; sub-grid fluctuations are modeled according to Smagorinsky [4]. The model constant is determined dynamically by the well known Germano approach [1]. Chemical processes are presently ignored in this work.

As computational domain, the cylinder between the nozzles is chosen. The grid consists of 65 cells in axial, respective 64 in tangential and 25 in radial direction, corresponding to a resolution of approximately 4 Kolmogorov scales. To incorporate the boundaries, the following conditions are used: An inflow condition (*von Neumann* for pressure, *Dirichlet* for velocities) is applied to both circular faces, describing the opposed jet and the inner part of the coflow. On the cylinder's abutting surface, an outflow condition (*von Neumann* for velocities, *Dirichlet* for pressure) is used.

Because inflow conditions are crucial for any LES, three approaches are examined to describe the turbulent inflow:

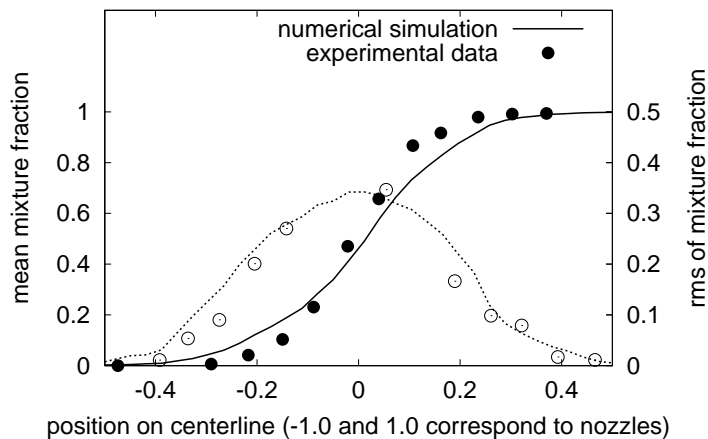
The most simple approach is to just add *random noise* to the mean velocities. A more sophisticated way consists of copying the instantaneous velocity field of a (fully developed turbulent) pipe flow to the inflow plain.

Finally, the flow through the turbulence generators can be simulated as well. This last approach removes the need for any experimental data to describe the boundaries. Fluid properties, geometry and bulk velocity are sufficient for the entire simulation. There is no parameter to be set to describe the turbulence or to adapt a model to this flow-field. This means that the acquired results

depend on the flow code only, not on turbulent boundary conditions or model constants.

From these considerations, it appears that simulating the flow in the perforated plate leads to the best results. Such results are presented in a plot, in which the results of a non-reactive simulation are compared to experimental data measured by K. Sardi [3]. The plot shows the standard deviation of the mixture fraction plotted along the axis of the counterflow. It is centered at the stagnation point; -0.5 representing the left nozzle, +0.5 the right.

The results (not all are shown here) of this study prove that LES is very capable to accurately predict flow and mixing for this configuration. These results are well, especially considering there is no parameter to be set and computation time on a modern workstation is just half a day.



## References

- [1] M. Germano, U. Piomelli, P. Moin und W.H. Cabot, *A dynamic subgrid-scale eddy viscosity model*, Phys. Fluids A, 3 (1991), §. 1760-1765
- [2] R. Hoffman, J.Y. Chen, *Numerical Study of a Turbulent Opposed Jet Flow*, Report, 1998, Technische Universität Darmstadt, University of California, Berkeley
- [3] K. Sardi, A. Taylor, J. Whitelaw, *Conditional scalar dissipation statistics in a turbulent counterflow*, Journal on Fluid Mechanics, 1998, vol. 361, pp. 1-24
- [4] J.S. Smagorinsky, *General circulation experiments with the primitive equations, 1. The basic experiment*, Monthly Weather Rev., 91 (1963), S. 99-164

# Prediction of NO formation in a bluff-body CH<sub>4</sub>/H<sub>2</sub> flame by the conditional moment closure model

Seung Hyun Kim and Kang Y. Huh

Department of Mechanical Engineering, Pohang University of Science and Technology, Korea

e-mail : shkcomb@postech.ac.kr and huh@postech.ac.kr

The first-order conditional moment closure (CMC) model is applied to a CH<sub>4</sub>/H<sub>2</sub> bluff-body flame with emphasis on formation of NO in the recirculation zone. The CMC model has been successfully applied to prediction of NO in turbulent jet diffusion flames [1, 2]. The jet flame calculation was based on a parabolic equation with the shear layer assumption, in which radial dependence of the conditional moments is neglected. However application of such method is questionable for a bluff-body flame due to the recirculating flow field near the nozzle. Recently elliptic CMC equations were solved for a methanol bluff-body flame with comparison against the measurements and results of the SLFM(Steady Laminar Flamelet Model)[3].

In this study the results of elliptic CMC for a CH<sub>4</sub>/H<sub>2</sub> bluff-body flame(HM1) are presented at different spatial locations. The flow and mixing fields are first calculated by the modified k- $\epsilon$ -g model and the conserved scalar approach. The probability density function (pdf) of the mixture fraction is assumed to be a beta function pdf, while the laminar flamelet with a strain rate of  $a = 100/s$  is assumed for the flow field. The reacting scalar fields are subsequently calculated by elliptic CMC under the initially given flow and mixing field. Details on the numerical simulation procedure may be found in [3]. Due to weak spatial dependence of the conditional averages a coarser spatial grid than that of the flow field is employed for the CMC equations. Here we used 70 $\times$ 50 grid points in the axial and radial direction for the flow field whereas 20 $\times$ 10 grid points for the CMC equations. The Miller-Bowman mechanism [4] and 14 step reduced mechanism based on the Miller-Bowman mechanism [5] are implemented for reaction of the given fuels and NO. Radiative heat loss is modeled by the optically thin assumption with the mean absorption coefficient taken from the website of the TNF workshop [6]. The CMC predictions for conditional mean temperature and species mass fractions are radially integrated at each axial location where the experimental data are available and compared with those from the measurements.

Calculation results show good agreement with the measured conditional mean concentrations of the major species, with some discrepancy on the fuel-rich side. The radially integrated conditional averages of temperature and OH, CO and NO mass fractions are shown in Figs. 1 and 2. The predicted conditional mean OH mass fractions are higher than the measurements while those for CO are lower than the measurements in Fig. 1. The discrepancy on the fuel rich side for the major species may be due to the first order closure of the conditional mean reaction rate and/or uncertainties in the chemical reaction mechanism. The reasons for overprediction of OH and underprediction of CO are not clear yet. The conditional mean temperature and NO mass fraction are shown in Fig. 2. Note that the CMC predictions of the conditional mean temperature are in good agreement with the measurements, although with slight underprediction on the fuel rich side. The results with the two different mechanisms, i.e., full Miller-Bowman mechanism and 14-step reduced mechanism, show no distinguishable difference for the conditional mean temperature. However the Miller-Bowman mechanism shows better agreement for the condition mean NO mass fraction in the recirculation zone in Fig. 1. The 14-step reduced mechanism tends to overpredict the conditional mean NO mass fraction on the fuel rich side. The conditional mean NO mass fraction is overpredicted in the neck zone and at further downstream locations. It seems to be due to failure of the k- $\epsilon$ -g model to reproduce intense mixing in the neck zone observed in the experiment.

## References

- [1] Smith, N. S. A., Bilger, R. W. and Chen, J. Y., *Proc. Combust. Inst.* 24:263-269(1992).

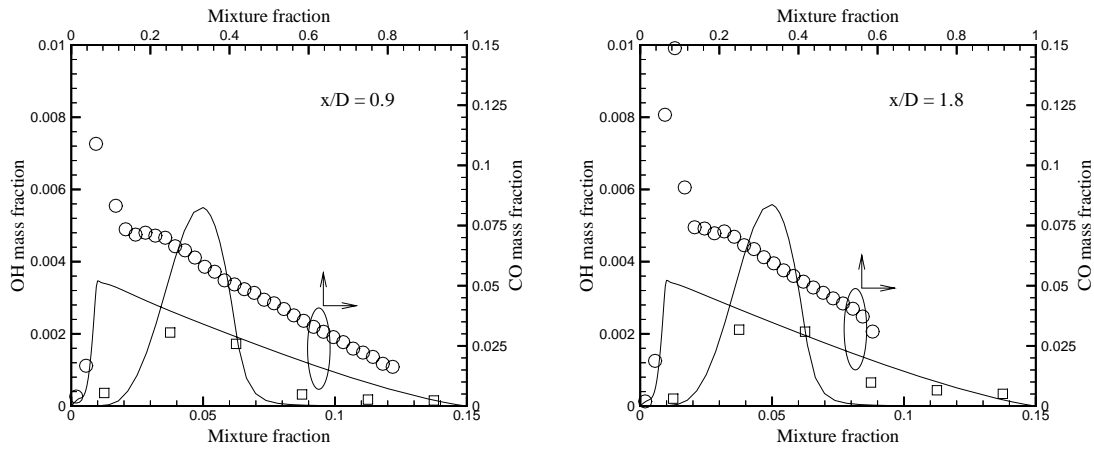


Figure 1: Conditional mean OH and CO mass fractions(symbols : measurements, lines : CMC with Miller-Bowman mechanism)

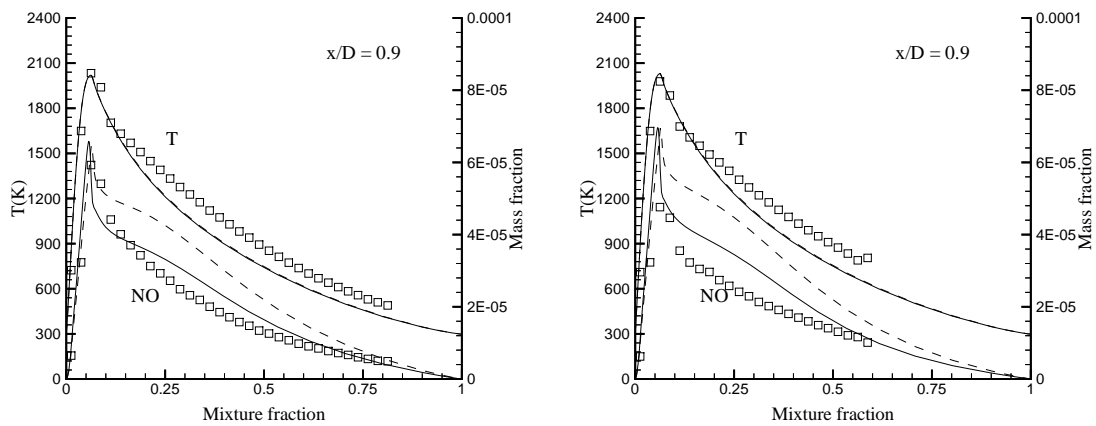


Figure 2: Conditional mean temperature and NO mass fraction(symbols : measurements, solid lines : CMC with Miller-Bowman mechanism, dashed lines : CMC with 14 step reduced mechanism)

- [2] Roomina, M. A. and Bilger, R. W., Conditional Moment Closure(CMC) Predictions of a Turbulent Methane-Air Jet Flame, *Combust. Flame* (in press)
- [3] Kim, S. H., Huh, K. Y. and Liu, T., *Combust. Flame* 120:75-90(2000).
- [4] Miller, J. A. and Bowman, C. T., *Prog. in Energy and Combust. Sci.* 15:287-338(1989).
- [5] Homma, R. and Chen, J. Y., <http://firebrand.me.berkeley.edu/homma/ASPACC99.htm>
- [6] <http://www.ca.sandia.gov/tdf/Workshop.html>

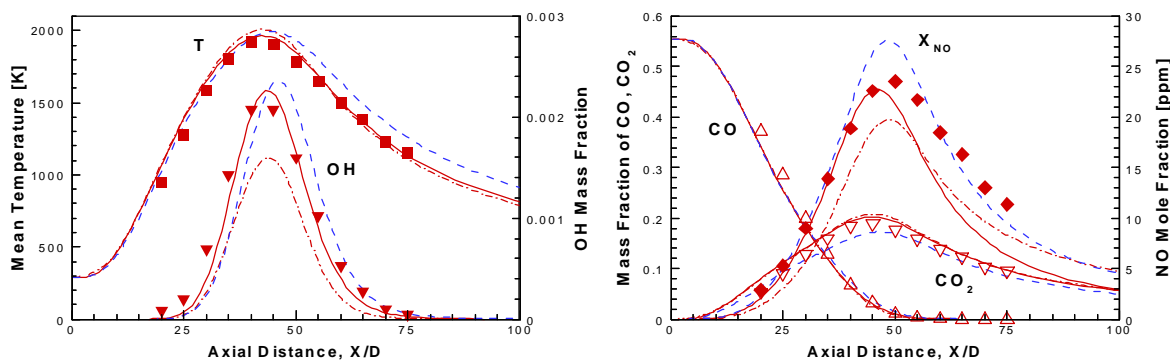
## Effects of Differential Diffusion and Radiation on the NO<sub>x</sub> Formation Characteristics of the Turbulent CO/H<sub>2</sub>/N<sub>2</sub> Jet Flames

Seong-Ku Kim, Sung-Mo Kang and Yong-Mo Kim\*

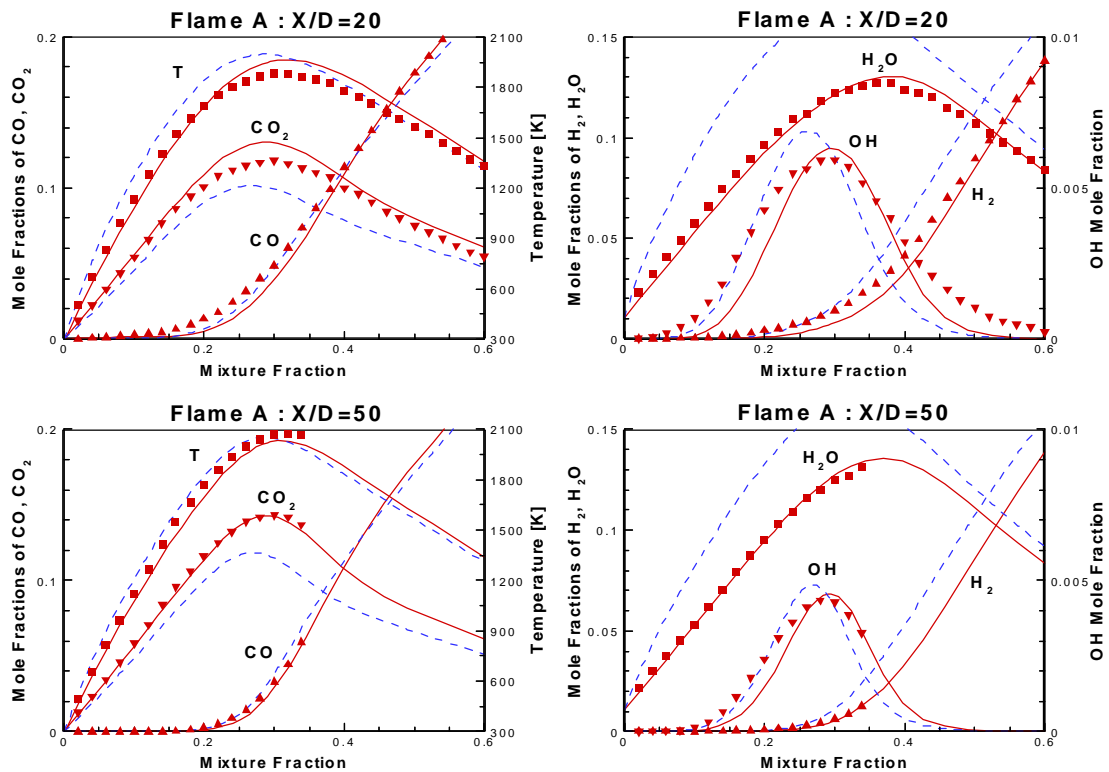
Department of Mechanical Engineering, Hanyang University  
17, Haengdang-Dong, Sungdong-Ku, Seoul 133-791, KOREA

E-mail : [ykim@email.hanyang.ac.kr](mailto:ykim@email.hanyang.ac.kr)

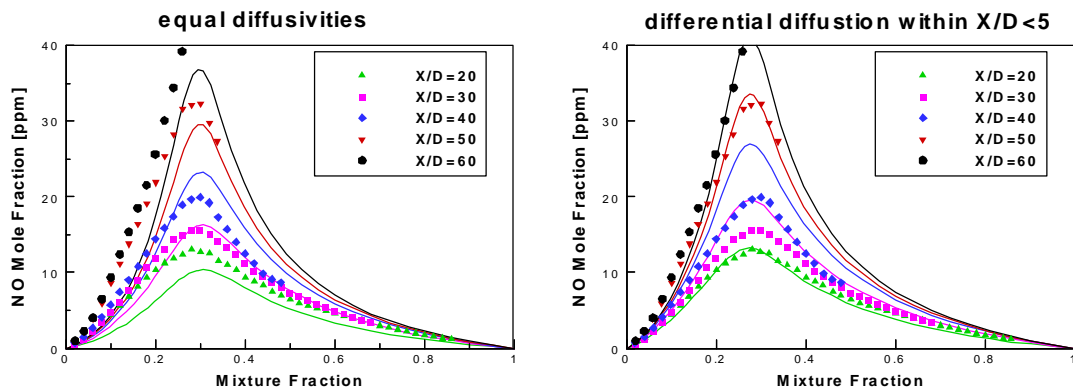
The unsteady flamelet model recently developed by Pitsch [1] has been applied to numerically investigate the detailed flame structure and NO formation process of Sandia/ETH-Zurich CO/H<sub>2</sub>/N<sub>2</sub> jet flames [2]. Main idea of this model is a Lagrangian treatment of local flamelet development, which, therefore, allows slow processes like NO formation and radiation to be incorporated directly into flamelet calculation. In order to minimize numerical diffusion in the physically complex turbulent reacting flows, the present numerical model employs the unstructured grid finite volume method with the adaptive refinement. For assessment of the prediction capability of this approach, numerical results are compared with experimental data and computational results of the steady model with flamelet library, in which NO concentration is inevitably determined by a post-processing step and radiation is taken into account by introducing enthalpy defect concept. The detailed discussions have been made for the crucial issues such as the turbulence-chemistry interaction, differential diffusion and radiative heat loss in the turbulent nonpremixed flames.



**Centerline Profiles in Flame A ; symbol : measured (Favre) ; dashdot : steady model ; solid : unsteady model with equal diffusivities ; dash : unsteady model including differential diffusion within X/D<5**



Steamwise evolution of local flame structure; symbol : measured conditional means; solid : unsteady flamelet with equal diffusivity; dash : unsteady flamelet including differential diffusion within  $X/D < 5$ .



## References

- [1] H. Pitsch, "Unsteady Flamelet Modeling of Differential Diffusion in Turbulent Jet Diffusion Flames," Combust. Flame, accepted, 1999.
- [2] R. S. Barlow, G. J. Fiechtner, C. D. Carter, and J.-Y. Chen, "Experiments on the Scalar Structure of Turbulent  $\text{CO}/\text{H}_2/\text{N}_2$  Jet Flames," Combust. Flame, 120:549-569, 2000.

# Scalar Measurements in Turbulent Swirling Flames

P.A.M. Kalt<sup>1</sup>, R.S.Barlow<sup>2</sup> and A.R. Masri<sup>1</sup>

<sup>1</sup>Department of Mechanical and Mechatronic Engineering, University of Sydney, NSW 2006, Australia

<sup>2</sup>Sandia National Laboratories, Livermore CA 94550, USA

Highly swirling flows form the next level of complexity after piloted and bluff-body stabilized flows, which have been the focus of the last few Workshops. The relevance of swirling flows in practical combustors is obvious, and the challenge here is to develop a laboratory burner that retains the basic physics and chemistry-flow interactions of swirling flames without the added complexity of intricate boundary conditions and other processes such as soot formation and two-phase flows. Such a burner is presented in this poster along with detailed measurements of the temperature and compositions fields in selected swirling flames. It is envisaged that such a burner will form the next model problem for this Workshop Series. A data bank will be made accessible to modelers providing information on the flow, mixing, and composition fields in swirling flames with a range of flow conditions and fuel mixtures.

A schematic of the new swirl burner used in this study is shown in Figure 1. It has a 50mm diameter bluff-body ( $D_B = 50\text{mm}$ ) with a 3.6mm central fuel jet. Surrounding the bluff-body is a 60mm diameter annulus for the primary swirling air stream. Swirl is introduced into the primary air stream by three tangential inlets, each 7mm in diameter, which are positioned 300mm upstream of the burner exit plane and inclined  $15^\circ$  upward to the horizontal plane. The swirl number may be easily varied by changing the relative flowrates of tangential and axial air in the primary stream. The burner assembly is situated in a wind tunnel providing a coflowing secondary air stream of 20 m/s with a free stream turbulence level of around 2%. The wind tunnel has an exit cross section of  $300 \times 300\text{mm}$ . Three fuels have been investigated: pure  $\text{CH}_4$ ,  $\text{CH}_4/\text{air}=1/2$  (by vol.) and  $\text{CH}_4/\text{H}_2=1/1$  (by vol.). Results for two flames of  $\text{CH}_4/\text{air}$  are presented in this abstract.

There are at least three parameters which control the stability characteristics and the physical properties of the flame. The bulk fuel jet velocity,  $\langle U_j \rangle$ , and the bulk axial and tangential velocities in the primary air stream,  $\langle U_s \rangle$ , and  $\langle W_s \rangle$ , respectively. The coflow velocity in the secondary air stream,  $\langle U_e \rangle$ , will also influence the flame but this is kept constant here at 20m/s. The stability characteristics of the flames have been studied and a number of flames covering a range of swirl numbers have been selected for further measurements.

Temperature and compositions measurements are performed at Sandia's CRF Turbulent Diffusion Flame Facility. The joint Rayleigh-Raman technique is used to obtain single-point measurements of temperature and the mass fractions of all stable species, and the LIF technique is used to measure CO, NO and OH.

Figure 2 shows scatter plots of temperature and mass fractions of  $\text{CH}_4$ , CO and NO measured at  $x=50\text{mm}$  in flames of  $\text{CH}_4/\text{air}$ . Data are presented for flames SMA2 (left column) and SMA3 (right column) with bulk fuel jet velocities of 65m/s and 130m/s, respectively. At 50mm downstream, the radial profiles pass through the necking region of both flames. Both flames have a geometric swirl number of 1.2 ( $\langle U_s \rangle = 16.6\text{m/s}$ ,  $\langle W_s \rangle = 20.2\text{m/s}$ ) and the flame blows off at a jet velocity of about 200m/s.

Temperature scatter plots show low temperature measurements occurring across the range of mixture fraction space and indicate the occurrence of local extinction. Local extinction occurs more frequently as fuel jet velocity increases. Additionally, higher  $\text{CH}_4$  concentrations across the whole mixture fraction space and increased scatter in CO and NO mass fractions in flame SMA3 compared to flame SMA2 are observed. Both indicate a higher mass fraction of unburnt hydrocarbons due to local extinction and a more intense mixing process.

Clearly, under conditions of high swirl the flame/turbulence interactions become significant. Detailed measurement of temperature and species in a variety of swirling flames are necessary for the testing and further development of combustion models. Data for other swirling flame conditions are to be presented in the accompanying poster.

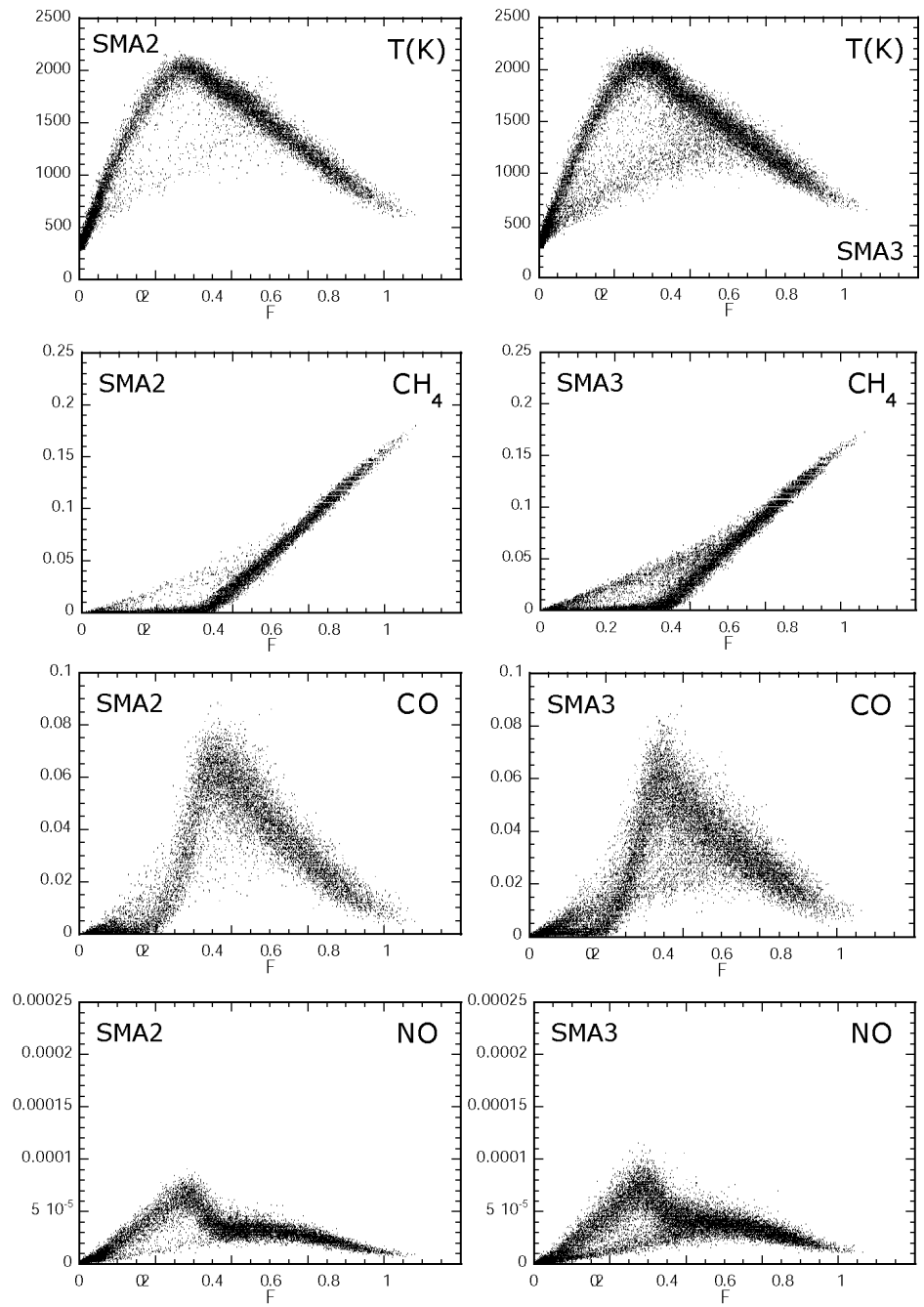
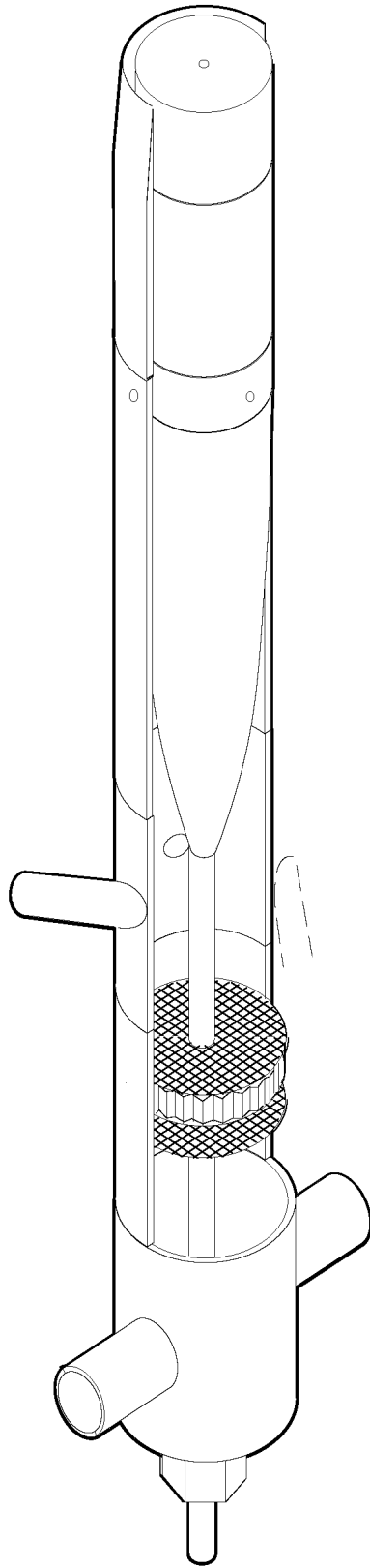


Fig. 2 Scatter plots of Temperature and  $\text{CH}_4$ , CO, and NO mass fractions at 50 mm above the burner exit for flames SMA2 (left column) and SMA3 (right column)

Fig. 1 Cut-away swirl burner schematic

## Flamelet modeling for 3-D simulation of high-temperature gas-fired furnaces

Denis Krasinsky, Theo H. van der Meer<sup>1</sup>, Dirk Roekaerts, Baifang Zuo<sup>2</sup>

Thermal and Fluids Sciences, Delft University of Technology,  
P.O. Box 5046, 2600 GA Delft, The Netherlands  
e-mail: dkr@ws.tn.tudelft.nl

In combustion systems where nonequilibrium effects are important, the assumption of local chemical equilibrium can lead to unrealistic results. From applied point of view, this assumption might be particularly inappropriate when the formation level of pollutant species, such as NO<sub>x</sub>, should be predicted with better accuracy. Flamelet models have been proposed as a general approach to include detailed nonequilibrium flame chemistry [1]. In this poster we elaborate the model further to make it more applicable in modeling of high-temperature gas-fired furnaces.

Because in high-temperature furnaces the corresponding Damköhler numbers are high, the assumption of the flamelet regime of combustion appears to be valid. Still till now, the "common" applications of flamelet modelling were mostly the turbulent reacting shear flows, free jet or confined jet flows, etc. For these types of flows, the scalar dissipation rate  $\chi_{st}$  is used as the only parameter characterizing each flamelet. However, 3-D furnace aerodynamics is always influenced by the flow recirculation, therefore the effect of additional mixing, or "dilution", of the fuel and air streams with backward streams coming from the post-flame zone becomes essential. With this, it should be noted that in 3-D field the local value of mixture fraction alone cannot adequately "distinguish" the presence of this dilution because the products from recirculating stream are already mixed (i.e., are at the (near) stoichiometric value of mixture fraction).

Therefore, to employ the flamelet approach in high-temperature furnaces modeling, an additional parameter of the flue gas dilution  $\alpha$ , characterizing flamelets at "diluted" or "non-diluted" conditions, has been suggested by B. Zuo [2]. The variation of this parameter, which can take values in the range between 0 and 1, is made in the flamelet library calculations through the variation of the composition of incoming streams by adding a volume percent of flue gases (products of stoichiometric combustion) to the basic fuel stream and air stream. It is assumed that  $\alpha=0$  for the pure air (fuel) stream, i.e. without dilution; while  $\alpha=1$  means that only product species are present in the flow, i.e. no reactants. The structure of each flamelet, as usual, is found from the numerical solution of the 1-D opposed-jet diffusion flame problem e.g by the OPPDIF program [3].

To account for the influence of radiative heat loss in high-temperature furnace on results of flamelet modelling, the parameter of inlet air (preheat) temperature  $T_{air}$  of the laminar flamelet has been proposed [2]. By varying  $T_{air}$  as parameter in OPPDIF calculations, it is possible to resemble the effect of non-adiabaticity on the maximal flame temperature.

The new features of the proposed flamelet model lie in its ability to consider the influences of the inlet temperature and dilution with flue gases, on the combustion process and pollutants formation. For simplicity, the assumption of constant strain rate is used, thus allowing to reduce the

---

<sup>1</sup> Present address: Mechanical Engineering, University Twente, The Netherlands

<sup>2</sup> Present address: Engine Research Center, University of Wisconsin - Madison, USA

dimensions of the library tabulation problem to three dimensions. Also the new model uses the chemical models for the prompt and thermal NO formation processes for which the appropriate mechanisms have been originally incorporated by B. Zuo into a general detailed chemical mechanism [4].

To incorporate this flamelet model into 3-D code FURNACE, which has been developed for the numerical simulation of gas-fired furnaces in the Section of Thermal and Fluids Sciences TU Delft, the transport equations for mass fractions of the "fuel" species  $Y_{\text{Fuel}}$  and the "product" species  $Y_{\text{Prod}}$  have been added to the set of solved equations. From these local values, the corresponding flamelet parameters  $\alpha$  and  $T_{\text{air}}$  can be estimated by a special procedure when identifying the relevant flamelet from the library during the FURNACE iterations.

Thus, the flamelet approach, as an improvement for modeling the non-equilibrium chemistry effects in turbulent flames including NO<sub>x</sub> formation processes, has been complemented by introducing the flue gas dilution and air inlet temperature as two new parameters to account for the dilution by product species and also for heat loss, which allows its application into 3-D numerical simulations of a gas-fired furnace.

The corresponding flamelet library has been constructed from a series of the opposed-jet diffusion flame calculations. The analysis of its data shows that, in particular, the dilution by flue gases significantly reduces the formation of both thermal and prompt NO.

In further work, results on the IFRF furnace simulations will be obtained through implementation of the proposed flamelet model into the FURNACE code. From there the validity of new model will be estimated.

## Acknowledgements

The financial support of this work by the European Commission is gratefully acknowledged (EURONITE project "New Industrial Furnaces of Higher Thermal Efficiency through Intensification of Heat Transfer from Flames" – contract No. JOE3-CT97-0083).

## References

1. N. Peters (1984). Laminar diffusion flamelet models in non-premixed turbulent combustion. *Progr. Energy Combust. Sci.*, vol.10, pp.319-339.
2. Th. H. van der Meer, B. Zuo. Flamelet Modeling of Turbulent Diffusion Flames. Abstracts of Symposiumdag "Verbrandingsonderzoek van Industrieel Belang", p.28. Arnhem, the Netherlands, 1999.
3. A.E. Lutz, R.J. Kee, J.F. Grcar, and F.M. Rupley. OPPDIF: A FORTRAN Program for Computing Opposed-Flow Diffusion Flames. Sandia National Laboratories Report SAND96-8243, 1997.
4. B. Zuo. Modeling of Pre-Vaporized Premixed Fuel-Oil Burner Combustion. PhD. Thesis, Katholieke Universiteit Leuven, Leuven, Belgium, 1997.

# TECFLAM swirl flame: Comparison of different turbulence and chemistry models

Oliver Kunz, Peter Gerlinger, Berthold Noll, Manfred Aigner

German Aerospace Center DLR, Institute of Combustion Technology,  
Pfaffenwaldring 38-40, 70569 Stuttgart, Germany  
oliver.kunz@dlr.de

Within the national German TECFLAM cooperation [1] numerical simulations of an experimentally investigated swirl burner are performed at the Institute of Combustion Technology, German Aerospace Center DLR, Stuttgart, Germany. Several combinations of turbulence and chemistry models are employed and compared. Additionally potential hardware influences of the TECFLAM setup on the flame are evaluated. The simulations are carried out with a DLR developed code (TRUST) and a commercially available code (FLUENT).

## Experimental Setup

The TECFLAM swirl burner consists of two concentric nozzles with inner diameters of 20 and 30 mm and annulus widths of 3 and 15 mm, respectively. The fuel stream in the inner annulus consists of natural gas with a typical composition of 98% methane, 0.8% higher alkanes, 0.2% carbon dioxide, and 1% nitrogen. The airflow in the outer annulus passes a movable block swirl generator which results in an effective swirl number of  $S = 0.9$ . The combustion chamber has an inner diameter of 500 mm and a variable length from 1200 to 1693 mm. The wall temperature is kept constant at about 70°C by water cooling. The combustion chamber exhaust consists of a partially blocked annulus with an inner diameter of 460 mm and a width of 20 mm.

The burner's thermal load is 150 KW at an air-to-fuel ratio of 1.2. Reynolds numbers based on exit bulk velocities are  $Re = 8000$  and  $Re = 42900$  for fuel and air stream, respectively.

The confined swirl flame thus represents a setup which is close to practical combustion devices. Especially the complex flow field links this laboratory burner with industrial applications. To demonstrate this crucial point the calculated local flame conditions of this burner are included into a Borghi-diagram [2] shown in Figure 1.

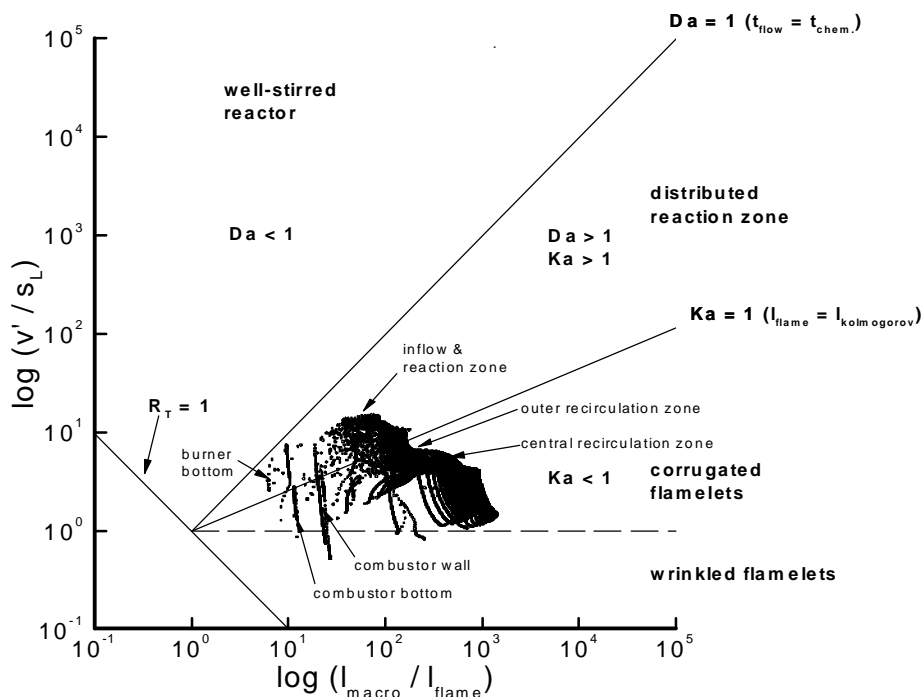


Figure 1: Borghi-diagram with calculated TECFLAM swirl burner conditions

### **Grid and computational domain**

Several 2D-axisymmetric unstructured grids are used for burner simulations. Grid sizes range from 14000 to 52000 hexahedron cells. At the inflow the grid is locally refined on a velocity gradient basis. The computational domain ranges from the bottom of the combustion chamber to the annular outflow. The calculation starts at the burner mouth thus the flow through the swirl generator is not modeled. Grid independence is guaranteed by several test calculations using refined grids.

### **Modeling Boundary Conditions and Numerical Scheme**

The cold flow is calculated using a standard k- $\epsilon$  model, two modified k- $\epsilon$  models (RNG and realizable) and a Reynolds stress model (RSM). For the reacting case a standard k- $\epsilon$  model or a RSM are employed. At the confining walls standard wall functions are used to approximate the boundary layer. Chemical reactions are taken into account by different combustion models (eddy break-up, Arrhenius finite rate, 5 species pdf and ILDM model).

Experimental results of LDA velocity measurements directly above the burner mouth are used as inflow boundary conditions for the stationary simulations. Incoming fuel is considered to be pure methane and the inflow water content of the air is neglected.

All convective terms are discretized by a second order upwind scheme while central discretization is used for the diffusive fluxes. Pressure-velocity coupling is performed using the SIMPLEC algorithm.

FLUENT calculations are carried out on an IBM RS6000, TRUST calculations on a DEC-Alpha. The corresponding CPU times range from a few hours (cold flow, small grid) to several days (reacting flow, large grid, ILDM). To obtain a converged solution the following strategy is applied: Cold flow and simple turbulence models are used to get a primary solution. Based on these results, more complex turbulence and reaction models are subsequently added.

### **Results and Discussion**

Comparisons between experimental data [3] and simulations show significant discrepancies both in velocity field structure and in species concentrations. Whereas the numerical calculation gives an open swirl flow core the measurements reveal a more closed form with a small but strong recirculation region. As a consequence the reaction zone obtained by simulation is not located on the axis as indicated by measurements.

As the length of the TECFLAM combustion chamber is variable, three different geometries are used within the calculations (1200 mm, 1350 mm and 1693 mm). Furthermore the influence of the partly blocked outflow is taken into account by size variations of the exhaust annulus. It is found that chamber length has no significant influence on the flow field near the nozzle. Concerning the variation of the outflow geometry it is found, that a wider annulus has a positive effect on convergence but leaves the burner flow field unaffected.

As to overcome the described flow field discrepancies an attempt is made to introduce features in the simulation that may have eventually influenced the experiment. Due to the variable geometry of the burner one could assume a slight inflow at the bottom corner of the chamber caused by insufficient sealing. Such a flow could have an effect on the outer recirculation zone and thus on the flame shape. However, it is found, that even a relatively strong axial inflow at the burner bottom edge has no significant influence on the overall flow field.

Thermal radiation is included by a discrete transfer radiation model (DTRM), without having any remarkable influence on the flow in the combustion region.

The influence of velocity inflow conditions is taken into account by using different experimental profiles stemming from experimental data 1 mm and 5 mm above the inflow. Numerical calculation shows that velocity profiles at these distances do not differ significantly from that at the burner mouth.

This statement should not be confused with the fact that the shape of the inlet profile has a great influence on both convergence rate and the flow field in the combustion region.

### **Conclusion/Outlook**

In this investigation several turbulence and chemistry models are used to simulate the confined TECFLAM swirl flame. Characteristics of sub models are demonstrated. Numerical results are compared to measurements. Several possible setup influences are considered and included in the simulation. It can be concluded that the numerical simulation employed is not yet able to predict the complex interaction between turbulence and chemistry sufficiently. Simulation results are depicted in a Borghi-diagram demonstrating the practical relevance of the TECFLAM swirl flame. Further improvements concerning turbulence and physico-chemical models are required.

### **References:**

- [1] <http://www.th-darmstadt.de/fb/mb/ekt/flamebase.html>
- [2] Borghi R., Progress in Energy and Combustion Science 14:245-292 (1988)
- [3] <http://www.dlr.de/VT>

# Joint Scalar PDF Monte Carlo Simulations of Methanol Turbulent Jet Diffusion Flames with Comprehensive Chemistry

R. P. Lindstedt, S. A. Louloudi and E. M. Vaos

e-mail:p.lindstedt@ic.ac.uk

Imperial College of Science, Technology and Medicine  
Mechanical Engineering Department  
London SW7 2BX, U.K.

Piloted methanol turbulent diffusion flames investigated experimentally by Masri and co-workers [1,2] have been modelled using a transported Probability Density Function (PDF) approach closed at the joint scalar level. The flames discussed here have Reynolds numbers of  $\sim 53500$  (Flame M2) and  $\sim 69600$  (Flame M4) respectively. The burner geometry features axisymmetric fuel jets with mean velocities of 90.3 and 117.4 m/s and an ambient air-coflow of 15.0 m/s. Both flames are stabilised by a premixed pilot flame with a velocity of 21.0 m/s.

In the present study the velocity field is modelled using the SSG (Speziale, Sarkar and Gatski [3]) second moment closure. The  $C_{\epsilon 2}$  constant in the dissipation rate equation is adjusted from 1.92 to 1.8 in order to improve the predicted spreading rate. Scalar mixing is modelled using the modified Curl's model of Janicka and Kollmann [4]. The equations are solved using a Monte Carlo approach featuring moving particles in a Lagrangian frame (eg. Hůlek & Lindstedt [5]). The flames are assumed adiabatic and computed using an implicit parabolic formulation with 100 cross stream cells with each containing on average 100 particles. About 1100 axial steps are used to cover 40 jet diameters. The approximate CPU time is 1 day on a Compaq XP1000. The chemistry [6] is based on the work of Lindstedt and co-workers [7] and the systematically reduced form used in the present work features 32 species of which 16 are treated as independent scalars.

The agreement with experimental data is mostly excellent. Conditional averages of experimental and computational (40 bins) temperature and mass fractions for  $CO$ ,  $OH$ ,  $CH_3OH$ ,  $CO_2$  and  $O_2$  are presented in Figure 1 for Flame M2. However, it may be noted that, consistent with CMC closure computations of Flames M1/M2 [8], the predicted  $CO$  and  $OH$  peaks are approximately 35% below the corresponding measured values.

The computed scatter plots of temperature,  $CO$ ,  $CH_3OH$  and  $OH$  at  $x/D=10$  for Flame M4 are compared with the measured profiles in Figure 2. Inspection reveals that the implemented modelling approach clearly predicts high levels of flame local extinction.

## References

- [1] Masri, A.R., Dibble, R.W. and Barlow, R.S., *Comb. Flame*, 89:167-185 (1992).
- [2] www.mech.eng.usyd.edu.au
- [3] Speziale, C.G., Sarkar, S. and Gatski, *JFM* 227:245-272 (1991).
- [4] Janicka, J. and Kollmann, W., *J. Non-equilib. Thermodyn.* 4-47 (1978).
- [5] Hůlek, T. and Lindstedt, R.P., *Combust. Sci. Tech.* 136:303-331 (1998).
- [6] Leung, K.M. and Lindstedt, R.P., *Brite Euram Contract 95-0056, Final Report*, April 1999.
- [7] Lindstedt, R.P. and Meyer, M., *in preparation*.
- [8] Roomina, M.R., *PhD thesis*, The University of Sydney (1998).

FLAME M2:  $x/D=20$

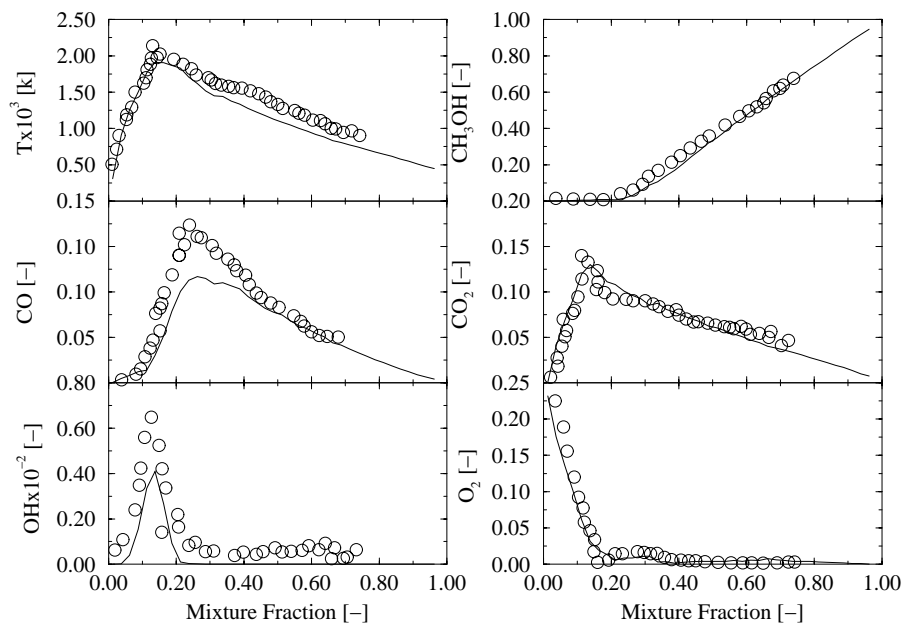


Figure 1: *Radial profiles of temperature and species in mixture fraction space at  $x/D=20$  for methanol flame M2. The circles and lines are conditional averages of experimental [2] and computed data.*

FLAME M4:  $x/D=10$

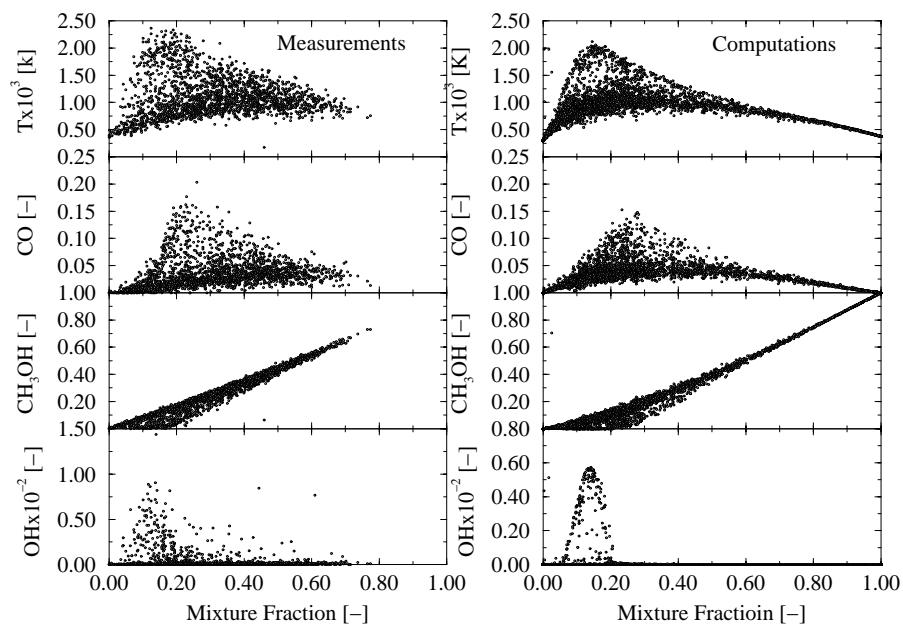


Figure 2: *Scatter plots of temperature and species profiles in mixture fraction space at  $x/D=10$  for methanol flame M4.*

## **JPDF Calculations of Bluff-Body Stabilized Flames**

K. Liu<sup>1</sup>, P. Jenny<sup>2</sup>, M. Muradoglu<sup>1</sup>, S. B. Pope<sup>1</sup> and D. A. Caughey<sup>1</sup>

1) Sibley School of Mechanical and Aerospace Engineering  
Cornell University, Ithaca, NY 14853, USA

Email: [kliu@mae.cornell.edu](mailto:kliu@mae.cornell.edu), [metinm@mae.cornell.edu](mailto:metinm@mae.cornell.edu),  
[pope@mae.cornell.edu](mailto:pope@mae.cornell.edu), [caughey@mae.cornell.edu](mailto:caughey@mae.cornell.edu).

2) Chevron Petroleum Technology Company

6001 Bollinger Canyon Rd., Bldg. D

San Ramon, CA 94583-0719

Email: [pjnn@chevron.com](mailto:pjnn@chevron.com)

### **ABSTRACT**

A joint velocity-composition-turbulence frequency PDF (JPDF) model is applied to calculate nonpremixed bluff-body flames, and also the corresponding non-reactive, cold flows. The present work concentrates on the numerical accuracy, sensitivity to inlet boundary conditions, and optimization of model constants. From the available experimental data, a test case is selected (namely BBHM1) in which there is little local extinction, so that a simple flamelet model can be used. This work is intended to establish a numerically accurate and well characterized set of calculations to form the basis for future investigations using detailed chemistry.

Bluff-body stabilized flames have simple and well-defined boundary conditions while they provide a complex turbulent field within the recirculation zone next to the bluff body. So they are well suited to investigate the interaction between turbulence and chemical reactions.

The calculations are made using a stand-alone particle method which solves the joint velocity-frequency-composition PDF (JPDF) transport equation. This method has been implemented in the code PDF2DV, which is discussed in detail by Xu and Pope[1] and has been successfully applied for various reacting and non-reacting flows including another target flow, the piloted jet flame.

In order to obtain numerically accurate results, based on the error analysis by Xu and Pope[1], the method of Deterministic Error Reduction with Richardson Extrapolation (DERRE) has been developed. In this method, three or more runs are performed with different grid sizes and numbers of particles per cell, and then an extended form of Richardson extrapolation is used to eliminate the leading-order numerical errors.

It is found that the calculation results are sensitive to the specified inlet boundary condition on mean turbulence frequency,  $\langle \omega \rangle$ , and also to the model constant  $C_{\omega 1}$  in the turbulence frequency model. An optimization method is applied to obtain the optimal inlet level of  $\langle \omega \rangle$  and value of the constant  $C_{\omega 1}$  so that the calculations are in the closest possible agreement to the experimental data. With these optimal specifications of the inlet boundary condition on  $\langle \omega \rangle$  and of  $C_{\omega 1}$ , the calculations are generally in good agreement with the experimental data[2].

The comparison with experimental data (Figure 1) shows that the radial profiles of the mean velocity, and of velocity variances and covariance are in very good agreement with the experimental data. For the reactive case the radial profiles of mean velocity, and of velocity variances and covariance are in good agreement. The profiles of the mixture fraction and its variance are well predicted within the recirculation zone while the agreement deteriorates further downstream.

### Reference

1. Xu, J. and Pope, S. B. "Assessment of Numerical Accuracy of PDF/Monte Carlo Methods for Turbulent Reactive Flows; *J. of Comp. Phys.* **152**, 192:230(1999).
2. Masri, A. S. <http://www.mesh.eng.usdy.edu.au/research/energy/#data>.

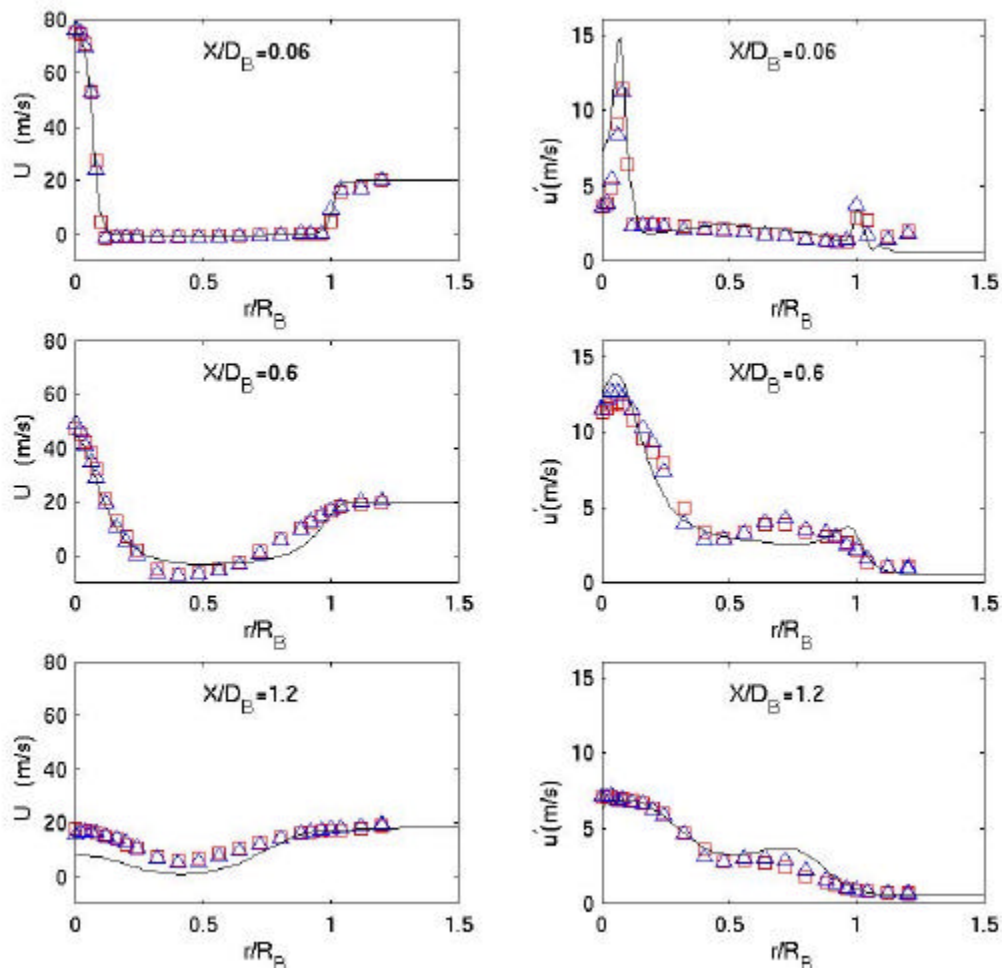


Figure 1. Cold-flow mean velocity  $\langle U \rangle$  and RMS  $u'$  profiles at three axial location.  $D_B$  is the diameter of Bluff-body,  $R_B$  is the radius of bluff-body. Symbols stand for experimental data of two nominally identical experiments. The lines represent the result of the JPDF simulation.

# Calculations of Turbulent Non-Premixed Jet Flames Using a Laminar Flamelet Model with Radiative Heat Transfer

C. Y. Ma, T. Mahmud\*, M. Fairweather, P. H. Gaskell and E. Hampartsoumian  
The University of Leeds, Leeds LS2 9JT, UK

\*Corresponding author, Email: [T.Mahmud@leeds.ac.uk](mailto:T.Mahmud@leeds.ac.uk)

## Abstract

It is well known that thermal radiation plays an important role in flames greater than certain lengths. In most applications of flamelet models, however, radiation has not been accounted for (see review in Ref. [1]) as the assumption of adiabatic combustion is generally invoked. This has led to a significant overprediction of temperatures. In the present study, the mixedness-reactedness flamelet (MRF) model of Bradley *et al.* [2] based on the assumption of adiabatic combustion has been extended to introduce the effect of radiative heat transfer using the concept of *enthalpy defect* [3]. The performance of the methodology is tested by computing well defined laboratory-scale flames, in which radiative heat transfer to the surroundings is significant. The flames considered are lifted, free, turbulent non-premixed natural gas flames, studied experimentally by Lockwood and Moneib [4]. Predictions obtained with and without radiative heat transfer are compared with the measured mean gas temperatures and flame lift-off heights.

An existing computer code [2,5] for the calculation of velocity, temperature and species concentration fields, based on the solution of the Favre-averaged conservation equations for mass, momentum, thermal-energy and chemical species using the MRF model, was adapted in this study. Turbulence is handled by the  $k-\epsilon$  model with standard values of the model constants. In the context of the MRF modelling approach [2], the volumetric heat release rate ( $q_v$ ) in a laminar flame can be expressed as a function of mixedness ( $c$ ) and reactedness ( $\theta$ ). The enthalpy defect is defined as the difference between the actual enthalpy and the adiabatic enthalpy of a flame, which is caused by the radiative heat loss ( $q_r$ ). This is then imposed on the flamelets as an additional parameter. The turbulent mean value of  $q_v$  under non-adiabatic conditions can be obtained using the joint PDF of  $c$ ,  $\theta$  and  $q_r$ . By assuming statistical independence between  $c$ ,  $\theta$  and  $q_r$ , and neglecting the effect of  $q_r$  fluctuation [3], the joint PDF can be decomposed into a product of individual PDFs. The radiative heat transfer is modelled by assuming free, jet flames to be optically thin. The absorption coefficients of the radiating species were obtained from data reported by Tien [6] based on the wide-band model. The laminar heat release data were generated from calculations of one-dimensional premixed methane-air flames with the GRI reaction mechanism, involving 49 species and 279 reaction steps, using the modified CHEMKIN code.

In the experiments [4], natural gas (93.63% by vol. methane) was injected through a burner of 7.74 mm inside diameter ( $D$ ) into the stagnant environment at velocities of 40, 53 and 80 m/s with corresponding  $Re = 15000, 20000$  and  $30000$ , respectively. The flames were lifted with visible lengths of 1.6, 1.73 and 1.88 m. Calculations were performed using the original adiabatic MRF model [2] and the non-adiabatic model accounting for the radiative heat loss as described above. Fig. 1 shows comparisons between the predicted radial distributions of mean temperature for both adiabatic and non-adiabatic flamelet models, along with measurements for the flame at  $Re = 15000$ . In the non-reacting lift-off region ( $x/D = 15.5$ ), the predicted temperature distributions obtained from both the models are in reasonable agreement with the experimental data, and are qualitatively correct in predicting the influence of the onset of combustion. Within the combustive zone of the jet, the adiabatic model significantly overpredicts the measured levels of temperature, particularly at  $x/D \geq 75.0$ . In contrast, the predictions of the present radiation adjusted model are, in general, in good agreement with measurements over the length of the flame. These findings are in line with previous predictions [1] of corresponding attached flames of Lockwood and Moneib [4], in which a diffusion flamelet model coupled with the optically thin gas radiation assumption was found to produce better agreement with the experimental data compared to an adiabatic model. Fig. 2 shows contours of turbulent mean heat release rate predicted using the adiabatic and radiation adjusted flamelets. The inclusion of radiative heat loss is seen to have a significant effect on flame structure predictions. Predicted lift-off heights for all three flames are compared against experimentally observed values [4] and those obtained from a correlation [7] in Fig. 3. Overall, reasonable agreement is obtained. In the present calculations, the lift-off heights were little affected by the inclusion of radiative heat loss.

### Acknowledgments

The authors are indebted to the *Engineering and Physical Sciences Research Council* of UK for their financial support, and to Professor D. Bradley of University of Leeds for providing the original combustion code.

### References

1. Marracino, B. and Lentini, D., *Combust. Sci. and Tech.* 128:23-48 (1997).
2. Bradley, D., Gaskell, P. H. and Lau, A. K. C., *Twenty-Third Symposium (International) on Combustion*, The Combustion Institute, Pittsburgh, PA, 1990, pp. 685-692.
3. Bray, K. N. C. and Peters, N., In *Turbulent Reacting Flows* (Libby, P. A. and Williams, F. A., Eds.), Academic Press, London, 1994, p. 78.
4. Lockwood, F. C. and Moneib, H. A., *Combust. Flame* 47:291-314 (1982).
5. Ma, C. Y., Mahmud, T., Gaskell, P. H. and Hampartsoumian, E., *Journal of Mech. Engng. Sci., Proc. Inst. Mech. Engrs., Part C*, 213:697-705 (1999).
6. Tien, C. L., *Adv. Heat Transfer*, 5:253-324 (1968).
7. Bradley, D., Gaskell, P. H., and Gu, X. J., *Twenty-Seventh Symposium (International) on Combustion*, The Combustion Institute, Pittsburgh, PA, 1998, pp. 1199-1206.

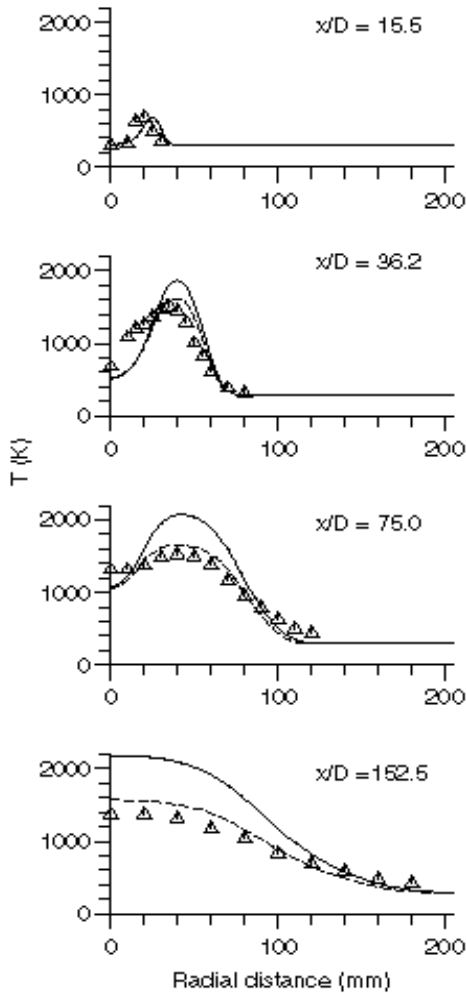


Fig. 1 Predicted and measured mean temperature distributions (— adiabatic flamelet model; - - - non-adiabatic flamelet model;  $\Delta$  measurements).

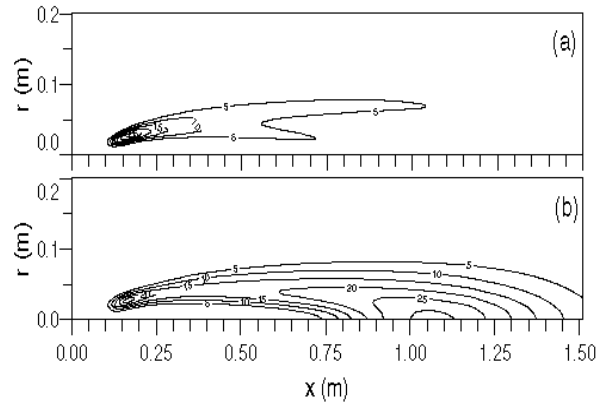


Fig.2 Predicted turbulent mean heat release patterns (a) without and (b) with radiative heat loss.

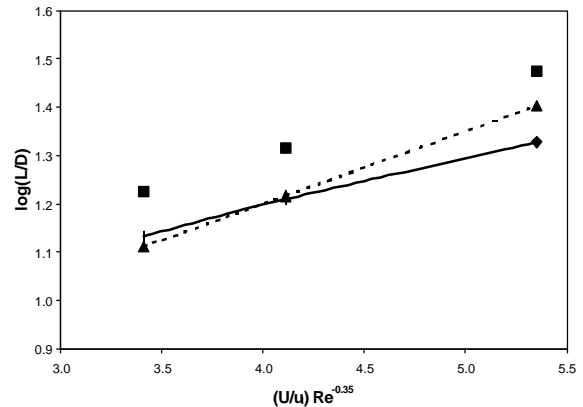


Fig. 3 Calculated and experimentally observed flame lift-off heights ( $\blacklozenge$  non-adiabatic flamelet model;  $\dots\blacktriangle\dots$  correlation;  $\blacksquare$  experiment; where  $L$  is the flame lift-off height,  $U$  the initial fuel jet velocity,  $u_l$  the laminar burning velocity of stoichiometric mixture).

## NUMERICAL AND EXPERIMENTAL INVESTIGATION OF TURBULENT NON-PREMIXED FLAMES OF INDUSTRIAL INTEREST

- P.Martinelli - M.Nutini -

- Pirelli Cavi e Sistemi S.p.A. -  
Viale Sarca 222 . 20126 Milano - Italy

e.mail: paolo.martinelli@pirelli.com  
massimo.nutini@pirelli.com

This work has been focused on the numerical simulation of turbulent, diffusive flames utilizing well-known turbulence and combustion models in round-robin comparison.

The numerical approach is also to be followed by an experimental study on the same flames utilizing laser diagnostics techniques for Species, Temperature and Velocity measurements.

In the context of our aims, preference has been given to the investigation on those models which are typically available to the industry and also applicable to the solution of complex industrial problems. Accordingly, the presented results have been all obtained utilizing the commercial code FLUENT 5.3 unstructured.

EKT flames have been chosen, since the availability of a vast class of experimental data [1] and the similarity to industrial burners configuration render them interesting as useful benchmarks.

Some experimental configurations have been selected. In detail, two situations have been considered. The first, labeled V1, is related to a CH<sub>4</sub>-H<sub>2</sub>- N<sub>2</sub> flame; the second, referred to as H5, is a H<sub>2</sub> - N<sub>2</sub> flame.

The numerical investigation involved simulations employing the standard k-epsilon, the RNG k-epsilon and the Reynolds Stress Model (RSM) for turbulence closure. The used constants of k-epsilon model are the standard ones [2] with the exception of  $C_{\mu}$  set to 0.06 [3]. Corrections to the constants  $C_{\epsilon 1}$  and  $C_{\epsilon 2}$ , respectively set to 1.60 [4] and to 1.83 [5] have also been considered, in order to better predict spreading rate and centerline decay.

Different combustion chemistry models have been used: among them; the equilibrium chemistry PDF model and an eddy dissipation model. The applied equilibrium chemistry model solves a transport equation for the mixture fraction  $\xi$  and its variance, 5 species (O<sub>2</sub>, H<sub>2</sub>, H<sub>2</sub>O, OH, N<sub>2</sub>) have been considered for H5 flame, while 8 species have been considered for V1 flame (O<sub>2</sub>, H<sub>2</sub>, H<sub>2</sub>O, OH, CH<sub>4</sub>, CO<sub>2</sub>, CO, N<sub>2</sub>) . The Eddy Dissipation Model used in the finite rate calculation couples a mixing- and an Arrhenius- rate term; a 1-step reaction scheme has been employed for H<sub>2</sub>, a 2-step reaction scheme for CH<sub>4</sub> combustion [6].

Consistent boundary conditions, fluid properties and discretization scheme were used for all cases to isolate the effect of closure models.

The experimental measurements are performed by laser diagnostics [7]. The system is based on a double Nd:YAG pulsed source of which, depending on the different techniques, the second (532nm) or fourth (266nm) harmonics is used. The laser radiation polarization can be rotated by means of ad-hoc motorized optics. An intensified, programmable-exposure camera is the detector and for the Raman technique a 300mm spectrometer is interposed between the flame and the detector. The whole measurement instrumentation is computer-controlled and synchronized.

2-D temperature fields are obtained by means of 90° Rayleigh scattering imaging of the UV laser sheet and by applying the ideal gas law.

1-D species concentrations along the focussed UV beam are measured by 90° Raman scattering. The principal species (i.e. mole fractions typically above 0.5% ) measured are O<sub>2</sub>, H<sub>2</sub>, H<sub>2</sub>O, CH<sub>4</sub>, CO<sub>2</sub>, CO, N<sub>2</sub>. The quantitative results are obtained by comparison to calibration flows/flames. In order to get rid of the interfering fluorescence from OH or O<sub>2</sub>, a crossed polarizations subtraction is applied. The Raman technique provides contemporary 1-D temperature measurement.

The 2-D measurement of the velocity field is performed by PIV. This technique requires the seeding of the gases with properly chosen solid particles, the illumination in sequence with two laser sheets (green radiation) and the imaging of the Mie-scattered light.

## Results

As an example, some results from simulation of flame H5 are shown in fig. 1, where they are plotted together with experimental values available in literature [1] represented by black circles. Temperature radial profiles at  $x/D = 10, 20, 40$  and  $80$  are reported. The general agreement of simulation results obtained with pdf-equilibrium chemistry model coupled with  $C_{\mu}=0.06$  k-epsilon (blue line) or RSM (red line) is visible. A result with RSM coupled with Eddy Dissipation is also shown (black line). At  $x/D = 10$  the equilibrium hypothesis does not provide a satisfactory solution. On the contrary in this region peak temperature is better predicted using an Eddy Dissipation Model. Moreover, results with RNG k-epsilon model (not shown) have been generally less accurate.

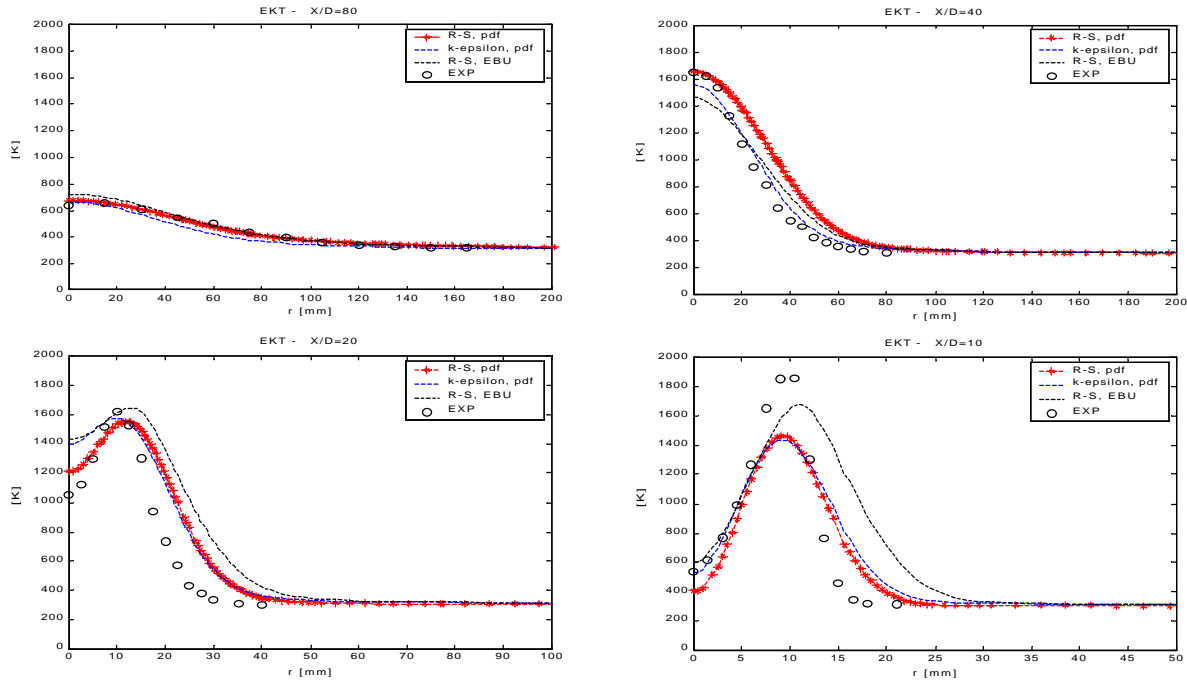


Fig. 1: H5 Flame. Temperature radial profiles at  $x/D=80, x/D=40, x/D=20$  and  $x/D=10$ .

Some further activity related to the introduction of other combustion models also applied to V1 flame is in progress. The main activity related to the application of laser diagnostics techniques is in progress as well.

## Bibliography

- [1] <http://www.dlr.de/VT/Datenarchiv/JetFlame.html>
- [2] B.E. Launder, D.B. Spalding, "The numerical computation of turbulent flows", *Comput. Methods Appl. Mech. Engrg.*, vol. 3., pp. 269-289, 1974
- [3] D.Garretton, G.Mariotti, *Proceedings of 2nd A.S.C.F. Workshop*, Pisa 1996, 1997
- [4] <http://www.ca.sandia.gov/tdf/Workshop/Submodels.html>
- [5] <http://www.tu-darmstadt.de/fb/mb/ekt/flamebase/ETHZuerich/>
- [6] Fluent 5 User Guide, 1988
- [7] E.Hassel, S.Linow, "Laser Diagnostics for Studies of Turbulent Combustion", *Meas. Sci. Technol.* 11, 2000

## Application of BEM and Analysis of the Role of Radiation Effects in Labscale Turbulent Diffusion Flames

Aristide Mbiock, Joan Teerling, and Dirk Roekaerts

Delft University of Technology,  
P.O. Box 5046, 2600 GA Delft, The Netherlands  
Phone +31-15-2781448, Fax +31-15-2781204  
E-mail: aristide@ws.tn.tudelft.nl

Turbulent diffusion flames are often studied in laboratory scales in relation with turbulence-chemistry interaction models. At temperatures of interest these flames emit heat by radiation, which in turn affect the flame temperature through the energy conservation equation. To obtain accurate predictions of the flame temperature, and other temperature related quantities; it is necessary to take account of the radiation effects in the analysis. This problem has been examined in previous TNF workshops [1] and it has been recommended that an "optically thin limit" approach, considering only emission, could be used. This conclusion is being challenged [2] and the object of this contribution is to explore the issue theoretically by using the boundary element method - BEM - for radiative heat transfer.

The Boundary Element Method approach provides a way to handle as exact as possible, and within adequate time constraints the radiative heat exchanges between the reacting flow and the combustion chamber boundaries [3]. The fundamental idea of the BEM, which is based on the energy balance relations, is the partition only of the boundary of the domain in which the problem is posed into a set of sub-domains. A suitable space of functions defined at the combustion chamber boundary is then approximated using basis functions, defined on each sub-domain with suitable matching conditions at interfaces. The method is general, and it has been shown that regardless of medium conditions, the radiative heat flux exists. A numerical solution method has been formulated that converges unconditionally to the exact answer. In examples, the accuracy and correctness of the algorithm was demonstrated (transparent medium, isothermal gray medium, non-isothermal gray medium, non gray medium). Subsequently the model was applied (disregarding turbulence-chemistry interaction effects) to semi-industrial scale gas and oil fired furnaces (M2-trials conducted at the International Flame Research Foundation in IJmuiden).

For the laboratory scale flame, an open-air flame - Flame D, which is subjected to analysis in this study, a specific application of the technique is utilised. The flame is placed within an ideal cavity of unit wall emissivity. Therefore, the intensity of incident radiation at any point  $p$  in the interior of the cavity, which originate from a point  $r$ , is written as:

$$I^i(r, p) = \frac{1}{\pi} (e_b(r)\tau(r, p) + L(r, p)), \quad L(r, p) = \int_{(r,p)} a(u)e_b(u)\tau(u, p)dL(u) \quad (1)$$

with  $a(u)$  being the coefficient of absorption at the point  $u \ni (r, p)$ , and  $\tau(u, p)$  being the transmissivity defined as:

$$\tau(r, p) = \exp\left(- \int_{(r,p)} a(u)dL(u)\right) \dots\dots\dots(2)$$

(Explicit wavelength dependence of all quantities can be included and in practice its treatment requires the use of band models). The radiative heat balance equation on a unit surface at a point  $p$  of the surface  $S$  shows that:

$$q(p) = e_b(p) - \int_S (e_b(r)\tau(r, p) + L(r, p)) \frac{\cos(\theta(r, p))\cos(\theta(p, r))}{\pi \|r - p\|_{R^3}^2} dS(r) \quad (3)$$

and on a control volume at a point  $p$  in the cavity interior  $V$ :

$$q_V(p) = a(p) \left( 4a(p)e_b(p) - \int_S (e_b(r)\tau(r, p) + L(r, p)) \frac{\cos(\theta(r, p))}{\|r - p\|_{R^3}^2} dS(r) \right). \quad (4)$$

In the present study, the net radiative heat source  $q_V$  is included in the overall energy balance equation through the enthalpy source term. A parametric study varying the coefficient of absorption and turbulence-chemistry interaction models is made. In particular the same constrained equilibrium chemistry model and the same presumed PDF approach is used as in Ref. [4], which also addresses Flame D.

#### **Acknowledgement:**

The work of the first author is sponsored by the Foundation for Fundamental Research on Matter (FOM), the Netherlands

#### **References**

1. Links to proceedings of previous workshops can be found at the TNF workshop web site: [www.ca.sandia.gov/tdf/Workshop.html](http://www.ca.sandia.gov/tdf/Workshop.html)
2. J. Frank et al., Proceedings of the Combustion Institute, Volume 28, 2000 (to be published)
3. Aristide Mbiok and Roman Weber, "Radiation in Enclosures - Elliptic Boundary Value Problem", Series in Scientific Computations, Springer-Verlag Berlin, ISSN 1434-8322; ISBN 3-540-66095-X; February 2000
4. B. Merci et al., The impact of the turbulence model and inlet boundary conditions on calculation results for reacting flows, Poster, Fifth International Workshop on Measurements and Computations of Turbulent Non-Premixed Flames, Delft, July 26-28, 2000

## Measurements and Simulations of the Turbulent DLR CH<sub>4</sub>/H<sub>2</sub>/N<sub>2</sub> Jet Diffusion Flame

Wolfgang Meier\*, Robert S. Barlow\*\*, Jyh-Yuan Chen\*\*\*

\* DLR-Institut für Verbrennungstechnik, Stuttgart, Germany

\*\* Sandia National Laboratories, Livermore, California, USA

\*\*\* UC Berkeley, Mechanical Engineering Department, Berkeley, California, USA

The DLR jet flame (fuel composition: 33.2% H<sub>2</sub>, 22.1% CH<sub>4</sub>, 44.7% N<sub>2</sub>, 8 mm nozzle diameter, Re=15200 and 22800) has been investigated in great detail in different laboratories (DLR Stuttgart, TU Darmstadt, Sandia National Laboratories, and Purdue University). An important feature of the flame is the combination of a simple flow field (without pilot or bluff body) with the possibility to study the methane chemistry in a turbulent flame (without partial premixing with air). The experimental data sets comprise measurements of velocity, temperature, mixture fraction, concentrations of all major species as well as OH and NO, and (qualitative) 2D images of OH, CH, NO and temperature.

In the poster, a brief summary of the experimental results will be given. A main part of the presentation concerns the comparison of measured and calculated results. In order to assess the influence of flame stretch and effects of Lewis number and finite-rate chemistry, the scatterplots are compared with results from steady, strained, laminar flame calculations. There is some influence of differential diffusion near the nozzle ( $x/D=5$ ) but the  $Le=1$  assumption is reasonable further downstream. Local flame extinction and finite-rate chemistry effects are clearly seen, especially for NO and OH, and are more pronounced for the flame with Re=22800 which is close to lift-off and extinction.

Calculations with different simulation codes are currently performed and results will be presented and discussed on the poster.

### References

[www.ca.sandia.gov/tdf/Workshop](http://www.ca.sandia.gov/tdf/Workshop)

V. Bergmann, W. Meier, D. Wolff, W. Stricker: Appl.Phys. B 66, 489 (1998)

W. Meier, R.S. Barlow, Y.-L. Chen, J.-Y. Chen: Combust. Flame, submitted

# The impact of the turbulence model and inlet boundary conditions on calculation results for reacting flows

B. Merci, D. Roekaerts\*, T.W.J. Peeters\*\* and E. Dick

Ghent University - Dept. of Flow, Heat and Combustion Mechs.  
 Sint Pietersnieuwstraat 41, B-9000 Gent, Belgium  
 Tel.: +/32/9/264.33.14, Fax: +/32/9/264.35.86, E-mail: Bart.Merci@rug.ac.be

\* Delft University of Technology, The Netherlands  
 \*\* Corus Group, The Netherlands

## Turbulence model

In turbulent reacting flow calculations, most effort usually goes to the chemistry model. The turbulence model, necessary to predict the flow field, is often a standard two-equation model with adjustment of model constants to match the results better with experimental data. Whereas, in principle, one cannot expect that any two-equation turbulence model can predict all possible turbulent flows, it makes sense to bring more physics into the model. In this work, this has been done in two ways. First, the classical, linear Boussinesq hypothesis has been replaced by a non-linear relation between the Reynolds stresses and the local mean velocity field (mean rate of strain and mean absolute rotation). Secondly, the transport equation for the dissipation rate has been altered. This way, 'constants' become quantities which automatically obtain a more appropriate value at different locations in the flow field. Low-Reynolds (LR) versions of the turbulence model have been used, thus avoiding the need for wall functions.

The turbulence model, at some points still under construction, is as follows:

$$\frac{\widetilde{v''_i v''_j}}{\widetilde{k}} - \frac{2}{3}\delta_{ij} = -2c_\mu S'_{ij} + q_1(S'_{ik}S'_{kj} - \frac{1}{3}\delta_{ij}S'_{lm}S'_{ml}) + q_2(\Omega'_{ik}S'_{kj} - S'_{ik}\Omega'_{kj}) \\ + c_1(S'_{mn}S'_{nm} + \Omega'_{mn}\Omega'_{nm})S'_{ij} + c_2(\Omega'_{ik}S'_{kl}S'_{lj} - S'_{ik}S'_{kl}\Omega'_{lj})$$

with  $S'_{ij} = \tau_t \left[ \frac{1}{2} \left( \frac{\partial v_i}{\partial x_j} + \frac{\partial v_j}{\partial x_i} \right) - \frac{1}{3} \delta_{ij} \frac{\partial v_k}{\partial x_k} \right]$  the nondimensional mean rate of strain and  $\Omega'_{ij} = \tau_t \left[ \frac{1}{2} \left( \frac{\partial v_i}{\partial x_j} - \frac{\partial v_j}{\partial x_i} \right) - \varepsilon_{ijk} \Omega_k \right]$  the nondimensional absolute rotation tensor. The turbulence time scale  $\tau_t = \sqrt{\frac{\mu}{\rho\varepsilon} + \frac{k}{\varepsilon}}$  (LR version).  $q_i$  and  $c_i$  are polynomial functions of  $S' = (2S'_{ij}S'_{ij})^{1/2}$  and  $\Omega' = (2\Omega'_{ij}\Omega'_{ij})^{1/2}$ .  $c_\mu$  is also a function of these quantities (instead of a constant such as 0.09), making the turbulence model realizable.

The dissipation rate transport equation is the standard one, except that a LR term has been added and the 'constant'  $c_{\varepsilon 2}$  (standard value 1.92) has been replaced by  $c_{\varepsilon 2} = f_2(1.83 + 0.075\Omega'/(1 + S'^2))$ .  $f_2$  is a damping function. As chemistry model, a simplified version of the constrained equilibrium model as in[1] has been used, within the framework of the conserved scalar approach with a pre-assumed  $\beta$ -pdf. Results are compared with different turbulence models (LR versions): the standard  $k - \varepsilon$ [2] model, the  $k - \omega$  based SST model[3] and the described non-linear  $k - \varepsilon$  model. Some results for flame D, with inlet boundary conditions as described on the web[4], are shown in fig. 1. The left picture is the mean mixture fraction along the symmetry axis, the right picture is its radial profile at  $x/D = 45$ .

## Inlet boundary conditions

Calculation results for turbulent flows can be sensitive to the inlet boundary values, particularly with respect to the dissipation rate, which cannot be directly measured. For calculations, the  $\varepsilon$  inlet profile can be determined from the given mean velocity and  $k$  profile, with an assumption of zero axial derivatives.

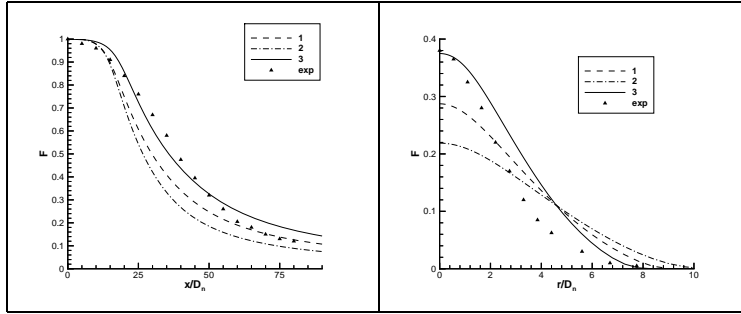


Figure 1: Results with different turbulence models. (1: linear  $k - \varepsilon$ ; 2: linear SST; 3: new cubic model)

Alternatively,  $\varepsilon$  can be estimated from  $\varepsilon = k^{3/2} c_\mu^{3/4} / l_m$ , with  $l_m$  the Prandtl mixing length.  $l_m$  is related to the radius  $R$  of the central jet as  $l_m = R/C$ ,  $C$  to be determined[5].  $C = 1$  seems a logical first guess, but  $C = 15$  gives much better results, as illustrated in fig. 2. Since the results are sensitive to the value of  $C$ .  $C$  is likely to differ from case to case, and moreover it is not clear what should be done for the annulus ( $R$  has been defined as half the hydraulic diameter there). Therefore, the more rigorous method firstly described seems the better one. The method is also applicable for  $k - \omega$  based models. Using a fixed method to obtain  $\varepsilon$ , we found that differences between the inlet profiles on the web[4] and the ones recently measured in Darmstadt[6], do not have a large effect (results not shown).

In the poster, results will be shown for the bluff-body geometry[7], too.

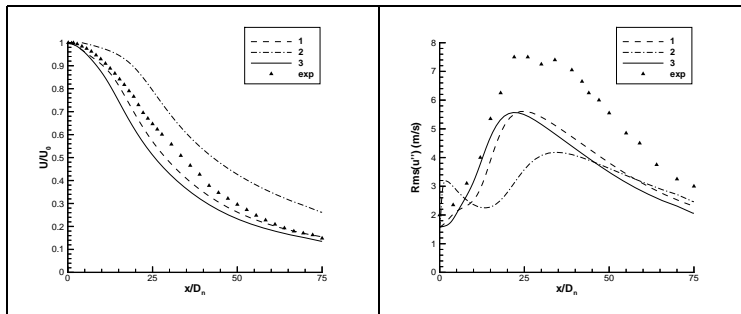


Figure 2: Influence of inlet boundary conditions. (1: inlet  $\varepsilon$  from  $U$  and  $k$ ; 2:  $\varepsilon = C k^{3/2} c_\mu^{3/4} / R$ ,  $C = 1$ ; 3: idem as 2, with  $C = 15$ )

## Acknowledgments

The first author works as Research Assistant of the Fund for Scientific Research - Flanders (Belgium) (FWO).

## References

- [1] Nooren P.A., Wouters H.A., Peeters T.W.J., Roekaerts D., Maas U. and Schmidt D. , ‘Monte Carlo PDF Modelling of a turbulent natural-gas diffusion flame’. *Comb. Theory and Modelling*, 1:79–96, 1997.
- [2] Yang Z.Y. and Shih T.H. , ‘New Time Scale Based  $k - \varepsilon$  Model for Near-Wall Turbulence’. *AIAA J.*, 31(7):1191–1198, 1993.
- [3] Menter F.R. , ‘Two-Equation Eddy-Viscosity Turbulence Models for Engineering Applications’. *AIAA J.*, 32(8):1598–1605, 1994.
- [4] Barlow R.S. and Frank J.H. ([www.ca.sandia.gov/tdf/Workshop.html](http://www.ca.sandia.gov/tdf/Workshop.html))
- [5] Jones W.P., Libby P.A. and Williams F.A. , ‘*Turbulent reacting flows*’, p. 353,354. Acad. Press, 1994.
- [6] Schneider C. *Private Communication*. 1999.
- [7] Masri A.R. Combustion data base, The University of Sydney and The Combustion Research Facility, Sandia National Laboratories. (<http://www.mech.eng.usyd.edu.au/research/energy/resources.html>)

## Time-Series Measurements of Scalars in H<sub>2</sub>/CH<sub>4</sub>/N<sub>2</sub> Jet Flames

Michael W. Renfro\*, Galen B. King, and Normand M. Laurendeau  
School of Mechanical Engineering  
Purdue University  
West Lafayette, Indiana 47907-1288 USA

\* Corresponding author: renfro@ecn.purdue.edu

Measurements of quantitative OH and CH concentrations and of the total number density have been separately obtained in a series of turbulent nonpremixed jet flames. The sampling rate for the measurements was sufficient to recover time series detailing the turbulence-induced fluctuations of the scalars. The fuel jet consisted of 33.2% hydrogen, 22.1 % methane, and 44.7% nitrogen. Seven jets were probed with Reynolds numbers from 2800 to 15,200 and burner diameters of 3.4 mm and 7.8 mm. One of these flames is nearly identical to a workshop target flame for which single-shot Raman and Rayleigh data are available [1,2]. The time-series data are used to compute power spectral densities (PSDs), probability density functions (PDFs), autocorrelation functions, and integral time scales. Except for the PDF, these statistics are not recovered by most existing diagnostics, yet some implicit assumptions regarding fluctuation rates are imbedded in many turbulent combustion models.

In the case of OH measurements, the signal-to-noise ratio is sufficient to visually resolve the scalar fluctuations in the time series. Hydroxyl time series are shown in Figure 1 for three Reynolds numbers and two burner diameters. Each time series is 20 ms of data at a single point in the flow ( $x/D=20$ , radial location of peak [OH]). The data were chosen randomly and are typical of the OH measurements at other points in the flow. A range of OH fluctuation rates is present at each point and these fluctuations are noticeably faster for higher Reynolds number or smaller burner diameter. This is also clear from the autocorrelation functions computed from these time series, shown in Figure 2a for several locations in each flame. Each autocorrelation function decays with a near exponential shape and can be characterized by its integral time scale. These time scales are observed to nearly collapse the data to a single "universal" OH autocorrelation function in Figure 2b. The implication of this result is that the entire range of fluctuation rates present at each point in Figure 1 is self similar from one point to the next and the integral time scale can be used to fully describe the observed variations in the time series. Similar results are observed for both CH and number density in the time-scale statistics; however, the poorer signal-to-noise ratios in both cases make the time series themselves somewhat noisy.

The variations of the OH, CH, and number density time scales have been compared to scaling for nonreacting jets and significant differences are observed. In nonreacting jets, mixture fraction fluctuation rates scale as [3,4],

$$\mathbf{t}_{i,z} = \frac{C}{\text{Re}} \int_{x/D}^2 \frac{U_{CL}(x/D)}{U(r/x)}$$

where  $\mathbf{t}_{i,z}$  is the mixture fraction integral time scale,  $U$  is the mean axial velocity,  $U_{CL}$  is the velocity on the centerline, and  $C$  is a constant which depends on the fuel density and viscosity.

From single-shot PLIF images of OH in these flames, the OH layer is often very narrow so that the presence of OH serves as a qualitative marker of the flame front. The OH-fluctuation statistics can then be interpreted as flame-sheet fluctuation statistics, which would depend

primarily on mixture fraction fluctuations. However, the OH time scales are observed to follow a relationship closer to

$$t_i \propto \text{Re}^{-1.4} (x/D)^{0.5} \frac{U_{CL}(x/D)}{U(r/x)}$$

The steeper dependence on Re may be an artifact of the dependence of the virtual origin on Re, and this is presently being investigated. The dependence on  $x/D$  is much less than for mixture fraction in a nonreacting jet. Each of the scalar measurements (OH, CH, and number density) separately confirm this departure from nonreacting jet scaling.

### References

1. Bergmann, V., Meier, W., Wolff, D., and Stricker, W. (1998). *Appl. Phys. B* **66**, 489-502.
2. Meier, W. (1999). <http://www.st.dlr.de/EN-CV/flamedat/intro.htm>
3. Becker, H. A., Hottel, H. C., and Williams, G. C. (1967). *J. Fluid Mech.* **30**, 285-303.
4. Birch, A. D., Brown, D. R., Dodson, M. G., and Thomas, J. R. (1978). *J. Fluid Mech.* **88**, 431-449.

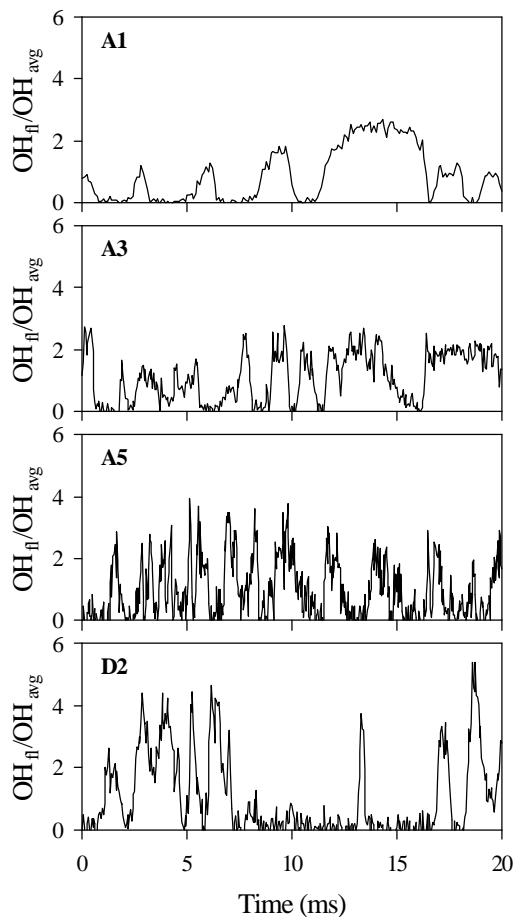


Figure 1. OH time series in flames A1 (Re=2800), A3 (Re=9000), and A5 (Re=15,200), each from a 3.4-mm jet, and flame D2 (Re=15,200) from a 7.8-mm jet.

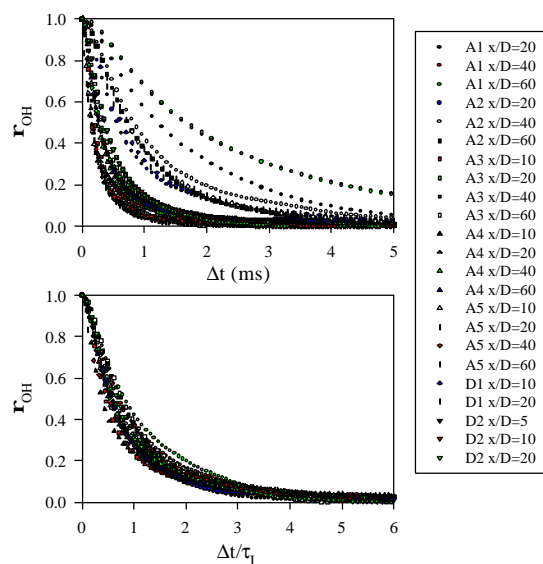


Figure 2. OH autocorrelation functions for various locations in the seven jet flames. The bottom plot has been normalized by the integral time scale for each curve.

# Experimental investigation of a confined swirling natural gas flame (TECFLAM)

Christoph Schneider, Andreas Dreizler, Johannes Janicka

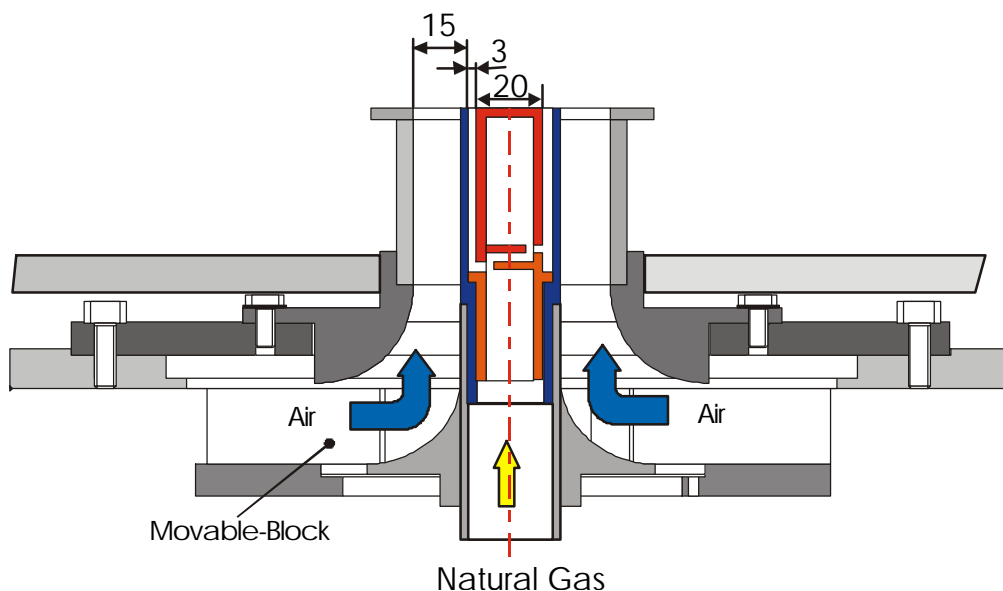
FG Energie- u. Kraftwerkstechnik, Technische Universität Darmstadt  
Petersenstr. 30, 64287 Darmstadt, Germany  
phone: +49-6151/16-2157, fax: +49-6151/16-6555, e-mail: ekt@hrzpub.tu-darmstadt.de

Egon Hassel  
Lehrstuhl für Technische Thermodynamik, Universität Rostock  
Albert-Einstein-Strasse 2, 18059 Rostock, Germany  
phone: +49-381/498-3227, fax: +49-381/498-3228, e-mail: egon.hassel@mbst.uni-rostock.de

Excessive LDV measurements of the velocity field of the TECFLAM swirl burner are performed. Data contain mean axial, radial and circumferential velocity components and the respective turbulence quantities for two swirl numbers  $S=0.9$  and  $S=1.4$ . For each case a fuel to air ratio of 1.2 was employed.

## Swirl burner

The swirl burner consists of a central bluff body, surrounded by one annulus of 3 mm width for the fuel (natural gas) and a second annulus for the combustion air. The air flow is swirled by a moveable block with a variable intensity between  $S=0\dots 2.0$  in terms of a theoretical swirl number. The thermal load amounts 150 kW. The chamber walls are water-cooled with 50% of the thermal power transferred. Geometry of the chamber is as follows: Height  $H_c=1200$  mm, Diameter,  $D_c=500$ mm.



Sketch of the burner

## Measurement technique

A two-component fiberoptic Laser-Doppler-Anemometer (Dantec) was used to determine the velocity characteristics of the flow field. A 4 W argon-ion laser served as light source. The laser beam was submitted to a transmitter box. A Bragg cell divided the incoming beam into different colours. Two beam pairs of the wavelengths  $\lambda_g = 514.5$  nm (green) and  $\lambda_b = 488$  nm (blue) were selected to survey the axial and the radial/circumferential velocity component, depending on the traversing direction. The first order beam of each colour was frequency shifted at 40 MHz. The laser beams (diameter of 2.2 mm) were then coupled into a fiber optic probe and collimated in the measurement volume with a front lens of  $f_l = 600$  mm focal length. A beam expander ( $m = 1.9$ ) was applied to reduce the size of the measurement volume to allow to analyse regions of high velocity gradients of the flow. The distance between the beam pairs was  $D_s = 72$  mm. With these values, the size of the probe volume could be calculated to a length of  $l_m = 0.780$  mm and to a diameter of  $d_m = 0.094$  mm. Photomultipliers observed the measurement volume through interference filters in backward scatter mode. The signal was electronically down mixed depending on the measured Doppler frequency. A digital auto-correlator evaluated the Doppler signals. Statistical averaging was transit time weighted to minimize velocity bias. An estimate of the statistical error concerning mean velocity was 5%, whereas fluctuations were accurate within 6%. Data obtained from the shear zone were even more accurate.

## Measurement positions

At the burner outlet 1 mm above the gas exit, a complete set of profiles of first and second order moments of velocity has been measured. Further down stream axial, radial as well as circumferential velocity components and the respective fluctuations were measured for a large variety of axial and radial positions.

The data are presented and discussed in the context of PDF calculations.

## Results

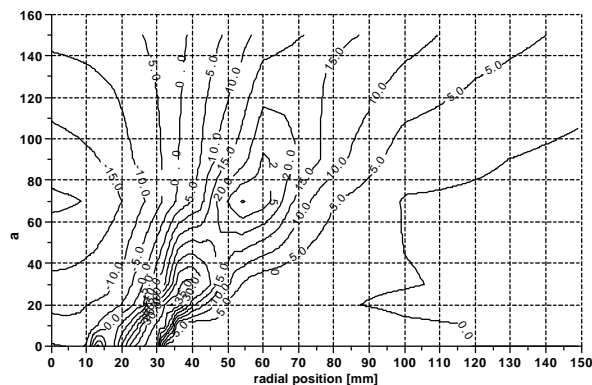


fig. 1: mean axial velocity distribution for  $S=0.9$

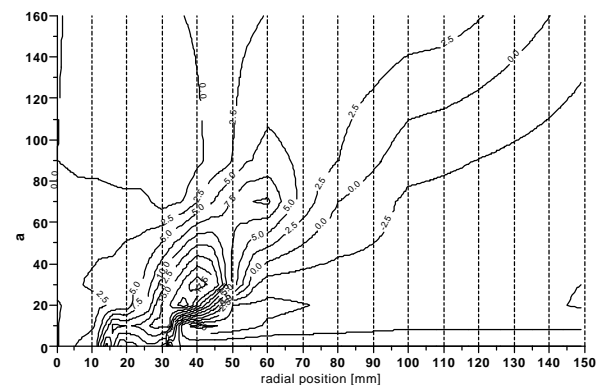


fig. 2: mean radial velocity distribution for  $S=0.9$

# Numerical Simulation of the Piloted Flame Type D

*Szasz Robert, Laszlo Fuchs*

*Lund Institute of Technology, Dept. of Heat and Power Engineering*

*Ole Römersväg 1, 22100, Lund, Sweden*

*szrobi@mail.vok.lth.se*

In our poster numerical simulations of the piloted methane-air flame type D are presented. The numerical results are compared to the experimental results of Barlow et al. [1].

Since the base models do not reproduce very well the experimental results, we carried out a series of studies to identify the effects of different sub-models. We compare the effects of

- i). turbulence model, ( $k$ - $\epsilon$ , realizable  $k$ - $\epsilon$  of Shih et al. [2] and a Reynolds Stress Model (RSM). LES have been started but no reliable results are available as yet.
- ii). Single-step vs two-step chemistry,
- iii). Modified combustion model by which one "freezes" the reactions once the methane concentration reaches the flammability limit of the rich flame [3].
- iv). Effects of differential diffusion
- v). Grid resolution

The simulations are made in two steps: first we run the calculations for the cold flow and after that we turned on the chemistry models. The reaction rates are evaluated both by Arrhenius-type equations and using the Eddy Dissipation Concept model of Magnussen and Hjertager [4], the calculations being made by the minimum value of these two. The base model includes also the standard  $k$ - $\epsilon$  model for turbulence. The geometry is assumed to be 2D axisymmetric, with 18291 nodes and 18000 faces, with higher density at the burner exit and near the axis. The boundary conditions were set in conformity with the recommendations found on the documentation website [1].

The main results can be summarized as follows:

- a. The effect of turbulence model shows that the RSM and the non-linear  $k$ - $\epsilon$  models are closer to each other than the standard  $k$ - $\epsilon$  model. The effects of the turbulence models are depicted in Figures 1. The figures show the axial distribution of the mixture fraction (1.a), temperature (1.b) and axial-velocity distributions (1.c).
- b. The effect of chemistry (single-step vs. a two-step mechanism) is rather small in terms of mixture fraction and velocity profiles along the axis of the flame. The peak temperature differ both in value and location. The two-step chemistry reproduces somewhat better the experimental data. The peak is located, for both models closer to the exit than in the measured data.
- c. The modified combustion model has been compared with the base model when using RSM as turbulence model. Figures 2 depict the results with this model set-up. As can be seen the modified combustion model yields somewhat better mixture fraction distribution (Figure 2.a) than the original one. The effect on the axial distribution of the temperature (Figure 2.b) is different from the original one, but it can hardly be termed as better as compared to experimental data. The situation is similar with respect to the axial-velocity distribution (Figure 2.c).
- d. Effects of differential diffusion exist but they are not so profound when used in terms of the Reynolds Averaged Navier-Stokes framework.
- e. Grid refinements and inclusion of the effects of radiation, have only minor effects

on the results and cannot be considered as of major importance for determining the source of discrepancy between modeling and experiments.

## References

1. [www.ca.sandia.gov/tdf/workshop.html](http://www.ca.sandia.gov/tdf/workshop.html)
2. T.H. Shih, W.W. Liou, A. Shabbir, and J. Zhu. A New k- $\epsilon$  Eddy Viscosity Model for High Reynolds Number Turbulent Flows - Model Development and Validation. *Computers Fluids*, 24(3):227-238, 1995.
3. Turns, R. S., An introduction to combustion, McGraw-Hill international editions, 1996
4. B.F. Magnussen and B.H.Hjertager. On mathematical models of turbulent combustion with special emphasis on soot formation and combustion. In 16<sup>th</sup> Symp. (Int'l) on Combustion. The Combustion Institute, 1976.

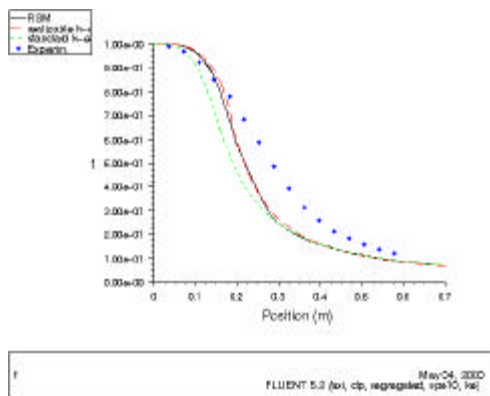


Fig. 1.a.

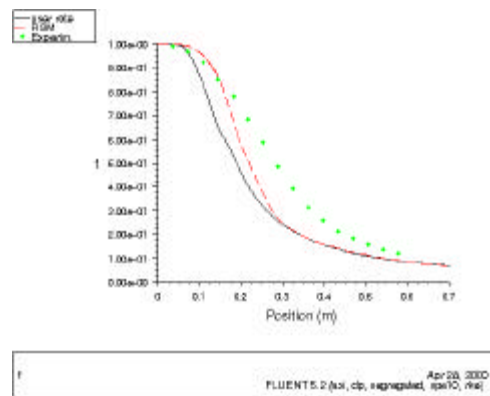


Fig. 2.a.

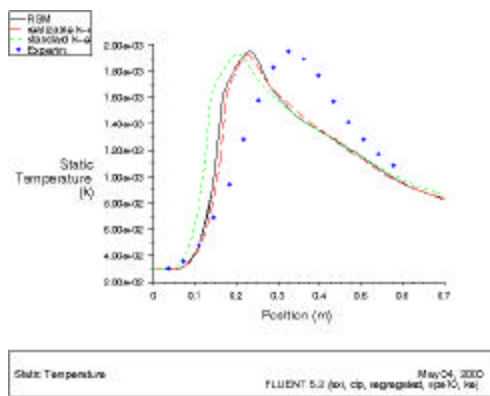


Fig. 1.b.

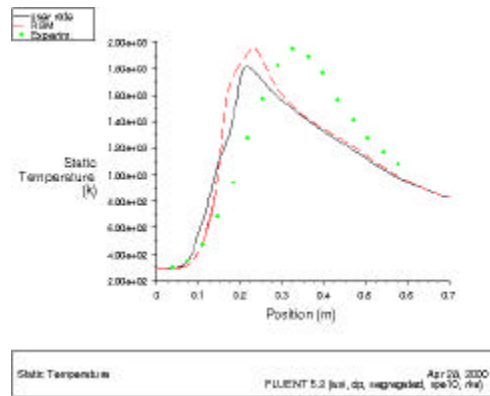


Fig. 2.b.

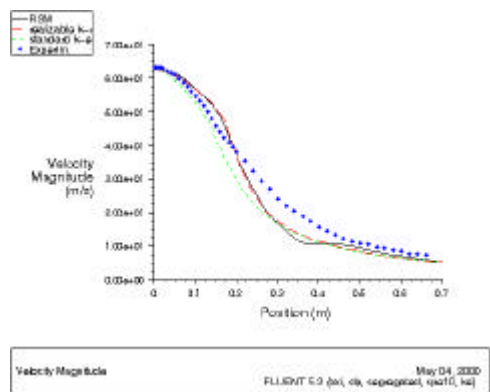


Fig. 1.c.

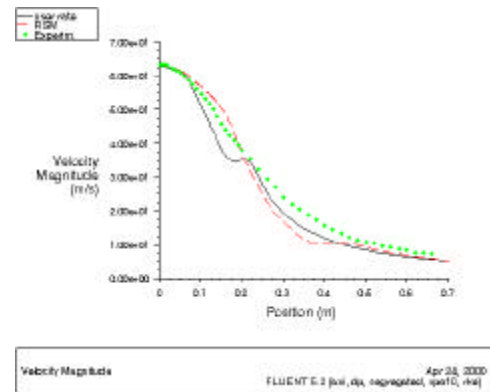


Fig. 2.c.

# PDF Calculations of NO Production in Piloted-Jet Turbulent Methane/Air Flame (Flame F)

**Qing Tang**

qtang@mae.cornell.edu

Sibley School of Mechanical and Aerospace Eng., Cornell Univ., Ithaca, NY 14850 USA.

**Jun Xu**

Combustion Design Engineering, GE Power System, Schenectady, NY 12345 USA

**Stephen B. Pope**

Sibley School of Mechanical and Aerospace Eng., Cornell Univ., Ithaca, NY 14850 USA.

## **ABSTRACT**

The velocity-composition-turbulence frequency joint PDF (JPDF) model has the distinction of taking into account both the chemical reactions and the convection in closed form. Hence, the turbulence effects on chemical reaction are treated exactly, and the gradient-diffusion assumption is avoided. This model also contains information on the turbulence time scale through modeling the turbulence frequency.

The JPDF method has been successfully used to calculate a series of piloted-jet non-premixed flames of methane/air (Flame D, E, and F of Barlow and Frank [1]) by Xu and Pope [2]. The calculation results are compared extensively with the experimental data, and demonstrate the ability of the JPDF model to represent, quantitatively, the processes of local extinction and re-ignition that occur in these flames. Tang and Pope [3] have also applied the JPDF method to piloted-jet flames with which the NO production can be calculated and reported excellent results for NO predictions for flames D and E.

Here we present JPDF predictions for Flame F. The burner has a fuel nozzle of radius  $R_j=3.6\text{mm}$  and a premixed pilot that extends to a diameter of  $D=18.2\text{mm}$ . The jet fuel is 25%  $\text{CH}_4$  and 75% air by volume and the pilot burns a lean pre-mixture of  $\text{C}_2\text{H}_2$ ,  $\text{H}_2$ , air,  $\text{CO}_2$ , and  $\text{N}_2$  with the same nominal enthalpy and equilibrium composition as methane/air at an equivalence ratio of 0.77. The bulk velocities of the fuel jet is 99.2m/s. The calculations are carried out down to  $x/R_j=120$ . The ingredients of the present model include the simplified Langevin model for velocity, a stochastic model of turbulence frequency and the EMST mixing model. An augmented reduced

mechanism (ARM2) for methane oxidation, which involves 19 species and 15 reactions (including NO chemistry) is incorporated in the JPDF calculations using the *in situ* adaptive tabulation (ISAT) algorithm [4]. The effects of radiative heat loss are studied using an optically thin limit model [5].

The numerical parameters used are identical to those used by Xu and Pope [2] who thoroughly characterized the numerical accuracy of their computations. The results are presented only where the numerical accuracy is assured, namely  $x/R_j < 60$  for unconditional quantities, and  $x/R_j < 90$  for conditional quantities.

In general, the flow and mixing field predictions are in good agreement with the experimental data. The radial profiles of unconditional Favre mean and the profiles of conditional (conditioned on mixture fraction) mean of temperature and the mass fractions of major species also show good agreement with the measurements on the fuel-lean side of the stoichiometric, while the peak values are over-predicted and there are discrepancies for these quantities on the fuel-rich side. It is found that the NO mass fraction in the flame are significantly over-predicted and the effects of radiative heat loss on NO production are not obvious.

#### **ACKNOWLEDGMENT**

This work was support in part by AIR FORCE Scientific Office of Research Grant F49620-97-1-0126, and in part by the U.S. Department of Energy, Federal Energy Technology Center under cooperative agreement No. DEFC21-92-MC29061 through the Advanced Gas Turbine Systems Research (AGTSR) program.

#### **REFERENCE**

- [1] R. S. Barlow and J. H. Frank. Proc. Combust. Inst. 27: 1087-1095 (1998)
- [2] J. Xu and S. B. Pope. Combust. Flame, (to be published) (2000).
- [3] Q. Tang and S. B. Pope. Proc. Combust. Inst. (to be published) (2000)
- [4] S. B. Pope. Combust. Theo. Modeling, 1:41-63, (1997).
- [5] Q. Tang and S. B. Pope. Report, FDA-99-05, MAE, Cornell University, (1999).